Scalable Synthesis of Dispersible Semiconducting Metal Chalcogenides Nanocrystals and their Application

by

Abhijit Bera
10CC14A26022

A thesis submitted to the
Academy of Scientific & Innovative Research
for the award of the degree of

DOCTOR OF PHILOSOPHY
in
SCIENCE

Under the supervision of
Dr. B. L. V. Prasad
Dr. Arup Kumar Rath

CSIR-National Chemical Laboratory, Pune

Academy of Scientific and Innovative Research
AcSIR Headquarters, CSIR-HRDC campus
Sector 19, Kamla Nehru Nagar,
Ghaziabad, U.P. – 201 002, India

June, 2021

Certificate

This is to certify that the work incorporated in this Ph.D. thesis entitled, "*Scalable Synthesis of Dispersible Semiconducting Metal Chalcogenides Nanocrystals and their Application",* submitted by *Abhijit Bera* to the Academy of Scientific and Innovative Research (AcSIR) in fulfillment of the requirements for the award of the Degree of *Doctor of philosophy in science*, embodies original research work carried-out by the student. We, further certify that this work has not been submitted to any other University or Institution in part or full for the award of any degree or diploma. Research material(s) obtained from other source(s) and used in this research work has/have been duly acknowledged in the thesis. Image(s), illustration(s), figure(s), table(s) etc., used in the thesis from other source(s), have also been duly cited and acknowledged.

(Signature of Student)	(Signature of Co-Supervisor)	(Signature of Supervisor)
Abhijit Bera	Dr. Arup Kumar Rath	Dr. B. L. V. Prasad
04.06.2021	04.06.2021	04.06.2021

STATEMENTS OF ACADEMIC INTEGRITY

I Abhijit Bera, a Ph.D. student of the Academy of Scientific and Innovative Research (AcSIR) with Registration No.10CC14A26022 hereby undertake that, the thesis entitled "Scalable Synthesis of Dispersible Semiconducting Metal Chalcogenides Nanocrystals and their Application" has been prepared by me and that the document reports original work carried out by me and is free of any plagiarism in compliance with the UGC Regulations on *"Promotion of Academic Integrity and Prevention of Plagiarism in Higher Educational Institutions (2018)"* and the CSIR Guidelines for "*Ethics in Research and in Governance (2020)".*

Signature of the Student
Date : 04.06.2021
Place : Pune

It is hereby certified that the work done by the student, under my/our supervision, is plagiarism-free in accordance with the UGC Regulations on *"Promotion of Academic Integrity and Prevention of Plagiarism in Higher Educational Institutions (2018)"* and the CSIR Guidelines for "*Ethics in Research and in Governance (2020)".*

Signature of the Co-supervisor (if any)
Name : Dr. Arup Kumar Rath
Date : 04.06.2021
Place : Pune

Signature of the Supervisor
Name : Dr. B. L. V. Prasad
Date : 04.06.2021
Place : Pune

Acknowledgement

During the entire period of my doctoral research, I have been acquainted, accompanied and supported by many people. Herein I take this opportunity to express my heart felt gratitude to all of them.

First of all, I would like to express my heart felt thanks to my supervisor, ***Dr. B. L. V. Prasad****, for his constant support and guidance throughout this journey. His precious knowledge, wise advices about life and generous help has significantly shaped the course of my doctoral journey and made me grow, not only as a researcher, but also as a wise and responsible human being. I also would like to express my heart felt thanks to my co-supervisor,* ***Dr. Arup K. Rath****, for his constant support and guidance throughout this journey. I feel immensely priviledged to be a part of their esteemed research group at CSIR-National Chemical Laboratory, where I have been constantly motivated to achieve my goals. It is this very pace, where I have learned to nurture a blend of hard work and discipline to shape my professional and personal aspects of life. It is under their supervision and guidance, where I have not only learned the art of culturing science, but also the art of thinking out of the box. What all I have gained and learned form them can never be repayed in any possible forms. I believe, a better way of thanking them would be through my future contributions to the scientific community. I wish both of them best of luck in their quest to perturb the limits of chemistry and physics, and may nothing but great things happen to them and their family.*

I owe to thank my doctoral advisory committee (DAC) members, Dr. Pradeep Kumar Tripathy, Dr. Manjusha Shelke and Dr. J Nithyanandhan for their constant support extended with guidance and suggestions. I am grateful to Prof. Dr. Ashish Lele (Director, CSIR-NCL), Prof. Dr. Ashwini K. Nangia (Former Director, CSIR-NCL), Prof. Dr. Sourav Pal (Former Director, CSIR-NCL), Dr. Anil Kumar (Former HoD, Division of Physical Chemistry, CSIR-NCL) and Dr. P. A. Joy (Former HoD, Division of Physical Chemistry, CSIR-NCL) for giving me this opportunity and providing me with advanced research infrastructure and facilities.

I would also like to express my gratitude to Mr. R. S. Gholap and Mr. S. S. Deo for helping in TEM analysis and XPS analysis, Mrs. Santhakumari for HRMS facility. I also would like to express my gratitude to Dr. P. R. Rajamohanan, Dr. Uday Kiran

Marelli, Dr. Ajith Kumar, Dinesh, Satish, Varsha, Meenakshi, Pramod for their timely support in recording NMR spectra. This list will be incomplete without expressing words of appreciation for Mr. Venkatesh and Mr. Tushar for helping me to collect electron microscopic images.

Herein I would also like to express my deep gratitude to my collaborators Dr. Leela Srinivas Panchakarla (IIT Bombay) and his students Mr. Vishal and Mr. Sushil for HRTEM analysis

I would also like to thank Prof. Dr. Ranga Rao (IIT Madras), under the guidance of whom I got my first exposure and experience in laboratory chemistry and research during my M. Sc. Dissertation.

It's my immense pleasure to thank my lab mates Dr. Balanagulu, Dr. Puspanjali, Dr. Jhumur, Dr. Prabhu, Dr. Arun, Dr. Pravin, Dr. Poulami, Dr. Vijay, Dr. Shankar, Dr. Kaustav, Dr. Gargi, Jayesh, Mayur, Pooja, Maya, Arun, Umasharan and Swapnali for devoting their precious time and providing me with valuable suggessions. I am also grateful to my another lab's mates, Dr. Srikanth, Debranjan, Prasenjit, Ashish, Chandan and Neha for helping me in device fabrication. A special thanks also goes to my co-authors and friend namely, Mr. Debranjan and Mr. Prasenjit for their fruitful suggessions and moral support throughout my research time especially device fabrication time. I would also like to express my heartfelt thanks to Sneha, Ruchira and Aparna for assisting me in my research projects.

No words are sufficient to acknowledge my prized friends in and out of NCL who have helped me at various stages of my life and my research work. I would love to thank Dr. Sibaprasad Midya, Dr. Pranab Deb, Dr. Bipul Biswas, Dr. Manoj K. Nandi, Dr. Santigopal Mondal, Dr. Arunava Maity, Dr. Saibal Bera, Dr. Subrata Mondal, Dr. Manjur, Dr. Arjun, Dr. Indradeep, Kaushik Maji, Debranjan Mondal, Pankaj Shaw Ashish Bera, Tapas Haldar, Tamal Das, Subhrasish Banerjee, Sanjukta Pahar, Susmita Bhowmik, Amarnath Singham, Dr. Arun Dadwal, Monika Malik, Monika Ghalawat, Supriya, Srijan, Deboreen, Rahul, Narugopal, Anirban, Vikash, Ravi, Swapnil Halnor for being a valuable part of my NCL family. Besides, I would like to express a deep sense of gratitude to Ishika Khatua for being there in the time of need

as a best friend and an uncomparable moral support during hard times throughout my masters (M. Sc.) and research tenure. I would also like to thank my friend out side of NCL, namely, Satyabrata Maity, Sayantan Ganguly, Sreejita Das, Dr. Chandramouli Ghosh, Priyangana, Debjit Bhar, Atanu, Arpan, Abhishek, Abhijit Manadal, Dr. Satyajit, Sukanya and Dr. Amrita for being their as a constant moral support. I really enjoyed the time that I spent with these awesome people.

Without the funding that I have received, this Ph. D. would not have been possible. Hence I would like to express my sincere appreciation to UGC-Rajib Gandhi National Fellowship(UGC-RGNF) for awarding me with JRF followed by SRF fellowship.

Words are inadequate to express my feelings and gratitude to my family for their unconditional love, care and support throughout my life. I would not have achieved anything without the support of my mom and dad, who gave me the freedom to explore my world and to explore who am I. With immense gratitude and reverence, I acknowledge my mom, Mrs. Kakali Bera and my dad, Mr. Ananda Bera for shaping my life and making me who I am today. I would not have achieved anything and would not have come here so far without the support of my beloved uncle Mr. Ashish K. Khatua, who always gave me positive support and encourage me.

Finally, with immense respect and gratitude, I bow down in front of the almighty for all that has been offered to me. I am, and will remain thankful for everything that has ever happened in my life, the good and the bad; for everything that I have achieved and few that I have lost. Some were blessings and some were lessons worth learning.

Abhijit Bera

Synopsis of the Thesis to be submitted to the Academy of Scientific and Innovative Research for Award of the Degree of Doctor of Philosophy in Chemistry	
Name of the Candidate	**Abhijit Bera**
Degree Enrollment No. & Date	**Ph.D. in Chemical Sciences (10CC14A26022); 16th July 2014**
Title of the Thesis	**Scalable Synthesis of Dispersible Semiconducting Metal Chalcogenides Nanocrystals and their Application**
Research Supervisor	**Dr. B. L. V. Prasad**
Research Co-Supervisor	**Dr. Arup Kumar Rath**

Keyword: Nanocrystals, quantum dots, single source precursor, metal thiolates, C_8DTCA, mixed metal thiolates.

Introduction:

Metal chalcogenide nanocrystals (NCs) or quantum dots (QDs) with excellent size-dependent and color-tunable emissions remained as one of the most exciting inventories in nanomaterials for the last few decades.[1] The term "quantum dot" is often used to refer to a quasi zero-dimensional (0-D) nanometer sized crystalline semiconductor particle where the active electronic components experience quantum confinement in all three spatial dimensions.[2] Such quantum confinement occurs when the diameters of such semiconductor NCs are smaller than the size of the material's exciton Bohr radius, (usually in the range of 1–10 nm).[3-5] One additional and interesting key advantage of QDs is the tunability of their optical and electrical properties based on the size.[1] Colloidal dispersion of these nano-meter-scaled semiconductor NCs are extremely useful materials for the development of numerous classes of solution-processed optoelectronic devices, including photovoltaic cells,[6, 7] photodetectors[6, 8] and light-emission devices.[9] Thus QDs are not only evoking interest among researchers but their commercial demand is also growing day by day. To fulfill their commercial demand, scalable synthesis of these materials without compromising their excellent properties is of utmost importance.

Statement of the problem

Though these QD NCs could be prepared by a variety of methods, including vapor- or solution-phase self-assembly and colloidal synthesis, the most important factor that their properties depend on their size and size distribution of particles and as expected particles with narrow size distributions (monodispersed) are highly desirable.[10, 11] The formation of monodisperse colloidal

quantum dots (CQDs) typically involves two steps: a rapid nucleation followed by a slow growth.[10] In the realm of colloidal synthetic methods two protocols,[10] in which the nucleation and growth processes are well separated, are generally employed. These are:

(i) Hot-Injection method: The hot-injection method is very effective in synthesizing high quality nanocrystals with good crystallinity and narrow size distributions as this procedure ensures the separation of nucleation and growth steps.[12, 13] The hot injection method involves the rapid injection of precursor(s) (mainly chalogenides sources) into a hot metal precursor solution with surfactant.[13] The injection temperature is critical, as it regulates the decomposition of the precursor(s). At this high temperature, nucleation is initiated due to the decomposition and the induced super saturation. Injecting a room temperature solution will decrease the overall reaction temperature, terminating the nucleation stage and commencing the growth stage.[13] Apart from the injection temperature the employment of appropriate active sulfur or selenium sources is also very important.[13]

(ii) Non-Injection method: In non-injection methods, the separation of nucleation and growth is realized by slowly heating up the solution in the presence of particular precursors.[14] The precursors should meet the requirement that they have negligible reactivity at a low temperature, but significant reactivity at elevated temperatures. When precursors are heated up to a certain temperature, a burst nucleation occurs followed by the growth of nanocrystals, which is similar to the process in hot-injection methods.[14-16] Compared to the hot-injection method, non-injection methods are far simpler and provide an alternative way to obtain CQDs at relatively low temperatures that is environmentally friendly and suited to scale-up.[16] Generally the non-injection methods are based on single source precursors and these methods are highly effective for generating metal chalcogenides QD materials if appropriate precursors can be chosen.[16, 17] The selected precursor must contain both the desired metal and corresponding chalcogen elements, which can decompose under a certain temperature to give metal chalcogenides compounds directly.[17] By adjusting the ratios of the starting reagents (including precursors, surfactant, and solvent) as well as the reaction temperature and reaction time, the size and morphology of the metal chalcogenides NCs can be precisely controlled.

A series of binary metal sulfide and metal selenide NCs like CdS, CdSe, ZnS, ZnSe, PbS, PbSe etc also including ternary metal sulfide like $CuInS_2$ and $AgInS_2$ NCs have been prepared by several research groups in the last few decades by using the above mentioned two conventional synthetic methods.[11, 18-20] Among all the binary metal chalcogenides, Pb chalcogenides (PbS and PbSe) are considered as a tricky material to synthesize in so far as their optical properties are concerned and non-injection procedures typically fail to produce good quality (sharp absorption and emission

peak) of PbS or PbSe QDs.[21-23] Thus till date hot-injection methods are considered the most effective methods in synthesizing high quality PbS QD with narrow size distribution.[13, 24] Several sulfur sources like elemental sulfur, ammonium sulfide, thiourea and thioacetamide were used in the hot injection method for PbS synthesis but unfortunately using these sulfur sources gives wide size distribution associated with imperfect surface passivation including poor air stability. Furthermore these PbS CQDs do not display a sharp excitonic peak preventing their utility in many applications like solar cells.[25-30] Therefore -bis (trimethylsilyl) sulfide $[(TMS)_2S]$[24] a highly reactive sulfur source is considered to be the best as far as PbS CQDs preparation is concerned.[24] In fact, all reported performance records of photovoltaic devices based on PbS CQDs have relied on the $[(TMS)_2S]$ based syntheses only.[31, 32] Unfortunately due to the pyrophoric nature of $[(TMS)_2S]$ or $[(TMS)_2Se]$ it is very difficult to scale-up the synthesis of metal chalcogenide NCs using them as chalcogenides source. This led to the search of other sulfur/selenides sources and recently Owen group from Columbia university reported the utilization of substituted thiourea[33] as a sulfur source to prepare a large scale quantity of PbS CQD characterized with sharp excitonic peak with tunable band gap including narrower size distribution. None the less, this procedure is also fraught with some problems like the necessity to synthesize a library of thiourea to get size control as the NC size obtained in this method crucially depends on the kinetics of thiourea decomposition.

So, there is obvious need of an alternate method that relies on more commonly available sulfur precursors as well as alternate single source metal precursors that can be employed for large scale synthesis of metal chalcogenide NCs.

In this context, we envisaged that metal thiolates (with one or more metal ions) could be good candidates as single source precursors for the synthesis of metal chalcogenide NCs as all the necessary ingredients like the metal ion, capping agent (which are essential for metal chalcogenides NCs synthesis) are inbuilt in the metal thiolate structure itself.

Accordingly, in this thesis we report our work on the synthesis of a series of metal thiolates (mono and mixed bimetal) and demonstrate that these metal thiolates and mixed bimetal thiolates are the good candidates as single source precursor for various metal chalcogenides NCs synthesis. We also found an alternate sulfur source called octyl ammonium octyl dithiocarbamate (C_8DTCA), which turned out to be an excellent sulfur precursor for the synthesis of binary metal sulfide NCs via solution based method (hot injection) as well as solvent-less solid state grinding method.

Objectives:

In this background, the work to be embedded in this thesis reports different procedures that provide easy accessibility to gram scale quantities of mono metal thiolates as well as bimemetallic mixed metal thiolates and their utility as precursors for the preparation of metal chalcogenide NCs. We also discovered an active air stable sulfur precursor called octyl ammonium octyl dithiocarbamate (C_8DTCA), which could be employed to access large quantities of metal sulfide NCs. This C_8DTCA could be used in solution based methods (hot injection) or solid state grinding methods for the preparation of metal sulfide NCs.

Quite satisfyingly while the monometallic thiolates were used to make simple metal sulfide/selenide NCs, the bimetallic mixed metal thiolates turned out to be excellent single source precursors for the preparation of bimetallic chalcogenides like $AgInS_2$, $CuInS_2$, as well as $AgInSe_2$ and $CuInSe_2$ NCs in large scale by simple solid state grinding methods. Most gratifyingly, all these NCs, though were prepared by a solvent less grinding method, could be easily dispersed in nonpolar solvents as the preparation method ensued the formation of organic molecule capped NCs.

Methodology:

First we synthesized a series of metal thiolates and simple thermal decomposition of these metal thiolates in a high boiling solvent gave uniform particles of metal chalcoginides. However, the optical properties of these metal chalcogenide NCs were poor probably due to the surface defects resulting from sulfur rich surface (anionic surface traps).[34, 35]

To reduce the thermal decomposition temperature and surface traps, we looked for a new air stable sulfur source and C_8DTCA fitted the bill perfectly. Accordingly, C_8DTCA was used as a sulfur source in the hot injection method to prepare a series of uniform sized metal sulfide NCs including most challenging PbS NCs and we found that the optical properties of the synthesized materials are as comparable to those obtained with the methods employing [$(TMS)_2S$) as the sulfur source.[36]

We could also demonstrate that the combination of metal thiolates and the air stable active sulfur source C_8DTCA works well to afford uniform sized binary metal sulfide NCs via mechano-chemical grinding methods and these binary metal sulfide NCs show excellent tunable optical properties.[37]

Extending this work we then prepared bimetallic mixed metal thiolates by simply mixing dodecanethiol with two metal salts. By grinding these mixed bimetal thiolates with an appropriate S-precursor solution (elemental S powder dissolved in minimal amount of oleyl amine) we could accomplish the synthesis of phase pure bimetallc sulfide NCs.

Summary:

1) We demonstrate metal thiolates as good single source precursors for various metal chalcogenide NCs synthesis.

2) We also establish C_8DTCA to be a useful sulfur precursor for the synthesis of binary metal sulfide NCs via solution based chemical method (hot injection) as well as solid state grinding methods.

3) A series of bimetallic thiolates were also synthesized and these were also utilized to synthesize the bimetallic sulfide NCs by mechano-chemical mothods.

All these developed procedures are scalable as well as can be improved to get good quality of metal chalcogenides NCs.

All the above results and step by step improvement of the different materials would be incorporated in the thesis titled "**Scalable Synthesis of Dispersible Semiconducting Metal Chalcogenides Nanocrystals and their Application**". This thesis is divided into five different chapters. A brief introduction to each chapter is provided below with the chapter titles.

Chapter-1: General Introduction

Brief background of the work and the motivation to carry out the work embedded in the thesis is included in this chapter.

Chapter-2: 2D Molecular Precursor for a One-pot Synthesis of Semiconducting Metal Sulphide Nanocrystals

This chapter focusses on the large scale synthesis of various 2D molecular precursors like metal thiolates and metal dithiocarbamate complexes (M-C_8DTCA) and their thermal decomposition to metal sulfide NCs via solution based methods.

Chapter-3: Generic and Scalable Method for the Preparation of Monodispersed Metal Sulfide Nanocrystals with Tunable Optical Properties.

In this chapter, we show that the fast decomposition of metal-C_8DTCA complexes can be accomplished in presence of primary amines and uniform metal sulfide CQDs can be prepared. This novel technique is generic and has been applied to prepare diverse CQDs, like CdS, MnS, ZnS, SnS, and In_2S_3, including more useful and in-demand PbS CQDs and plasmonic nanocrystals of Cu_2S. Based on several control reactions, it is postulated that the reaction involves the in situ formation of a metal–C_8DTCA complex, which then reacts with oleylamine at slightly elevated temperature to decompose into metal sulfide CQDs at a controlled rate, leading to the formation of the metal sulfide NCs with good optical characteristics. Controlled sulfur precursor's

reactivity and stoichiometric reaction between C_8DTCA and metal salts affords high conversion yield and large-scale production of monodisperse CQDs. Tunable and desired crystal size could be achieved by controlling the precursor reactivity by changing the reaction temperature and reagent ratios. Finally, the photovoltaic devices fabricated from PbS CQDs displayed a power conversion efficiency of 4.64% that is comparable with the reported values of devices prepared with PbS CQDs synthesized by the standard methods.

Chapter-4: Solvent-Less Solid State Synthesis of Dispersible Metal and Semiconducting Metal Sulfide Nanocrystals.

In this chapter we show metal thiolates as possible precursors for the preparation of monolayer protected metal and metal sulfide NCs via solid state grinding method. More precisely we show that a large variety of uniform-sized semiconducting NCs of metal sulfides including PbS, CdS, ZnS, MnS, Ag_2S, and CuS NCs could be synthesized via the solid state route by grinding the metal thiolates with C_8DTCA and in some cases C_8DTCA plus small amount of oleylamine as sulfur source. Interestingly, using this simple technique sub-3 nm NCs like Ag_2S, PbS, and CuS could be prepared which are otherwise difficult to prepare by the conventional high temperature solution routes also. Most gratifyingly, all these NCs, though prepared by a solvent less grinding method, could be easily dispersed in nonpolar solvents as the preparation method ensued the formation of organic molecule capped NCs.

Chapter-5: Synthesis and Characterization of Mixed Bimetal Thiolates and Their Utilization for the Preparation of Bimetallic Chalcogenide Nanocrystals through Mechano-chemical Grinding.

In this chapter, we establish that even mixed bimetal thiolates like copper-indium thiolate and silver-indium thiolate also exist as lamellar sheets similar to the thiolates the individual metals and these sheets consist of both metal ions arranged in a random fashion. We also demonstrate that these mixed metal thiolates could be employed as single source precursors for the preparation of series of bimetallic chalcogenide nanocrystals (NCs) through mechano-chemical routes by grinding them with an appropriate chalcogenide source. Quite notably these bimetallic chalcogenide NCs, though synthesized via a mechano-chemical route get easily dispersed in non-polar solvents as the thiolate molecules that get released during the grinding process passivate the metal sulphide/selenide NCs being formed. These ternary NCs display a strong and tunable photoluminescence in the visible to near-infrared region.

Conclusion and Future Perspective:

We have developed single source precursor called metal thiolates where metal thiolates could be a mono metal thiolate or also could be mixed bimetal thiolates. We have also developed an active sulfur precursor called octyl ammonium octyl dithiocarbamate (C_8DTCA) and utilized it in the synthesis of various metal sulfide NCs by solution based method (hot injection) or solid state grinding method. We have so far made a scalable quantity of various metal sulfide and selenide NCs including ternary metal sulfide or selenide NCs using mono metal thiolates or mixed bimetal thiolates. These materials have many applications such as in LED, photovoltaics and biological cell imaging. For these emerging applications, there are still plenty of rooms to develop new materials (especially quaternary metal chalcogenide NCs and one new class of materials called chalcogenide perovskite) and to improve their surface passivation for their better optical properties.

Even our single source precursor, metal thiolates are interesting class of materials which exist as 2D materials analogous to graphene or MoS_2. As it has been postulated earlier that completely new and exotic materials could be prepared by making hetero-structures from 2D materials. As we already have various metal thiolates and these could be easily realized by an easy and convenient route. Since some of these metal thiolates are soluble in organic solvents, so composite 2D hetero-structures of two different metal thiolates nanosheets could easily be prepared and composite 2D hetero-structure are expected to display unprecedented properties leading to novel applications such as in energy generation and catalysis. So, these mono metal thiolates and mixed bimetal thiolates, prepared by very convenient solid state method prescribed in this thesis, open another avenue for further investigation to understand the nanosheet-nanosheet hetero-structures of two different metal thiolates and utilization of those hetero-structure in the preparation of functional nanomaterials for the improvement of the photovoltaic performance as well as in LED, biological cell imaging and catalysis.

List of Publications:

1. Abhijit Bera, Bhagavatula L V Prasad, 2D molecular precursor for a one-pot synthesis of semiconducting metal sulphide nanocrystals. *Bull. Mater. Sci*. **2018**, 41:125.
2. Abhijit Bera, Debranjan Mandal, Prasenjit N. Goswami, Arup K. Rath, and Bhagavatula L. V. Prasad, Generic and Scalable Method for the Preparation of Monodispersed Metal Sulfide Nanocrystals with Tunable Optical Properties. *Langmuir* **2018**, 34, 5788−5797.
3. Abhijit Bera, Balanagulu Busupalli and Bhagavatula L. V. Prasad, Solvent-Less Solid State

Synthesis of Dispersible Metal and Semiconducting Metal Sulfide Nanocrystals. *ACS Sustainable Chem. Eng*. **2018**, 6, 12006−12016.

4. Abhijit Bera, Bhagavatula L. V. Prasad, Synthesis and Characterization of Mixed Bimetal Thiolates and Their Utilization for the Preparation of Bimetallic Chalcogenide Nanocrystals through Mechano-chemical Grinding (to be communicate soon)

References:

1. Norris, D. J.; Efros, A. L.; Rosen, M.; Bawendi, M. G., Size dependence of exciton fine structure in CdSe quantum dots. *Phys. Rev. B* **1996,** *53* (24), 16347.
2. Nirmal, M.; Norris, D. J.; Kuno, M.; Bawendi, M. G.; Efros, A. L.; Rosen, M., Observation of the" dark exciton" in CdSe quantum dots. *Phys. Rev. Lett.* **1995,** *75* (20), 3728.
3. Zhang, Y.; Liu, Y.; Li, C.; Chen, X.; Wang, Q., Controlled synthesis of Ag2S quantum dots and experimental determination of the exciton Bohr radius. *J. Phys. Chem. C* **2014,** *118* (9), 4918-4923.
4. Ramvall, P.; Tanaka, S.; Nomura, S.; Riblet, P.; Aoyagi, Y., Observation of confinement-dependent exciton binding energy of GaN quantum dots. *Appl. Phys. Lett.* **1998,** *73* (8), 1104-1106.
5. Fu, H.; Wang, L.-W.; Zunger, A., Excitonic exchange splitting in bulk semiconductors. *Phys. Rev. B* **1999,** *59* (8), 5568.
6. McDonald, S. A.; Konstantatos, G.; Zhang, S.; Cyr, P. W.; Klem, E. J.; Levina, L.; Sargent, E. H., Solution-processed PbS quantum dot infrared photodetectors and photovoltaics. *Nat. Mater.* **2005,** *4* (2), 138-142.
7. Rekemeyer, P. H.; Chang, S.; Chuang, C. H. M.; Hwang, G. W.; Bawendi, M. G.; Gradečak, S., Enhanced photocurrent in pbs quantum dot photovoltaics via ZnO nanowires and band alignment engineering. *Adv. Energy Mater.* **2016,** *6* (24), 1600848.
8. Kufer, D.; Nikitskiy, I.; Lasanta, T.; Navickaite, G.; Koppens, F. H.; Konstantatos, G., Hybrid 2D–0D MoS2–PbS quantum dot photodetectors. *Adv. Mater.* **2015,** *27* (1), 176-180.
9. Sun, Q.; Wang, Y. A.; Li, L. S.; Wang, D.; Zhu, T.; Xu, J.; Yang, C.; Li, Y., Bright, multicoloured light-emitting diodes based on quantum dots. *Nat. Photonics* **2007,** *1* (12), 717-722.
10. Gao, M.-R.; Xu, Y.-F.; Jiang, J.; Yu, S.-H., Nanostructured metal chalcogenides: synthesis, modification, and applications in energy conversion and storage devices. *Chem. Soc. Rev.* **2013,** *42* (7), 2986-3017.
11. Kershaw, S. V.; Susha, A. S.; Rogach, A. L., Narrow bandgap colloidal metal chalcogenide quantum dots: synthetic methods, heterostructures, assemblies, electronic and infrared optical properties. *Chem. Soc. Rev.* **2013,** *42* (7), 3033-3087.
12. LaMer, V. K.; Dinegar, R. H., Theory, production and mechanism of formation of monodispersed hydrosols. *J. Am. Chem. Soc.* **1950,** *72* (11), 4847-4854.
13. Murray, C.; Norris, D. J.; Bawendi, M. G., Synthesis and characterization of nearly monodisperse CdE (E= sulfur, selenium, tellurium) semiconductor nanocrystallites. *J. Am. Chem. Soc.* **1993,** *115* (19), 8706-8715.
14. Aboulaich, A.; Billaud, D.; Abyan, M.; Balan, L.; Gaumet, J.-J.; Medjadhi, G.; Ghanbaja, J.; Schneider, R. l., One-pot noninjection route to CdS quantum dots via hydrothermal synthesis. *ACS Appl. Mater. Interfaces* **2012,** *4* (5), 2561-2569.
15. Nam, D.-E.; Song, W.-S.; Yang, H., Noninjection, one-pot synthesis of Cu-deficient CuInS2/ZnS core/shell quantum dots and their fluorescent properties. *J. Colloid Interface Sci.* **2011,** *361* (2), 491-496.
16. Zhang, W.; Zhang, H.; Feng, Y.; Zhong, X., Scalable single-step noninjection synthesis of

high-quality core/shell quantum dots with emission tunable from violet to near infrared. *ACS Nano* **2012,** *6* (12), 11066-11073.
17. Du, Y.; Xu, B.; Fu, T.; Cai, M.; Li, F.; Zhang, Y.; Wang, Q., Near-infrared photoluminescent Ag2S quantum dots from a single source precursor. *J. Am. Chem. Soc.* **2010,** *132* (5), 1470-1471.
18. van Embden, J.; Chesman, A. S.; Jasieniak, J. J., The heat-up synthesis of colloidal nanocrystals. *Chem. Mater.* **2015,** *27* (7), 2246-2285.
19. Castro, S. L.; Bailey, S. G.; Raffaelle, R. P.; Banger, K. K.; Hepp, A. F., Nanocrystalline chalcopyrite materials (CuInS2 and CuInSe2) via low-temperature pyrolysis of molecular single-source precursors. *Chem. Mater.* **2003,** *15* (16), 3142-3147.
20. Yu, K.; Liu, X.; Zeng, Q.; Yang, M.; Ouyang, J.; Wang, X.; Tao, Y., The Formation Mechanism of Binary Semiconductor Nanomaterials: Shared by Single-Source and Dual-Source Precursor Approaches. *Angew. Chem.* **2013,** *125* (42), 11240-11245.
21. Ouyang, J.; Schuurmans, C.; Zhang, Y.; Nagelkerke, R.; Wu, X.; Kingston, D.; Wang, Z. Y.; Wilkinson, D.; Li, C.; Leek, D. M., Low-temperature approach to high-yield and reproducible syntheses of high-quality small-sized PbSe colloidal nanocrystals for photovoltaic applications. *ACS Appl. Mater. Interfaces* **2011,** *3* (2), 553-565.
22. Hughes, B. K.; Ruddy, D. A.; Blackburn, J. L.; Smith, D. K.; Bergren, M. R.; Nozik, A. J.; Johnson, J. C.; Beard, M. C., Control of PbSe quantum dot surface chemistry and photophysics using an alkylselenide ligand. *ACS Nano* **2012,** *6* (6), 5498-5506.
23. de Mello Donegá, C.; Liljeroth, P.; Vanmaekelbergh, D., Physicochemical evaluation of the hot-injection method, a synthesis route for monodisperse nanocrystals. *Small* **2005,** *1* (12), 1152-1162.
24. Hines, M. A.; Scholes, G. D., Colloidal PbS nanocrystals with size-tunable near-infrared emission: observation of post-synthesis self-narrowing of the particle size distribution. *Adv. Mater.* **2003,** *15* (21), 1844-1849.
25. Joo, J.; Na, H. B.; Yu, T.; Yu, J. H.; Kim, Y. W.; Wu, F.; Zhang, J. Z.; Hyeon, T., Generalized and facile synthesis of semiconducting metal sulfide nanocrystals. *J. Am. Chem. Soc.* **2003,** *125* (36), 11100-11105.
26. Li, Z.; Ji, Y.; Xie, R.; Grisham, S. Y.; Peng, X., Correlation of CdS nanocrystal formation with elemental sulfur activation and its implication in synthetic development. *J. Am. Chem. Soc.* **2011,** *133* (43), 17248-17256.
27. Zhang, H.; Hyun, B.-R.; Wise, F. W.; Robinson, R. D., A generic method for rational scalable synthesis of monodisperse metal sulfide nanocrystals. *Nano Lett.* **2012,** *12* (11), 5856-5860.
28. Zhang, L.-J.; Shen, X.-C.; Liang, H.; Guo, S.; Liang, Z.-H., Hot-injection synthesis of highly luminescent and monodisperse CdS nanocrystals using thioacetamide and cadmium source with proper reactivity. *J. Colloid Interface sci.* **2010,** *342* (2), 236-242.
29. Cademartiri, L.; Montanari, E.; Calestani, G.; Migliori, A.; Guagliardi, A.; Ozin, G. A., Size-dependent extinction coefficients of PbS quantum dots. *J. Am. Chem. Soc.* **2006,** *128* (31), 10337-10346.
30. Yuan, M.; Kemp, K. W.; Thon, S. M.; Kim, J. Y.; Chou, K. W.; Amassian, A.; Sargent, E. H., High-performance quantum-dot solids via elemental sulfur synthesis. *Adv. Mater.* **2014,** *26* (21), 3513-3519.
31. Liu, M.; Voznyy, O.; Sabatini, R.; de Arquer, F. P. G.; Munir, R.; Balawi, A. H.; Lan, X.; Fan, F.; Walters, G.; Kirmani, A. R., Hybrid organic–inorganic inks flatten the energy landscape in colloidal quantum dot solids. *Nat. Mater.* **2017,** *16* (2), 258-263.
32. Xu, J.; Voznyy, O.; Liu, M.; Kirmani, A. R.; Walters, G.; Munir, R.; Abdelsamie, M.; Proppe, A. H.; Sarkar, A.; de Arquer, F. P. G., 2D matrix engineering for homogeneous quantum

dot coupling in photovoltaic solids. *Nat. Nanotech.* **2018,** *13* (6), 456-462.
33. Hendricks, M. P.; Campos, M. P.; Cleveland, G. T.; Jen-La Plante, I.; Owen, J. S., A tunable library of substituted thiourea precursors to metal sulfide nanocrystals. *Science* **2015,** *348* (6240), 1226-1230.
34. Bera, A.; Prasad, B. L., 2D molecular precursor for a one-pot synthesis of semiconducting metal sulphide nanocrystals. *Bull. Mater. Sci.* **2018,** *41* (5), 125.
35. Houtepen, A. J.; Hens, Z.; Owen, J. S.; Infante, I., On the origin of surface traps in colloidal II–VI semiconductor nanocrystals. *Chem. Mater.* **2017,** *29* (2), 752-761.
36. Bera, A.; Mandal, D.; Goswami, P. N.; Rath, A. K.; Prasad, B. L., Generic and scalable method for the preparation of monodispersed metal sulfide nanocrystals with tunable optical properties. *Langmuir* **2018,** *34* (20), 5788-5797.
37. Bera, A.; Busupalli, B.; Prasad, B. L., Solvent-Less Solid State Synthesis of Dispersible Metal and Semiconducting Metal Sulfide Nanocrystals. *ACS Sustainable Chem. Eng.* **2018,** *6* (9), 12006-12016.

Student: **Abhijit Bera**
Date: **11/12/2020**

Research Guide: **Dr. B. L. V. Prasad**

Date: **11/12/2020**

Co-Guide: **Dr. Arup Kr. Rath**

Date: **11/12/2020**

Table of Content

Chapter 1
Introduction

Table of Content

Chapter 2

2D Molecular Precursor for a One-pot Synthesis of Semiconducting Metal Sulfide Nanocrystals

Table of Content

Chapter 3

Generic and Scalable Method for the Preparation of Monodispersed Metal Sulfide Nanocrystals with Tunable Optical Properties

Chapter 4

Solvent-Less Solid State Synthesis of Dispersible Metal and Semiconducting Metal Sulfide Nanocrystals

Table of Content

List of Figures

List of Tables

1.1 Introduction

Recapitulating the developments that happened over several million years it is probably safe to say that the evolution of human beings is essentially linked to the development of materials. In fact, after satiating the basic needs like food, cloth, and shelter the human life style has undergone a big change with other factors like comfort, commerce, conflict, communication and curiosity taking a central stage. For this changed lifestyle development of technology was the key. In the recent times this changed life style is also closely associated with miniaturization where small gadgets with multifunctional abilities are becoming a norm. For example until few years back we used to store data on a 3.5 inches floppy disk with a capacity of 800 KB to 2.8 MB. Similarly the popular audio cassette tapes could store 12- 20 songs and a reel camera was being used to capture photos. Now using a small gadget like mobile phone we are able to accomplish all these in a very convenient way.

Obviously, all this requires the development of new materials and tweaking their properties for the desired applications. While for a long time this relied only on finding new materials with different properties, thanks to the advent of nanoscience it became possible to append properties to materials that they otherwise are not known to display. This hitherto unknown aspect of size-dependent properties of nanoscale materials has drawn huge attention both from researchers as well as common people. Some of the examples of the size-dependent properties are surface plasmon resonance in some metal particles, emission in semiconductor particles due to quantum confinement and super para-magnetism in magnetic materials due to their single domain nature.[1]

1.1.1 Nanomaterials

Though there is lot of curiosity towards nanomaterials these days, but they are not new to the world; they were used unknowingly by Roman artisans during the fourth century (eg. Lycurgus cup)[2, 3] and also used by Mesopotamians in ninth century for creating a glittering effect on the surface of pots.[4] But the term “nanomaterials” and the deliberate preparation of such special class of materials and their utilization for different applications began few decades ago. Nobel laureate Richard Feynman is regarded as the father of modern nanotechnology based on his lecture now popularly

known as "There's Plenty of Room at the Bottom"[5] where he described a vision of using molecules and atoms to construct smaller machines at nanoscale level, though he never specifically used the term nanoscience or nanotechnology.[6-9] The usage of the term "nanotechnology" for the first time is credited to Norio Taniguchi; a Japanese scientist who in 1974 defined it as "nanotechnology mainly consists of the processing of separation, consolidation, and deformation of materials by one atom or one molecule."[10, 11]This vision, coupled with the relentless efforts of many researchers led to the development of the new field called nanoscience and nanotechnology. Nanoscience and nanotechnology is nothing but synthesizing and manufacturing matter at the nanoscale and by observing, measuring, manipulating, assembling, controlling, and employ them for useful applications.[11-15] As time progressed, materials, with at least one dimension in size range of 1-100 nm were started to be termed as nanomaterials.[12-14]This size range is intermediate between bulk and atomic or molecular materials and the nanoparticles of different materials possess unusual properties, differing from their bulk counterparts.[13-16] This is partly because, as particle diameter decreases, surface area per unit mass increases, such that at the nanoscale the specific surface area will be huge.[16] Further, for bulk materials of sizes larger than one micrometre, the percentage of atoms at the surface is minuscule relative to the total number of atoms present in the material whereas, at the nanoscale, the percentage of atoms at the surface of a material becomes significant.[15, 16] Hence their activity towards any processes that occur at their surface (such as catalysis and sensing) is greatly increased. Apart from this, some unique changes occur to the electronic structures of the materials also (especially metallic and semiconductor systems) leading to exquisite properties.[17-20]

In this thesis, we will be majorly dealing with metal chalcogenide semiconductor nanoparticles capped with a covalently bound organic molecule. Most of the metal chalcogenides are crystalline semiconductor compounds in their bulk form, and at certain sizes (as defined below) if their crystalline nature is preserved, they experience quantum confinement effect.[21] For this quantum confinement to occur the diameter of the particle/crystal should be smaller than twice the size of the material's exciton Bohr radius, (usually in the range of 1–10 nm).[22-24]Such tiny semiconductor nanocrystals (NCs) are also popularly denoted as quantum dots (QDs). Colloidal dispersion of these nano-meter-scaled

semiconductor NCs are extremely useful materials for the development of numerous classes of solution-processed optoelectronic devices,[25-27] including photovoltaic cells,[28-30]photodetectors[31-33] and light-emission devices.[34-36] Thus metal chalcogenide QDs are not only evoking interest among researchers but their commercial demand is also growing day by day. To fulfil their commercial demand, scalable synthesis of these materials without compromising their excellent properties is of utmost importance. In the following we briefly explain their salient features and the characteristics they should possess for them to display the excellent properties they are known for.

1.1.1.1 Metal chalcogenides

Metal chalcogenides area group of inorganic chemical compounds consisting of at least one chalcogen anion and at least one more electropositive metal element. Although, the elements from group VI_A are all called chalcogens, but the term metal chalcogenides is mainly reserved for sulfides, selenides, and tellurides, rather than oxides and polonium compounds. As we go down the group VI_A of periodic table, the metallic character of elements increases. Thus the first element of group VI_A, oxygen, shows extremely strong non-metallic properties while the last element of group VI_A, polonium (Po), shows strong metallic properties. On the other hand, the three other elements (S, Se and Te) are totally different from the oxygen and polonium. For example, O_2 is a gas while the others are solid, and the temperature coefficient of electrical resistivity for S, Se and Te is negative, while Po has resistivity typical of metal. The properties and details of chalcogens elements are shown in Table 1.1 and in Figure 1.1 the electropositive metals are highlighted. Besides, when the non-metallic chalcogen (S, Se and Te) anions react with electropositive metals under appropriate reaction conditions, metal chalcogenides with various kinds of structure and compositions are formed.[37] The compositions are directly related to the available oxidation state of electropositive metal and properties of chalcogen, leading to huge variety of metal chalcogenides as detailed below.

Table 1.1 Properties of chalcogen elements (S, Se and Te)

	Sulphur (S)	**Selenium (Se)**	**Tellurium (Te)**
Atomic Mass	32.07	78.96	127.6

Atomic Number	16	34	52
Electronic Configuration	$[Ne]3s^23p^4$	$[Ar]3d^{10}4s^24p^4$	$[Kr]4d^{10}5s^25p^4$
Atomic Radius (10^{-10} m)	1.00	1.20	1.40
X^{2-} Ionic Radius (10^{-10} m)	1.03	1.16	1.37
Electronegativity (Pauling's Data)	2.58	2.55	2.10
Standard Redox Potential	-0.48	-0.92	-1.14

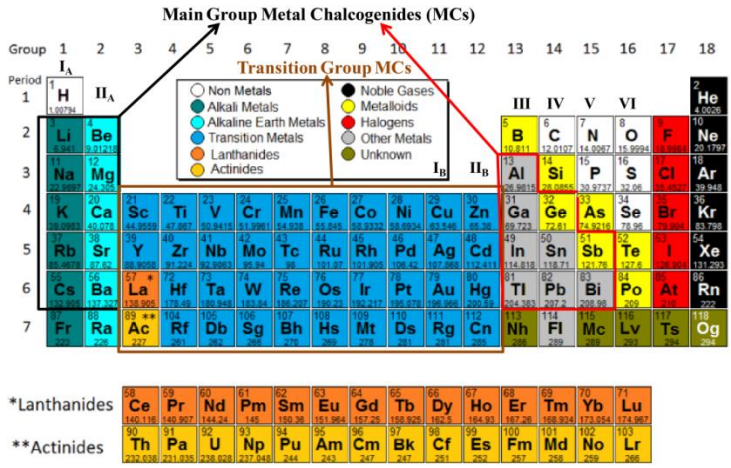

Figure 1.1 Periodic Table and main group metal chalcogenides and transition group metal chalcogenides.

1.1.1.1.1 Category, structure and properties of metal chalcogenides

The non-metallic chalcogens (S, Se and Te) and the polychalcogenide anions (S^{2-} and S_n^{2-}) react with metals, (which possesses unfilled d orbitals –like group 3 to Group 12 transition metals), resulting in the formation of off stoichiometry compounds, such as FeS, FeS_2, Fe_2S_3; CuS, $Cu_{1.75}S$, $Cu_{1.97}S$, Cu_2S,etc. On the other hand, most of the main group metal chalcogenides form stoichiometric compound such as PbS, PbSe, PbTe

and Bi_2S_3. Thus there are vast numbers of metal chalcogenides with a huge diversity and these could be categorized in many different ways. One such categorization is based on the number of metals present, such as binary Na_2X, Ag_2X, MoX_2, WX_2, ZnX, MnX, Cu_2X, PbX, CdX, Bi_2X_3(where X= S, Se orTe); ternary $AgInX_2$, $CuInX_2$, $CuAlX_2$, $CuGaX_2$, $CuFeX_2$, $AgBiX_2$ (where X= S or Se); quaternary Cu_2ZnSnX_4, $CuIn_XGa_{1-X}X_2$, etc. (where X= S or Se). As it would be vast and complicated to discuss all the possible combinations of metal chalcogenides, we have restricted our discussion to binary and ternary metal chalcogenide (where only one/two metals and any one of the chalcogen are engaged) systems. Additionally we also focussed our attention only on chalcogenides of main group and transition metals (as elaborated in Figure 1.1) as the variety of systems will become too large otherwise. Here, the binary metal chalcogenides could be formed when any of the non-metallic chalcogens from group VI react with any of the metals and few different types of the combination and corresponding metal chalcogenidesare shown in Table 1.2. Few important ternary chalcogenides, including I-III-VI_2 and I_2-II-IV-VI_4 family that are pertinent to this thesis work are also included in Table 1.2.

Table 1.2 Different types of main group and transition group metal chalcogenides

Group	**I**		**II**		**III**	**IV**	**V**	**VI**	Possible Metal Chalcogenides
System	I_A	I_B	II_A	II_B					
I_2-VI	M^1= Li, Na, K, Rb and Cs	Cu, Ag						S, Se and Te	$M^1{}_2X$ (M= Li, Na, K, Rb and Cs) Ag_2X and Cu_2X (X= S, Se and Te)
II-VI			M^2=Mg, Ca, Sr and Ba	Zn, Cd and Hg				S, Se and Te	M^2X (M= Mg, Ca, Sr and Ba) ZnX, CdX and HgX (X= S, Se and Te)

III_2-VI_3			Al, Ga and In			S and Se	In_2S_3, In_2Se_3, Ga_2S_3 and Ga_2Se_3
IV-VI				Sn^{2+} and Pb		S, Se and Te	SnX and PbX (X= S, Se and Te)
V_2-VI_3					Sb and Bi	S, Se and Te	Sb_2X_3 and Bi_2X_3(X= S, Se and Te)
I-III-VI_2	Cu, Ag		Al, Ga and In			S and Se	$CuAlX_2$, $AgAlX_2$, $CuGaX_2$, $AgGaX_2$, $CuInX_2$ and $AgInX_2$(X= S and Se)
I_2-II-IV-VI_4	Cu	Zn		Sn^{4+}		S and Se	Cu_2ZnSnX_4 (X= S, Se)

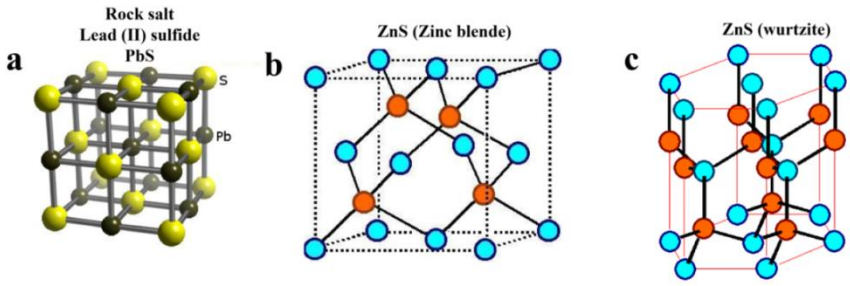

Figure 1.2 Metal chalgogenide basic structures a) Rock salt, b) Zinc blende and c) Wurtzite type.

Most of the above mentioned metal chalcogenides crystallize in the three basic forms: NaCl type (rock salt), zinc blende type (ZB), and wurtzite type, and these are shown in Figure 1.2. The rock salt (NaCl) structure has a face-centered cubic unit cell where the chalcogen anions are in cubic close packing type of arrangement, i.e., it contains

chalcogen anions at the corners and at the center of each face of the cube and metal cations occupy the octahedral voids (PbS as an example of rock salt structure is shown in Figure 1.2). For the zinc blende (ZB) structure, the chalcogenides show a cubic symmetry (cubic close packing and the Zn occupy half of the tetrahedral holes only), which leads to a diamond like frame work. In the wurtzite structure, the chalcogenide atoms are arranged in hexagonal close packing and Zn occupy half of the tetrahedral holes only, but shows different crystal symmetry from ZB (Figure 1.2).

Beside these three basic types of structure, some other types of structure also are there. For instance Ag (group I_B) metal chalcogenides mostly crystallize with monoclinic structure (acanthite (β-form), stable below 179 °C).[38] Interestingly, though copper also belongs to group I_B, the binary copper chalcogenides shows variety of crystal structures with various stoichiometries and polymorphs because of the many defects in these structures.[39,40] For example, in the Cu-S system, Cu_2S (chalcocite), pyrite-type CuS_2, $Cu_{2-x}S$, $Cu_{1.96}S$, $Cu_{1.9}4S$, $Cu_{1.8}S$, Cu_7S_4, Cu_9S_8, CuS (covellite) etc. exist.[41, 42] For example, copper monosulfide (where $1.6 \leq Cu/S \leq 2$, no direct S-S bond) consist of isolated sulfide anions that are closely related to either hcp or fcc lattices.[43] Other interesting copper sulfides are mixed copper monosulfide or disulfide (where copper contain both monosulfide (S^{2-}) as well as disulfide $(S_2)^{n-}$ which consists of an S-S bond and Cu:S ratios between 1.0 and 1.4). These crystal structures usually consist of alternating hexagonal layers of monosulfide and disulfide anions with Cu cations in trigonal and tetrahedral interstices.[43]

As the chalcogenide anions are polarizable, most of the metal-chalcogen bonds are covalent in nature except those with few alkali metals (M-X, where M=Li, Na, K, Rb) and silver. This covalency is mainly due to a strong mixing of the valence s and p orbitals of the chalcogen (e.g. 3s and 3p for sulfur, etc.) with the outer s and p orbitals of the electropositive metal (e.g. 4s and 4p for 3d transition and post-transition elements). The overlap of these molecular orbitals leads to the formation of a broad valence band and conduction band. The contribution to the valence band (bonding) is mainly due to the electronegative elements, i.e. the chalcogen. Similarly the conduction band (antibonding) is mainly associated with the metal. In most cases, an energy gap gets generated between valence band and conduction band, which is the band gap of the material. It may be noted that, copper monosulfides and disulfides

behave either as semiconductors or as metallic conductors depending on their composition.[44] In case of metallic conductors they also display surface plasmon resonance in the NIR region. Most of the other metal chalcogenides can be regarded as semiconductors, where the energy gap is generally higher in sulfides than selenides and tellurides; since sulfur is much more electronegative than the selenium and tellurium.[45] Typically, for any metal chalcogenide, the gap in sulfides is in the range is 1 to 3 eV, where as in selenides and particularly in tellurides it tends to be much smaller. Also this difference in band gap is mainly associated with the changes in the valence band whereas the conduction band related to metal remains much less affected.

When a photon is absorbed by a semiconductor, an electron from the lower electron energy level (ground state/valence band) is excited to a higher electron energy level (excited state/conduction band), leaving behind a hole in the valence band. The excited electrons then relax and combine with the hole and this result in the emission of light (radiative recombination) or heat (non-radiative recombination).[46] The emitted energy is usually smaller than the absorbed energy which is termed as the Stokes shift.[47] Fascinatingly, when the size of the crystalline particles of these metal chalcogenides are in the nanosize regime and fulfil the condition of their size being less than twice the Bohr excitonic radius of that particular material, they experience quantum confinement effect.[21, 47, 48] The most impressive result of quantum confinement in QDs is the tunability of their band gap and the ensuing size dependent photoluminescence from them.[49, 50]

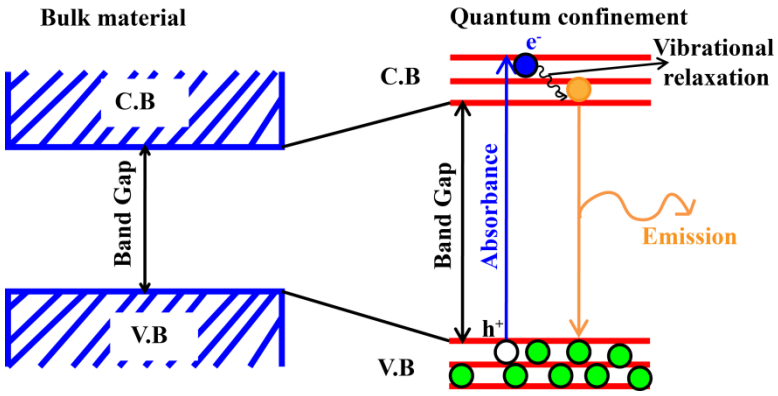

Figure 1.3 Band structures of bulk and QDs. Schematic illustrations of luminescence mechanisms in semiconductors NCs.

Figure 1.3 is a schematic illustration showing the difference between electronic properties of bulk semiconductor material and their QDs. The left portion of the schematic shows the overlapped electronic energy levels (bands) in bulk semiconducting material (as example CdSe), whereas, the right portion shows the discrete electronic energy levels when the material is in the form of QDs.

As mentioned above for these semiconductors to be qualified QDs their size should be less than twice the Bohr exciton radius, leading to quantum confinement. The Bohr exciton radius (r_B) of a particle is given by:

$$r_B = \frac{\hbar^2 \varepsilon}{e^2} \left(\frac{1}{m_e} + \frac{1}{m_h}\right)$$

Where, ε is the dielectric constant of the material, m_e and m_h are the effective mass of the electron and hole respectively, and r_B is Bohr exciton radius of the material.

For example, the Bohr exciton radius of CdSe QD is ~3 nm.[51] Thus a CdSe particle of size below ~6 nm ($2r_B$= 6 nm) or less they will start showing size dependent absorption and emission properties as presented in Figure 1.4 a-c. Here it can be noticed that a QD with a diameter of ~2 nm emits light in the blue region (high energy), while that with a diameter of 5.5 nm emits in the red region (low energy). The size dependent energy gap in spherical QDs can be explained using "particle in a box model" and it can be estimated by the effective mass approximation using the following relation:

$$E_g = E_{g,bulk} + \frac{h^2 \pi^2}{2R^2} \left(\frac{1}{m_e} + \frac{1}{m_h}\right) - \frac{1.8e^2}{\varepsilon R}$$

Where, R is the radius of the particle, E_g is the energy gap (band gap), $E_{g,bulk}$ is the energy gap of the bulk material, h is Plank's constant, m_e is the effective mass of electron, m_h is the effective mass of hole, and ε is the effective dielectric constant.

From the above equation it becomes clear that, increasing the size of QDs results in lower energy gap (band gap decreases). Thus as the size of the QD increases, the absorption and emission peak positions shifts to the red. Figure 1.4 shows size dependent change in emission for CdSe QDs by varying their diameter from ~2 nm to 5.5 nm. This illustrates that some QDs can be engineered to emit throughout the visible and near infrared spectrum by just changing their size.

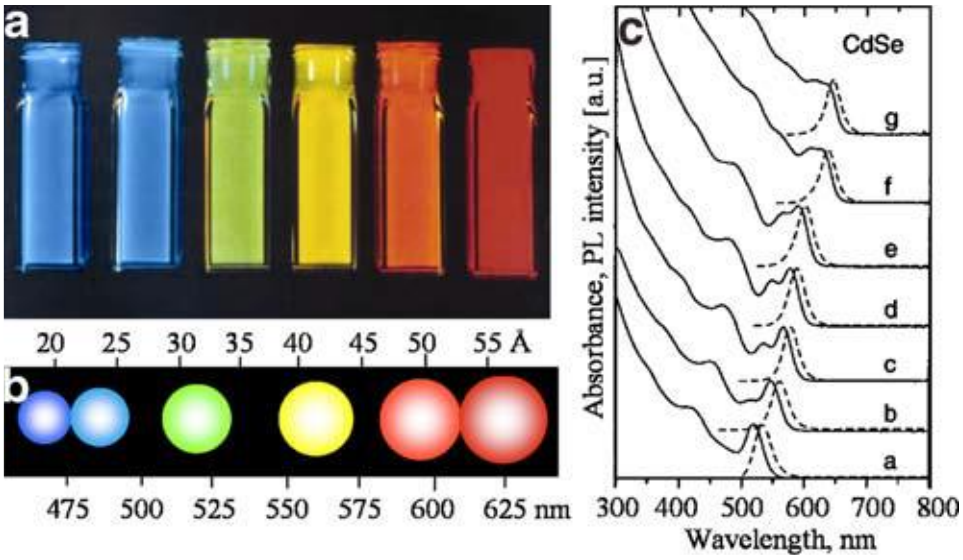

Figure 1.4 (a) Size-dependent PL color and (b) schematic presentation of size, color, and PL wavelength of CdSe–ZnS QDs. (c) Absorption (solid lines) and PL (broken lines) spectra of CdSe QDs with various sizes.[52] Figure has been taken with permission from ref 52. Copyright (2008) Springer Nature.

1.1.2 Important characteristics of metal chalcogenide QDs

The most exciting property of semiconducting metal chalcogenide QDs is photoluminescence (PL) as described above. In case of PL, the quality of metal chalcogenide QDs are decided by the factor called photoluminescence quantum yield (PLQY), which is measured on a scale from 0 to 1.0 (100%, often represented it as a percentage). PLQY is a measure of the efficiency of photon emission as defined by the ratio of the number of photons emitted to the number of photons absorbed.

Apart from the band gap (which is directly related to size of the particles) and composition, the PLQY of QDs is also strongly affected by both surface and intrinsic defects (crystalline defects).[53-55]The intrinsic defects in II-VI or I-III-VI compound semiconductor are lattice vacancies and host interstitials as well as atom arrangements (imperfect crystalline patterns) associated with the metal and chalcogenide sublattices.[56-58] The presence of defects or impurities in the crystal lattice causes symmetry breaking and bond distortions (Jahn–Teller effect), giving rise to electronic energy levels between the valence and conduction bands that trap the excited electron.[58, 59] This results in a non-radiative relaxation that competes strongly with the

radiative exciton recombination, decreasing the PLQY significantly and causing a red shift and broadening of the emission band.

The surface of QDs has very strong influence in the photoluminescence.[60-62] The pioneer of quantum physics and Nobel laureate, Wolfgang Pauli once stated that "God made the bulk; the surface was invented by the devil" as the surfaces are incredibly important and yet remarkably complex.[63, 64] Surface atoms have dangling bonds due to non-existent nearest neighbour atoms, which results in lower coordination compared to atoms in the bulk of the crystal. These dangling bonds at the surface of QDs can strongly influence their chemical, physical, and optoelectronic properties. Similar to crystalline defects (intrinsic defects), defects on the surface create additional electronic states within the band gap, which can act as traps for electrons or holes.[46, 65] High surface defect densities can lead to a decrease in PLQY, and a red-shifted emission band due to the trap states. Moreover, the surface states near the band edges can mix with the intrinsic states, and these can change the energy gap of the QDs. These surface related defects and intrinsic defects are commonly observed in any binary or ternary metal chalcogenide QDs and decrease their PLQY and limit their applications. For instance, binary metal chalcogenide systems like ZnSe and CdSe show point defects which leads to lattice vacancies and as well as imperfect crystalline patterns. Similarly ternary system like $CuInS_2$ could form off-stoichiometric compounds ($Cu_xIn_yS_2$) where point defects, lattice displacements, lattice vacancies as well as imperfect crystallinity which strongly affect their optical and electronic properties.[58, 66-69]

The problems related to crystalline and surface defects can be minimized by heating the QDs with proper surface protecting ligands or surface passivation.[54, 70, 71] The heating (even in a solvent) can improve the crystallinity and the surface defects can be removed by capping the QDs with a surface protecting ligands or thin layer of another semiconductor which is elaborated below.[71]

1.1.2.1 Surface passivation

Passivation of QD surfaces can suppress the non-radiative recombination mechanisms such as trap states, and enhance luminescence. This passivation can be carried out either with organic molecules or by creating inorganic shells.[71-73] In organic surface passivation, an organic ligand is used to cap and form a monolayer on the QD surface

which can make bonds with the surface defects, remove the trap states and stabilize the electronic state of the particle.[74, 75] The choice of ligand is determined by its coordination chemistry with QD surface atoms.[76] On the basis of the Lewis concept of acids and bases, a hard Lewis acid will favour bonding to a hard Lewis base such as oxygen. By contrast, metal cations with a lower charge to size ratio (soft acids) prefer bonding to soft bases (like thiols). In inorganic surface passivation, an inorganic material with a similar crystal structure to that of the parent QD, with a close lattice parameter, and a wider band gap is used to cap and remove surface dangling bonds and consequently enhance luminescence.[77, 78] For example, $CuInS_2$ QDs passivated by the larger band gap material ZnS shows an enhancement in PLQY from 1-5 % for un-passivated to 50-65 % for passivated system as shown in Figure 1.5.[79]

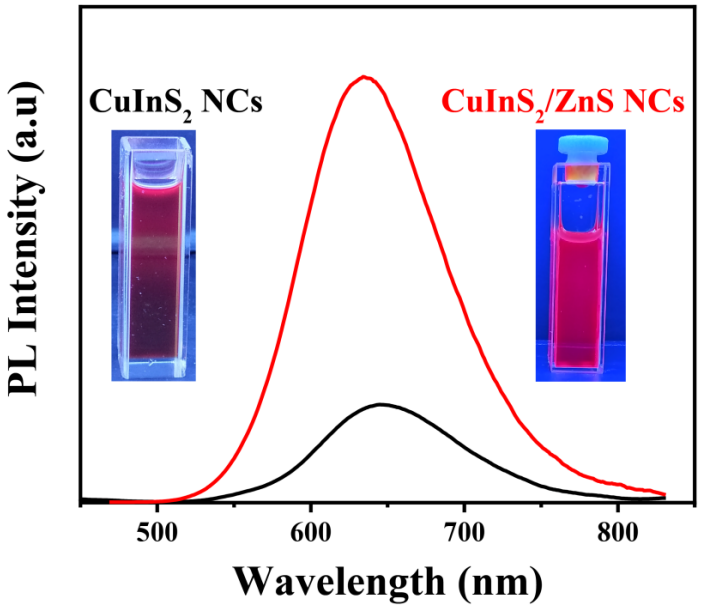

Figure 1.5 Normalized PL spectra of copper indium sulfide QDs before and after ZnS passivation.

1.1.2.2 Applications of QDs

As mentioned briefly above due to extraordinary properties of QDs, they have emerging application in various fields including solar cells,[28-30] optoelectronics,[25-27] biomedical imaging[34-36] and security.[80] Some of these applications are discussed below.

1.1.2.2.1 Quantum dot solar cell

The energy of solar radiation is distributed across a wide spectral range of 350 to 2500 nm, of which 47% is visible light and 52% is NIR light (700-2500 nm). Due to the polychromatic nature of the solar radiation the theoretical limit of a single-junction solar cell is 32% (Shockley and Queisser limit) for the optimum semiconductor bandgap of 1.3eV.[81-83] Commerciallyavailable Si based solar cells have reached the highest efficiency of 25%, as of date.[82, 83] Some of the recently developed metal chalcogenides QDs have the potential to exceed this 32% limit.[84] The use of QDs for making solar cells offers several advantages over other conventional materials: (i) they can be manufactured in an energy-saving low-temperature process; (ii) they can be made from earth abundant, inexpensive materials that do not require extensive purification, as is required for Si; (iii) the synthetic control and the size tenability allows the use of different size QDs to absorb a broad range of the solar spectrum (according to required band gap, the particular size QDs could be prepared). Also QDs possess higher extinction coefficients and they can be applied on a variety of inexpensive and even flexible substrate materials, such as light weight plastics. Few of the solar cells developed using QDs such as CdTe, PbS, $CuInS_2$, $CuInSe_2$, $CuIn_xGa_{1-x}Se_2$ and Cu_2ZnSnS_4 display remarkable power conversion efficiencies; 13.8 % for PbS QDs, 21 % for CdTe and $CuIn_xGa_{1-x}Se_2$ and 12.6% in case of Cu_2ZnSnS_4.[85-91]

1.1.2.2.2 Quantum dots for solid state lightning

Solid-state lightening (SSL) utilizes light-emitting diodes (LEDs).[92] LEDs have high energy conversion efficiency, compact structure, and longer user-life compared to conventional lamps.[92] White light SSL are used in car lights, traffic signs, displays, and general illumination while, multi-color LEDs are used for displays, bio-imaging, and lasers.[92-95] White light SSL can be made by mixing red, green, and blue QDs. Now days, QDs are also being used to fabricate TV and mobile screens. Because QDs are both photo-active (photoluminescent) and electro-active (electroluminescent) they are expected to play a crucial role in developing next-generation displays. Samsung and LG launched their QLED TVs in 2015, and a few other companies followed not long after. QD-based materials have purer colors, longer lifetime, lower

manufacturing cost, and lower power consumption. In this context, availability of colloidal QDs makes it very advantageous because they can be deposited on virtually any substrate, and printable, flexible even rollable QD displays of all sizes may be realized. Cadmium and lead based QDs have excellent optical properties; however these materials have high toxicity to animals and plants. Hence, significant efforts are now focused on development of QDs free from cadmium and lead. $CuInS_2$/ZnS QDs are one of these promising materials that may substitute cadmium and lead based QDs.[96, 97] However, low PLQY and broad full width at half maxima (FWHM) of these QDs has been a challenge, and may limit their application areas.

1.1.2.2.3 Biomedical Imaging

QDs are also finding important medical applications, including potential cancer treatments.[98, 99] QDs can be appropriately designed so that they accumulate in particular parts of the body and due to the luminescence properties they can be traced and also utilized to deliver anti-cancer drugs to specific parts of the body in a targeted way.[100] This can reduce the unpleasant side effects that are characteristic of untargeted, traditional chemotherapy.[101, 102] QDs can also be used in place of organic dyes for medical imaging.[103] In this purpose low toxic and highly photoluminescent materials such as $CuInS_2$/ZnS and $AgInS_2$/ZnS could be used as these materials can be transferred to the aqueous medium easily.[97]

1.1.3 Metal chalcogenide NC or QDs synthesis

From the above discussion it is clear that colloidal QDs are extremely useful materials for the development of numerous classes of solution-processed optoelectronic devices,[25-27] including photovoltaic cells,[28-30] photodetectors,[31-33] and light-emission devices.[34-36] According to the IDTechEx forecast report, demand for QDs will grow from less than 100 kg in 2015 to over 2 metric tons in 2026, which is more than a 20-fold increase ("Demand for quantum dots will increase 20-fold over next decade" IDTechEx Research forecasts report by Dr. Guillaume Chansin on December 15, 2015). Thus QDs are not only evoking interest among researchers but their commercial demand is also growing day by day. To fulfil this commercial demand, scalable synthesis of these materials without compromising their excellent properties

is of utmost importance. Scalable synthesis of QDs is an extremely challenging task and should be accomplished by keeping the following issues in view:

1) Purity, stability and dispersibility: The final materials have to be chemically pure (no impurity), stable (air stable) and dispersible in any solvent.
2) Monodispersity and crystallinity: As PL properties directly related to band gap and which is again size dependent, the QDs should be uniform in size with good crystallinity. (otherwise it may show intrinsic defects which affect their PLQY)
3) Surface should be properly passivated (minimal trap states)
4) Reproducibility (lab to lab and batch to batch)

It is to be noted that for QDs to be useful for many applications, the most important factor is the syntheses of monodispersed particles with narrow size distribution. Studies on the mechanism underlying the formation of colloidal systems have improved our knowledge on the factors that control their size and size distribution of QDs and led to innovative routes for their synthesis.

The formation of monodisperse QDs typically involves two steps: a rapid nucleation followed by a slow growth (Figure 1.6).[104, 105] In a typical colloidal QD synthesis, reaction precursors are initially dispersed or dissolved in proper solvents, followed by the generation of monomers due to the chemical reaction between precursors (Figure 1.6I).[104-107] As the concentration of monomers increases to the super-saturation level, nuclei are formed by the aggregation and self-nucleation of these monomers (Figure 1.6II).[105, 107] With the continuous deposition of monomers on these pre-existing nuclei, the growth process of nanocrystals occurs until the concentration of monomers drops below the critical level (Figure 1.6III). It should be noted that new nuclei are also formed during the growth of nanocrystals, which often results in a widening size distribution of the nanocrystals. Therefore separation of nucleation and growth is considered to be important for obtaining QDs with narrow size distribution.[105, 107]

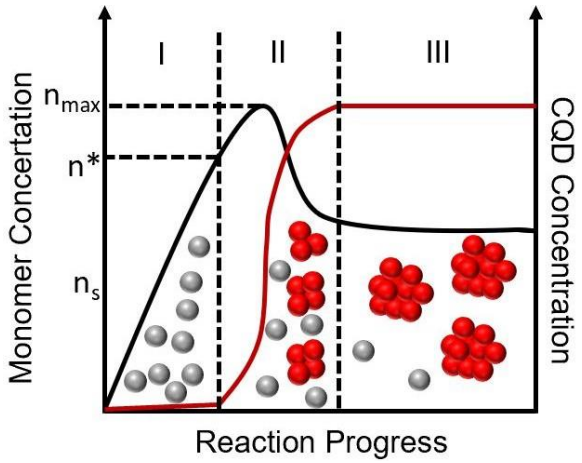

Figure 1.6 Plot of LaMer model for the generation of atoms, nucleation, and subsequent growth of colloidal NCs synthesis (LaMer and Dinegar 1950).[105] Figure redrawn from ref 105.

The major factors that control the rate of nanocrystal nucleation are temperature, interfacial tension, and degree of super saturation in solution. Nucleation can be terminated either by a reduction in concentration below a critical level or by a rapid drop in reaction temperature induced by fast injection of the precursor(s) into a hot coordinating solvent (hot-injection method– *vide infra*).[104] Following nucleation, nanocrystal growth begins with molecular addition of the monomeric precursor(s) remaining in solution.

Another routine practice during the synthesis of colloidal QDs is the employment of surfactants/surface-passivating reagents/ ligands. The majority surfactant molecules used are comprised of a long hydrocarbon tail and a polar head; and the examples include oleic acid, oleylamine, trioctylphosphine oxide, or dodecanethiol.[108] These surfactants can tune the reactivity of the precursors, improving control over the nucleation and growth rates.[108] In addition, the phase, morphology, and optical properties of QDs also can be tuned on the basis of the choice of surfactant.[109, 110]

1.1.3.1 Synthetic methods

Basically two types of synthetic methods for the synthesis of colloidal QDs are known which reasonably satisfy the above mentioned conditions, which are as follows:

(i) Non-Injection method

(ii) Hot-Injection method

In non-injection methods, the QDs are synthesized by slowly heating up the solution in presence of suitable precursors. The precursors should meet the requirement that they have negligible reactivity at a low temperature, but significant reactivity at elevated temperatures.[111] When precursors are heated up to a certain temperature, a burst nucleation should occur followed by the growth of nanocrystals.[111] These, non-injection methods are simpler and provide a way to obtain QDs at relatively low temperatures. Several types of non-injection synthesis of QD are described below:

1.1.3.1.1 Non-injection method

1.1.3.1.1.1 Single-source precursor method

The so-called single source precursor method has been proved to be a very popular non-injection strategy. For this the chosen precursor must contain both the desired metal and corresponding chalcogen elements, which can decompose at a certain temperature to give QDs directly. By adjusting the ratios of the starting reagents (including precursors, ligands, and solvent) as well as the reaction temperature and reaction time, the size and morphology of the QDs can be precisely controlled. Lead sulfide (PbS) nanocrystals have been grown up in polymer thin film matrix from single molecular precursors.[112] When dithiocarbamate complexes were used as single source precursors, anisotropic PbS nanoparticles could be obtained.[113-115] Single-crystalline, monodisperse Ag_2S QDs with a size of ~10 nm synthesized using a single source precursor (SSP) of Ag(DDTC)[$(C_2H_5)_2NCS_2Ag$] as presented in Fig. 1.7.[116]

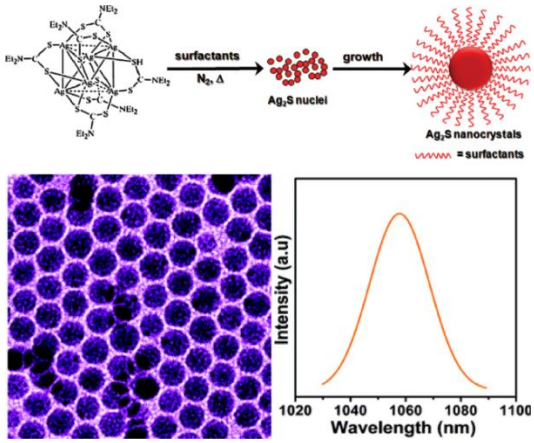

Figure 1.7 Synthesis of Ag_2S NIR QDs from a Single SourcePrecursor of Ag(DDTC). Figure has redrawn with permission from ref 116. Copyright (2010) American Chemical Society.

1.1.3.1.1.2 Solvo-thermal synthesis (organic medium) of QDs

Solvo-thermal methods (in aqueous medium the same is called hydrothermal) have been extensively utilized for nanoparticle synthesis. However, the earlier efforts to synthesize QDs by these methods largely resulted in products with inferior characteristics. Also, many times such methods resulted in large size particles/crystals that did not fulfil the quantum confinement conditions, thus restricting the practical utility of such methods. Recently, a number of reports on the solvo-thermal synthesis of QDs in organic solvents have appeared. For example CdS,[117] CdSe and CdSe/CdS core/shell,[118] PbSe,[119] InP,[120] and $CuInS_2$ QDs[121] have been reported via these approaches. Solvo-thermal conditions could provide desired temperature and pressure thus generating unique synthesis condition for nanocrystal growth. The solvo-thermal method employs similar synthesis method as the normal batch synthesis, usually starting from the mixing of two individual precursors at lower temperature, and then raising the temperature to the desired level in a sealed autoclave for the nanocrystal production. In a typical solvo-thermal growth of PbSe quantum dots, Pb precursor was prepared by dissolving $Pb(CH_3COO)_2 \cdot 3H_2O$ in octadecylamine to form a clear solution at 80 °C.[119] Then Se powder was rapidly added into Pb precursor and stirred vigorously for ~10 min.[119] The mixture was then transferred to a sealed Teflon-lined stainless steel autoclave and the same was maintained at 200 °C for 1.5 h. Different sized PbSe nanocrystals could be obtained by this method by simply varying the initial Pb-to-Se ratio.[119] Although the synthesized quantum dots show narrow size distribution and quantum confined absorption spectra, the reported photoluminescence efficiency was found to be still lower than those reported from other methods. This indicates the formation of lower quality of QDs which possibly originate from higher defect levels.

QDs of ternary metal chalcogenides such as $CuInS_2$ and $AgInS_2$ offer exciting opportunities because of their tunable size and composition. $CuInS_2$ QDs are the most widely studied representatives of this family as they can be easily prepared with good size control and in high yield by solvo-thermal decomposition method. In one such typical method Liang Li et al. obtained $CuInS_2$ QDs by reacting the metal precursors (copper iodide and indium acetate) with dodecanethiol (1-DDT).[122] In this reaction, DDT was used along with 1-octadecene (ODE) and DDT plays the triple role of being the sulfur source, surface ligand, and solvent. The synthesis involves two steps, first

one at around 100 °C ("complexation, a polymeric complex called metal thiolates formed") and second one carried out at 230 °C where the polymeric complex thermally decomposes to $CuInS_2$ ("nucleation and growth" scheme was shown in Figure 1.8).[123] This method has many advantageous features due to its simple implementation (heat-up approach), high reproducibility and reaction yield.

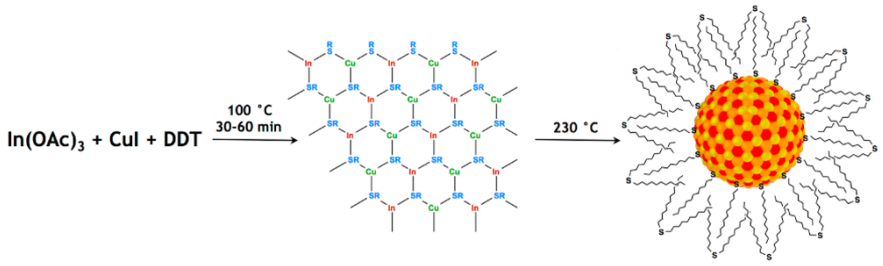

Figure 1.8 Conventional syntheses of $CuInS_2$ NCs by solvo-thermal decomposition of lamellar metal thiolate complex.[123] Figure has taken with permission from ref 123. Copyright (2017) American Chemical Society.

1.1.3.1.1.3 Aqueous and hydrothermal synthesis of QDs

QDs made from aqueous synthesis are especially attractive for biological application due to their compatibility with water.[124, 125]Also compared to the organic-based synthesis, aqueous synthesis is cheaper, less toxic and more environmental friendly. Unfortunately, the QDs prepared in aqueous media have relatively low PLQY and large size distribution compared to those carried out in organic solvents.[125]

1.1.3.1.1.4 Limitation of non-injection methods

Although non-injection method has the advantage like single step synthesis and scalable process, the difficulty to avoid defects and the associated low PLQY makes this a less favoured mode of synthesis. Even though few metal sulfides like CdS, MnS, ZnS and SnS with good optical properties have been prepared by this method; in case of tricky materials like PbS and PbSe QDs the optical properties are still observed to be poor.[112, 119]So these limitations leave the search for better synthetic procedures open.

1.1.3.1.2 Hot-injection method

The hot-injection method is one of the most effective in synthesizing high quality NCs with good crystallinity and narrow size distributions as this procedure ensures

the separation of nucleation and growth steps. This method involves the rapid injection of precursor(s) (mainly chalogenides sources) into a hot metal precursor plus surfactant solution in a high boiling solvent. The injection temperature is critical, as it regulates the decomposition of the precursor(s) (scheme showed in Figure 1.9). At this high temperature, nucleation is initiated due to the decomposition of the metal precursor and its reaction with the chalcogen sources inducing a super saturation of the metal chalcogenide monomers. Injecting a room temperature solution will decrease the overall reaction temperature, terminating the nucleation stage and commencing the growth stage. Apart from the injection temperature the employment of appropriate active sulfur or selenium sources is also very important in these procedures.

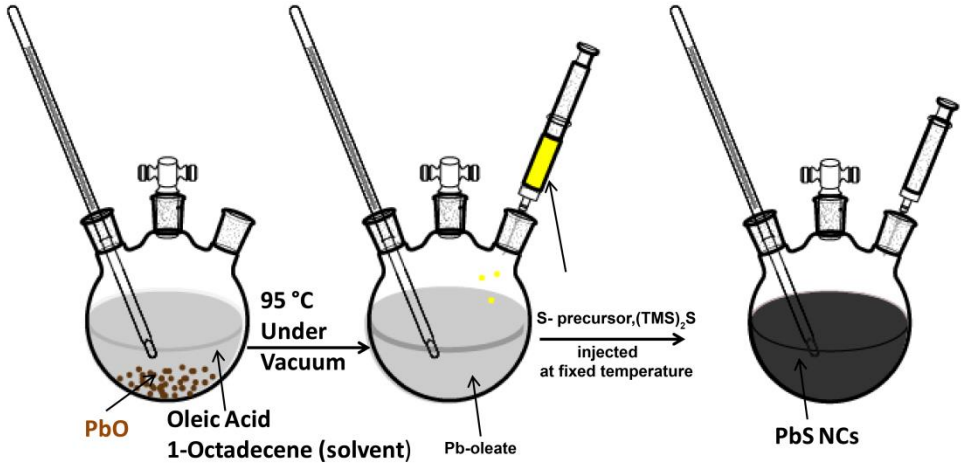

Figure 1.9 Hot-injection method for PbS NCs synthesis, with nucleation occurring upon the injection of a room temperature "S" precursor into a high-temperature Pb-oleate solution, followed by reaction cooling leading to the growth phase.

The hot-injection method was first used by Prof. Bawendi and his co-workers to prepare monodisperse CdSe nanocrystals.[104] Since then, many other high-quality semiconductor NCs have also been successfully synthesized by this method, including II–VI, III–V, and IV–VI semiconductor NCs. Various metal chalcogenide NCs have been successfully synthesized by this method, such as PbS,[126-128] GeTe,[129] ZnS,[130, 131] Bi_2S_3,[132] Ag_2E (E = S, Se, Te),[133] In_2S_3,[134] SnSe,[135] Cu_2S,[136] and including ternary metal chalcogenides such as $CuInSe_2$, and $AgInSe_2$ NCs.[137, 138]

1.1.3.1.2.1 Limitation of hot-injection method

Till date hot-injection method turned out to be the most effective method in synthesizing high quality CQD with narrow size distribution. Several high quality (good optical properties, narrower size distribution) metal sulfide QDs like CdS QD, MnS QD, ZnS QD, SnS QD, In_2S_3 QD and Cu_2S QD have been synthesized using hot injection method and elemental sulfur[104, 139] or sulfur containing ligands (like thiourea),[140] ammonium sulfide[141] and thioacetamide[142] as sulphur source. In these methods generally sulphur solution is prepared by dissolving the sulphur powder in oleylamine that leads to the generation of S^{2-}disulfide or S_n^{2-} polysulfide which have relatively low nucleation threshold.[139, 143, 144] It may be noted that like silver and gold in case of metallic nanoparticles PbS system is often taken as a model system while developing new QD synthetic method. The understanding here is that if the method works for PbS usually it can extended to other metal chalcogenides also because in case of PbS system the optical properties and PLQY are very sensitive and crucially depend on the quality of QDs. It may be noted here that in case of PbS QDs traditional synthetic methods using elemental sulphur also do not provide good quality material and the reaction yield is also low.[145, 146] Further the prepared materials also suffer from other disadvantages like huge batch-to-batch variation and wide size distribution with low PLQY.[145, 146] Hence, it becomes difficult to realize the true application potential of these PbS QDs in applications like photovoltaic solar cells.

To address these issue researchers started looking for alternative sulfur sources. Bakueva, et al. were the first to successfully synthesize stable and monodispersed PbS QDs with diameters of 4 nm ± 1 nm in aqueous solutions using a mixture of thioglycerol (TGL) and dithioglycerol (DTG) as both stabilizing agent and sulfur source also.[127] The PbS QD, using these thioglycerol as a sulfur source, did not show good optical properties (shows broad absorption spectra).[127]

Some alternative organic compound which contains sulfur, such as thiourea and thioacetamide are also used as a sulphur source for PbS CQD synthesis.[147, 148] PbS nanocrystal have been synthesized first by using lead nitrate and thiourea in controlled ratios of mixed ligands cum solvents hexadecylamine (HDA) and trioctylphosphine oxide (TOPO).[147] But PbS QDs prepared using procedures based on thiourea were

found to be featured with poor optical properties with polydispersity in size and improper surface passivation.[147, 148]So, thiourea based PbS QD also fail to get utilized for photovoltaic cell applications.

Recently Jonathan S. Owen's group reported the preparation of different metal sulfide QDs (including the tricky PbS QDs) using derivatives of thiourea.[128] They prepared library of substituted thiourea derivative and used as a sulphur source for various metal sulfide QD synthesis. They were successful in preparing reasonably large scale of PbS QDs with tunable band gap including narrower size distribution and good optical properties.[128] However, this procedure also suffers from the necessity to use different thiourea derivatives for different sized PbS QDs and higher decomposition temperatures.

In this context it is to be noted that amongst all the reported synthesis methods for high-quality PbS QDs the one that uses a highly reactive sulfur source, bis (trimethyl silyl) sulfide [TMS] is reported to be the best.[126] The use of TMS facilitates a fast reaction, yielding PbS QDs with a relatively narrow size distribution. To date, all published performance records for optoelectronic devices based on PbS QDs have relied on the TMS based syntheses.[149-150] Unfortunately TMS is both pyrophoric and expensive. The TMS source accounts for over 80% of the PbS QDs synthesis materials cost, limiting the potential for the scale-up and their utilization in QD based technologies.

1.2 Statement of problem

Although several research groups have reported different synthetic methods for the preparation of binary metal sulfide and metal selenide QDs like CdS, CdSe, ZnS, ZnSe, In_2S_3, PbS, PbSe etc. and ternary metal sulfide like QDs $CuInS_2$ and $AgInS_2$, using one of the above mentioned two conventional synthetic methods, many of them fail to produce good quality (sharp absorption and emission peak) QDs.[151-158]

It is worth mentioning that the synthesis of ternary QDs is even more challenging because of the distinct reactivity of the two cations. For eg., in $CuInS_2$, In^{3+} is a hard Lewis acid, whereas both Cu^+ and S^{2-} are soft in character. Therefore, if the reactivity of Cu^+ toward sulfur sources is not attenuated the formation of copper sulfide binary system overtakes the formation of $CuInS_2$ QDs.[66, 159-162]

So, there is obvious need of finding synthetic methods that rely on more conveniently available sulfur precursors as well as alternate single source metal precursors that can be employed for large scale synthesis of metal chalcogenide QDs to fulfil the commercial demand.

In this context, we envisaged that metal thiolates, consisting of one (for binary metal chalcogenides) or more metals (for ternary metal chalcogenides) could be good candidates as single source precursors for the synthesis of metal chalcogenide QDs. This is because all the necessary ingredients like the metal ion, capping agent (which are essential for metal chalcogenides QDs synthesis) are inbuilt in the metal thiolate structure itself.[163,164] On the other hand, for the preparation of ternary metal chalcogenide such as $CuInS_2$ QDs the in-situ formation 2D lamellar polymeric complex which gets thermally decomposed to the desired ternary system was found to be useful.[123] Keeping this in view, we envisaged that if we could make mixed metal thiolates like $A^+B^{3+}(SR)_n$ [where A=Cu,Ag and B=In, Bi] and if they are treated with a very active chalcogen source, the simultaneous release of equimolar amounts of A^+ and B^{3+} ions could occur, promoting the formation of phase pure ABX_2 NCs(X: S and Se) without the formation of the individual binary chalcogenides as impurities.

1.3 Objectives:

With this aim, the work embedded in this thesis reports different procedures that provide easy accessibility to gram scale quantities of mono metal thiolates as well as bimetallic mixed metal thiolates and their utility as precursors for the preparation of metal chalcogenide QDs. We also discovered that octyl ammonium octyldithiocarbamate (C_8DTCA), could be employed as an active sulfur source to access large quantities of metal sulfide QDs via solution based (hot injection) or solid state grinding methods for the preparation of metal sulfide QDs.[163, 165]

Quite satisfyingly while the monometallic thiolates could be used to make a wide variety of metal sulfide/selenide QDs, the bimetallic mixed metal thiolates turned out to be excellent single source precursors for the preparation of bimetallic chalcogenides like $AgInS_2$, $CuInS_2$ as well as $AgInSe_2$ and $CuInSe_2$ QDs in large scale by simple solid state grinding methods.

1.4 Methodology:

First we synthesized a series of metal thiolates and simple thermal decomposition of these metal thiolates in a high boiling solvent afforded reasonably uniform metal chalcoginide QDs.[164] However, the optical properties of these metal chalcogenide QDs were poor probably due to the surface defects resulting from sulfur rich surface (anionic surface traps).

To reduce the thermal decomposition temperature and surface traps, we looked for a new air stable sulfur source and C_8DTCA fitted the bill perfectly.[165] Accordingly, C_8DTCA was used as a sulfur source in the hot injection method to prepare a series of uniform sized metal sulfide QDs including most challenging PbS QDs and we found that the optical properties of the synthesized materials were as comparable to those obtained with the methods employing [$(TMS)_2S$) as the sulfur source.

We could also demonstrate that the combination of metal thiolates and the air stable active sulfur source C_8DTCA works well to afford uniform sized binary metal sulfide QDs via mechano-chemical grinding methods and these binary metal sulfide QDs show excellent tunable optical properties.[163]

Extending this work we then prepared bimetallic mixed metal thiolates by simply mixing dodecanethiol with two metal salts. By grinding these mixed bimetal thiolates with an appropriate S-precursor solution (elemental S powder dissolved in minimal amount of oleyl amine) we could accomplish the synthesis of phase pure bimetallc sulfide QDs.

Most gratifyingly, all these latter QDs, though prepared by a solvent less grinding method, could be easily dispersed in nonpolar solvents as the preparation method ensued the formation of organic molecule capped QDs.

1.5 Outline of thesis:

This thesis is divided into five different chapters. A brief introduction to each chapter is provided below with the chapter titles.

Chapter-1: General Introduction

Brief background of the work and the motivation to carry out the work embedded in the thesis is included in this chapter.

Chapter-2: 2D Molecular Precursor for a One-pot Synthesis of Semiconducting Metal Sulfide Nanocrystals

This chapter focuses on the large scale synthesis of various 2D molecular precursors like metal thiolates and metal dithiocarbamate complexes (M-C_8DTCA) and their thermal decomposition to metal sulfide QDs via solution based methods.

Chapter-3: Generic and Scalable Method for the Preparation of Monodispersed Metal Sulfide Nanocrystals with Tunable Optical Properties.

In this chapter, we show that the fast decomposition of metal-C_8DTCA complexes can be accomplished in presence of primary amines and uniform metal sulfide QDs can be prepared. This novel technique is generic and has been applied to prepare diverse QDs, like CdS, MnS, ZnS, SnS, and In_2S_3, including more useful and in-demand PbS QDs and plasmonic nanocrystals of Cu_2S. Based on several control reactions, it is postulated that the reaction involves the in situ formation of a metal–C_8DTCA complex, which then reacts with oleylamine at slightly elevated temperature to decompose into metal sulfide QDs at a controlled rate, leading to the formation of the desired material with good optical characteristics. Controlled sulfur precursor's reactivity and stoichiometric reaction between C_8DTCA and metal salts affords high conversion yield and large-scale production of monodisperse QDs. Tunable and desired crystal size could be achieved by controlling the precursor reactivity by changing the reaction temperature and reagent ratios. Finally, the photovoltaic devices fabricated from PbS QDs displayed a power conversion efficiency of 4.64% that is comparable with the reported values of devices prepared with PbS QDs synthesized by the standard methods.

Chapter-4: Solvent-Less Solid State Synthesis of Dispersible Metal and Semiconducting Metal Sulfide Nanocrystals.

In this chapter we show metal thiolates as possible precursors for the preparation of monolayer protected metal and metal sulfide QDs via solid state grinding method.

More precisely we show that a large variety of uniform-sized semiconducting QDs of metal sulfides including PbS, CdS, ZnS, MnS, Ag_2S, and CuS could be synthesized via the solid state route by grinding the metal thiolates with C_8DTCA and in some cases C_8DTCA plus small amount of oleylamine as sulfur source. Interestingly, using this simple technique sub-3 nm QDs like Ag_2S, PbS, and CuS could be prepared which are otherwise difficult to prepare by the conventional high temperature solution routes also. Most gratifyingly, all these QDs, though prepared by a solvent less grinding method, could be easily dispersed in nonpolar solvents as the preparation method ensued the formation of organic molecule capped QDs.

Chapter-5: Synthesis and Characterization of Mixed Bimetal Thiolates and Their Utilization for the Preparation of Bimetallic Chalcogenide Nanocrystals through Mechano-chemical Grinding.

In this chapter, we establish that even mixed bimetal thiolates like copper-indium thiolate and silver-indium thiolate also exist as lamellar sheets similar to the thiolates the individual metals and these sheets consist of both metal ions arranged in a random fashion. We also demonstrate that these mixed metal thiolates could be employed as single source precursors for the preparation of series of bimetallic chalcogenide QDs through mechano-chemical routes by grinding them with an appropriate chalcogenide source. Quite notably these bimetallic chalcogenide QDs, though synthesized via a mechano-chemical route get easily dispersed in non-polar solvents as the thiolate molecules that get released during the grinding process passivate the metal sulfide/selenide QDs being formed. These ternary CQDs display a strong and tunable photoluminescence in the visible to near-infrared region.

1.6 References

1. Alivisatos, A. P., Semiconductor clusters, nanocrystals, and quantum dots. *Science* **1996,***271*, 933-937.

2. Freestone, I.; Meeks, N.; Sax, M.; Higgitt, C., The Lycurgus cup—a roman nanotechnology. *Gold Bull.* **2007,***40*, 270-277.

3. Barber, D. J.; Freestone, I. C., An investigation of the origin of the colour of the Lycurgus Cup by analytical transmission electron microscopy. *Archaeometry* **1990,***32*, 33-45.

4. Chazan, M.; Lehner, M., An ancient analogy: pot baked bread in ancient Egypt and Mesopotamia. *Paléorient* **1990**, 21-35.

5. Feynman, R. P., There's plenty of room at the bottom. *California Institute of Technology, Engineering and Science magazine* **1960**.

6. Feynman, R. P., There's Plenty of Room at the Bottom: An Invitation to Enter a New Field of Physics. *Handbook of Nanoscience, Engineering and Technology* **2003**.

7. Hochella Jr, M. F., There's plenty of room at the bottom: Nanoscience in geochemistry. *Geochim. Cosmochim. Acta* **2002,***66*, 735-743.

8. Bououdina, M., *Handbook of research on nanoscience, nanotechnology, and advanced materials*. IGI Global: **2014**.

9. Whitesides, G. M., Nanoscience, nanotechnology, and chemistry. *Small* **2005,***1*, 172-179.

10. Taniguchi, N., On the basic concept of nanotechnology. *Proceeding of the ICPE* **1974**.

11. Cao, G., *Nanostructures & nanomaterials: synthesis, properties & applications*. Imperial college press: **2004**.

12. Ratner, M. A.; Ratner, D., *Nanotechnology: A gentle introduction to the next big idea*. Prentice Hall Professional: **2003**.

13. Goddard III, W. A.; Brenner, D.; Lyshevski, S. E.; Iafrate, G. J., *Handbook of nanoscience, engineering, and technology*. *CRC press*: **2002**.

14. Varghese, P.; Pradeep, T., *A textbook of nanoscience and nanotechnology*. *Tata McGraw-Hill Education*: **2003**.

15. Rao, C.; Müller, A.; Cheetham, A., "Nanomaterials–an introduction." *The chemistry of nanomaterials* **2006**, 1-11.

16. Roduner, E., Size matters: why nanomaterials are different. *Chem. Soc. Rev.* **2006,***35*, 583-592.

17. Dai, Y.; Hu, H.; Wang, M.; Xu, J.; Wang, S., Stretchable transistors and functional circuits for human-integrated electronics. *Nat. Electron.* **2021**, 1-13.

18. Gaponenko, S. V., *Optical properties of semiconductor nanocrystals*. *Cambridge university press*: **1998**.

19. Smith, A. M.; Mohs, A. M.; Nie, S., Tuning the optical and electronic properties of colloidal nanocrystals by lattice strain. *Nat. Nanotech.* **2009,***4*, 56-63.

20. Smith, A. M.; Nie, S., Semiconductor nanocrystals: structure, properties, and band gap engineering. *Acc. Chem. Res.* **2010,***43*, 190-200.

21. Jun, Y.-w.; Choi, C.-S.; Cheon, J., Size and shape controlled ZnTe nanocrystals with quantum confinement effect. *Chem. Comm.* **2001,** 1, 101-102.

22. Cassidy, J.; Zamkov, M., Nanoshell quantum dots: Quantum confinement beyond the exciton Bohr radius. *J. Chem. Phys.* **2020,***152*, 110902-11909.

23. Zhang, Y.; Liu, Y.; Li, C.; Chen, X.; Wang, Q., Controlled synthesis of Ag_2S quantum dots and experimental determination of the exciton Bohr radius. *J. Phys.l Chem. C* **2014,***118*, 4918-4923.

24. Norris, D. J.; Bawendi, M., Measurement and assignment of the size-dependent optical spectrum in CdSe quantum dots. *Phys. Rev. B* **1996,***53*, 16338.

25. Wu, J.; Chen, S.; Seeds, A.; Liu, H., Quantum dot optoelectronic devices: lasers, photodetectors and solar cells. *J.Phys. D: Appl. Phys.* **2015,***48*, 363001.

26. Lee, S.; Choi, M.-J.; Sharma, G.; Biondi, M.; Chen, B.; Baek, S.-W.; Najarian, A. M.; Vafaie, M.; Wicks, J.; Sagar, L. K., Orthogonal colloidal quantum dot inks enable efficient multilayer optoelectronic devices. *Nat. Comm.* **2020,***11*, 1-8.

27. Panzer, M. J.; Aidala, K. E.; Bulović, V., Contact printing of colloidal nanocrystal thin films for hybrid organic/quantum dot optoelectronic devices. *Nano Rev.* **2012,***3*, 16144.

28. Dong, H.; Xu, F.; Sun, Z.; Wu, X.; Zhang, Q.; Zhai, Y.; Tan, X. D.; He, L.; Xu, T.; Zhang, Z., In situ interface engineering for probing the limit of quantum dot photovoltaic devices. *Nat. Nanotech.* **2019,***14*, 950-956.

29. Azmi, R.; Oh, S.-H.; Jang, S.-Y., High-efficiency colloidal quantum dot photovoltaic devices using chemically modified heterojunctions. *ACS Energy Lett.* **2016,***1*, 100-106.

30. Bakulin, A. A.; Neutzner, S.; Bakker, H. J.; Ottaviani, L.; Barakel, D.; Chen, Z., Charge trapping dynamics in PbS colloidal quantum dot photovoltaic devices. *ACS Nano* **2013,***7*, 8771-8779.

31. Konstantatos, G.; Howard, I.; Fischer, A.; Hoogland, S.; Clifford, J.; Klem, E.; Levina, L.; Sargent, E. H., Ultrasensitive solution-cast quantum dot photodetectors. *Nature* **2006,***442* , 180-183.

32. Clifford, J. P.; Konstantatos, G.; Johnston, K. W.; Hoogland, S.; Levina, L.; Sargent, E. H., Fast, sensitive and spectrally tuneable colloidal-quantum-dot photodetectors. *Nat. Nanotech.* **2009,***4*, 40-44.

33. McDonald, S. A.; Konstantatos, G.; Zhang, S.; Cyr, P. W.; Klem, E. J.; Levina, L.; Sargent, E. H., Solution-processed PbS quantum dot infrared photodetectors and photovoltaics. *Nat. Mater.* **2005,***4*, 138-142.

34. Choi, M. K.; Yang, J.; Kang, K.; Kim, D. C.; Choi, C.; Park, C.; Kim, S. J.; Chae, S. I.; Kim, T.-H.; Kim, J. H., Wearable red–green–blue quantum dot light-emitting diode array using high-resolution intaglio transfer printing. *Nat. Comm.* **2015,***6*, 1-8.

35. Caruge, J.; Halpert, J. E.; Wood, V.; Bulović, V.; Bawendi, M., Colloidal quantum-dot light-emitting diodes with metal-oxide charge transport layers. *Nat. Photonics* **2008,***2* , 247-250.

36. Shirasaki, Y.; Supran, G. J.; Bawendi, M. G.; Bulović, V., Emergence of colloidal quantum-dot light-emitting technologies. *Nat. Photonics* **2013,***7*, 13-23.

37. Devillanova, F. A.; Du Mont, W.-W., *Handbook of chalcogen chemistry: new perspectives in sulfur, selenium and tellurium*. *Royal Society of Chemistry:***2013**; Vol. 1.

38. Sadanaga, R.; Sueno, S., X-ray study on the α-β transition of Ag_2S. *Mineral. Mag.* **1967,***5*, 124-143.

39. Zhao, K.; Blichfeld, A. B.; Eikeland, E.; Qiu, P.; Ren, D.; Iversen, B. B.; Shi, X.; Chen, L., Extremely low thermal conductivity and high thermoelectric performance in liquid-like $Cu_2Se_{1-x}S_x$ polymorphic materials. *J. Mater. Chem. A* **2017,***5*, 18148-18156.

40. Zhao, K.; Blichfeld, A. B.; Eikeland, E.; Qiu, P.; Ren, D.; Iversen, B. B.; Shi, X.; Chen, L., Extremely low thermal conductivity and high thermoelectric performance in liquid-like $Cu_2Se_{1-x}S_x$ polymorphic materials. *J. Mater. Chem. A* **2017**,18, 18148-18165.

41. Zhao, Y.; Burda, C., Development of plasmonic semiconductor nanomaterials with copper chalcogenides for a future with sustainable energy materials. *Energy Environ. Sci.* **2012,***5*, 5564-5576.

42. Jiang, X.; Xie, Y.; Lu, J.; He, W.; Zhu, L.; Qian, Y., Preparation and phase transformation of nanocrystalline copper sulfides (Cu_9S_8, Cu_7S_4 and CuS) at low temperature. *J. Mater. Chem.* **2000,***10*, 2193-2196.

43. Liu, H.; Shi, X.; Xu, F.; Zhang, L.; Zhang, W.; Chen, L.; Li, Q.; Uher, C.; Day, T.; Snyder, G. J., Copper ion liquid-like thermoelectrics. *Nat. Mater.* **2012,***11*, 422-425.

44. O'Connor, G.; Eksteen, J., A critical review of the passivation and semiconductor mechanisms of chalcopyrite leaching. *Miner. Eng.* **2020,***154*, 106401.

45. Lezal, D.; Pedlikova, J.; Zavadil, J.; Kostka, P.; Poulain, M., Preparation and characterization of sulfide, selenide and telluride glasses. *J. Non-cryst. Solids* **2003,***326*, 47-52.

46. Nirmal, M.; Brus, L., Luminescence photophysics in semiconductor nanocrystals. *Acc. Chem. Res.* **1999,***32*, 407-414.

47. Han, N.; Liu, C.; Zhao, Z.; Zhang, J.; Xie, J.; Han, J.; Zhao, X.; Jiang, Y., Quantum dots in glasses: size-dependent stokes shift by lead chalcogenide. *Int. J. Appl. Glass Sci.* **2015,***6*, 339-344.

48. Thambidurai, M.; Muthukumarasamy, N.; Agilan, S.; Murugan, N.; Vasantha, S.; Balasundaraprabhu, R.; Senthil, T., Strong quantum confinement effect in nanocrystalline CdS. *J. Mater. Sci.* **2010,***45*, 3254-3258.

49. Sobhana, S. L.; Devi, M. V.; Sastry, T.; Mandal, A. B., CdS quantum dots for measurement of the size-dependent optical properties of thiol capping. *J. Nanoparticle Res.* **2011,***13*, 1747-1757.

50. Norris, D. J.; Sacra, A.; Murray, C.; Bawendi, M., Measurement of the size dependent hole spectrum in CdSe quantum dots. *Phys. Rev. Lett.* **1994,***72*, 2612.

51. Norris, D. J.; Efros, A. L.; Rosen, M.; Bawendi, M. G., Size dependence of exciton fine structure in CdSe quantum dots. *Phys. Rev. B* **1996,***53*, 16347.

52. Biju, V.; Itoh, T.; Anas, A.; Sujith, A.; Ishikawa, M., Semiconductor quantum dots and metal nanoparticles: syntheses, optical properties, and biological applications. *Anal. Bioanal. Chem.* **2008,***391*, 2469-2495.

53. Liu, Y.; Kim, D.; Morris, O. P.; Zhitomirsky, D.; Grossman, J. C., Origins of the stokes shift in PbS quantum dots: impact of polydispersity, ligands, and defects. *ACS Nano* **2018,***12*, 2838-2845.

54. Subila, K.; Kishore Kumar, G.; Shivaprasad, S.; George Thomas, K., Luminescence properties of CdSe quantum dots: role of crystal structure and surface composition. *J. Phys. Chem. Lett.* **2013,***4*, 2774-2779.

55. Wang, X.; Qu, L.; Zhang, J.; Peng, X.; Xiao, M., Surface-related emission in highly luminescent CdSe quantum dots. *Nano Lett.* **2003,***3*, 1103-1106.

56. Lany, S.; Zunger, A., Intrinsic D X Centers in Ternary Chalcopyrite Semiconductors. *Phys. Rev. Lett.* **2008,***100*, 016401.

57. Mao, B.; Chuang, C.-H.; Wang, J.; Burda, C., Synthesis and photophysical properties of ternary I–III–VI $AgInS_2$ nanocrystals: intrinsic versus surface states. *J. Phys. Chem. C* **2011,***115*, 8945-8954.

58. Komarala, V. K.; Xie, C.; Wang, Y.; Xu, J.; Xiao, M., Time-resolved photoluminescence properties of $CuInS_2$/ZnS nanocrystals: Influence of intrinsic defects and external impurities. *J. Appl. Phys.* **2012,***111*, 124314.

59. Zhang, S.; Wei, S.-H.; Zunger, A., Overcoming doping bottlenecks in semiconductors and wide-gap materials. *Physica B: Condens. Matter* **1999,***273*, 976-980.

60. Wuister, S. F.; de Mello Donega, C.; Meijerink, A., Influence of thiol capping on the exciton luminescence and decay kinetics of CdTe and CdSe quantum dots. *J. Phys. Chem. B* **2004,***108*, 17393-17397.

61. Wegner, K. D.; Lanh, P. T.; Jennings, T.; Oh, E.; Jain, V.; Fairclough, S. M.; Smith, J. M.; Giovanelli, E.; Lequeux, N.; Pons, T., Influence of luminescence quantum yield, surface coating, and functionalization of quantum dots on the sensitivity of time-resolved fret bioassays. *ACS Appl. Mater. Interfaces* **2013,***5*, 2881-2892.

62. Guyot-Sionnest, P.; Wehrenberg, B.; Yu, D., Intraband relaxation in CdSe nanocrystals and the strong influence of the surface ligands. *J. Chem. Phys.* **2005,***123*, 074709.

63. Cardon, M., The Devil and the Surfaces. *Shot Peener* **2006,***20*, 38.

64. Mudunkotuwa, I. A.; Grassian, V. H., The devil is in the details (or the surface): impact of surface structure and surface energetics on understanding the behavior of nanomaterials in the environment. *J. Environ. Monit.* **2011,***13*, 1135-1144.

65. Brus, L. E., Electron–electron and electron-hole interactions in small semiconductor crystallites: The size dependence of the lowest excited electronic state. *J. Chem. Phys.* **1984,***80*, 4403-4409.

66. Leach, A. D.; Shen, X.; Faust, A.; Cleveland, M. C.; La Croix, A. D.; Banin, U.; Pantelides, S. T.; Macdonald, J. E., Defect luminescence from wurtzite $CuInS_2$ nanocrystals: Combined experimental and theoretical analysis. *J. Phys. Chem. C* **2016,***120*, 5207-5212.

67. Chen, B.; Zhong, H.; Zhang, W.; Tan, Z. a.; Li, Y.; Yu, C.; Zhai, T.; Bando, Y.; Yang, S.; Zou, B., Highly emissive and color-tunable $CuInS_2$-based colloidal semiconductor nanocrystals: off-stoichiometry effects and improved electroluminescence performance. *Adv. Funct. Mater.* **2012,***22*, 2081-2088.

68. Hughes, K. E.; Ostheller, S. R.; Nelson, H. D.; Gamelin, D. R., Copper's Role in the Photoluminescence of $Ag_{1-x}Cu_xInS_2$ Nanocrystals, from Copper-Doped $AgInS_2$ (x∼ 0) to $CuInS_2$ (x= 1). *Nano Lett.* **2018,***19*, 1318-1325.

69. Nelson, H. D.; Gamelin, D. R., Valence-band electronic structures of Cu^+-doped ZnS, alloyed Cu–In–Zn–S, and ternary $CuInS_2$ nanocrystals: a unified description of photoluminescence across compositions. *J. Phys. Chem. C* **2018,***122*, 18124-18133.

70. Jung, S. M.; Kang, H. L.; Won, J. K.; Kim, J.; Hwang, C.; Ahn, K.; Chung, I.; Ju, B.-K.; Kim, M.-G.; Park, S. K., High-performance quantum dot thin-film transistors with environmentally benign surface functionalization and robust defect passivation. *ACS Appl. Mater. Interfaces* **2018,***10*, 3739-3749.

71. Kirkwood, N.; Monchen, J. O.; Crisp, R. W.; Grimaldi, G.; Bergstein, H. A.; Du Fossé, I.; Van Der Stam, W.; Infante, I.; Houtepen, A. J., Finding and fixing traps in II–VI and III–V colloidal quantum dots: the importance of Z-type ligand passivation. *J. Am. Chem. Soc.* **2018,***140* , 15712-15723.

72. Evans, C. M.; Cass, L. C.; Knowles, K. E.; Tice, D. B.; Chang, R. P.; Weiss, E. A., Review of the synthesis and properties of colloidal quantum dots: the evolving role of coordinating surface ligands. *J. Coord. Chem.* **2012,***65*, 2391-2414.

73. Singh, S.; Tomar, R.; Ten Brinck, S.; De Roo, J.; Geiregat, P.; Martins, J. C.; Infante, I.; Hens, Z., Colloidal CdSe nanoplatelets, a model for surface

chemistry/optoelectronic property relations in semiconductor nanocrystals. *J. Am. Chem. Soc.* **2018,***140*, 13292-13300.

74. Tang, J.; Kemp, K. W.; Hoogland, S.; Jeong, K. S.; Liu, H.; Levina, L.; Furukawa, M.; Wang, X.; Debnath, R.; Cha, D., Colloidal-quantum-dot photovoltaics using atomic-ligand passivation. *Nat. Mater.* **2011,***10*, 765-771.

75. Anderson, N. C.; Hendricks, M. P.; Choi, J. J.; Owen, J. S., Ligand exchange and the stoichiometry of metal chalcogenide nanocrystals: spectroscopic observation of facile metal-carboxylate displacement and binding. *J. Am. Chem. Soc.* **2013,***135*, 18536-18548.

76. Yuan, M.; Zhitomirsky, D.; Adinolfi, V.; Voznyy, O.; Kemp, K. W.; Ning, Z.; Lan, X.; Xu, J.; Kim, J. Y.; Dong, H., Doping control via molecularly engineered surface ligand coordination. *Adv. Mater.* **2013,***25*, 5586-5592.

77. Ip, A. H.; Thon, S. M.; Hoogland, S.; Voznyy, O.; Zhitomirsky, D.; Debnath, R.; Levina, L.; Rollny, L. R.; Carey, G. H.; Fischer, A., Hybrid passivated colloidal quantum dot solids. *Nat. Nanotech.* **2012,***7*, 577-582.

78. Jin, H.; Choi, S.; Xing, G.; Lee, J.-H.; Kwon, Y.; Chong, W. K.; Sum, T. C.; Jang, H. M.; Kim, S., SnS_4^{4-}, SbS_4^{3-}, and AsS_3^{3-}Metal Chalcogenide Surface Ligands: Couplings to Quantum Dots, Electron Transfers, and All-Inorganic Multilayered Quantum Dot Sensitized Solar Cells. *J. Am. Chem. Soc.* **2015,***137*, 13827-13835.

79. Jia, L.; Wang, Y.; Nie, Q.; Liu, B.; Liu, E.; Hu, X.; Fan, J., Aqueous-synthesis of $CuInS_2$ core and $CuInS_2$/ZnS core/shell quantum dots and their optical properties. *Mater. Lett.* **2017,***200*, 27-30.

80. Zheng, X.; Zhu, Y.; Liu, Y.; Zhou, L.; Xu, Z.; Feng, C.; Zheng, C.; Zheng, Y.; Bai, J.; Yang, K., Inkjet-Printed Quantum Dot Fluorescent Security Labels with Triple-Level Optical Encryption. *ACS Appl. Mater. Interfaces* **2021,***13*, 15701-15708.

81. Krogstrup, P.; Jørgensen, H. I.; Heiss, M.; Demichel, O.; Holm, J. V.; Aagesen, M.; Nygard, J.; i Morral, A. F., Single-nanowire solar cells beyond the Shockley–Queisser limit. *Nat. Photonics* **2013,***7*, 306-310.

82. Green, M. A. In *High efficiency silicon solar cells*, Seventh EC Photovoltaic Solar Energy Conference, Springer: **1987**; pp 681-687.

83. Swanson, R. M. In *Approaching the 29% limit efficiency of silicon solar cells*, Conference Record of the Thirty-first IEEE Photovoltaic Specialists Conference, **2005**., IEEE: **2005**; pp 889-894.

84. Essig, S.; Allebé, C.; Remo, T.; Geisz, J. F.; Steiner, M. A.; Horowitz, K.; Barraud, L.; Ward, J. S.; Schnabel, M.; Descoeudres, A., Raising the one-sun conversion efficiency of III–V/Si solar cells to 32.8 % for two junctions and 35.9 % for three junctions. *Nat. Energy* **2017,***2*, 1-9.

85. Bang, J. H.; Kamat, P. V., Quantum dot sensitized solar cells. A tale of two semiconductor nanocrystals: CdSe and CdTe. *ACS Nano* **2009,***3*, 1467-1476.

86. Cao, Y.; Stavrinadis, A.; Lasanta, T.; So, D.; Konstantatos, G., The role of surface passivation for efficient and photostable PbS quantum dot solar cells. *Nat. Energy* **2016,***1*, 1-6.

87. Scheer, R.; Walter, T.; Schock, H.; Fearheiley, M.; Lewerenz, H., $CuInS_2$ based thin film solar cell with 10.2 % efficiency. *Appl. Phys. Lett.* **1993,***63*, 3294-3296.

88. Weil, B. D.; Connor, S. T.; Cui, Y., $CuInS_2$ solar cells by air-stable ink rolling. *J. Am. Chem. Soc.* **2010,***132*, 6642-6643.

89. Feurer, T.; Carron, R.; Torres Sevilla, G.; Fu, F.; Pisoni, S.; Romanyuk, Y. E.; Buecheler, S.; Tiwari, A. N., Efficiency improvement of near-stoichiometric $CuInSe_2$ solar cells for application in tandem devices. *Adv. Energy Mater.* **2019,***9*, 1901428.

90. Wang, W.; Su, Y.-W.; Chang, C.-h., Inkjet printed chalcopyrite $CuIn_xGa_{1-x}Se_2$ thin film solar cells. *Sol. Energy Mater. Sol. Cells* **2011,***95*, 2616-2620.

91. Ahmed, S.; Reuter, K. B.; Gunawan, O.; Guo, L.; Romankiw, L. T.; Deligianni, H., A high efficiency electrodeposited Cu_2ZnSnS_4 solar cell. *Adv. Energy Mater.* **2012,***2*, 253-259.

92. Jo, D.-Y.; Yang, H., Synthesis of highly white-fluorescent Cu–Ga–S quantum dots for solid-state lighting devices. *Chem. Comm.* **2016,***52*, 709-712.

93. Shea-Rohwer, L. E.; Martin, J. E.; Cai, X.; Kelley, D. F., Red-emitting quantum dots for solid-state lighting. *ECS J. Solid State Sci. Technol.* **2012,***2*, R3112.

94. Kim, J.-H.; Kim, B.-Y.; Jang, E.-P.; Han, C.-Y.; Jo, J.-H.; Do, Y. R.; Yang, H., A near-ideal color rendering white solid-state lighting device copackaged with

two color-separated Cu–X–S (X= Ga, In) quantum dot emitters. *J. Mater. Chem. C* **2017,***5*, 6755-6761.

95. Kim, S.; Im, S. H.; Kim, S.-W., Performance of light-emitting-diode based on quantum dots. *Nanoscale* **2013,***5*, 5205-5214.

96. Chuang, P.-H.; Lin, C. C.; Liu, R.-S., Emission-tunable $CuInS_2$/ZnS quantum dots: structure, optical properties, and application in white light-emitting diodes with high color rendering index. *ACS Appl. Mater. Interfaces* **2014,***6*, 15379-15387.

97. Huang, W.-T.; Yoon, S.-Y.; Wu, B.-H.; Lu, K.-M.; Lin, C.-M.; Yang, H.; Liu, R.-S., Ultra-broadband near-infrared emission $CuInS_2$/ZnS quantum dots with high power efficiency and stability for the theranostic applications of mini light-emitting diodes. *Chem. Comm.* **2020,***56*, 8285-8288.

98. Zhang, H.; Yee, D.; Wang, C., Quantum dots for cancer diagnosis and therapy: biological and clinical perspectives. *Nanomedicine***2008**, 3, 1.

99. Luo, G.; Long, J.; Zhang, B.; Liu, C.; Ji, S.; Xu, J.; Yu, X.; Ni, Q., Quantum dots in cancer therapy. *Expert Opin. Drug Deliv.* **2012,***9*, 47-58.

100. Nurunnabi, M.; Cho, K. J.; Choi, J. S.; Huh, K. M.; Lee, Y.-k., Targeted near-IR QDs-loaded micelles for cancer therapy and imaging. *Biomaterials* **2010,***31*, 5436-5444.

101. Narayanan, S. S.; Sinha, S. S.; Pal, S. K., Sensitized emission from a chemotherapeutic drug conjugated to CdSe/ZnS QDs. *J. Phys. Chem. C* **2008,***112*, 12716-12720.

102. Zayed, D. G.; Ebrahim, S. M.; Helmy, M. W.; Khattab, S. N.; Bahey-El-Din, M.; Fang, J.-Y.; Elkhodairy, K. A.; Elzoghby, A. O., Combining hydrophilic chemotherapy and hydrophobic phytotherapy via tumor-targeted albumin–QDs nano-hybrids: covalent coupling and phospholipid complexation approaches. *J. Nanobiotechnology* **2019,***17*, 1-19.

103. Arya, H.; Kaul, Z.; Wadhwa, R.; Taira, K.; Hirano, T.; Kaul, S. C., Quantum dots in bio-imaging: revolution by the small. *Biochem. Biophys. Res. Comm.* **2005,***329*, 1173-1177.

104. Murray, C.; Norris, D. J.; Bawendi, M. G., Synthesis and characterization of nearly monodisperse CdE (E= sulfur, selenium, tellurium) semiconductor nanocrystallites. *J. Am. Chem. Soc.* **1993,***115*, 8706-8715.

105. LaMer, V. K.; Dinegar, R. H., Theory, production and mechanism of formation of monodispersed hydrosols. *J. Am. Chem. Soc.* **1950,***72*, 4847-4854.

106. Kwon, S. G.; Hyeon, T., Formation mechanisms of uniform nanocrystals via hot-injection and heat-up methods. *Small* **2011,***7*, 2685-2702.

107. de Mello Donegá, C.; Liljeroth, P.; Vanmaekelbergh, D., Physicochemical evaluation of the hot-injection method, a synthesis route for monodisperse nanocrystals. *Small* **2005,***1*, 1152-1162.

108. Elimelech, O.; Aviv, O.; Oded, M.; Banin, U., A Tale of Tails: Thermodynamics of CdSe Nanocrystal Surface Ligand Exchange. *Nano Lett.* **2020,***20*, 6396-6403.

109. Subramanian, S.; Ganapathy, S.; Rajaram, M.; Ayyaswamy, A., Tuning the optical properties of colloidal Quantum Dots using thiol group capping agents and its comparison. *Mater. Chem. Phys.* **2020,***249*, 123127.

110. Yarema, O.; Yarema, M.; Wood, V., Tuning the composition of multicomponent semiconductor nanocrystals: The case of I–III–VI materials. *Chem. Mater.* **2018,***30*, 1446-1461.

111. Zhang, W.; Zhang, H.; Feng, Y.; Zhong, X., Scalable single-step noninjection synthesis of high-quality core/shell quantum dots with emission tunable from violet to near infrared. *ACS Nano* **2012,***6*, 11066-11073.

112. Lewis, E. A.; McNaughter, P. D.; Yin, Z.; Chen, Y.; Brent, J. R.; Saah, S. A.; Raftery, J.; Awudza, J. A.; Malik, M. A.; O'Brien, P., In situ synthesis of PbS nanocrystals in polymer thin films from lead (II) xanthate and dithiocarbamate complexes: evidence for size and morphology control. *Chem. Mater.* **2015,***27*, 2127-2136.

113. Akhtar, J.; Malik, M. A.; O'Brien, P.; Helliwell, M., Controlled synthesis of PbS nanoparticles and the deposition of thin films by Aerosol-Assisted Chemical Vapour Deposition (AACVD). *J. Mater. Chem.* **2010,***20*, 6116-6124.

114. Nyamen, L. D.; Pullabhotla, V. R.; Nejo, A. A.; Ndifon, P. T.; Warner, J. H.; Revaprasadu, N., Synthesis of anisotropic PbS nanoparticles using heterocyclic dithiocarbamate complexes. *Dalton Trans.* **2012,***41*, 8297-8302.

115. Mandal, T.; Piburn, G.; Stavila, V.; Rusakova, I.; Ould-Ely, T.; Colson, A. C.; Whitmire, K. H., New mixed ligand single-source precursors for PbS

nanoparticles and their solvothermal decomposition to anisotropic nano-and microstructures. *Chem. Mater.* **2011,***23,* 4158-4169.

116. Du, Y.; Xu, B.; Fu, T.; Cai, M.; Li, F.; Zhang, Y.; Wang, Q., Near-infrared photoluminescent Ag2S quantum dots from a single source precursor. *J. Am. Chem. Soc.* **2010,***132,* 1470-1471.

117. Arellano, I. H. J.; Mangadlao, J.; Ramiro, I. B.; Suazo, K. F., 3-component low temperature solvothermal synthesis of colloidal cadmium sulfide quantum dots. *Mater. Lett.* **2010,***64,* 785-788.

118. Wang, Q.; Pan, D.; Jiang, S.; Ji, X.; An, L.; Jiang, B., Luminescent CdSe and CdSe/CdS core-shell nanocrystals synthesized via a combination of solvothermal and two-phase thermal routes. *J. Lumin.* **2006,***118,* 91-98.

119. Xu, J.; Ge, J.-P.; Li, Y.-D., Solvothermal synthesis of monodisperse PbSe nanocrystals. *J. Phys. Chem. B* **2006,***110,* 2497-2501.

120. Nag, A.; Sarma, D., Solvothermal synthesis of InP quantum dots. *J. Nanosci. Nanotechnology* **2009,***9,* 5633-5636.

121. Nakamura, H.; Kato, W.; Uehara, M.; Nose, K.; Omata, T.; Otsuka-Yao-Matsuo, S.; Miyazaki, M.; Maeda, H., Tunable photoluminescence wavelength of chalcopyrite $CuInS_2$-based semiconductor nanocrystals synthesized in a colloidal system. *Chem. Mater.* **2006,***18,* 3330-3335.

122. Li, L.; Pandey, A.; Werder, D. J.; Khanal, B. P.; Pietryga, J. M.; Klimov, V. I., Efficient synthesis of highly luminescent copper indium sulfide-based core/shell nanocrystals with surprisingly long-lived emission. *J. Am. Chem. Soc.* **2011,***133,* 1176-1179.

123. Gromova, M.; Lefrançois, A. l.; Vaure, L.; Agnese, F.; Aldakov, D.; Maurice, A.; Djurado, D.; Lebrun, C.; de Geyer, A.; Schülli, T. U., Growth mechanism and surface state of $CuInS_2$ nanocrystals synthesized with dodecanethiol. *J. Am. Chem. Soc.* **2017,***139,* 15748-15759.

124. Mazing, D.; Korepanov, O.; Aleksandrova, O.; Moshnikov, V., Synthesis of ternary metal chalcogenide colloidal nanocrystals in aqueous solutions. *Opt. Spectrosc.* **2018,***125,* 773-776.

125. Xia, Z.; Zhong, J.; Leng, M.; Hu, L.; Xue, D.-J.; Yang, B.; Zhou, Y.; Liu, X.; Qin, S.; Cheng, Y.-B., Generalized water-processed metal chalcogenide complexes: synthesis and applications. *Chem. Mater.* **2015,***27,* 8048-8057.

126. Hines, M. A.; Scholes, G. D., Colloidal PbS nanocrystals with size-tunable near-infrared emission: observation of post-synthesis self-narrowing of the particle size distribution. *Adv. Mater.* **2003,***15*, 1844-1849.

127. Bakueva, L.; Gorelikov, I.; Musikhin, S.; Zhao, X. S.; Sargent, E. H.; Kumacheva, E., PbS quantum dots with stable efficient luminescence in the near-IR spectral range. *Adv. Mater.* **2004,***16*, 926-929.

128. Hendricks, M. P.; Campos, M. P.; Cleveland, G. T.; Jen-La Plante, I.; Owen, J. S., A tunable library of substituted thiourea precursors to metal sulfide nanocrystals. *Science* **2015,***348*, 1226-1230.

129. Polking, M. J.; Zheng, H.; Ramesh, R.; Alivisatos, A. P., Controlled synthesis and size-dependent polarization domain structure of colloidal germanium telluride nanocrystals. *J. Am. Chem. Soc.* **2011,***133*, 2044-2047.

130. Yu, J. H.; Joo, J.; Park, H. M.; Baik, S.-I.; Kim, Y. W.; Kim, S. C.; Hyeon, T., Synthesis of quantum-sized cubic ZnS nanorods by the oriented attachment mechanism. *J. Am. Chem. Soc.* **2005,***127*, 5662-5670.

131. Li, L. S.; Pradhan, N.; Wang, Y.; Peng, X., High quality ZnSe and ZnS nanocrystals formed by activating zinc carboxylate precursors. *Nano Lett.* **2004,***4*, 2261-2264.

132. Malakooti, R.; Cademartiri, L.; Akçakir, Y.; Petrov, S.; Migliori, A.; Ozin, G. A., Shape-controlled Bi_2S_3 nanocrystals and their plasma polymerization into flexible films. *Adv. Mater.* **2006,***18*, 2189-2194.

133. Sahu, A.; Qi, L.; Kang, M. S.; Deng, D.; Norris, D. J., Facile synthesis of silver chalcogenide (Ag_2E; E= Se, S, Te) semiconductor nanocrystals. *J. Am. Chem. Soc.* **2011,***133*, 6509-6512.

134. Park, K. H.; Jang, K.; Son, S. U., Synthesis, Optical Properties, and Self-Assembly of Ultrathin Hexagonal In_2S_3 Nanoplates. *Angew. Chem.* **2006,***118*, 4724-4728.

135. Franzman, M. A.; Schlenker, C. W.; Thompson, M. E.; Brutchey, R. L., Solution-phase synthesis of SnSe nanocrystals for use in solar cells. *J. Am. Chem. Soc.* **2010,***132*, 4060-4061.

136. Wu, Y.; Wadia, C.; Ma, W.; Sadtler, B.; Alivisatos, A. P., Synthesis and photovoltaic application of copper (I) sulfide nanocrystals. *Nano Lett.* **2008,***8*, 2551-2555.

137. Zhong, H.; Wang, Z.; Bovero, E.; Lu, Z.; Van Veggel, F. C.; Scholes, G. D., Colloidal $CuInSe_2$ nanocrystals in the quantum confinement regime: synthesis, optical properties, and electroluminescence. *J. Phys. Chem. C* **2011,***115*, 12396-12402.

138. Langevin, M.-A.; Ritcey, A. M.; Allen, C. N., Air-stable near-infrared $AgInSe_2$ nanocrystals. *ACS Nano* **2014,***8*, 3476-3482.

139. Joo, J.; Na, H. B.; Yu, T.; Yu, J. H.; Kim, Y. W.; Wu, F.; Zhang, J. Z.; Hyeon, T., Generalized and facile synthesis of semiconducting metal sulfide nanocrystals. *J. Am. Chem. Soc.* **2003,***125*, 11100-11105.

140. Kaderavkova, A.; Loghina, L.; Chylii, M.; Slang, S.; Placek, P.; Frumarova, B.; Vlcek, M., N, N′, N′-trisubstituted thiourea as a novel sulfur source for the synthesis of Mn-doped ZnS QDs. *J. Alloys Compd.* **2020,***831*, 154814.

141. Zhang, H.; Hyun, B.-R.; Wise, F. W.; Robinson, R. D., A generic method for rational scalable synthesis of monodisperse metal sulfide nanocrystals. *Nano Lett.* **2012,***12*, 5856-5860.

142. Zhang, L.-J.; Shen, X.-C.; Liang, H.; Guo, S.; Liang, Z.-H., Hot-injection synthesis of highly luminescent and monodisperse CdS nanocrystals using thioacetamide and cadmium source with proper reactivity. *J. Colloid Interface Sci.* **2010,***342*, 236-242.

143. Li, Z.; Ji, Y.; Xie, R.; Grisham, S. Y.; Peng, X., Correlation of CdS nanocrystal formation with elemental sulfur activation and its implication in synthetic development. *J. Am. Chem. Soc.* **2011,***133*, 17248-17256.

144. Thomson, J. W.; Nagashima, K.; Macdonald, P. M.; Ozin, G. A., From sulfur− amine solutions to metal sulfide nanocrystals: peering into the oleylamine− sulfur black box. *J. Am. Chem. Soc.* **2011,***133*, 5036-5041.

145. Cademartiri, L.; Montanari, E.; Calestani, G.; Migliori, A.; Guagliardi, A.; Ozin, G. A., Size-dependent extinction coefficients of PbS quantum dots. *J. Am. Chem. Soc.* **2006,***128*, 10337-10346.

146. Yuan, M.; Kemp, K. W.; Thon, S. M.; Kim, J. Y.; Chou, K. W.; Amassian, A.; Sargent, E. H., High-performance quantum-dot solids via elemental sulfur synthesis. *Adv. Mater.* **2014,***26*, 3513-3519.

147. Khan, A. H.; Thupakula, U.; Dalui, A.; Maji, S.; Debangshi, A.; Acharya, S., Evolution of long range bandgap tunable lead sulfide nanocrystals with photovoltaic properties. *J. Phys. Chem. C* **2013,***117*, 7934-7939.

148. Huang, Z.; Zhai, G.; Zhang, Z.; Zhang, C.; Xia, Y.; Lian, L.; Fu, X.; Zhang, D.; Zhang, J., Low cost and large scale synthesis of PbS quantum dots with hybrid surface passivation. *Cryst. Eng. Comm.* **2017,***19*, 946-951.

149. Liu, M.; Voznyy, O.; Sabatini, R.; de Arquer, F. P. G.; Munir, R.; Balawi, A. H.; Lan, X.; Fan, F.; Walters, G.; Kirmani, A. R., Hybrid organic–inorganic inks flatten the energy landscape in colloidal quantum dot solids. *Nat. Mater.* **2017,***16*, 258-263.

150. Xu, J.; Voznyy, O.; Liu, M.; Kirmani, A. R.; Walters, G.; Munir, R.; Abdelsamie, M.; Proppe, A. H.; Sarkar, A.; de Arquer, F. P. G., 2D matrix engineering for homogeneous quantum dot coupling in photovoltaic solids. *Nat. Nanotech.* **2018,***13*, 456-462.

151. Kershaw, S. V.; Susha, A. S.; Rogach, A. L., Narrow bandgap colloidal metal chalcogenide quantum dots: synthetic methods, heterostructures, assemblies, electronic and infrared optical properties. *Chem. Soc. Rev.* **2013,***42*, 3033-3087.

152. van Embden, J.; Chesman, A. S.; Jasieniak, J. J., The heat-up synthesis of colloidal nanocrystals. *Chem. Mater.* **2015,***27*, 2246-2285.

153. Castro, S. L.; Bailey, S. G.; Raffaelle, R. P.; Banger, K. K.; Hepp, A. F., Nanocrystalline chalcopyrite materials ($CuInS_2$ and $CuInSe_2$) via low-temperature pyrolysis of molecular single-source precursors. *Chem. Mater.* **2003,***15*, 3142-3147.

154. Pandit, MA.; Sai, H. K. D.; Billakanti, S.; Ramadoss, M.; Muralidharan, K., Chalcopyrite with Magnetic and Dielectric Properties: An Introductory Catalyst for 4-Nitrophenol Reduction. *J. Phys. Chem. C.* **2020**, *124*, 18010-18019.

155. Billakanti, S.; Krishnamurthi, M., Facile preparation of surfactant or support material free CdS nanoparticles with enhanced photocatalytic activity. *J. Environ. Chem. Eng*. **2018**, *6*, 1250-1256.

156. Gottapu, S.; Muralidharan, K., Room temperature synthesis of organic surfactant-free PbS and PbSe nanoparticles exhibiting NIR absorption. *New J. Chem.* **2016**, *40*, 832-837.

157. Kumar, B.G.; Muralidharan, K., Hexamethyldisilazane-assisted synthesis of indium sulfide nanoparticles. *J. Mater. Chem*. **2011**, *21*, 11271-11275.

158. Yu, K.; Liu, X.; Zeng, Q.; Yang, M.; Ouyang, J.; Wang, X.; Tao, Y., The Formation Mechanism of Binary Semiconductor Nanomaterials: Shared by Single-Source and Dual-Source Precursor Approaches. *Angew. Chem.* **2013,***125*, 11240-11245.

159. Nairn, J. J.; Shapiro, P. J.; Twamley, B.; Pounds, T.; Von Wandruszka, R.; Fletcher, T. R.; Williams, M.; Wang, C.; Norton, M. G., Preparation of ultrafine chalcopyrite nanoparticles via the photochemical decomposition of molecular single-source precursors. *Nano Lett.* **2006**, *6*, 1218-1223.

160. Kolny-Olesiak, J.; Weller, H., Synthesis and application of colloidal $CuInS_2$ semiconductor nanocrystals. *ACS Appl. Mater. Interfaces* **2013**, *5*, 12221-12237.

161. Xie, R.; Rutherford, M.; Peng, X., Formation of high-quality I− III− VI semiconductor nanocrystals by tuning relative reactivity of cationic precursors. *J. Am. Chem. Soc*. **2009**, *131*, 5691-5697.

162. Zhong, H.; Lo, S. S.; Mirkovic, T.; Li, Y.; Ding, Y.; Li, Y.; Scholes, G. D., Noninjection gram-scale synthesis of monodisperse pyramidal $CuInS_2$ nanocrystals and their size-dependent properties. *ACS Nano***2010,***4*, 5253-5262.

163. Bera, A.; Busupalli, B.; Prasad, B. L., Solvent-less solid state synthesis of dispersible metal and semiconducting metal sulfide nanocrystals. *ACS Sustain. Chem. Eng*. **2018**, *6*, 12006-12016.

164. Bera, A.; Prasad, B. L. V., 2D Molecular precursor for a one-pot synthesis of semiconducting metal sulfide nanocrystals. *Bull. Mater.Sci*. **2018,***41*, 125.

165. Bera, A.; Mandal, D.; Goswami, P. N.; Rath, A. K.; Prasad, B. L., Generic and scalable method for the preparation of monodispersed metal sulfide nanocrystals with tunable optical properties. *Langmuir* **2018,** *34*, 5788-5797.

Chapter 2

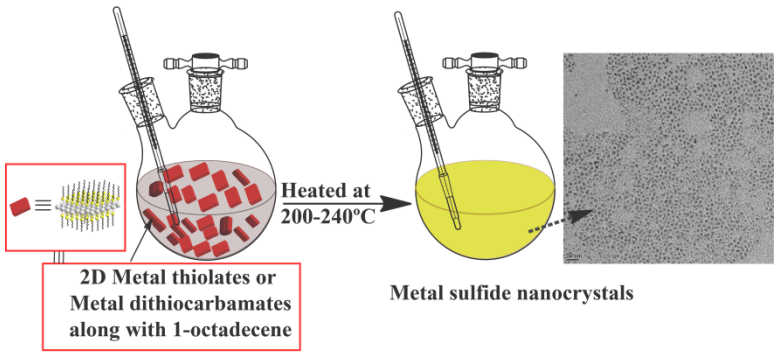

This chapter presents the synthesis of semiconducting metal sulfidenanocrystals using 2D molecular precursor by thermal decomposition.

2.1 Introduction

Metal chalcogenide nanocrystals (NCs) exhibit remarkable size-tunable optical properties including absorbance extending over a wide wavelength range and bright, narrow emission.[1-5] Furthermore, these optical properties can be tuned by particle size via quantum confinement or changing the composition.[5,6-8] Even a slight change of size, morphology, or composition of NCs has been shown to display considerable effect on the optical properties including the energies of the absorption onset, fluorescence emission, and surface plasmons.[1-5] As mentioned briefly in the previous chapter due to extraordinary properties of QDs (Note: the metal chalcogenide NCs with appropriate sizes could be classified as QDs), they have emerging application in various fields including solar cells,[9-11] optoelectronics,[12-14] biomedical imaging[15-17] and security.[18] Thus their commercial demands are also growing day by day. According one estimate the demand for QDs which was less than 100 kg in 2015, is expected to be over 2 metric tons in 2026, which is more than a 20-fold increase (according to the IDTechEx forecast report).[19] Thus, the synthesis of monodisperse, single crystalline metal sulfide NCs (that qualify to be called as QDs) is highly desired not just for investigating their excellent optical properties but for their on growing commercial demand. To fulfil this commercial demand, scalable synthesis of these materials without compromising their excellent properties is of utmost importance. While there are many ways to synthesize NCs, solution based colloidal synthesis often yields high quality materials, with desired monodispersity displaying uniform properties. Over the past several years, several groups have reported the synthesis of metal sulfide NCs using various solution based colloidal synthetic routes, including the hot injection method,[20-23] thermolysis of single-source precursors,[24-28] solvent-less synthesis,[29-32] thermolysis of metal-oleylamine complexes,[33] and a simple organic amine assisted hydrothermal process[34] but due to different issues such as the number of steps/reagents involved, the necessity to carry out reactions in inert atmosphere etc. the scalability of these routes is in question. We reckoned that for a scalable synthesis of metal sulfide NCs we need a much simplified procedure and for that first we have to see the constituents of a metal sulfide nanocrystals (akin to retro-synthesis strategy adapted by organic synthetic chemists). Monolayer protected metal sulfide nanocrystals have mainly two constituents; the inorganic metal chalcogenide

complex as core and an organic molecule as shell (simplified schematic of retro synthesis of a metal sulfide NCs is shown in Figure 2.1). So, if we can design any single source precursor where these ingredients (metal source and capping agent) are already present, then the scalable synthesis of metal sulfide NCs could be realized. Noticing that metal thiolates and metal dithiocarbamate complexes have these ingredients inbuilt in their structure itself, we investigated them as possible precursors for the preparation of monolayer protected metal sulfide nanocrystals (NCs) via thermolysis method.[35-36] Previous examples of thermal decomposition method (thermolysis method) to synthesize the metal sulfide NCs include reacting metal precurosrs with thiols (which is expected result in the formation of metal thiolates *insitu)* and subjecting them to thermolysis. Zhongbin Zhuang et al reported a generic route to prepare a series of metal sulfide nanocrystals with the assistance of alkylthiol, where they had shown the reaction undergoes in two steps: i)in the first step a key intermediate compound, metal thiolate, is generated, and ii) in the second step, it melts and disperses into the solvent at a relatively low temperature, and then the dispersed metal thiolates decomposes into metal sulfide upon heating.[37] Similar to metal thiolates, some other single source precursors like metal dithiocarbamate or metal xanthate also were used earlier to synthesize metal sulfide NCs by thermal decomposition.[38-43] Pradhan et al. and later his group did extensive studies on the thermal decomposition of various precursors such as metal xanthates and metal dithiocarbamates to synthesize tunable fluorescing semiconductor chalcogenide nanoparticles like CdS and ZnS.[38-40,43] Prof. Graeme Hogarth and his co-workers also did significant work in this research area to develop different type of dithiocarbamate ligands and studied the formation of corresponding metal dithiocarbamate complexes and their thermal decomposition to metal sulfide NCs.[44-45] Thermal decomposition temperature and rate of these metal dithiocarbamates complex depends on few factors like amine concentration. It is well studied that any amine helps to decompose the metal dithiocarbamate complex at faster rate and at comparatively lower temperature. Prof. Graeme Hogarth and his co-workers have shown that addition of oleylamine to the thermally stable $[Ni(S_2CNBui_2)_2]$ complex reduces its solvo-thermal decomposition temperature from 310 °C to 145 °C to result in the formation of NiS NPs.[44] According to Jung et al. an amine attacks the electron deficient thionyl carbon atom in the metal dithiocarbamate complex, causing a weakening ofthe C−S bond and

breaks it at comparatively lower temperature at faster rate and promoting metal sulfide formation.[46] Similarly, several groups reported the synthesis of monometallic sulfide (like CdS and ZnS) and bimetallic self-coupled sulfide hetero-structures (like $Cu_{2-x}S$-ZnS, $Cu_{2-x}S$-CuS and Ag-$AgInS_2$) by simply heating the single source precursors in presence of amine.[38,39, 41-47] In this premise, we initiated our work towards developing single source precursors for the simplified large scale synthesis of metal sulfide NCs. In our work we specifically focused on PbS NCs as it is considered as a tricky material to synthesize, from single source precursors and no previous reports existed. In this chapter, our efforts towards the development of a general "solvothermal–decomposition" approach for the synthesis of metal sulfide NCs (including the above mentioned tricky PbS NCs) using metal thiolates and metal dithiocarbamate complexes as single source precursors are presented.

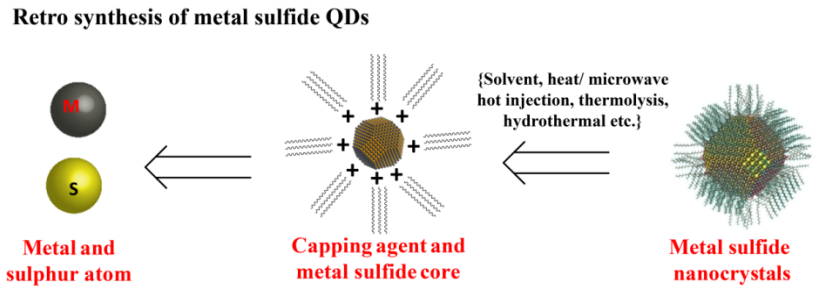

Figure 2.1 Schematic shows the retro synthesis of metal sulfide NCs.

We started our endeavour by preparing a series of 2D molecular precursors (metal thiolates and dithiocarbamate complexes of different metal like Cu, Pb, Cd and Zn) using a protocol developed previously with slight modification.[48] These metal alkyl thiolates or metal dithiocarbamate complexes are coordination compounds and exist as lamellae or stacked sheets in the solid state and they have ideal reactivity to be converted to metal sulfides (schematic of a metal thiolate is shown in Figure 2.2).

Our idea was to achieve a short nucleation process by direct heating of these metal thiolates at or above their decomposition temperature. We thought that at these high temperatures, the decomposition of thiols leads to the formation of metal sulfides and at the termination of the reaction, the particles get *insitu* capped with a layer of intact thiols. Furthermore, metal thiolates of different metals are easy to prepare in a large scale by simple solvent-less process which are highly air stable below the

decomposition temperature. Accordingly, we show in this chapter that by the decomposition of a suitable metal thiolate in a high boiling solvent like 1-octadecene, a series of metal sulfides NCs, such as Cu_2S, PbS, ZnS, MnS and CdS, can be successfully synthesized. Interestingly their size also could be controlled by varying the decomposition temperature. This method avoids injecting a second reagent during the reaction and uses air-free manipulation, which is very suitable for large-scale synthesis.

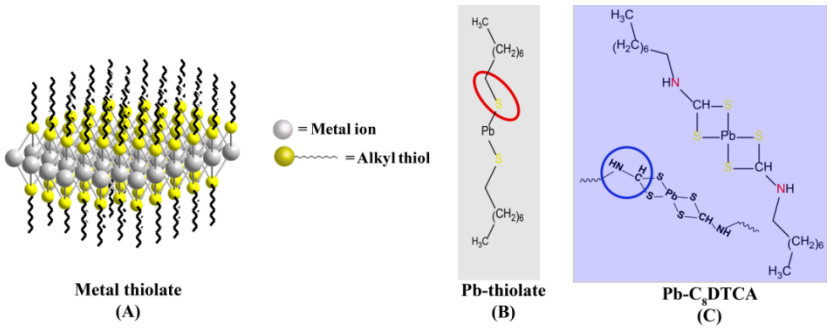

Figure 2.2 (A) Schematic of the metal thiolate sheet, which contain metal and alkyl thiol as capping agents. The detailed bonding in (B) Pb-thiolate and (C) Pb-C_8DTCA (C_8DTCA: octyl ammonium octyl dithio carbamate) complex are also shown, where the C-S bond (marked with a red circle in Pb-thiolate) and C-N bond (marked by a blue circle in Pb-C_8DTCA) have to break to get the corresponding PbS NCs.

2.1.1 Experimental section

Chemicals required:

Octanethiol ($C_8H_{17}SH$), octylamine ($C_8H_{17}NH_2$) and 1-octadecene (1-ODE) were purchased from Sigma Aldrich and was used as received. Copper acetate, cuprous (I) iodide, cadmium acetate, manganese acetate, zinc acetate and lead acetate were purchased from Sigma Aldrich. Solvents such as ethanol, toluene and 1-ODE etc. were also purchased from Merck Chemicals and were used as received.

2.1.1.1 Synthesis of metal thiolates

A series of thiolates of different metals like Cu, Pb, Cd, Mn and Zn) were synthesized following a protocol previously developed by Prasad and co-workers.[48] Briefly, metal precursors (such as metal acetate or metal iodide) were taken in glass vial and alkyl

thiol (octane thiol) was added into that which immediately leads to a colour change due to M-S co-ordination indicating the formation of metal thiolate (the generic procedure for metal thiolate synthesis is shown in Figure 2.3). The mixture was washed thoroughly with ethanol, and the product was dried inside vacuum oven at room temperature.

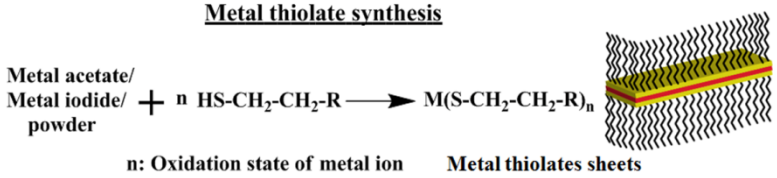

Figure 2.3 Schematic representation of the metal thiolate synthesis and bilayer of metal thiolate.

2.1.1.1.1 Synthesis of lead (II)thiolate:

500 mg of lead acetate (II) trihydrate was taken in 15 mL glass vial and 1 mL of octanethiol was added into the solid directly, and the tube was shaken vigorously. The reaction mixture turned yellow in colour instantaneously. The mixture was washed thoroughly with ethanol, and the yellow product was dried inside vacuum oven at room temperature. The obtained yellow powder was characterized using PXRD and SEM.

2.1.1.1.2 Synthesis of cadmium (II) thiolate:

500 mg of cadmium acetate was taken in 15 mL glass vial and 1 mL of octanethiol was added into the solid directly, and the tube was shaken vigorously. The reaction mixture turned milky white in colour instantaneously. The mixture was washed thoroughly with ethanol, and the white product was dried inside vacuum oven at room temperature. The obtained white powder was characterized using PXRD and SEM.

2.1.1.1.3 Synthesis of manganese (II) thiolate:

500 mg of manganese acetate was taken in 15 mL glass vial and 1 mL of octanethiol was added into the solid directly, and the tube was shaken vigorously. The reaction mixture turned white in colour instantaneously. The mixture was washed thoroughly

with ethanol, and the pinkish white product was dried inside vacuum oven at room temperature. The obtained pinkish white powder was characterized using PXRD and SEM.

2.1.1.1.4 Synthesis of zinc (II) thiolate:

500 mg of zinc acetate was taken in 15 mL glass vial and 1 mL of octanethiol was added into the solid directly, and the tube was shaken vigorously. The reaction mixture turned milky white in colour instantaneously. The mixture was washed thoroughly with ethanol, and the white product was dried inside vacuum oven at room temperature. The obtained white powder was characterized using PXRD and SEM.

2.1.1.1.5 Synthesis of copper thiolate:

500 mg of cupper acetate or copper (I) iodide was taken in 15 mL glass vial and 1 mL of octanethiol was added into the solid directly, and the tube was shaken vigorously. The reaction mixture turned yellow in colour instantaneously. The mixture was washed thoroughly with ethanol, and the yellow product was dried inside vacuum oven at room temperature. The obtained yellow powder was characterized using PXRD and SEM.

Caution: All these reactions are exothermic; mixture became warm upon addition of alkylthiol, so proper safety precaution should be taken care during large scale synthesis and the reaction should be performed in ice cold condition.

2.1.2 General procedure for the preparation of metal sulfide NCs:

200 mg of metal thiolate powder was taken along with 15 mL of 1-ODE in 100 mL RB flask. First the reaction mixture was heated at mild temperature (130-140ºC) which led to the formation of a homogeneous clear solution. The temperature was then raised to (200– 240ºC) and the heating was continued for 30min. This reaction mixture was precipitated and washed with methanol to obtain pure metal sulfide NCs. These products obtained were characterized by PXRD and UV-Vis absorption, fluorescence spectra and TEM. The general synthesis method is shown in Figure 2.4.

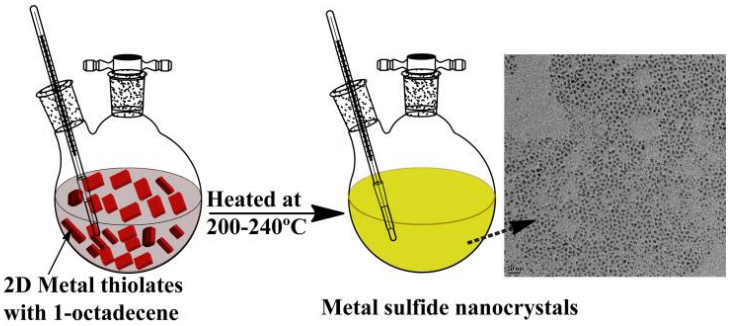

Figure 2.4 Method for generic metal sulfide NC synthesis.

2.1.3 Synthesis of octylammonium octyl dithiocarbamate (C_8DTCA)

About 10 mL dry dichloromethane (DCM) was taken in 100 mL Rb flask and cooled. To this 50 mmol of CS_2 (large excess) was added and stirred for some time in argon atmosphere. After 15 min 10 mmol of octylamine was added drop-wise into the CS_2 solution and stirred for 30 min. A white coloured precipitate formed immediately. This was dried under vacuum. The powder was recrystallised from toluene. The dried shiny crystals were analyzed by NMR, DEPT and HRMS (please see the characterisation details in Annexure Chapter 2 Figure A.C.2.1-4).The final crystallised product is a stable zwitter ionic form $[C_8H_{17}NHCS_2]^-[C_8H_{17}NH_3]^+$ and it is denoted as C_8DTCA in all over this thesis. The reaction scheme and C_8DTCA molecular structure is shown in Figure 2.5)

Caution: Reaction is exothermic; solution became warm upon addition of amine, so reaction should be performed in ice cold condition and addition of amine should be drop wise. Otherwise some part of desired compound can convert to thiourea.

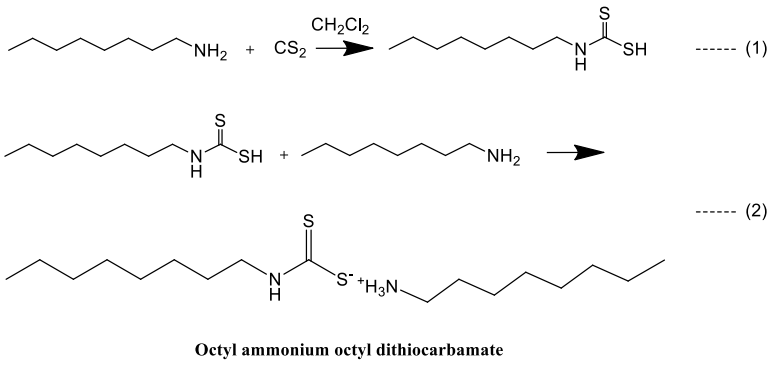

Figure 2.5 Synthetic scheme of octyl ammonium octyl dithiocarbamate (C_8DTCA).

2.1.3.1 Synthesis of metal dithiocarbamate complex

Similar to metal thiolate preparation, metal precursors (such as metal acetate or metal iodide) were taken in glass vial and ethanolic solution of C_8DTCA was added into that and immediately led to a colour change due to M-S co-ordination indicating the formation of metal dithiocarbamate complex. The mixture was washed thoroughly with ethanol, and the product was dried inside vacuum oven at room temperature.

Note: Some of the metal dithiocarbamate complexes like Pb-C_8DTCA are highly unstable (moisture sensitive), and they decompose to PbS in even at room temperature (25 °C) in presence of air and moisture. So, we had prepared the Pb-C_8DTCA complex in slightly different way (solution based method) under inert atmosphere by the following procedure which provides comparatively stable Pb-C_8DTCA complex.

2.1.4 Reaction 2A- Preparation of lead oleate: PbO (450 mg, 2 mmol) was mixed with 1.5 mL of oleic acid and 10 mL of 1-octadecene in the 100 mL three-neck round bottom flask. The system was connected to the vacuum gas manifold and heated to 100 °C under vacuum. The turbid yellow solution turns colorless, indicating formation of a lead (II) oleate solution.

2.1.5 Reaction 2B -Preparation of lead octyl dithiocarbamate (Pb-C_8DTCA) complex: Initially the lead oleate was made as mentioned in reaction 2A. First C_8DTCA dissolved in dry $CHCl_3$ (used very less amount of $CHCl_3$ mixedwith toluene) was injected into this lead oleate solution at room temperature (25°C) under inert atmosphere. Immediately the colourless lead oleate solution became pale yellow. Addition of dry acetone to this solution led to the formation of a yellowish brown coloured precipitate. This precipitate is highly soluble in non-polar solvents like toluene and chloroform. Based on different characterizations this compound was determined to be Pb(C_8DTCA)$_2$.

Note: The Pb-C_8DTCA complex is highly moisture sensitive. It can decompose to PbS NPs in presence of air and moisture. The yellowish brown coloured Pb-(C_8DTCA)$_2$ turns black when exposed to moisture.

2.1.6 Reaction 2C -Preparation of PbS by heating Pb-C_8DTCA complex without OlAm: Initially the lead oleate was made as mentioned in reaction 2A. After 2 h, the

setup is backfilled with nitrogen and left for an additional 20 min for temperature stabilization (100 °C). Into this lead oleate solution C_8DTCA dissolved in dry $CHCl_3$ (at RT) was injected. Immediately the colourless lead oleate solution becomes pale yellow. Then the temperature was increased slowly to 140-150 °C leading to the formation of a dark brownish black coloured product. When dry acetone was added a brownish black coloured precipitate got separated from the solution. This precipitate was washed two times with acetone (centrifuged at 5000 rpm for 3 min) to remove excess surfactants. This precipitate was then dried under Argon flow and redispersed into tetrachloroethylene or toluene for various measurements. Analysis of this product indicated the formation of PbS NCs.

2.1.7 Reaction 2D -Preparation of PbS by heating Pb-C_8DTCA complex with OlAm: The Pb-C_8DTCA complex was prepared as mentioned in reaction 2B. The system was connected to the vacuum gas manifold and heated to 50-100 °C under vacuum. Into this 0.5 mL of OlAm was injected very fast (<1 sec). Immediately the pale yellow Pb-C_8DTCA solution turned into brownish black indicating formation of PbS. Immediately after OlAm injection, the heating was stopped and the system was removed from the heating batch and was allowed to naturally cool to room temperature (which took ~45 minutes). The product of this reaction was collected by precipitating it with acetone addition and after washing it two times with acetone (centrifuged at 5000 rpm for 3 min) and one time with a mixture of acetone and methanol (1:3 by volume) the precipitate was dried under Argon flow. The precipitate was redispersed into tetrachloroethylene or toluene for various measurements. Analysis of this product indicated the formation of PbS NCs.

2.2 Results and discussion

2.2.1 Characterization of metal thiolate and metal dithiocarbamate complex

2.2.1.1 Powder X-ray diffraction (PXRD) of metal thiolate and metal dithiocarbamate complex

Metal alkyl thiolatesor metal dithiocarbamate complexes are coordination compounds and exist as lamellae or stacked sheets in the solid state.[48] Metal thioates are characterized with zig-zag strands of –S(R)–M–S(R)–M– segments and these zig-zag segments associate into lamellar or multi-bilayer type structures.[48] The PXRD pattern

of different metal thiolates and Pb-dithiocarbamate complex are shown in Figure2.6a and b, which shows periodically spaced (*00l*) reflections.

For example, in Pb(I) thiolates, the lead ions sit in a plane and the sulfur atoms are attached to them from both above and below their plane and the carbon chain conformation are almost exclusively in trans orientation. This structure can be very well correlated with the two dimensional self-assembled monolayers (2D-SAMs).

2.2.1.2 Morphological studies of metal thiolate and metal dithiocarbamate complex

The PXRD patterns of different metal thiolates and Pb-C_8DTCA complex (Pb-dithiocarbamate complex); prepared as part of this study are displayed in Figure 2.6. They show (*00l*) reflections indicating the layer like structure. SEM images (shown in Figure 2.7a-e and Figure 2.7f) of these metal thiolates and Pb-C_8DTCA complex also clearly indicate that all of the metal-thiolates and Pb-C_8DTCA are featured with layered like structure and justify the sheet like (2D) morphology. Such metal thiolates and metal-C_8DTCA complexes could be easily prepared by a simple and generic solvent-less method which is scalable and the resulting materials are also highly air stable.

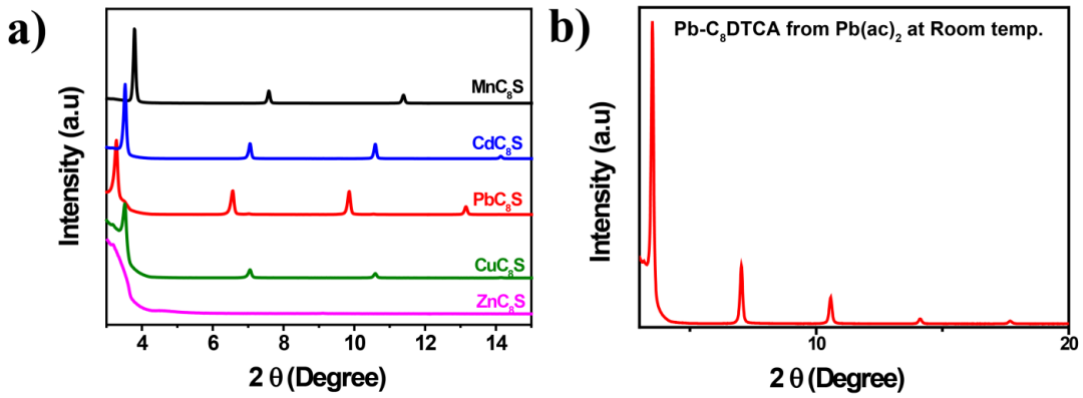

Figure 2.6 a) PXRD of metal thiolates, manganese octanethiolate denoted as MnC_8S (black), cadmium octanethiolate (CdC_8S, blue), lead octanethiolate (PbC_8S, red), copper octanethiolate (CuC_8S, green), zinc octanethiolate (ZnC_8S, pink); b) PXRD of Pb-C_8DTCA complex.

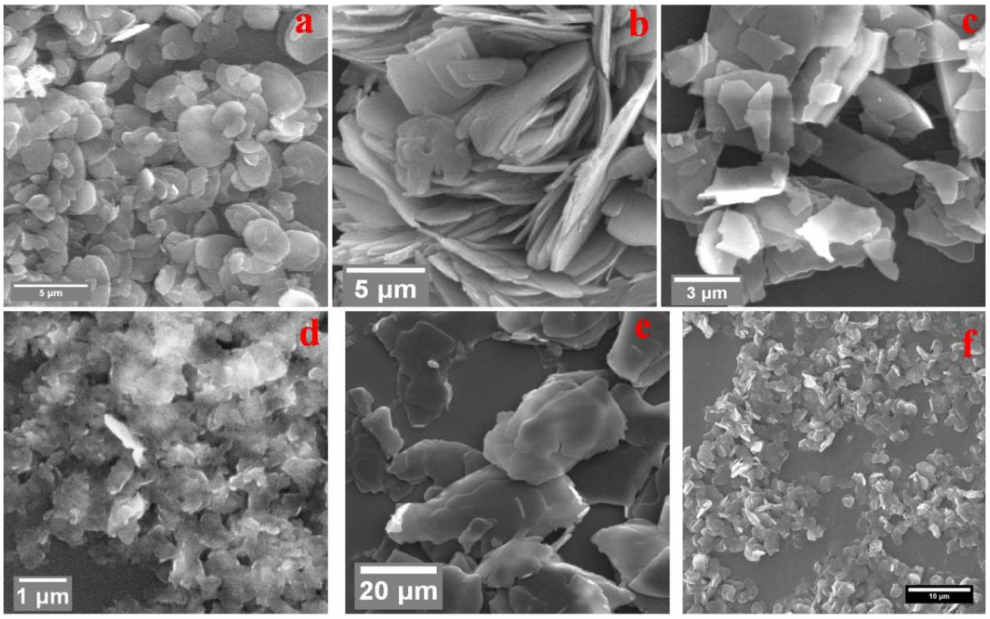

Figure 2.7 SEM images of metal thiolates; a) CuC_8S, b) CdC_8S, c) PbC_8S, d) ZnC_8S and e) MnC_8S; f) SEM image of Pb-C_8DTCA complex.

2.2.2 Synthesis and characterization of metal sulfide NCs

An interesting aspect, of some these metal thiolates is that they become dispersible in a high boiling solvent like 1-ODE when heated to mild temperatures (120-140 ºC). This dispersion of metal thiolates (which have been shown to exist as individual sheet like structures in solution) decomposes into metal sulfide when they are subjected to heating at higher temperatures. The side product of this reaction is an alkene and some of the undecomposed alkylthiol caps/passivates the surface of the ensuing NCs (proposed reaction mechanism showed in Figure 2.8, according to Sang-Hyun Choi et al).[49] In the following the synthetic procedure is explained in detail by taking the CdS NCs as an example. First, 200 mg of the Cd-octanethiolate 2D molecular complex was taken along with 1- ODE and the temperature was raised to 130 ºC to get a homogeneous clear solution. The temperature was then raised to 200-240 ºC under argon flow and the reaction was kept at this temperature for 30 min. The colourless solution became pale yellow indicating formation of CdS. The heating was stopped immediately after the color change and the system was allowed to naturally cool to room temperature (which took ~45 minutes). The product of this reaction was collected by precipitating it with acetone/ethanol addition and after washing it two times with acetone/ethanol (centrifuged at 5000 rpm for 3 min) and the precipitate

was dried under Argon flow. The precipitate was re-dispersed into tetrachloroethylene or toluene for various measurements. Similar to the synthesis of CdS NCs, nearly monodisperse NCs of other metal sulfides could also be synthesized by heating the corresponding metal thiolate precursor in 1-ODE solution at 200 ºC.

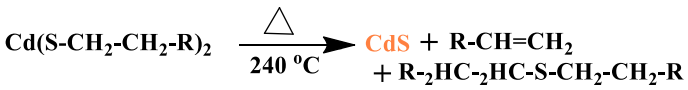

Figure 2.8 Proposed reaction mechanism for thermal decompositon of metal thiolates to metal sulfide NCs.

2.2.2.1 Powder X-ray diffraction (PXRD) of metal sulfide NCs

The PXRD pattern of the purified materials clearly matched with the CdS cubic phases (Figure 2.9; corresponding JCPDS card No#43-1469). In case of other sulfide systems also the PXRD patterns clearly matched with the corresponding JCPDS numbers as listed here: PbS with rock salt structure JCPDS card No#05-0592. ZnS, zinc blend JCPDS card no. 75-1546; Cu_2S, JCPDS card no. 84-0206; MnS, JCPDS card No#00-006-0518.

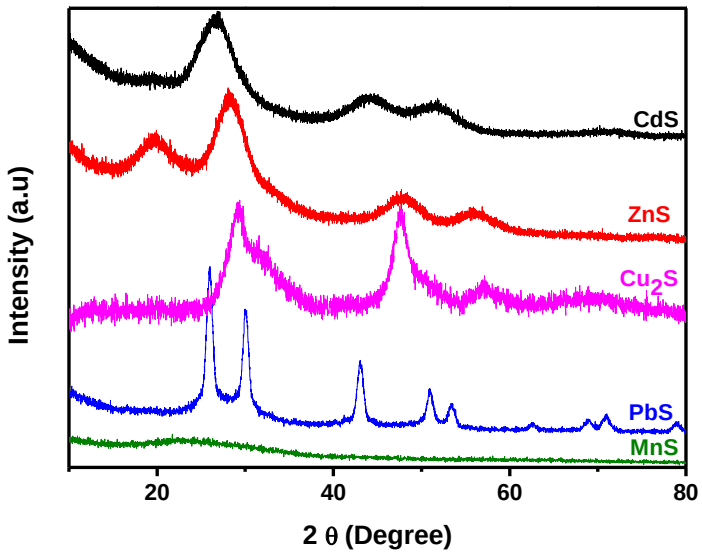

Figure 2.9 PXRD of metal sulfide NCs CdS, JCPDS card no. 43-1469; ZnS, JCPDS card no. 75-1546; Cu_2S, JCPDS card no. 84-0206; PbS, JCPDS card no. 05-0592; MnS, JCPDS card No#00-006-0518.

2.2.2.2 Optical properties of metal sulfide NCs

Figure 2.10 shows the UV−vis absorption spectra of CdS NCs synthesized by heating Cd-thiolate at 200 to 240 °C. As can be noticed, all spectra exhibit sharp band gap absorption features, indicating the formation of nearly monodisperse CdS NCs. It may be noticed that the samples display well defined excitonic peak and the peak position varied gradually from 370 to 385 to 405 nm as the reaction temperature was varied from 200 to 220 to 240 ºC (Figure 2.10). The absorption peak also becomes narrow and the peak shifts towards red (Figure 2.10). The photoluminescence (PL) of CdS NCs (Figure 2.10) shows both a sharp band gap emission as well as trap state emission centred around 450-700 nm. The trap state emission is significantly depressed as the reaction temperature was increased and the bandgap emission dominates for the materials synthesized above 200 ºC (Figure 2.10).

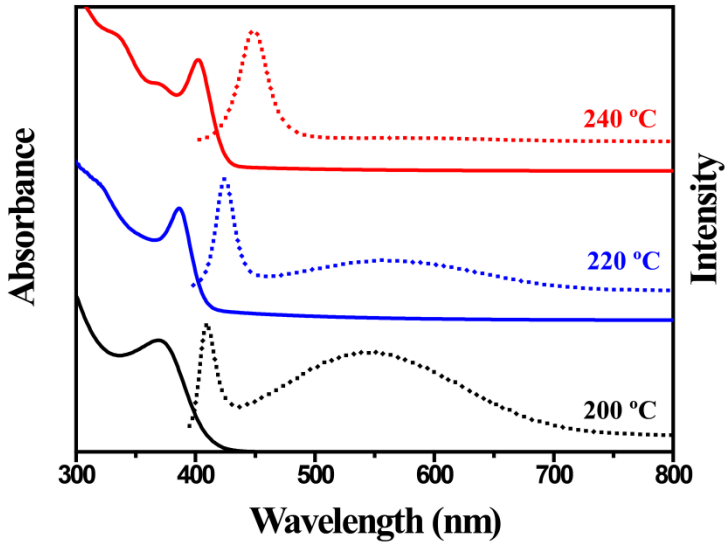

Figure 2.10 Absorption (solid line) and emission (dotted line) spectra of CdS NCs synthesized at different temperatures (200-240 ºC).

The absorbance and photoluminescence (PL) of ZnS NCs (Figure 2.11a) also display sharp peak at ~410 nm attributed to the bandgap emission. The photoluminescence (PL) of MnS NCs synthesized at different reaction temperature show a sharp bandgap emission in the range 470-490 nm (Figure 2.11b). Figure 2.11c and Figure 2.11d represent the absorbance spectra of PbS and Cu_2S NCs respectively. Here it can be noticed that PbS does not show any characteristic excitonic peak.

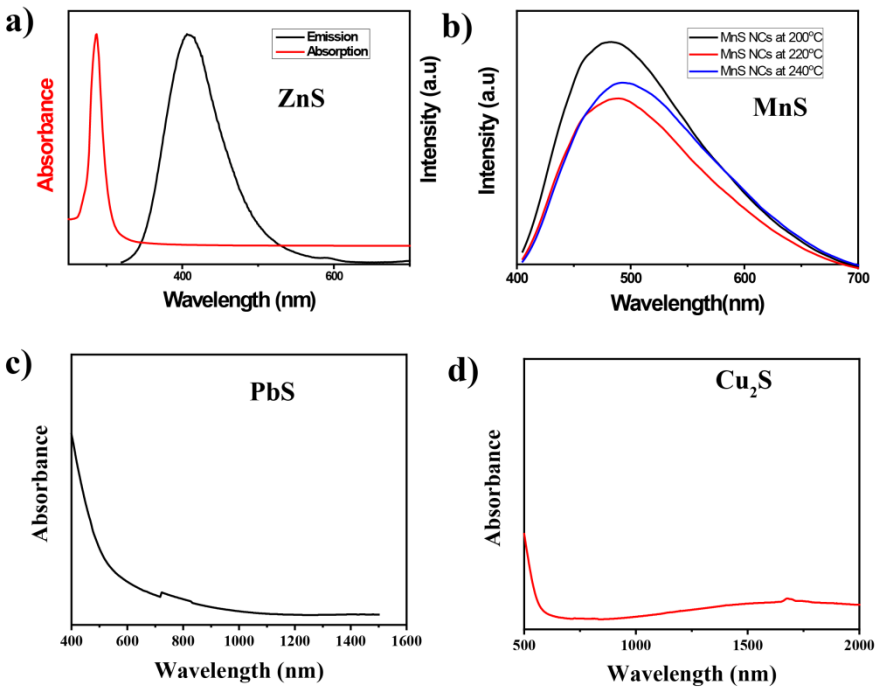

Figure 2.11 a) absorbance and PL spectra of ZnS; b) PL spectra of MnS; absorbance spectra of c) PbS and d) Cu_2S NCs.

2.2.2.3 Morphological studies of metal sulfide NCs

TEM images reveal that almost all the materials synthesized by above mentioned procedure are nearly spherical in shape. The CdS NCs are featured with an average size of ~3 nm and the size can be tuned between ~3 and 5 nm, with longer reaction times and higher reaction temperatures favouring the formation of larger nanocrystals (Figure 2.12a-c). Nearly monodisperse sub-13 nm PbS NCs could be synthesized by heating Pb-octanethiolate precursor in ODE solution at 200 ºC. As in the case of CdS and PbS NCs, monodisperse ~sub-3 nm ZnS and MnS could also be synthesized by thermal decomposition of zinc octanethiolate and Mn-octanethiolate in ODE at 240 ºC (See Figure 2.12d, Figure 2.12e and Figure 2.12f for TEM image of PbS, ZnS NCs and MnS NCs respectively).

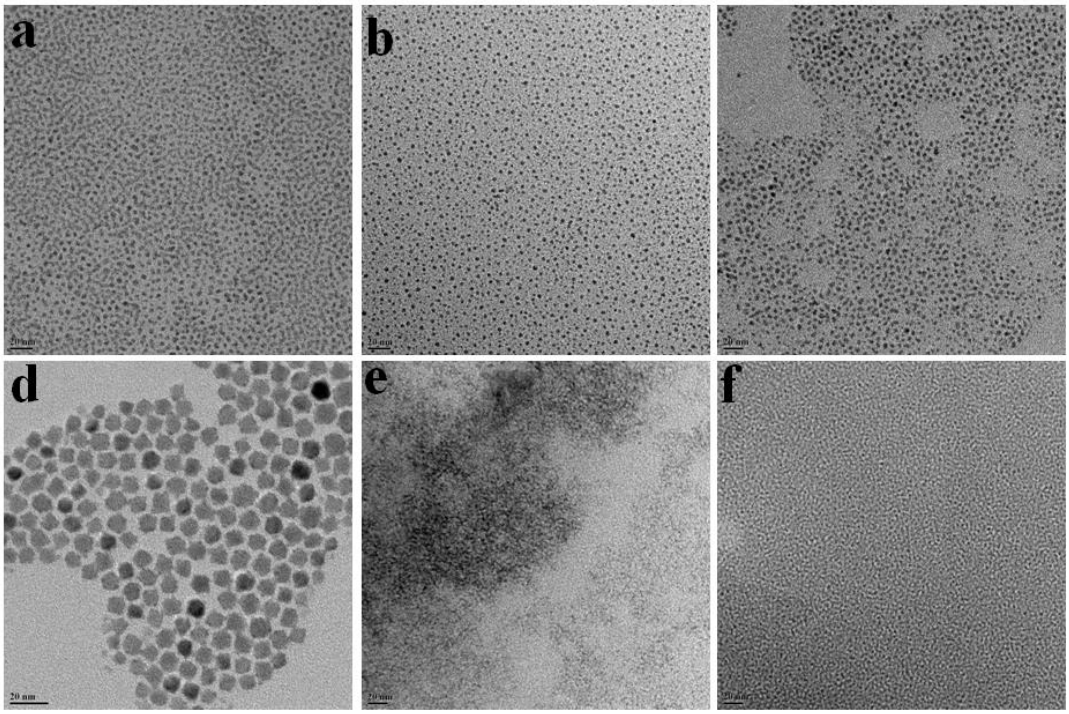

Figure 2.12 TEM images of different metal sulfide quantum dots synthesized using their corresponding thiolates as precursors; a-c) CdS at different temperature, a) 200ºC, b) 220 ºC, c) 240 ºC; d) PbS at 200 ºC, e) ZnS at 200 ºC and f) MnS at 200 ºC. In all images the scale bar corresponds to 20 nm**.**

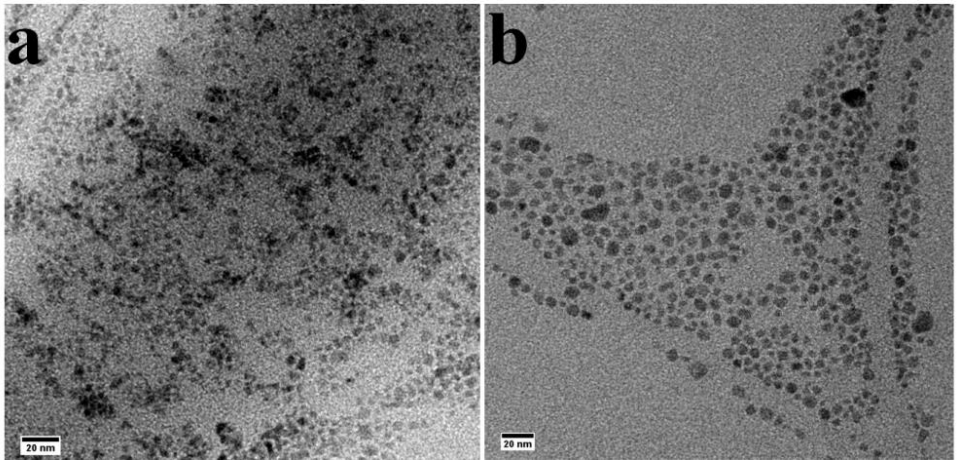

Figure 2.13 TEM images of Cu_2S prepared by thermolysis from Cu-octanethiolate (a) at 200 ºC, b) 240 ºC.

Similar to the synthesis of different NCs described above, monodisperse NCs of ~6-10 nm spherical sized Cu_2S were also synthesized by the thermal decomposition of copper octanethiolate in ODE at 200-240 ºC (TEM images showed in Figure 2.13a-b).

The Cu_2S NCs obtained by heating the copper-octanethiolate at 200 ºC under argon flow, leads to the formation around 6 nm sized spherical particles and with increasing the temperature to 240 ºC around ~10-nm-sized spherical NCs were obtained.

It is clear that we could synthesize a series of metal sulfide NCs by just simple heating their corresponding metal thiolates and those NCs show reasonably good optical properties (absorption and emission). However PbS NCs synthesized by this procedure do not show any optical properties (absorption and emission). But PbS colloidal QDs are very important attractive materials for use in photovoltaic applications due to their facile solution processing, their potential for efficient multiple exciton generation and harvesting, and their spectral tunability based on the quantum-size-effect.[50,51] Since the report of the first PbS QD solar cell in 2005, rapid progress in QD photovoltaic device architectures and improvements in electronic material properties have led to certified AM 1.5 solar power conversion efficiencies of 11%.[51]

High performance and low cost materials will be required simultaneously for a competitive PbS QD-based technology. This provides further impetus to develop improved processing and growth paradigms with low cost syntheses of PbS QDs with tunable sizes. For these reasons the synthesis of PbS in good quantities could turn out to be very useful. Also in case of all the other NCs the size of the NCs, their size distributions and their optical properties are not really of the desired quality.

We hypothesized the reasons for the poor quality optical properties of PbS NC prepared by us could be the following. One, the temperature required is very high (more than 200 ºC) to decompose Pb-octanethiolate to PbS. Also Pb is a very reactive material and such a high temperature results in uncontrolled growth leading to bigger sized polydispersed particles (10-20 nm) and their surfaces also have chance to oxidise or is characterized with sulphur rich materials causing them to show surface defects with poor optical properties.

So, to overcome the high temperature decomposition of lead alkyl thiolates, we thought of using C_8DTCA which instantly reacts with highly reactive Pb^{2+} metal and forms a Pb-C_8DTCA complex. This complex is also characterized with equidistant peaks (PXRD pattern shown in Figure 2.6b and the structure of Pb-C_8DTCA complex

presented in Figure 2.2C) suggesting its lamellar structure similar to several other metal thiolates.[48] Here we choose C_8DTCA as this bidentate ligand strongly binds to the metal and shows similar characteristic features like metal thiolates. But in the M-C_8DTCA structure, the chemically active –NH proton is very reactive and we surmised that this could help to decompose the complex at comparatively lower temperature. During the thermolysis of M-C_8DTCA, the –NH proton could help to form isothiocyanate and break the C-S bond at comparative lower temperature than that is required for the decomposition of metal thiolates. Here, we wish to mention that the Pb-C_8DTCA complex is itself very unstable (in air) and decomposes to form PbS even at room temperature (in presence of moisture). Unfortunately these PbS NCs also do not show any good optical properties. Thus we proceeded to heat the Pb-C_8DTCA complex to 150 °C in 1-ODE (without exposing to moisture). When the heating temperature reached immediately a black precipitate (indicating PbS formation) was seen to form within 1-2 minutes (reaction 2B and 2C). The PXRD pattern of this powder could be assigned to PbS rock salt structure which is similar to that observed in case of the product obtained with thermal decomposition of single source precursors like lead alkyl thiolates.[37,49] However compared to the PbS NCs obtained by the decomposition of Pb-thiolate, the particle sizes were more uniform (TEM images and particle size distribution is shown in Figure 2.14).The absorption spectrum shown in Figure 2.14b is featured with two peaks, one at ~1500 nm and other peak at 2000 nm (major peak), (due to very different size and morphology particles, some of them are spherical and some are in cubic shape) which indicates the formation of larger sized PbS particles.

From the optical properties, TEM images shown in Figure 2.14, it is clear that the self-decomposition of Pb-C_8DTCA complex was not suitable for good quality of PbS QDs which has been ascribed to the bigger sized particles (similar or beyond their excitonic Bohr radius) and probably surface defects.

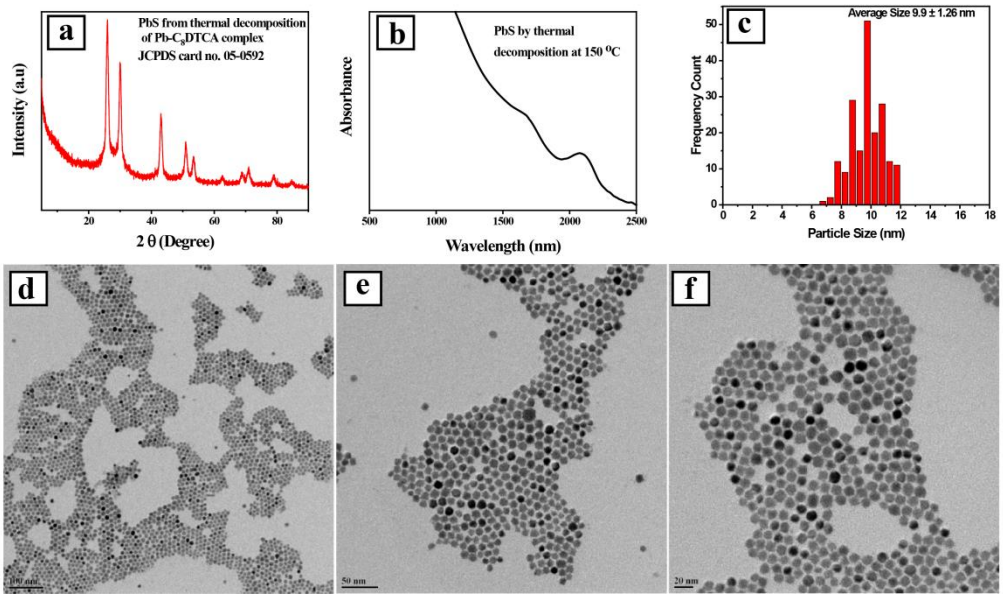

Figure 2.14 a) PXRD of PbS NCs prepared by thermal decomposition of Pb-C_8DTCA complex at 150° C, b) absorption spectra of the same, c) size distribution plot of the same PbS NCs, d-f)TEM images of PbS NC prepared by thermal decomposition of Pb-C_8DTCA complex at 150°C.

In this context it has been reported that addition of oleyl amine to the thermally stable [Ni(S_2CNBui$_2$)$_2$] complex reduces its solvo-thermal decomposition temperature from 310 °C to 145 °C to result in the formation of NiS NPs.[44] We thus wanted to see whether oleyl amine addition would lead to the reduction in the Pb-C_8DTCA decomposition temperature. Indeed, when oleyl amine was injected to the pre-formed Pb-C_8DTCA complex in 1-ODE at 120 °C, its color immediately changed to deep brownish black, indicating that the Pb-C_8DTCA complex is decomposing to PbS NPs. The absorption spectra of the samples obtained when oleyl amine was injected at 120 °C displayed a sharp peak at 1427 nm as may be noticed from Figure 2.15b. The FWHM of this sharp peak is deduced to be 92 nm. However, this sharp peak is overlaid on a broad absorbance which is characterized with four more shoulder/hump like features, indicating different sized and different morphologies particles are getting formed. The TEM images (Figure 2.15d-f) recorded from these PbS QDs also support the presence of different sized particles with average size 6.52±2.16 nm [please see the size distribution plot in Figure 2.15c]. Thus it is clear that the PbS QDs prepared by the decomposition of pre-formed Pb-C_8DTCA complex both in the

absence and presence of OlAm led to the formation of larger particles or polydispersed particles that show broad absorbance features. But OlAm aided decomposition showed at least one sharp excitonic peak in the absorbance spectra and TEM images also showed most of the particles are spherical with uniform size (although few bigger sized particles are also there Figure 2.15d-f). So this indicated that to get PbS NCs with uniform size distributions and better optical properties we need to optimise the reaction conditions further more.

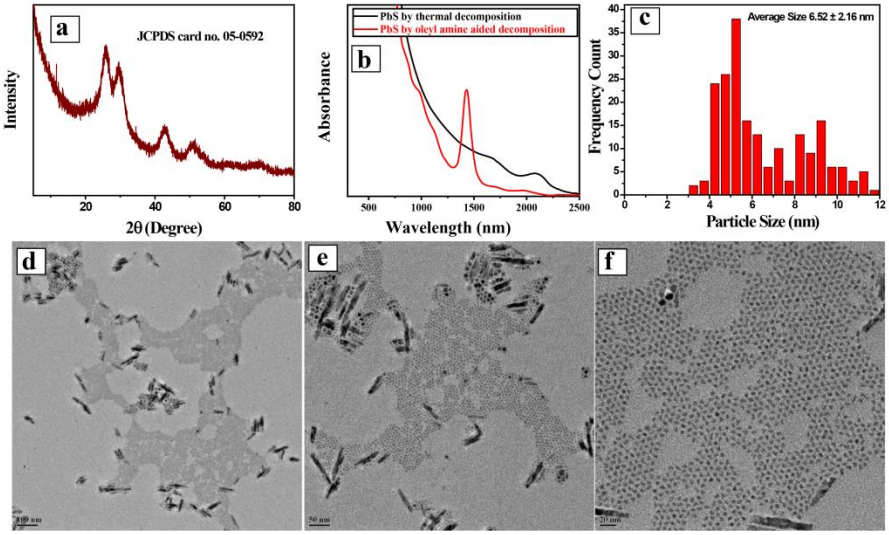

Figure 2.15 a) PXRD of PbS NCs prepared by OlAm aided decomposition of Pb-C_8DTCA complex at 120° C, b) absorption spectra of PbS NCs by OlAm aided decomposition of Pb-C_8DTCA (red solid line) and for comparison thermal decomposition without OlAm also showed (black solid line) , c) Size distribution plot of the same PbS NCs prepared by OlAm aided decomposition, d-f) TEM images of PbS NC prepared by OlAm aided decomposition of Pb-C_8DTCA complex at 120° C.

2.3 Summary and leads for the next chapter

To summarize the work incorporated in this chapter, a simple and general direct-heating solvothermal–decomposition synthetic method using 2D molecular precursors has been developed for the synthesis of different metal sulfide NCs like Cu_2S, PbS, CdS, MnS and ZnS. The synthesis of starting material (metal thiolate 2D sheets) is also very simple and scalable. We also show that the size and shape of the nanocrystals could be controlled by changing the reaction temperature and changing the metal precursor (used for metal thiolate preparation).

In case of PbS NCs (synthesised from Pb-thiolate by thermal decomposition) we did not get any optical properties indicating that the material prepared is characterized could be highly defective and polydispersed. To resolve this we then examined another organic ligand called octyl ammonium octyl dithiocarbamate which instantly reacts with highly active Pb^{2+} metal and formed a Pb-C_8DTCA complex. This new Pb-C_8DTCA complex decomposes at comparatively low temperature (150 °C). This temperature could be brought down to 120 °C by the addition of oleyl amine. PbS NCs obtained by the thermal decomposition of Pb-C_8DTCA complex at least shows very weak and broad absorption at NIR region, whereas those obtained with oleyl amine aided decomposition showed very sharp absorption peak overlaid on a broad absorbance which is characterized with four more shoulder/hump. These PbS NCs with weak and broad absorbance are not useful in photovoltaics, but we get an indication that if we can modify the oleyl amine aided decomposition we may get good quality of PbS NCs. Therefore we have focused on this aspect to obtain better quality of PbS QDs by modifying the synthetic conditions and our efforts are highlighted in the next chapter.

2.4 References

1. Jun, Y.-w.; Choi, C.-S.; Cheon, J., Size and shape controlled ZnTe nanocrystals with quantum confinement effect. *Chem. Comm.* **2001,** 1, 101-102.

2. Thambidurai, M.; Muthukumarasamy, N.; Agilan, S.; Murugan, N.; Vasantha, S.; Balasundaraprabhu, R.; Senthil, T., Strong quantum confinement effect in nanocrystalline CdS. *J. Mater. Sci.* **2010,***45*, 3254-3258.

3. Sobhana, S. L.; Devi, M. V.; Sastry, T.; Mandal, A. B., CdS quantum dots for measurement of the size-dependent optical properties of thiol capping. *J. Nanoparticle Res.* **2011,***13*, 1747-1757.

4. Norris, D. J.; Sacra, A.; Murray, C.; Bawendi, M., Measurement of the size dependent hole spectrum in CdSe quantum dots. *Phys. Rev. Lett.* **1994,***72*, 2612.

5. Norris, D. J.; Efros, A. L.; Rosen, M.; Bawendi, M. G., Size dependence of exciton fine structure in CdSe quantum dots. *Phys. Rev. B* **1996,***53*, 16347.

6. Chen, B.; Zhong, H.; Zhang, W.; Tan, Z. a.; Li, Y.; Yu, C.; Zhai, T.; Bando, Y.; Yang, S.; Zou, B., Highly emissive and color-tunable $CuInS_2$-based colloidal semiconductor nanocrystals: off-stoichiometry effects and improved electroluminescence performance. *Adv. Funct. Mater.* **2012,** *22*, 2081-2088.
7. Hughes, K. E.; Ostheller, S. R.; Nelson, H. D.; Gamelin, D. R., Copper's Role in the Photoluminescence of $Ag_{1-x}Cu_xInS_2$ Nanocrystals, from Copper-Doped $AgInS_2$ (x~ 0) to $CuInS_2$ (x= 1). *Nano Lett.* **2018,** *19*, 1318-1325.
8. Nelson, H. D.; Gamelin, D. R., Valence-band electronic structures of Cu^+-doped ZnS, alloyed Cu–In–Zn–S, and ternary $CuInS_2$ nanocrystals: a unified description of photoluminescence across compositions. *J. Phys. Chem. C* **2018,** *122*, 18124-18133.
9. Dong, H.; Xu, F.; Sun, Z.; Wu, X.; Zhang, Q.; Zhai, Y.; Tan, X. D.; He, L.; Xu, T.; Zhang, Z., In situ interface engineering for probing the limit of quantum dot photovoltaic devices. *Nat. Nanotech.* **2019,** *14*, 950-956.
10. Azmi, R.; Oh, S.-H.; Jang, S.-Y., High-efficiency colloidal quantum dot photovoltaic devices using chemically modified heterojunctions. *ACS Energy Lett.* **2016,** *1*, 100-106.
11. Bakulin, A. A.; Neutzner, S.; Bakker, H. J.; Ottaviani, L.; Barakel, D.; Chen, Z., Charge trapping dynamics in PbS colloidal quantum dot photovoltaic devices. *ACS Nano* **2013,** *7*, 8771-8779.
12. Wu, J.; Chen, S.; Seeds, A.; Liu, H., Quantum dot optoelectronic devices: lasers, photodetectors and solar cells. *J.Phys. D: Appl. Phys.* **2015,***48*, 363001.
13. Lee, S.; Choi, M.-J.; Sharma, G.; Biondi, M.; Chen, B.; Baek, S.-W.; Najarian, A. M.; Vafaie, M.; Wicks, J.; Sagar, L. K., Orthogonal colloidal quantum dot inks enable efficient multilayer optoelectronic devices. *Nat. Comm.* **2020,** *11*, 1-8.
14. Panzer, M. J.; Aidala, K. E.; Bulović, V., Contact printing of colloidal nanocrystal thin films for hybrid organic/quantum dot optoelectronic devices. *Nano Rev.* **2012,** *3*, 16144.
15. Choi, M. K.; Yang, J.; Kang, K.; Kim, D. C.; Choi, C.; Park, C.; Kim, S. J.; Chae, S. I.; Kim, T.-H.; Kim, J. H., Wearable red–green–blue quantum dot

light-emitting diode array using high-resolution intaglio transfer printing. *Nat. Comm.* **2015,** *6,* 1-8.

16. Caruge, J.; Halpert, J. E.; Wood, V.; Bulović, V.; Bawendi, M., Colloidal quantum-dot light-emitting diodes with metal-oxide charge transport layers. *Nat. Photonics* **2008,** *2* , 247-250.
17. Shirasaki, Y.; Supran, G. J.; Bawendi, M. G.; Bulović, V., Emergence of colloidal quantum-dot light-emitting technologies. *Nat. Photonics* **2013,** *7,* 13-23.
18. Zheng, X.; Zhu, Y.; Liu, Y.; Zhou, L.; Xu, Z.; Feng, C.; Zheng, C.; Zheng, Y.; Bai, J.; Yang, K., Inkjet-Printed Quantum Dot Fluorescent Security Labels with Triple-Level Optical Encryption. *ACS Appl. Mater. Interfaces* **2021,** *13,* 15701-15708.
19. "Demand for quantum dots will increase 20-fold over next decade" IDTechEx Research forecasts report by Dr. Guillaume Chansin on December 15, 2015, https://www.idtechex.com/en/research-article/demand-for-quantum-dots-will-increase-20-fold-over-next-decade/8814.
20. Murray, C.; Norris, D. J.; Bawendi, M. G., Synthesis and characterization of nearly monodisperse CdE (E= sulfur, selenium, tellurium) semiconductor nanocrystallites. *J. Am. Chem. Soc.* **1993,** *115,* 8706-8715.
21. Hines, M. A.; Scholes, G. D., Colloidal PbS nanocrystals with size-tunable near-infrared emission: observation of post-synthesis self-narrowing of the particle size distribution. *Adv. Mater.* **2003,** *15,* 1844-1849.
22. Bakueva, L.; Gorelikov, I.; Musikhin, S.; Zhao, X. S.; Sargent, E. H.; Kumacheva, E., PbS quantum dots with stable efficient luminescence in the near-IR spectral range. *Adv. Mater.* **2004,** *16,* 926-929.
23. Hendricks, M. P.; Campos, M. P.; Cleveland, G. T.; Jen-La Plante, I.; Owen, J. S., A tunable library of substituted thiourea precursors to metal sulfide nanocrystals. *Science* **2015,***348,* 1226-1230.
24. Lewis, E. A.; McNaughter, P. D.; Yin, Z.; Chen, Y.; Brent, J. R.; Saah, S. A.; Raftery, J.; Awudza, J. A.; Malik, M. A.; O'Brien, P., In situ synthesis of PbS nanocrystals in polymer thin films from lead (II) xanthate and

dithiocarbamate complexes: evidence for size and morphology control. *Chem. Mater.* **2015,** *27*, 2127-2136.

25. Akhtar, J.; Malik, M. A.; O'Brien, P.; Helliwell, M., Controlled synthesis of PbS nanoparticles and the deposition of thin films by Aerosol-Assisted Chemical Vapour Deposition (AACVD). *J. Mater. Chem.* **2010,** *20*, 6116-6124.
26. Nyamen, L. D.; Pullabhotla, V. R.; Nejo, A. A.; Ndifon, P. T.; Warner, J. H.; Revaprasadu, N., Synthesis of anisotropic PbS nanoparticles using heterocyclic dithiocarbamate complexes. *Dalton Trans.* **2012,***41*, 8297-8302.
27. Mandal, T.; Piburn, G.; Stavila, V.; Rusakova, I.; Ould-Ely, T.; Colson, A. C.; Whitmire, K. H., New mixed ligand single-source precursors for PbS nanoparticles and their solvothermal decomposition to anisotropic nano-and microstructures. *Chem. Mater.* **2011,** *23*, 4158-4169.
28. Du, Y.; Xu, B.; Fu, T.; Cai, M.; Li, F.; Zhang, Y.; Wang, Q., Near-infrared photoluminescent Ag_2S quantum dots from a single source precursor. *J. Am. Chem. Soc.* **2010,***132*, 1470-1471.
29. Wang, W.; Liu, Z.; Zheng, C.; Xu, C.; Liu, Y.; Wang, G., Synthesis of CdS nanoparticles by a novel and simple one-step, solid-state reaction in the presence of a nonionic surfactant. *Mater. Lett.* **2003,** *57*, 2755-2760.
30. Chawla, P.; Sharma, G.; Lochab, S.; Singh, N., Photoluminescence and optical characterization of CdS nanoparticles prepared by solid-state method at low temperature. *Radiation Effects & Defects in Solids* **2009,** *164*, 755-762.
31. Liu, J.; Cao, J.; Li, Z.; Ji, G.; Deng, S.; Zheng, M., Low-temperature solid-state synthesis and phase-controlling studies of CdS nanoparticles. *J. Mater. Sci.* **2007,** *42*, 1054-1059.
32. Liu, J.; Zhao, C.; Li, Z.; Chen, J.; Zhou, H.; Gu, S.; Zeng, Y.; Li, Y.; Huang, Y., Low-temperature solid-state synthesis and optical properties of CdS–ZnS and ZnS–CdS alloy nanoparticles. *J. Alloys Compd.* **2011,** *509*, 9428-9433.
33. Yu, J.H.; Joo J.; Park, H.M.; Baik, S.I.; Kim, Y.W.; Kim, S.C.; Hyeon, T., Synthesis of quantum-sized cubic ZnS nanorods by the oriented attachment mechanism. J. Am. Chem. Soc. **2005,** *127*, 5662-70.

34. Lu, Q.; Gao, F.; Zhao, D., One-step synthesis and assembly of copper sulfide nanoparticles to nanowires, nanotubes, and nanovesicles by a simple organic amine-assisted hydrothermal process. *Nano Lett*. **2002,** *2*,725-8.
35. Bera, A.; Prasad, B. L. V., 2D Molecular precursor for a one-pot synthesis of semiconducting metal sulfide nanocrystals. *Bull. Mater.Sci*. **2018,** *41*, 125.
36. Bera, A.; Mandal, D.; Goswami, P. N.; Rath, A. K.; Prasad, B. L., Generic and scalable method for the preparation of monodispersed metal sulfide nanocrystals with tunable optical properties. *Langmuir* **2018,** *34*, 5788-5797.
37. Zhuang, Z.; Lu, X.; Peng, Q.; Li, Y., A facile "dispersion–decomposition" route to metal sulfide nanocrystals. *Chem. Eur. J.***2011,** *17*, 10445-10452.
38. Pradhan, N.; Katz, B.; Efrima, S., Synthesis of High-Quality Metal Sulfide Nanoparticles from Alkyl Xanthate Single Precursors in Alkylamine Solvents., *J. Phys. Chem. B*, **2003**, *107*, 13843-13854.
39. Pradhan, N.; Efrima, S., Single-Precursor, One-Pot Versatile Synthesis under near Ambient Conditions of Tunable, Single and Dual Band Fluorescing Metal Sulfide Nanoparticles. *J. Am. Chem. Soc.*,**2003**, *125*, 2050-2051.
40. Karan, N. S.; Sarkar, S.; Sarma, D. D.; Kundu, P.; Ravishankar, N.; Pradhan, N., Thermally controlled cyclic insertion/ejection of dopant ions and reversible zinc blende/wurtzite phase changes in ZnS nanostructures. *J. Am. Chem. Soc*., **2011,** *133*, 1666-9.
41. Han, S. K.; Gong, M.; Yao, H. B.; Wang, Z. M.; Yu, S. H. One-Pot Controlled Synthesis of Hexagonal-Prismatic $Cu_{1.94}S$-ZnS, $Cu_{1.94}S$-ZnS-$Cu_{1.94}S$, and $Cu_{1.94}S$-ZnS-$Cu_{1.94}S$-ZnS-$Cu_{1.94}S$ Heteronanostructures. *Angew.Chem. Int. Ed.* **2012,** *51*, 6365–6368.
42. Han, S. K.; Gu, C.; Zhao, S.; Xu, S.; Gong, M.; Li, Z.; Yu, S. H. Precursor Triggering Synthesis of Self-Coupled Sulfide Polymorphs with Enhanced Photoelectrochemical Properties. *J. Am. Chem. Soc.* **2016,** *138*, 12913−12919.
43. Li, L. S.; Pradhan, N.; Wang, Y.; Peng, X., High quality ZnSe and ZnS nanocrystals formed by activating zinc carboxylate precursors. *Nano Lett.* **2004,** *4*, 2261-2264.
44. Hollingsworth, N.; Roffey, A.; Islam, H.-U.; Mercy, M.; Roldan, A.; Bras, W.; Wolthers, M.; Catlow, C. R. A.; Sankar, G.; Hogarth, G. Active nature of

primary amines during thermal decomposition of nickel dithiocarbamates to nickel sulfide nanoparticles. *Chem. Mater.* **2014,** *26*, 6281-6292.

45. Hogarth, G., Transition metal dithiocarbamates: 1978–2003. *Prog. Inorg. Chem.,* **2005,** *53*, 71-561.
46. Jung, Y. K.; Kim, J. I.; Lee, J.-K. Thermal decomposition mechanism of single-molecule precursors forming metal sulfide nanoparticles. *J. Am. Chem. Soc.* **2009,** *132*, 178-184.
47. Han, S. K.; Gong, M.; Yao, H. B.; Wang, Z. M.; Yu, S. H. One-Pot Controlled Synthesis of Hexagonal-Prismatic $Cu_{1.94}S$-ZnS, $Cu_{1.94}S$-ZnS-$Cu_{1.94}S$, and $Cu_{1.94}S$-ZnS-$Cu_{1.94}S$-ZnS-$Cu_{1.94}S$ Hetero nanostructures. *Angew. Chem. Int. Ed.* **2012,** *51*, 6365–6368.
48. Busupalli, B.; Kummara, S.; Kumaraswamy, G.; Prasad, B. L. V. Ultrathin sheets of metal or metal sulfide from molecularly thin sheets of metal thiolates in solution. *Chem. Mater*. **2015,** *26*, 3436-3442.
49. Choi, S. H.; An, K.; Kim, E. G.; Yu, J. H.; Kim, J. H.; Hyeon, T. Simple and generalized synthesis of semiconducting metal sulfide nanocrystals. *Adv. Funct. Mater*. **2009,** *19*, 1645-1649.
50. Liu, M.; Voznyy, O.; Sabatini, R.; de Arquer, F. P. G.; Munir, R.; Balawi, A. H.; Lan, X.; Fan, F.; Walters, G.; Kirmani, A. R., Hybrid organic–inorganic inks flatten the energy landscape in colloidal quantum dot solids. *Nat. Mater.* **2017,** *16*, 258-263.
51. Xu, J.; Voznyy, O.; Liu, M.; Kirmani, A. R.; Walters, G.; Munir, R.; Abdelsamie, M.; Proppe, A. H.; Sarkar, A.; de Arquer, F. P. G., 2D matrix engineering for homogeneous quantum dot coupling in photovoltaic solids. *Nat. Nanotech.* **2018,** *13*, 456-462.

Chapter 3

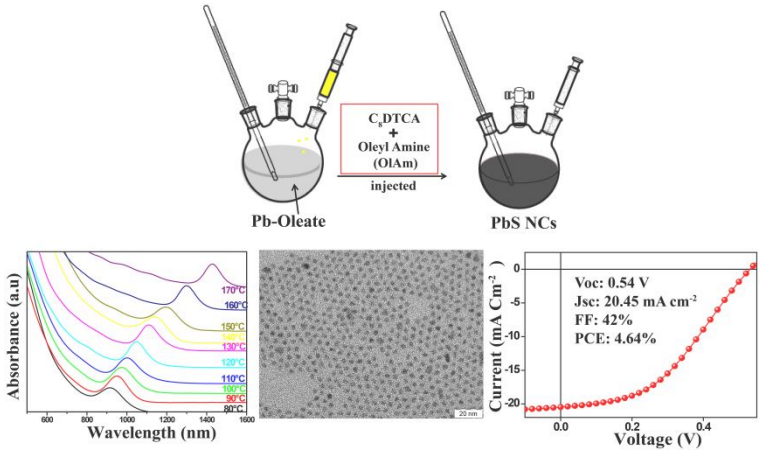

This chapter presents a generic and scalable method to prepare monodispersed metal sulfide NCs including PbS NCs with tunable optical properties.

3.1 Introduction

In the previous chapter the results about the preparation of binary metal sulfide NCs like CdS, ZnS, Cu_2S, MnS and PbS by thermolysis of the corresponding metal thiolates has been described. The results obtained indicated that the materials obtained (especially at lower temperatures) were featured with intrinsic defects and that the optical properties displayed by them were not of the desired quality. The poor optical properties of the materials prepared by this process were clearly evident in the case of PbS QDs as they did not show any absorbance or emitting features. To address this we tried the thermolysis of the Pb-C_8DTCA complex surmising this complex would decompose faster and also at lower temperatures leading to better quality materials. This new Pb-C_8DTCA complex also displayed equidistant peaks in PXRD suggesting its lamellar structure similar to several other metal thiolates.[1] Though this Pb-C_8DTCA complex decomposed at comparatively lower temperatures (~150 °C) resulting in the formation of PbS QDs, their optical properties were also not up to the mark. It should be noted however that these PbS QDs at least showed very weak and broad absorption at NIR region (absorption spectra was shown in Figure 2.14b (in the second chapter)), unlike the PbS QDs obtained from Pb-thiolates which were completely featureless (absorption spectra was shown in Figure 2.11c (in the second chapter)). As mentioned in the previous chapter PbS QDs due to their tunable absorption edge from the near-infrared through the visible region are highly attractive for solar energy conversion.[2-4] Accordingly, solar cells based on the p-n junction between a wide band-gap n-type semiconductor (eg. TiO_2, ZnO) and a p-type lead-rich PbS colloidal quantum dot (QD) film have seen rapid advances in recent years, progressing from the first report of an infrared solar cell to recent reports of a ~11.28% solar AM1.5 power conversion efficiency.[3] Therefore, it is not surprising to see that a large number of researchers dedicating their efforts to find methods for the preparation of large scale high quality metal sulfide QDs, especially PbS.[5-8] Though a plethora of synthetic methods to synthesize metal sulfide QDs with the desired characteristics have been reported, the procedure referred to as hot-injection methods are considered the best.[5,9,10] In case of synthesis of many QDs (including the most tricky PbS), the preferred sulfur source used in this method happens to be bis (trimethylsilyl) sulfide [$(TMS)_2S$].[3,5] The use of [$(TMS)_2S$] provides a fast reaction,

yielding QDs with a relatively narrow size distribution.[5] Till date, all reported performance records for photovoltaic devices based on PbS QDs have relied on the [$(TMS)_2S$] based synthesis.[3,4] Unfortunately [$(TMS)_2S$] is pyrophoric, toxic and expensive.[11] Though [$(TMS)_2S$] can be used to prepare PbS near room temperature as it is highly reactive, this rapid reactivity causes problems due to limitations in mixing during the injection step that may also hinder the reaction scalability.[11] Therefore, there exists a gap between the desire to get good quality PbS QDs at large scale to what we can achieve in the sense that the scalable methods that we attempted (based on Pb-thiolates and Pb-C_8DTCA complexes) did not result in good quality materials and the good quality methods that use [$(TMS)_2S$] are not scalable.

We attribute the failure to obtain good quality PbS QDs when pre-formed Pb-thiolate or Pb-C_8DTCA complexes were subjected to heating to their uncontrollable decomposition. We also showed in the previous chapter that oleyl amine helps to decompose the Pb-C_8DTCA complex at faster rate and at lower temperature. Also, the absorption spectra of the samples obtained when oleyl amine was injected at 120 °C into Pb-C_8DTCA complex displayed a sharp peak at 1427 nm (absorption spectra was shown in Figure 2.15b, red solid line (in the second chapter)). However, the optical properties of this PbS NCs are also not to the level that we can use them for applications like solar cell device fabrication.[12] Nevertheless; this gave us an indication that OlAm can increase the decomposition rate of Pb-C_8DTCA. Consequently, we wanted to see what happens when we add the C_8DTCA-OlAm solution (C_8DTCA solid powder dissolved in oleyl amine and 1-ODE) into a Pb-oleate complex at desired temperature (120 °C). Quite gratifyingly this small change in the reaction conditions lead to a remarkable improvement in the quality of PbS NCs obtained and we could exercise great control in different aspects of the material prepared such as size control, narrow size distribution good optical properties etc.[13]

We also tried to understand the mechanism of PbS NCs formation and show that in this process the highly reactive bidentate ligand C_8DTCA first reacts with metal-precursor leading to the formation of metal-C_8DTCA complex.[13] The OlAm present in the solution immediately attacks this Pb-C_8DTCAcomplex *in situ* resulting in the formation of PbS NCs.[13] We also show that great control over the particle sizes and size distribution can be achieved by just adjusting the reaction parameter like

temperature, time and oleyl amine concentration. While the full details of the study are described with the more difficult PbS system, we could easily extend this method to obtain others metal sulfide like CdS, MnS, ZnS etc. Finally to prove that the PbS QDs thus prepared could indeed be used for device fabrication, we prepared photo-voltaic devices that displayed a power conversion efficiency of 4.64 % which is comparable with reported values where PbS QDs obtained using TMS have been utilized.[13]

3.1.1 Experimental section

Chemicals required:

Octylamine ($C_8H_{17}NH_2$) and 1-octadecene (1-ODE) were purchased from Sigma Aldrich and were used as received. Lead oxide (PbO), copper acetate, cuprous (I) iodide, cadmium acetate, manganese acetate, zinc acetate and lead acetate were purchased from Sigma Aldrich. Solvents such as ethanol and toluene etc were purchased from Merck Chemicals and were used as received.

Synthesis

3.1.1.1 Reaction 3A -In situ preparation of PbS using Pb-oleate, C_8DTCA and OlAm: Initially the lead oleate was made as mentioned in Chapter 2 reaction 2A. Into this lead oleate the mixture of C_8DTCA and OlAm (0.3 - 0.75 mL) solution in 1-octadecene (1-ODE) was injected very fast (<1 s). During the injection the temperature of the Pb-oleate was maintained between 80-160 °C. Immediately after the addition colourless Pb-oleate became brownish black. The heating was stopped immediately after the injection of C_8DTCA plus OlAm and the system was allowed to naturally cool to room temperature (which took ~45 minutes). The product of this reaction was collected by precipitating it with acetone addition and after washing it two times with acetone (centrifuged at 5000 rpm for 3 min) and one time with a mixture of acetone and methanol (1:3 by volume) the precipitate was dried under Argon flow. The precipitate was re-dispersed into tetrachloroethylene or toluene for various measurements. Analysis of this product indicated the formation of PbS nanoparticles.

Note: The other metal sulfide NCs were also synthesized in the similar way to PbS NCs synthesis and were shown in Annexure of chapter 3.

3.2 Results and discussion

The absorption spectra of the PbS QDs obtained under the above mentioned condition showed only one sharp peak at 1050 nm (Figure 3.1a -black solid line) with an FWHM of ~95 nm. In addition to the narrow absorption line width, this sample also displayed a strong emission in the infra-red region. The emission spectra (red solid line, Figure 3.1a, excitation max = 1125 nm) has a FWHM of ~100 nm with a minimal Stokes shift (~75 nm). The intense photoluminescence (quantum yield ~42 %) indicates that the emission is purely band gap emission, devoid of any significant emission from trapped states. The PXRD pattern of these PbS NCs is shown in Figure 3.1b, which shows a high degree of crystallinity with all the peaks matching with the Bragg reflections of the standard cubic rock-salt structure of PbS (JCPDS #05-0592). The TEM image of this sample (Figure 3.1c and 3.1d) unveils the presence of monodispersed particles [size 3.32 ± 0.47 nm; σ = 4.7 %; size distribution plot shown in Annexure Chapter 3 Figure A.C.3.1d] which is also exemplified by their self-assembly into two dimensional hexagonally close packed structures. High resolution TEM images showed in Figure 3.1d (inset) indicate that the particles are highly crystalline with well-resolved lattice planes corresponding to an interplanar spacing of 0.29 ± 0.02 nm, consistent with the (200) d-spacing of the PbS bulk rock salt structure (lattice fringes shown in Figure 3.1d inset).

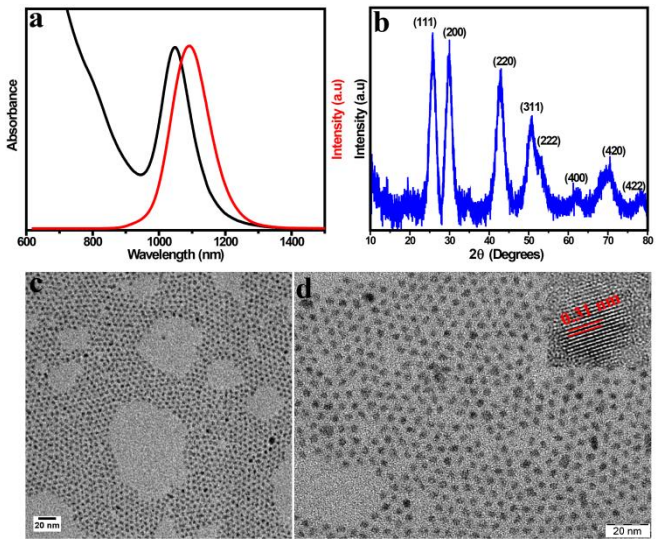

Figure 3.1 a) Optical characterization of PbS QDs prepared at 120 °C; Absorption spectra (black solid line) and photoluminescence Spectra (red solid line), normalized

for same peak amplitude.(b) PXRD of PbS QDs, (c and d) TEM images of PbS QDs. The HRTEM image of one PbS QD is shown in the inset of (d).

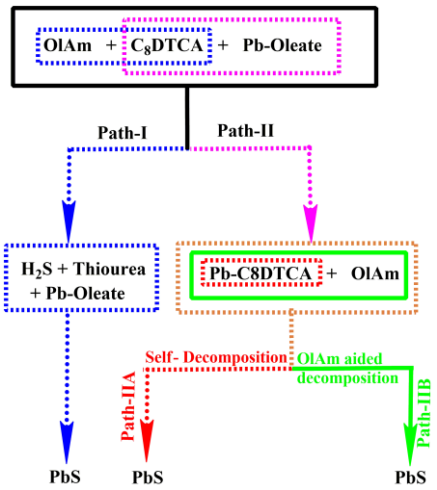

Figure 3.2 Probable pathways of PbS formation. Please see text for details.

It may be recalled that the successful synthetic strategy to obtain PbS QDs with controlled sizes comprised the addition of C_8DTCA and OlAm together into pre-heated Pb-oleate. We reckoned that there could be several possible ways through which these PbS QDs form. In the first of such scenario the OlAm could react with C_8DTCA forming thiourea and releasing H_2S gas (Path -I, please see Figure 3.2). This H_2S gas could then react with Pb-oleate and form PbS QDs. To gain more insights in to this aspect we recorded the ^{1}H NMR spectra of C_8DTCA and n-butyl amine (n-butyl amine was used as it is more reactive) mixture (at room temp. 25°C) and C_8DTCA and OlAm mixture (at 50ºC) which clearly revealed the presence of the individual species that are intact (no extra peaks observed that can be related to the reaction products (thiourea) between C_8DTCA and amine- please see in Annexure Chapter 3 FigureA.C.3.2 and A.C.3.3). However, when the same mixture was heated to 140 °C for several hours (1 - 2 h) we could see signatures of thiourea with a concomitant release of H_2S (as evidenced by the blackening of lead acetate paper. For NMR spectra of the reaction products please see Annexure Chapter 3 Figure A.C.3.4 and A.C.3.5). We also noticed that the liberation rate of H_2S species by this route is much slower (30 min - 1h) than the overall reaction time taken to form PbS QDs by the addition of C_8DTCA and OlAm together into pre-heated Pb-oleate which was just few minutes. Thus we ruled out that Path -I (possibility of H_2S gas getting released by

the reaction between OlAm and C_8DTCA) as the possible route by which PbS QDs are getting formed in the current study.

The other possibility is the formation of a stable Pb-C_8DTCA complex which undergoes self- decomposition (Path-IIA) when subjected to high temperature heating or OlAm aided decomposition (Path-IIB) giving rise to the respective QDs which get subsequently capped/passivated by the oleic acid/OlAm present in the system. We have shown in chapter 2 (Figure 2.14 and 2.15) that products acquired when such reactions were carried out also were also featured with large or polydispersed particles with anisotropic structure (Figure 2.15d-e, Chapter 2). Thus the results of the above two experiments suggested thateither the reaction of H_2S gaswith Pb-oleate ortheself-decomposition of pre formed Pb-C_8DTCA complex do not provide the PbS QDs with the desired optical characteristics.

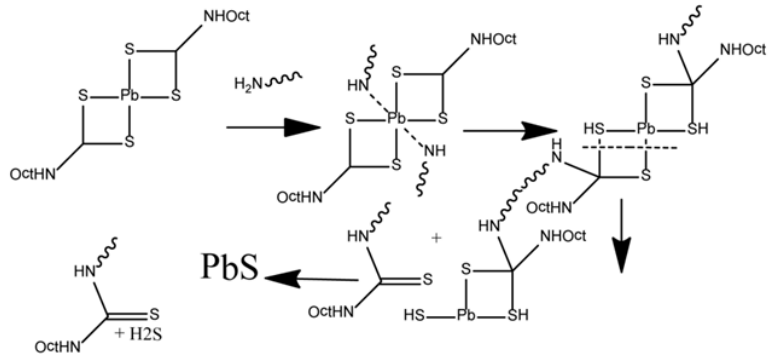

Figure 3.3 Probable mechanism of decomposition of Pb-C_8DTCA complex to PbS in presence of OlAm. Adapted from ref 14.

Then how does the current procedure afford highly monodispersed PbS QDs with tunable optical characteristics? The third and final possibility we envisaged is that Pb-oleate and C_8DTCA react first, forming the Pb- C_8DTCA complex which then reacts *in situ* with OlAm to form the PbS nanocrystals (Figure 3.2, Path-IIB). This could happen as follows. After injection of C_8DTCA-OlAm solution into Pb-oleate, the bidentate ligand (C_8DTCA) first reacts with Pb-oleate to form the highly reactive Pb-C_8DTCA complex (unstable in ambient atmosphere). The OlAm present in the solution immediately attacks this complex *in situ* resulting in the formation of PbS nanoparticles (the reaction mechanism drawn based on the one suggested by Jung et al. is shown in Figure 3.3).[14] We further postulate that the reaction of the Pb-C_8DTCA with oleyl amine results in the formation of N,N´-octylthiourea as the side product

and no further decomposition of this thiourea takes place. To support this we have independently prepared the N,N´-octyl thiourea derivative. It was seen that this compound required a temperature of ~150-170 °C to decompose which is higher than that we have generally used in our reaction. Also when we used this N,N´-octylthiourea as a sulfur source for PbS synthesis, particles with poor optical properties (with excitonc peak near around ~1300 nm -Annexure Chapter 3 Figure A.C.3.6) formed. This supports our contention that the attack of oleyl amine on Pb-C_8DTCA with the release of H_2S and the formation of thiourea as a by-product is the main reaction. The H_2S thus released reacts with the liberated Pb^{2+} species to form PbS nanoparticles. We hasten to add here that we cannot rule out the possibility of some amount of thiourea decomposing and releasing active sulfur species which also participate in the formation of PbS.

3.2.1 Tunablity of PbS size and absorbance and emission spectra

Our next aim was to find reaction conditions that allow us to gain control over the particle sizes and their optical properties. To achieve this, we synthesized PbS at different injection temperatures (T_{inj}) by keeping the reaction parameters like OlAm concentration and Pb: C_8DTCA ratio same as above. The absorption spectra of PbS QDs obtained by varying the T_{inj} temperatures (80-160 °C) are plotted in Figure 3.4a. It can be clearly seen that each of the sample displays well defined excitonic peak and the peak position varied gradually from 915 to 1300 nm (1.35 - 0.95 eV) as the T_{inj} temperature is varied in the range 80 - 160 °C. At 80 °C the excitonic peak is positioned at 915 nm (1.35 eV) and the peak is comparatively broader (the FWHM for this peak could not be determined exactly). The TEM images (Figure 3.4c) of this sample indicate that the average particle size is ~ 2.4 nm with slightly broader particle size dispersion (5.1%, please see Annexure Chapter 3 Figure A.C.3.1a for size distribution plots). As the T_{inj} is raised to 90 °C, the excitonic peak becomes noticeably narrower (FWHM =157 nm). As the T_{inj} is increased further (100 to 120 °C) the FWHM of the first excitonic peak gets further narrowed down to 95 nm, with a concomitant red shift in the peak. After a certain T_{inj} temperature (120 °C) no further change in the FWHM is observed while the peak position keeps shifting to the right. In Figure 3.4b, the near infrared emission spectra of all the samples are plotted, which demonstrate that all the samples display bright and narrow emission peaks. The

Stokes shift changes observed with different samples obtained at various T_{inj} are found to be minimal (110 - 50 nm), which indicate pure band gap emission from these QDs. In Figure 3.4c-h the TEM images of PbS QDs synthesized at different T_{inj} temperatures, are presented which clearly point to the monodispersity in the the particle sizes. The average particles sizes for these particles are shown in Table 3.1 and for the size distribution plots of the same please see Annexure Chapter 3 Figure A.C.3.1.

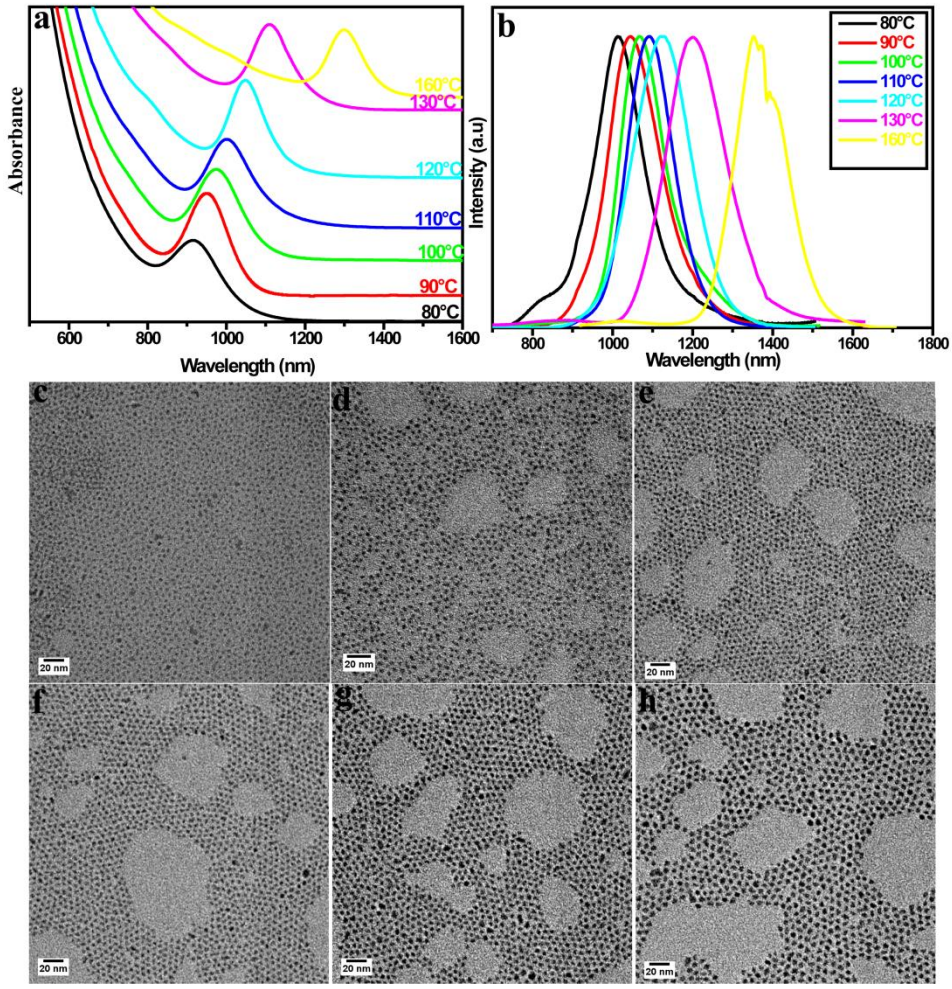

Figure 3.4 (a) Absorbance spectra of PbS QDs prepared by adding C_8DTCA and OlAm to Pb-oleate at a Pb:S ratio of 3:1 at different temperatures. (b) Near infrared photoluminescence spectra of the PbS QDs synthesized at different temperatures. All the enission spectra were normalized to have the same peak amplitude. The absorbance spectra were offset vertically for clarity. (c-h) TEM images of PbS QDs synthesized at different temperatures (c) at 80°C, (d) at 90°C, (e) at 100°C, (f) at

120°C, (g) 130°C and (h) at 160°C. All QDs were dispersed in tetrachloroethylene for the absorption and PL spectra.

Table-3.1: The summary of particle sizes and optical spectral parameters of PbS QDs prepared at different temperatures.

PbS at different temp.	Particle Size From TEM (nm)	Absorption wavelength (nm)	FWHM		Emission wavelength (nm)	Stokes Shift (nm)
			(nm)	(eV)		
80 °C	2.4 ± 0.5	915	. . . . .	.....	1015	100
90 °C	2.7 ± 0.5	946	157	7.8	1045	99
100 °C	2.8 ± 0.5	972	147	8.4	1068	96
120 °C	3.3 ± 0.5	1050	95	13.0	1125	75
130 °C	3.9 ± 0.6	1110	95	13.0	1200	90
160 °C	4.8 ± 0.7	1300	92	13.4	1371	71

3.2.2 Scalability and stability studies

One of the most attractive features of the procedure we present here is the possibility to scale up without compromising the product quality. This is demonstrated by carrying out the above reaction at 10 mmol scale. As may be noticed the optical properties of the product remain almost the same even when the concentration was increased five times (Figure 3.5a). In addition the PbS QDs synthesized using the recipe developed here showed excellent air stability as evidenced by the intact optical characteristics from the sample recorded after storing it in normal lab atmosphere (not in inert atmosphere) for several months. In Figure 3.5b, we compare the absorbance spectra for three different sized of PbS QDs immediately after synthesis and after 3 months of storage. It can be easily noticed that the absorption peak positions remain almost the same even when the sample is stored for 3 months under ambient conditions.

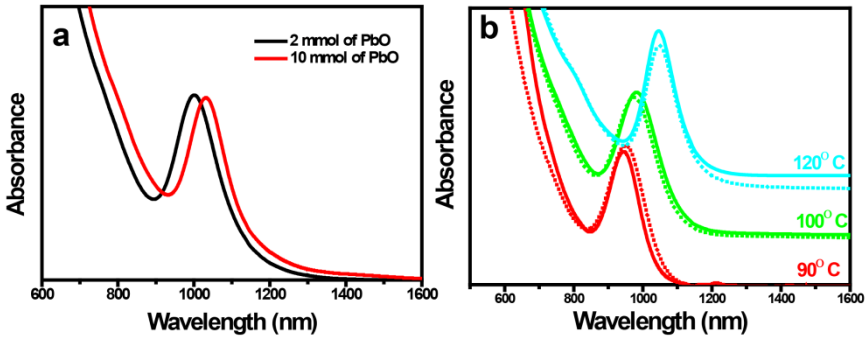

Figure 3.5 (a) Absorption spectra of PbS QDs synthesized at different ~mmol scales. Black solid line represents 2mmol batch synthesis and red solid line is the spectrum recorded from 10mmol batch. (b) Absorption spectra of different sized PbS QDs immediately after synthesis (solid line) and after 3 months of storage (dotted line).

In addition to PbS QDs we could synthesize other metal sulfide QDs by following the same procedure described above (Figure 3.6).This generic approach is optimized for PbS QD synthesis and as has been demonstrated we could exercise great control over the particle sizes and size distribution of these QDs by just adjusting the reaction parameter like temperature, time and oleyl amine concentration. However it may be noted that in case of some of the other metal sulfide QDs the method has not been optimized and therefore the as prepared materials here are characterized with broad size distribution as well as irregular size. This could be due to the fact that the decomposition temperature and other reaction conditions (eg. amount of OlAm needed) for different M-C_8DTCA complexes will be different and each may need further optimization of the conditions which are currently being pursued in our group.

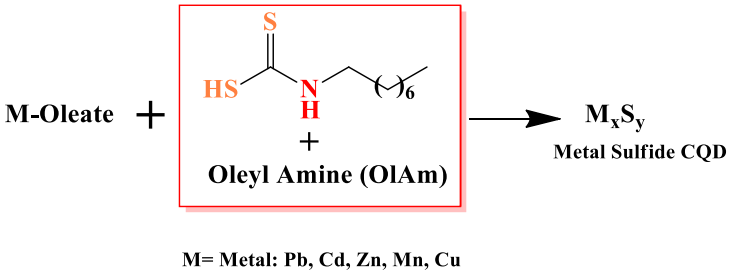

Figure 3.6 Method for generic metal sulfide QDs Synthesis.

3.2.3 Characterization of other metal sulfide QDs

The other QDs synthesized by the above described generic procedure included, CdS, ZnS, MnS, In_2S_3, SnS and Cu_2S. In all these cases the sulfur precursor solution -

prepared by dissolving C_8DTCA into OlAm (at room temp. 25°C) -was injected into the previously prepared corresponding metal-oleate solution at an appropriate temperature (140 – 200°C) depending on the type of QDs to be prepared. The TEM images of all the metal sulfide QDs prepared by this simple method are presented in Figure 3.7 and other characterizations (PXRD, UV-Vis and PL spectra) of all these metal sulfides are summarized in (Table 3.2 and Figure 3.8, 3.9, 3.10, 3.11 and 3.12). Thus it is clearly established that this simple one step synthesis process can be easily applied for the synthesis of different metal sulfide QDs.

Table-3.2: The summary of the other metal sulfide QDs characterisation.

Metal Sulfide	Crystal System JCPDS No	Size (nm)	Absorption Wavelength (nm)	Emmision Wavelength (nm)
CdS	75-0581	3.3 ± 0.493	401	448
ZnS	05-566	6.3 ± 1.048	395	444
MnS	00-006-0518	6.9 ± 1.603	495	547
In_2S_3	65-0459	4.3 ± 0.855	……	481
SnS	39-0354	8.3 ± 1.962	……	433
Cu_2S	84-0206	8.4 ± 2.095	1235	----------

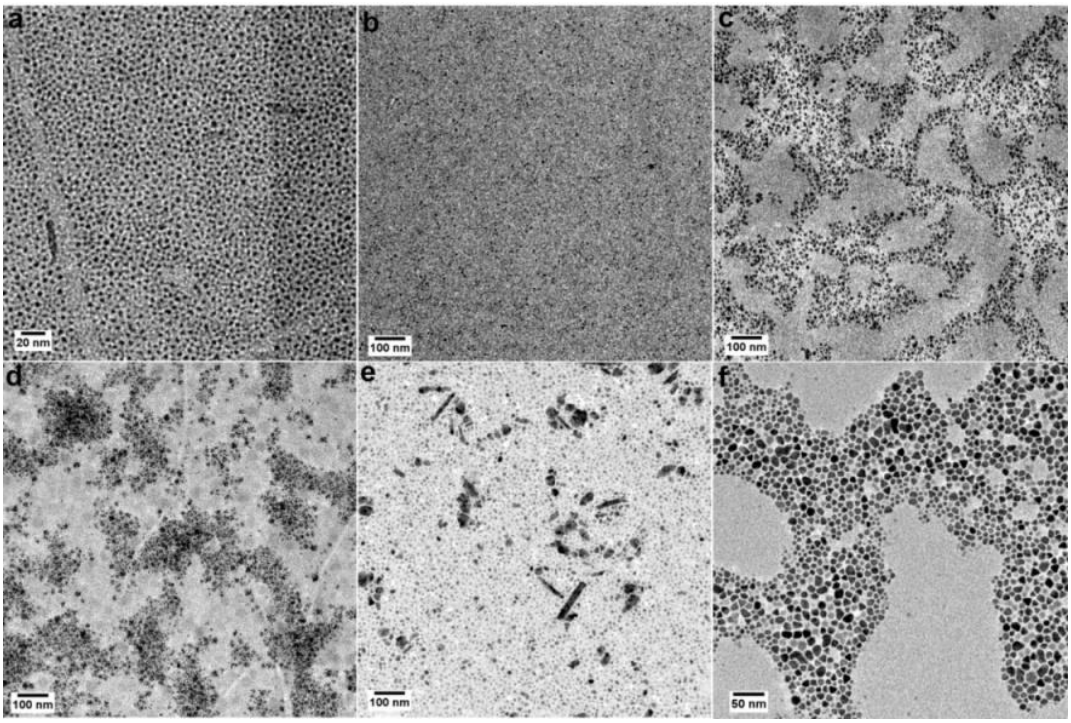

Figure 3.7 TEM images of other metal sulfides; (a) CdS QDS, (b) ZnS QDs, (c) MnS QDs, (d) In_2S_3 NCs, (e) SnS NCs, (f) $Cu_{2-x}S$ NCs.

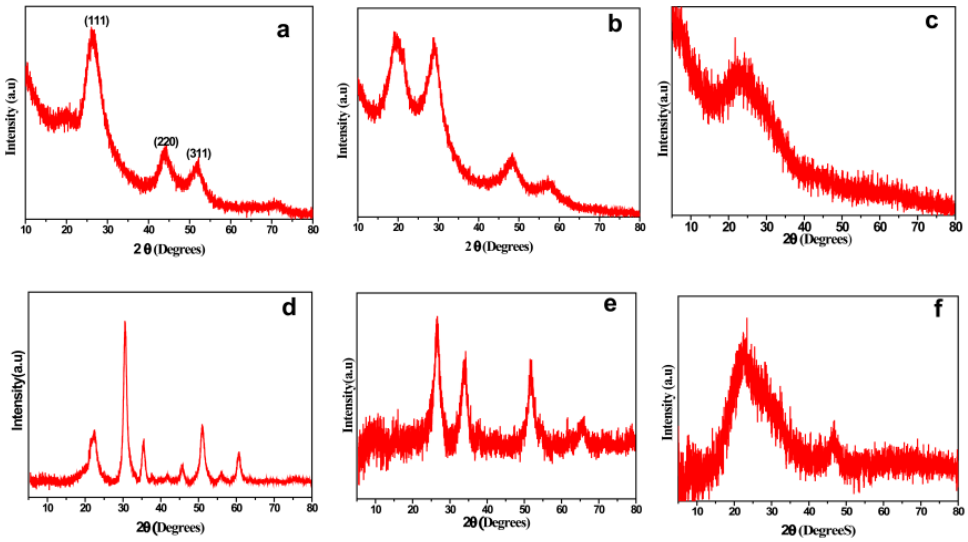

Figure 3.8 PXRD patterns of various metal sulfide QDs; (a) CdS prepared at 200 °C, (b) ZnS (c) MnS (d) In_2S_3 (e) SnS (f) $Cu_{2-x}S$ (all prepared at 140°C).

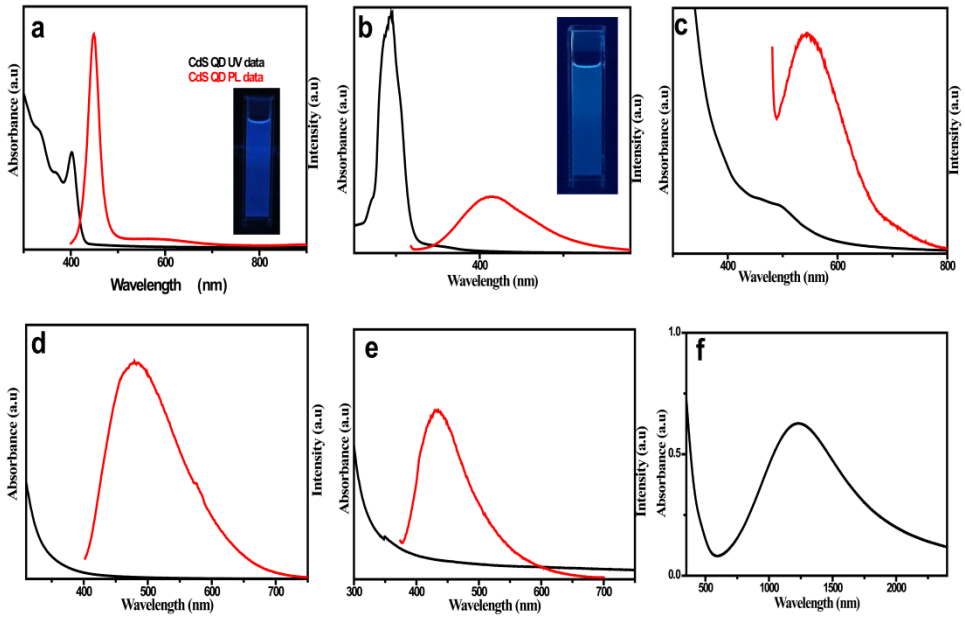

Figure 3.9 Uv-Vis/ Photoluminescence spectra of metal sulfide QDs; (a) CdS (b) ZnS (c) MnS (d) In_2S_3 (e) SnS (f) $Cu_{2-x}S$. In each case black solid line indicates UV-Vis spectra and red solid line photoluminescence spectra.

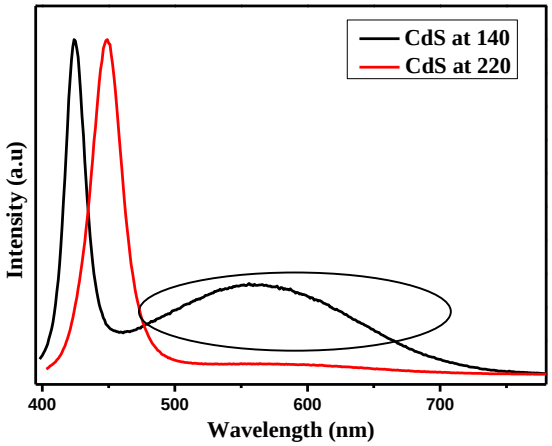

Figure 3.10 PL Spectra of CdS QDs prepared at different temperature; black solid line (at 140 °C), red solid line (at 220 °C). At high temperature synthesis reduces the trap state density.

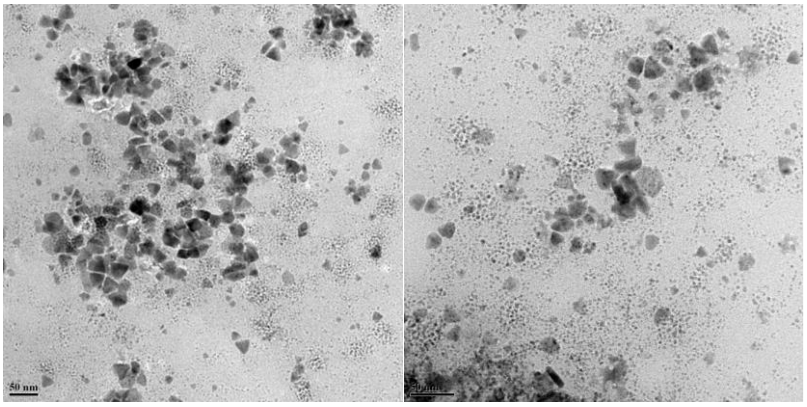

Figure 3.11.TEM images of Cu_2S prepared at 60°C. Polydispersed particles with anisotropic morphology are present.

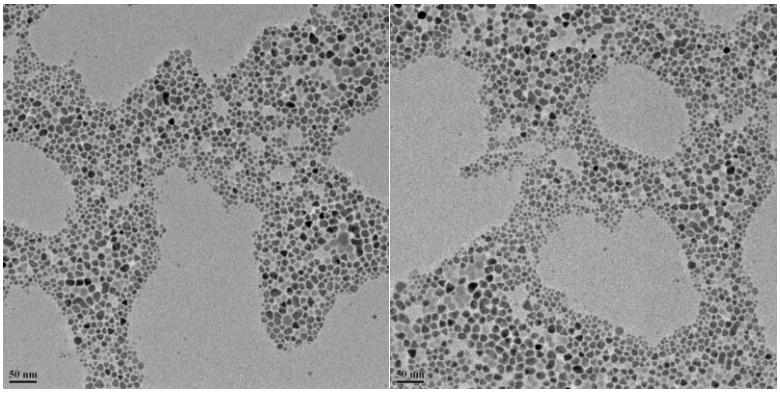

Figure 3.12.TEM images of Cu_2S prepared at 140 °C. At high temperature synthesis polydispersity reduced and almost similar morphology particles formed.

3.2.4 Photovoltaic device fabrication and results

For any QDs, in order to perform as an active layer in photovoltaic application, both good optical and electronic properties are a perquisite. Therefore, to test the usefulness of the PbS QDs synthesized from the present strategy we have tested their performance as an active layer in photovoltaic devices. Solar cell devices were made according to the earlier report and the device structure is shown in Figure 3.13a (methods for solar cell device fabrication details was shown in Annexure of chapter 3).[15] Here, ZnO layer acts as n-type window layer through which light can pass without any absorption to shine upon the active layer. $MAPbI_3$ capped PbS QD layer acts as main light absorbing layer and 1, 2 ethane dithiol (EDT) caped PbS QD layer acts as p-type electron blocking and hole transport layer for the solar cell. Au was deposited as counter electrode to establish ohmic contact with EDT capped PbS layer for seamless collection of holes from the solar cell. J-V characteristic under solar illumination for the best performing solar cell is shown in Figure 3.13b. As can be seen, power conversion efficiency (PCE) as high as 4.64 % is achieved in the PbS QD based solar cells synthesized using the present approach. We further studied photovoltaic figure of merits of the different sized PbS QDs. Shockley–Queisser equation[16] predicts that semiconductor band gap in between 1.1 eV to 1.3 eV are best suited for single junction solar cell application.

Figure 3.13c shows the evolution of V_{oc}, J_{sc}, fill factor (FF) and power conversion efficiency (PCE) with band gap of PbS QDs. It can be seen that lower band gap PbS QDs produces higher J_{sc} values but both V_{oc} and FF decrease significantly with decrease in band gap. Best PCE is achieved in case of 1.3 eV band gap PbS QDs. Doping density and depletion width of the best performing PbS QD layer (1.3 eV band gap) are determined to further assess their quality from capacitance–voltage study as shown in Figure 3.13d.[17] Capacitance-voltage study suggests near-complete depletion of PbS-$MAPbI_3$ layer at short circuit condition. Doping density of the PbSQD layer as determined from Mott-Schottky analysis is found to be 5×10^{16} cm^{-3}, matching closely with the high performing PbS QD based photovoltaic devices.[15] We further characterized electronic properties of the PbS QD layer through light intensity dependent current and voltage generation measurements. Photocurrent generation in solar cells with illumination intensity is governed by the equation $J \infty \phi^{\alpha}$, where J is current density; ϕ is the illumination intensity and α is the power exponent.[18]As

shown in Figure 3.13e, slope of the logarithmic plot of J_{sc} and light intensity is determined to be 1.

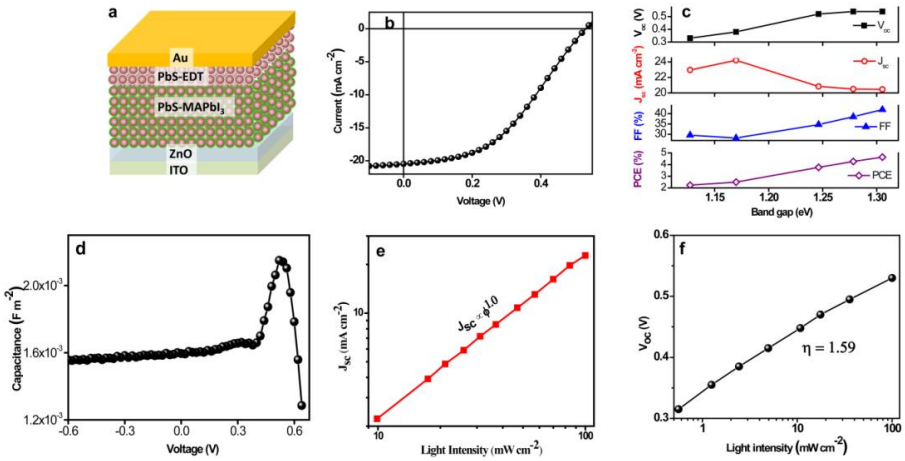

Figure 3.13 (a) Schematic device structure of the photovoltaic device. (b) J-V characteristics of the best performing solar cell under 1.5 AM illumination. (c) Comparison of photovoltaic figure of merits for different band gap PbS QDs. (d) Capacitance-voltage plot for best performing PbSQD (1.3 eV band gap) based solar. (e) and (f) depicts the evolution of short circuit current (J_{sc}) and opencircuit voltage (V_{oc}) respectively for best performing PbS QD based solar cell.

This implies that current extraction is generation limited and transport of both electron and hole carriers are balanced through the PbS layer in our photovoltaic devices. Diode ideality factor η is determined from the intensity vs V_{oc} evolution measurement (Figure 3.13f).[19] η= 1.59 suggests the involvement of intermediate trap states of PbS QD layer in the recombination process of the photo carriers. Further, literature reports suggest that PbS QD synthesized from the established optimised method shows similar η values in their solar cell applications.[19]

3.3 Summary and leads for the next chapter

We have developed a convenient procedure for the preparation of good quality PbS QDs by the addition of C_8DTCA and OlAm together into pre-heated Pb-oleate. We showed that this procedure involves the formation of Pb-C_8DTCA complex which reacts with oleyl amine (in situ) decomposing very fast at comparatively low temperatures. We also disclose that the Pb-C_8DTCA complex's decomposition can be delicately controlled by adjusting the reaction parameter like temperatures and oleyl

amine concentration. The PbS QDs thus synthesized display tunable infrared emission with small Stokes shifts and quantum yields of 15-40 %. The synthesis could be easily scaled up to produce 1.2-3.5 gm of PbS QDs from one batch of reaction. We observed that the as synthesized QDs are air-stable for several months (more than 3months) and they readily self-assemble into ordered lattices and the PbS NCs prepared here when used in a solar cell displayed a power conversion efficiency of 4.64 % which is close to the previous reported ones where PbS QDs prepared using $[(TMS)_2S]$ as sulfur source were used. Thus this scalable synthesis of PbS QDs opens new avenues for the development of large area photovoltaic cells based on them.

Apart from PbS the developed method has been extended for the preparation of other metal sulfide NCs as well. Interestingly, during the course of our studies incorporated in this chapter, we noticed that C_8DTCA to be a very reactive sulfur source. So we wondered whether this could be utilized to prepare metal sulfide nanocrystals (NCs) via solid state grinding method. The results of our experiments in this direction are included in the next chapter.

3.4 References

1. Busupalli, B.; Kummara, S.; Kumaraswamy, G.; Prasad, B. L. V. Ultrathin sheets of metal or metal sulfide from molecularly thin sheets of metal thiolates in solution. *Chem. Mater*. **2015,***26*, 3436-3442.

2. Yuan, M.; Kemp, K. W.; Thon, S. M.; Kim, J. Y.; Chou, K. W.; Amassian, A.; Sargent, E. H., High-performance quantum-dot solids via elemental sulfur synthesis. *Adv. Mater.* **2014,***26*, 3513-3519.
3. Liu, M.; Voznyy, O.; Sabatini, R.; de Arquer, F. P. G.; Munir, R.; Balawi, A. H.; Lan, X.; Fan, F.; Walters, G.; Kirmani, A. R., Hybrid organic–inorganic inks flatten the energy landscape in colloidal quantum dot solids. *Nat. Mater.* **2017,***16*, 258-263.
4. Xu, J.; Voznyy, O.; Liu, M.; Kirmani, A. R.; Walters, G.; Munir, R.; Abdelsamie, M.; Proppe, A. H.; Sarkar, A.; de Arquer, F. P. G., 2D matrix engineering for homogeneous quantum dot coupling in photovoltaic solids. *Nat. Nanotech.* **2018,***13*, 456-462.

5. Hines, M. A.; Scholes, G. D., Colloidal PbS nanocrystals with size-tunable near-infrared emission: observation of post-synthesis self-narrowing of the particle size distribution. *Adv. Mater.* **2003,***15*, 1844-1849.
6. Joo, J.; Na, H. B.; Yu, T.; Yu, J. H.; Kim, Y. W.; Wu, F.; Zhang, J. Z.; Hyeon, T., Generalized and facile synthesis of semiconducting metal sulfide nanocrystals. *J. Am. Chem. Soc.* **2003,***125*, 11100-11105.
7. Cademartiri, L.; Montanari, E.; Calestani, G.; Migliori, A.; Guagliardi, A.; Ozin, G. A., Size-dependent extinction coefficients of PbS quantum dots. *J. Am. Chem. Soc.* **2006,***128*, 10337-10346.
8. Hendricks, M. P.; Campos, M. P.; Cleveland, G. T.; Jen-La Plante, I.; Owen, J. S., A tunable library of substituted thiourea precursors to metal sulfide nanocrystals. *Science* **2015,***348*, 1226-1230.
9. LaMer, V. K.; Dinegar, R. H., Theory, production and mechanism of formation of monodispersed hydrosols. *J. Am. Chem. Soc.* **1950,***72*, 4847-4854.
10. Murray, C.; Norris, D. J.; Bawendi, M. G., Synthesis and characterization of nearly monodisperse CdE (E= sulfur, selenium, tellurium) semiconductor nanocrystallites. *J. Am. Chem. Soc.* **1993,***115*, 8706-8715.
11. Yuan, M.; Kemp, K. W.; Thon, S. M.; Kim, J. Y.; Chou, K. W.; Amassian, A.; Sargent, E. H. High□Performance Quantum□Dot Solids via Elemental Sulfur Synthesis. *Adv. Mater.* **2014,** 26, 3513-3519.
12. Chuang, C.-H. M.; Brown, P. R.; BuloviÄ, V.; Bawendi, M. G. Improved performance and stability in quantum dot solar cells through band alignment engineering. *Nat. Mater.* **2014,** 13, 796-801.
13. Bera, A.; Mandal, D.; Goswami, P. N.; Rath, A. K.; Prasad, B. L., Generic and scalable method for the preparation of monodispersed metal sulfide nanocrystals with tunable optical properties. *Langmuir* **2018,** *34*, 5788-5797.
14. Jung, Y. K.; Kim, J. I.; Lee, J.-K. Thermal decomposition mechanism of single-molecule precursors forming metal sulfide nanoparticles. *J. Am. Chem. Soc.* **2009,** 132, 178-184.

15. Yang, Z.; Janmohamed, A.; Lan, X.; García de Arquer, F. P.; Voznyy, O.; Yassitepe, E.; Kim, G.-H.; Ning, Z.; Gong, X.; Comin, R.; Sargent, E. H. Colloidal Quantum Dot Photovoltaics Enhanced by Perovskite Shelling. Nano Lett. **2015**, 15, 7539−7543.

16. Shockley, W.; Queisser, H. J. Detailed Balance Limit of Efficiency of p-n Junction Solar Cells. *J. Appl. Phys.*, **1961**, 32, 510-519.

17. Johnston, K. W.; Pattantyus-Abraham, A. G.; Clifford, J. P.; Myrskog, S. H.; Hoogland, S.; Shukla, H.; Klem, E. J. D.; Levina, L.; Sargent, E. H. Efficient Schottky-quantum-dot photovoltaics: The roles of depletion, drift, and diffusion. *Appl. Phys. Lett.* **2008,** 92, 122111.

18. Zhao, N.; Osedach, T. P.; Chang, L.-Y.; Geyer, S. M.; Wanger, D.; Binda, M. T.; Arango, A. C.; Bawendi, M. G.; Bulovic, V. Colloidal PbS quantum dot solar cells with high fill factor. *ACS Nano.* **2010,**4, 3743-3752.

19. Chuang, C.-H. M.; Maurano, A.; Brandt, R. E.; Hwang, G. W.; Jean, J.; Buonassisi, T.; BulovicÌ, V.; Bawendi, M. G. Open-circuit voltage deficit, radiative sub-bandgap states, and prospects in quantum dot solar cells. *Nano Lett.* **2015,**15, 3286-3294.

Chapter 4

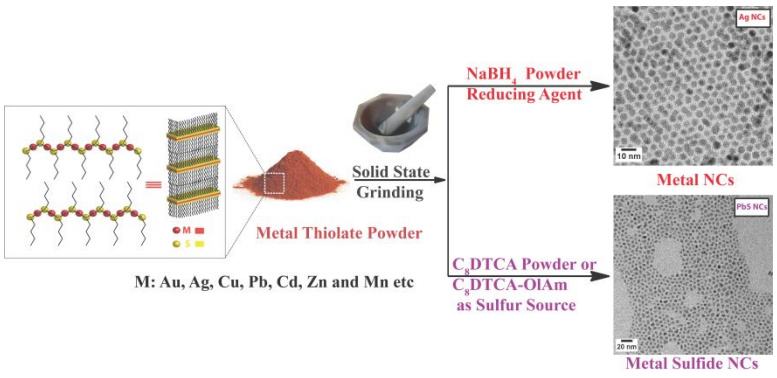

This chapter presents the solvent-less solid state grinding method for the synthesis of dispersible semiconducting metal sulfide and selenide Nanocrystals

4.1 Introduction

Monolayer protected metal chalcogenide NCs have mainly two constituents; the inorganic chalcogenide complex as core and an organic molecules as shell to protect the tiny core. Metal thiolates have these ingredients inbuilt in their structure itself, and they turned out to be good precursors for the preparation of monolayer protected metal chalcogenide NCs via solution based routes as discussed in the previous two chapters. The extraordinary properties of metal chalcogenide NCs and their on growing commercial demand for various applications require large quantities of these materials to be prepared. In fact, it is argued that obtaining large enough quantities of these materials is the main hurdle in translating their potential applications into practicing technologies. Thus, efforts to develop methods for large scale preparation of monolayer protected metal chalcogenide nanocrystals (NCs) are picking up steam. Many solution based methods (as described in the previous two chapters and being practiced by many researchers) afford monolayer protected particles with excellent control over their size and shape.[1-4]Unfortunately, many of these synthetic procedures are time consuming and complicated and also require multiple reagents and lot of solvents during the reaction and for the purification of material. All these make scaling up these reactions challenging and thus accessing large amounts of these materials turns out to be difficult. Thus a method for synthesis of metal chalcogenideNCs which can be scaled up and yet can be carried out under solvent-less environment, is highly desirable. In this context, engagement of reagents or some inorganic metal complexes consisting distinct moieties that can play the role of different ingredients (such as the core of the desired NC, the capping agents etc.) would lead to the simplification of the synthetic procedure and thus would be an attractive prospect. In addition, if the reaction is carried out under ambient atmosphere, at room temperature (~25 °C) and in a solvent-less environment, it adds greenness to the process and could lead to mass production of these materials that are highly sought after for many applications.

In fact, a few solid state routes were indeed reported for the synthesis of metallic NCs. For example, a high-speed vibration milling has been used for the synthesis of gold NCs, where sodium borohydride was used for the reduction of the gold salt and poly vinyl pyrrolidonewas used as a protecting agent.[5] Similarly macroscopic quantities of

bimetallic Au–Ag alloy NCs were prepared through sequential reduction by simple mortar grinding using a chitosan biopolymer as both a stabilizing and reducing agent.[6] In another example, a silver cluster having the composition $Ag_9(H_2MSA)_7$ (H_2MSA=mercapto succinic acid) was synthesized by Prof. Pradeep group from IIT Madras in macroscopic quantities using a solid-state route.[7] More precisely, when a reaction between $AgNO_3$ and H_2MSA is carried out silver thiolate was seen to form by solid state reaction. In the next step this silver thiolate was ground with sodium borohydride resulting in the formation of a brownish black silver cluster powder consisting of a nine-atom core protected with mercapto succinic acid (H_2MSA).[7]Like in the case of metallic NCs and nanoclusters described above, a few solid state routes for the preparation of semi conducting systems have also been published. Amongst these the noteworthy one is the synthesis of ultra-small monodispersed 2 nm sized Bi_2S_3 NCs.[8] In addition, reports on the preparation of cadmium sulfide NCs have also appeared.[9 – 12] In some of these non-ionic surfactants were employed as one ingredient and the resultant NCs were polydispersed and displayed broad absorption spectra. [9 –12] It may be worth noting here that there have been few studies focused on the synthesis of PbS NCs based on solid state routes also.[13,14] In one of them PbS NCs in the size regime 10-15 nm were prepared in presence of a surfactant while in the other paper the preparation of PbS nanocubes using lead dodecylsulfate and Na_2S as precursors was described.[14] In both cases the resulting PbS NCs did not display any characteristic excitonic peak, which are extremely important in terms of their application potential.[13,14]

In the previous chapters we have demonstrated the synthesis of a series of thiolates of different metal ions like Pd (II), Ni (II), Hg (II), Pb(II), Cd(II), Zn(II) and Mn(II). Similarly Ag (I), Au (I) and Cu (I) have also been prepared by Prasad and co-workers and they established that these thiolates also exist as lamellar sheets in the bulk state.[15,16–20] Realizing that these thiolates have the two main ingredients -the metal ion that can become part of the metal chalcogenide NCs and the thiol molecule, capable of becoming a capping/passivating agent -in built in their structures we reckoned that they could be utilized as precursors for the synthesis of metal chalcogenide NCs. Indeed these metal alkyl thiolates were previously used for the synthesis of functional nanomaterials like metal NCs[21–26] and metal sulfide NCs[27–30] by solution based solvo-

thermal routes, but they have never been used as precursors in a solvent less solid-state based method.

In the previous chapter (chapter 3), we have also described that the octyl ammonium octyldithiocarbamate (C_8DTCA) could be utilized as sulfur precursor to prepare metal sulfide nanocrystals (NCs) via solution based routes.[31] As C_8DTCA is a reactive sulfur source we hypothesized that it could be tried for the preparation of metal sulfide NCs via solid state grinding method. Accordingly in this chapter we demonstrate the synthesis of metal chalcogenide NCs like CdS, ZnS, MnS including the highly sought after PbS, Ag_2S and CuS NCs through a simple and convenient solid state route wherein grinding the corresponding metal thiolate and a C_8DTCA based sulfur source (C_8DTCA or C_8DTCA dissolved in few µL of oleyl amine) has been shown to yield monolayer protected metal sulfide NCs. The most gratifying aspect of this procedure is that the resultant NCs were monodispersed and could be easily dispersed in non-polar solvents though no solvent has been used during their preparation. These NCs also displayed very good optical characteristics exemplifying their compositional purity and crystalline nature.

4.1.1 Experimental section

Chemicals required:

Octanethiol ($C_8H_{17}SH$) and octyl amine (C_8NH_{19}) were purchased from Sigma Aldrich and were used as received. Silver nitrate, silver acetate, gold (I) iodide, cuprous (I) iodide, cadmium acetate, cadmium iodide, manganese acetate, zinc acetate and lead acetate were purchased from Sigma Aldrich. Solvents such as ethanol and toluene etc were also purchased from Merck chemicals and were used as received.

4.1.1.1 Synthesis of metal thiolate precursors

Thiolates of different metals like Cu, Pb, Cd, Mn and Zn were synthesized following a protocol previously developed by Prasad and co-workers and already described in the chapter 2 experimental section 2.2.1.[15] The generic procedure for metal thiolate synthesis is also shown in chapter 2 (Figure 2.3). Here in this chapter, the synthesis of thiolates of few more metals like Ag (I) and Au (I) is described. These metal thiolates also are found to be lamellar in nature; the only differences being these are insoluble

in non-polar solvent. The insolubility of these metal thiolates in non-polar solvents prevents their utilization as precursors for the synthesis of NCs via solution based routes, whereas no such difficulty exists if they can be used in the solid state grinding methods.

4.1.1.1.1 Synthesis of silver (I) thiolate:

To 500 mg of silver nitrate or silver acetate, 1000 µL of n- octanethiol was added and the reaction mixture was shaken vigorously. The reaction mixture turned white immediately, indicating the formation of Ag (I) thiolates. The mixture was then washed thoroughly with ethanol (1-2 times).The obtained powder was dried at ambient conditions and was analyzed using several characterization techniques like powder XRD and SEM.

4.1.1.1.2 Synthesis of gold (I) thiolate:

Gold (I) thiolates were synthesized in an easy manner to furnish gram quantities of materials. Approximately 250 mg of gold (I) iodide was taken in an eppendorf tube. To this 500 µL of n- octanethiol (in ethanol) cold solution was added and the reaction mixture was shaken vigorously. After sometime the colour of this mixture changed to white. The resulting product was washed thoroughly several times (1-2 times) with ethanol. The obtained powder was dried at ambient conditions and was analyzed using several characterization techniques like powder XRD and SEM.

Caution! Addition of thiol solution to the solid Au(I)I was found to be highly exothermic and thiol has ability to reduce the gold. Therefore instead of pure thiol, cold ethanolic solutions of thiol need to be used for gold (I) thiolate preparation. Otherwise, bulk gold metal could form as an impurity apart from gold-thiolates.

4.1.1.2 Preparation of selenium precursor solution

The Se^{2-} precursor solution was prepared following reported procedures with slight modifications.[32] About 82 mg of elemental Se powder was taken in an Eppendorf tube and 200 µL of 1-DDT was added to it. Then 200 µL of OlAm was added to this mixture and immediately the color changed to deep brownish red in color. This solution was used for the preparation of metal selenide NCs.

4.1.1.3. Synthesis of metal nanocrystals

4.1.1.3.1 Ag NCs from Ag-thiolates

125 mg (0.5 mmol) of Ag (I) octanethiolate was weighed and ground with 150 mg (3 mmol) of sodium borohydride (excess amount). Here Ag-thiolates and $NaBH_4$ both are white in colour and insoluble in toluene. After sometime the colour of the mixture changed to brown indicating metal nanoparticle formation. When little amount of toluene was added to it, whatever Ag (I) octanethiolate was converted to Ag NCs got disperse in toluene. This pure Ag NCs dispersion could be separated by decanting. The remaining solid was unreacted thiolates and $NaBH_4$.The remaining residue was again ground and Ag NCs was collected by adding toluene. This process could be continued for 3-5times and up to 90% of Ag-thiolates was converted to Ag NCs.

4.1.1.3.2 Au NCs from Au thiolate

Au (I) octanethiolate was used as the precursor for the gold NC synthesis. 25 mg (~0.01 mmol) of the as prepared gold (I) octanethiolate and 50 mg (1 mmol) of sodium borohydride was taken in mortor-pestle and ground as was done above for the Ag NCs preparation. After sometime the colour of the mixture changed to reddish and bluish mixtures. When toluene was added to this mixture, Au NCs got dispersed in toluene. In case of Au two different sized (<3nm and ~10~25nm) NCs formed. These were separated by centrifuging where the bigger particles settled down at the bottom and ultra small particles were in supernatant.

4.1.1.4. Synthesis of metal sulfide nanocrystals

4.1.1.4.1 Synthesis of Ag_2S NCs

About 250 mg (1 mmol) of silver thiolate ($Ag(C_8H_{17}S)$) was taken and ground well till it spreads uniformly inside the mortar. To this, ~0.75 mmol of C_8DTCAwas added and ground for 10 minutes. The colour of the mixture changed to brownish black. To this mixture toluene was added and the dispersion was collected in Eppendorf tubes. After some time, some precipitate appeared at the bottom of the Eppendorf, which was discarded. The remaining supernatant was precipitated and washed with methanol to obtain pure Ag_2S NCs. This product was characterized by PXRD and UV-Vis absorption and fluorescence spectra.

4.1.1.4.2 Synthesis of PbS NCs

500 mg (1 mmol) of lead thiolate ($Pb(C_8H_{17}S)_2$) was taken and ground well till it spreads uniformly inside the mortar. To this, (0.05 mmol-0.5 mmol) of C_8DTCA was added and ground for 10 minutes. The colour of the mixture changed to brownish black. To this mixture toluene was added and the dispersion was collected in Eppendorf tubes. After some time, some precipitate appeared at the bottom of the Eppendorf, which was discarded. The remaining supernatant was precipitated and washed with methanol to obtain pure PbS NCs. These again could be re-dispersed in most of the non-polar organic solvents like toluene. This product was characterized by PXRD and UV-Vis absorption and fluorescence spectra.

Caution: Appropriate precautions (like wearing gloves, masks and carrying out the reactions in fume cupboard) should take while dealing with Pb salts, Cd salts and alkanethiols.

4.1.1.4.3 Synthesis of CdS NCs

500 mg (~1.25 mmol) of cadmium thiolate ($Cd(C_8H_{17}S)_2$) was taken and ground well till itspreads uniformly inside the mortar. To this, C_8DTCA-OlAm (~0.75 mmol of C_8DTCA dissolved in 200µL OlAm) was added and ground for 10 minutes. The colour of the mixture changed to pale yellow. To this mixture toluene was added and collected in Eppendorf tubes, sonicated it for 5-10 min for proper mixing. Then it was centrifuged to obtain the supernatant. This supernatant was precipitated and washed with methanol to obtain pure CdS NCs. This product was characterized by PXRD and UV-Vis absorption and fluorescence spectra.

4.1.1.4.4 Synthesis of ZnS NCs

500 mg (~1.5 mmol) of zinc thiolate ($Zn(C_8H_{17}S)_2$) was taken and ground well till it spreads uniformly inside the mortar. To this, C_8DTCA-OlAm (~0.75 mmol of C_8DTCA dissolved in 200µL OlAm) was added and ground for 10 minutes. The colour of the mixture changed to pale yellow. To this mixture toluene was added and the dispersion was collected in Eppendorf tubes. After some time, some precipitate appeared at the bottom of the Eppendorf, which was discarded. The remaining supernatant was precipitated and washed with methanol to obtain pure ZnS NCs. This product was characterized by PXRD and UV-Vis absorption and fluorescence spectra.

4.1.1.4.5 Synthesis of MnS NCs

500 mg (~1.5 mmol) of manganese thiolate ($Mn(C_8H_{17}S)_2$) was taken and ground well till it spreads uniformly inside the mortar. To this, C_8DTCA-OlAm (~0.75 mmol of C_8DTCA dissolved in 200µL OlAm) was added and grinded for 10 minutes. The colour of the mixture changed to pale yellow. To this mixture toluene was added and the dispersion was collected in Eppendorf tubes. After some time, some precipitate appeared at the bottom of the Eppendorf, which was discarded. The remaining supernatant was precipitated and washed with methanol to obtain pure MnS NCs. This product was characterized by PXRD and UV-Vis absorption and fluorescence spectra.

4.1.1.4.6 Synthesis of CuS NCs

200 mg (~1 mmol) of copper thiolate ($Cu(C_8H_{17}S)$) was taken and ground well till it spreads uniformly inside the mortar. To this, C_8DTCA-OlAm (~1 mmol of C_8DTCA dissolved in 200µL OlAm) was added and grinded for 10 minutes. The colour of the mixture changed to greenish black. To this mixture toluene was added and the dispersion was collected in Eppendorf tubes. After some time, some precipitate appeared at the bottom of the Eppendorf, which was discarded. The remaining supernatant was precipitated and washed with methanol to obtain pure CuS NCs. This product was characterized by PXRD and UV-Vis absorption and fluorescence spectra.

4.1.1.5 Synthesis of metal selenide nanocrystals

4.1.1.5.1 Synthesis of CdSe NCs

1 mmol of Cd $(ac)_2$ or CdI_2 was taken in mortar pestle and ground properly to get fine powder and then about 500 µL of 1-DDT was added into the fine powder and the grinding was continued for 5-10 mins more, resulting in the formation of a pure milky white paste. Then varied amount (0.25 mmol to 1 mmol) of Se-precursor solution (elemental Se powder + DDT + OlAm) was added into the milky white paste and these two was ground thoroughly using a mortar and pestle. After 5-10 mins grinding the mixture colour changed to deep orange yellow indicating CdSe formation. Non-polar solvent toluene was added to the mixture to collect CdSe NCs from the unreacted Cd-thiolates. The CdSe NCs were purified by adding acetone or

methanol into the dispersion, followed by centrifugation and the extracted NCs were dispersed in toluene. The purified CdSe NCs were characterized by PXRD, UV-Vis spectroscopy, PL spectra and TEM.

4.1.1.5.2 Synthesis of ZnSe NCs

1mmol of Zn $(ac)_2$ was taken in mortar pestle and ground properly to get fine powder and then about 500 µL of 1-DDT was added into the fine powder and the grinding was continued for 5-10 mins more, resulting in the formation of a pure milky white paste. Then varied amount 0.5 mmol of Se-precursor solution (elemental Se powder + DDT + OlAm) was added into the milky white paste and these two was ground thoroughly using a mortar and pestle. After 5-10 mins grinding the mixture colour changed to deep yellow indicating ZnSe formation. Non-polar solvent toluene was added to the mixture to collect ZnSe NCs from the unreacted Zn-thiolates by centrifuge. The ZnSe NCs were purified by adding acetone or methanol into the dispersion, followed by centrifugation and the extracted NCs were dispersed in toluene. The purified ZnSe NCs were characterized by PXRD, UV-Vis spectroscopy, PL spectra and TEM.

4.1.1.6 Ligand Exchange with oleic acid

The thiol/oleyl amine ligands were replaced by adding oleic acid to semiconducting NCs dispersed in a 1:1 toluene + 1-octadecene (ODE) solution (40 mg/mL) in a ratio of 1:10 oleic acid: solvent (toluene + ODE) under inert atmosphere at 50-60 ºC. After precipitation with ethanol and centrifugation, the semiconducting NCs were re-dispersed in toluene. This dispersion was characterized by PXRD and UV-Vis absorption, fluorescence spectra and FTIR spectra.

4.1.1.7 Metal halide ($CdCl_2$ treatment) post-treatment

Metal halide ($CdCl_2$) treatment was done as per the previously published report.[33] A stock $CdCl_2$ precursor solution was prepared by dissolving 600 mg of $CdCl_2$ (3.2 mmol) and 66 mg (0.24 mmol) of tetradecylphosphonic acid (TDPA) in 10 mL of oleyl amine, then heated to 100 °C for 1 h under nitrogen. The PbS NCs toluene solution was heated to 60 °C under vacuum for 30 min; then 1.0 mL of metal halide

precursor was introduced into the reaction flask. A 6:1 Pb:Cd molar ratio was maintained during the treatment. The temperature was kept at 60 °C for 30 min and then cooled to room temperature. The NCs were isolated by the addition of acetone followed by centrifugation. The NCs were then purified by dispersion in toluene and re-precipitation with ethanol. Finally, they were re-dissolved in anhydrous toluene or octane.

4.2 Results and discussion

4.2.1 Characterization of metal thiolate

4.2.1.1 Powder X-ray diffraction (PXRD) of metal thiolate

Metal alkyl thiolates are coordination compounds and exist as lamellae or stacked sheets in the solid state.[15] Metal thioates are characterized with zig-zag strands of –S(R)–M–S(R)–M– segments and these zig-zag segments associate into lamellar or multi-bilayer type structures.[15–20] The PXRD pattern of different metal thiolates are shown in chapter 2 Figure 2.6a, which shows periodically spaced (*00l*) reflections. This structure can be very well correlated with the two dimensional self-assembled monolayers (2D-SAMs).

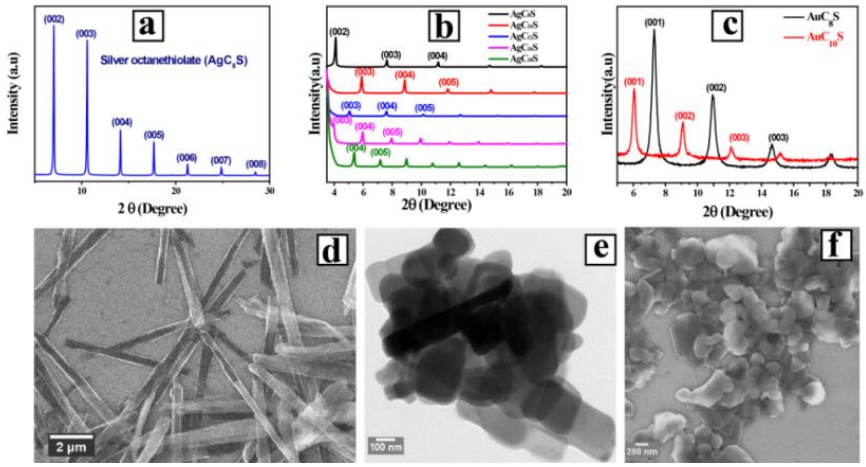

Figure 4.1 PXRD of a) Ag-octanethiolate denoted as AgC_8S; b) Silver thiolates of different chain length alkyl thiols, chain length C_8 to C_{18} and silver octadecanethiolate denoted as $AgC_{18}S$; c) PXRD of Au-thiolates with octanethiol (AuC_8S,black) and decanethiol ($AuC_{10}S$, red); d) SEM and e) TEM image of AgC_8S; f) SEM image of AuC_8S.

4.2.1.2 Morphological studies of Ag-thiolate and Au-thiolate

The PXRD patterns of Ag and Au-octanethiolates are displayed in Figure 4.1a-c. They show (*00l*) reflections indicating the layer like structure. SEM images (shown in Figure 4.1d (for Ag-octanethiolate) and Figure 4.1f (for Au-octanethiolate)) of these metal thiolates also clearly indicate that the metal-thiolates are featured with layered like structure and justify the sheet like (2D) morphology.[15,34] TEM image of Ag-octanethiolate also shown in Figure 4.1e also reveal the layered like structure.

4.2.2 Characterization of metal NCs

The XRD pattern of the obtained material after grinding Ag thiolates with $NaBH_4$, shown in Figure 4.2a, clearly display reflections for pure cubic phase Ag(0) that are in agreement with the JCPDS data (JCPDS No. 03-0931). It may be noticed that, no reflections corresponding to the silver thiolates can be seen. The conversion of Ag-C_8S to Ag NCs has also been supported by X-ray photoelectron spectroscopy (XPS). The high-resolution XPS spectra for Ag-C_8S and Ag NCs are presented in Annexure Chapter 4 Fig. A.C.4.1. The Ag-C_8S thiolate shows the $3d_{5/2}$ peak at 368.37 eV and the corresponding spectra of Ag NCs shows the $3d_{5/2}$ peak at 367.88 eV (single component), confirming the conversion of Ag(I) to Ag(0) as suggested by the previous studies.[35,36]The well defined surface plasmon resonance (SPR) band in the UV–vis spectrum at 448 nm (as shown in the Figure 4.2b) further confirmed the formation of small size Ag NCs. The TEM images of Ag NCs obtained from above reaction are shown in Figure 4.2c. The TEM images clearly indicate that the NCs are nearly monodispersed with average size 4.04±0.45nm (size distribution plot shown in inset of Figure 4.2c).

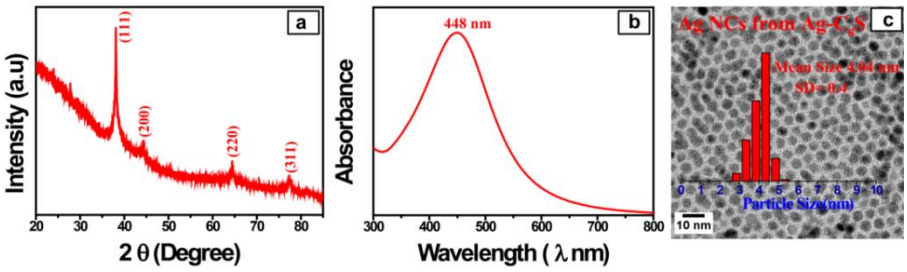

Figure 4.2 a) PXRD of Ag NCs obtained from Ag-octanethiolate. b) UV-Vis spectra of Ag NCs obtained from Ag-C_8S (Ag-octanethiolate). c) TEM images of Ag NCs

obtained from Ag-C_8S.Thesize distribution plot of the Ag NCs obtained is shown in the inset.

In a similar manner when we ground the Au-C_8S with sodium borohydride, we observed that the XRD pattern (please see Figure 4.3a) of obtained product clearly shows reflections for pure cubic phase Au(0) that are in agreement with the JCPDS data (JCPDS No. 04-0784). Here again no reflections corresponding to the gold thiolates could be seen. The UV-vis spectra (please see Figure 4.3b) displays a clear but broad surface plasmon resonance (SPR) peak positioned at 536 nm where the peak broadening could be to the presence of larger sized particles. Very interestingly, the TEM images of the product revealed the presence NCs of two different sized (Figure 4.3c-e) particles where the average size of the small Au NCs was 2.0±0.4 nm and the larger sized Au NCs were of the size 17.4±5.7 nm. When we separated these two NCs from one another by centrifuge and looked at the TEM images of them again, the small Au NCs (which formed flocculent precipitate upon standing) were seen to assemble in a 1D nanowire (NW) fashion.[34] These NWs mostly consist of single strands with lengths of up to several hundred nanometers, as shown in Figure 4.3f-g.

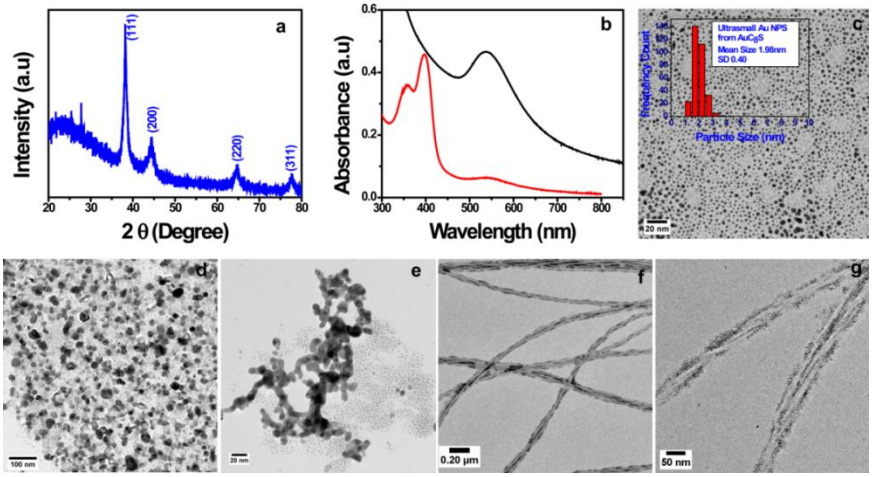

Figure 4.3 a) PXRD of Au NCs. b) UV-Vis spectra of Au NCs from gold octanethiolates (AuC_8S) [black is for bigger sized particles and red is for small sized particles]. TEM images of Au NCs; c) smaller sized particles from Au-octanethiolate (AuC_8S). The inset shows the size distribution plot. d) Bigger sized particles from Au-octanethiolate (AuC_8S), e) mixed sized particles from Au-octanethiolate (AuC_8S)[no

separation], f) self-assembled chain of smaller sized Au NCs, g) enlarged TEM image of self-assembled chain of smaller sized Au NCs.

4.2.3 Characterization of metal sulfide NCs

As we have seen, solid state grinding of AgC_8S with $NaBH_4$ gives uniform monodispersed Ag NCs. Hence we were curious whether we would be able to prepare metal sulfide nanocrystals (NCs) via solid state grinding method. In this context, we had tried solid-state reaction with different sulfur sources like elemental sulfur (sulfur powder dissolved in oleyl amine), sodium sulfide and thiourea. When all these sulfur sources were ground with different metal thiolates a precipitate which was more like bulk material (as concluded by its non-dispersibility in any solvent) formed. The small amount of dispersible materials that formed was found to be featured (on examination by electron microscopy and X-ray diffraction) with particles of broad size distributions. As expected the optical properties of these products were not good as established by the presence of very broad absorption peaks and multiple emission peaks (results shown in Annexure Chapter 4 Figure A.C.4.2 and Figure A.C.4.3 where metal sulfides were prepared using S-OlAm as sulfur source). When we changed the sulfur source to thiourea no reaction took place when it was ground with different metal thiolates (especially with those of Ag, Pb, Cd and Cu).

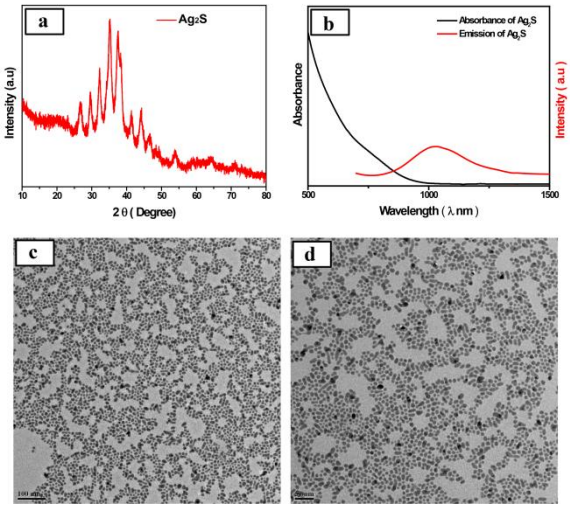

Figure 4.4 a) PXRD of Ag_2S NCs synthesized by solid state, using C_8DTCA as a sulfur source. b) NIR UV-Vis spectra (black solid line) and NIR PL spectra (red solid line) of Ag_2S NCs. c-d) TEM images of Ag_2S NCs.

Our search for a suitable sulfur source lead us to C_8DTCA which we have previously used to make a library of metal sulfide NCs in a solution based method (chapter 3). As a first attempt we tried solid state grinding of AgC_8S with C_8DTCA. Here again the Ag-C_8S was taken along with C_8DTCA in mortar pestle and these two were ground to make a consistent mixture. As soon as we start grinding the white colour of Ag-C_8S changed to deep brownish black indicating Ag_2S formation. The PXRD pattern of as prepared purified material shown in Figure 4.4a is consistent with the pattern of monoclinic α-Ag_2S (JCPDS 14-0072) and TEM images obtained from this sample (Figure 4.4c-d), display nearly monodispersed particles with the average particle size of 6.71 nm and a standard deviation of 13.9% (size distribution plot showed in Annexure Chapter 4 Figure A.C.4.4d). It is observed that the absorption spectra of as prepared purified Ag_2S NCs are featureless with no discrete absorption feature (Figure 4.4b, black solid line), which is different from the II−VI NCs that usually exhibit an evident absorption feature. This could be due to overlap of other transitions with the excitonic transition. Figure 4.4b (solid red line) presents the PL of Ag_2S NCs, in which the fluorescence of Ag_2S NCs is slightly broad with FWHM 316 nm and peak position at 1027 nm.

Encouraged by the successful preparation of nearly monodispersed Ag_2S NCs with good optical properties by this solid state route, we wanted to extend this simple method to prepare other important metal sulfide NCs.

Accordingly, we could extend this procedure to prepare several NCs including those in high demand like PbS, Ag_2S and CuS as well as CdS, MnS and ZnS with good optical characteristics (the overall generic synthetic procedure for metal NCs and also for the metal sulfide NCs preparation is shown in Figure 4.5). Based on the sulfur source used the type of NCs being prepared could be separated into two classes. For instance, for the synthesis of PbS and Ag_2S, the ingredients were the respective metal thiolates and only C_8DTCA was used as sulfur source. On the other hand, in case of CdS, MnS, ZnS and Cu_2S while the metal thiolates could still be used as the metal precursor, we had to use C_8DTCA-OlAm (C_8DTCA+few μL of oleylamine) as the sulfur source. In the following the full details of the study are described with the PbS and CdS systems from these two different classes.

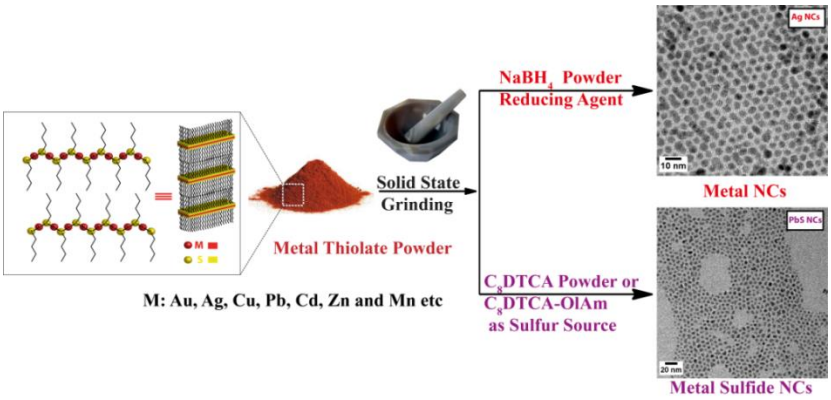

Figure 4.5 Schematic shows the preparation of metal and metal sulfide NCs by solid state grinding method.

As PbS NCs synthesis is the most challenging task with respect to the optical properties they display, we explain the preparation of PbS NCs, in more detail. For their synthesis about 250 mg of lead-octanethiolate (Pb-C_8S, 0.5 mmol) powder was taken in a mortar pestle to which 0.25 mmol of C_8DTCA was added. These two were ground for 5-10 min in air atmosphere. During the grinding, the yellow colour of Pb-C_8S changed to brownish black indicating PbS formation (for detailed synthesis procedures and isolation of dispersible PbS NCs please see the experimental section 4.2.4.2). The PXRD pattern of the purified materials clearly matched with the PbS with rock salt structure (please see Figure 4.6a solid black line), which corresponds to JCPDS card No#05-0592). The conversion of Pb-C_8S to PbS NCs has also been supported by X-ray photoelectron spectroscopy (XPS). The high-resolution XPS Pb 4f spectra and S 2p spectra for both Pb-C_8S and PbS NCs are presented in Annexure Chapter 4 Figure A.C.4.5. The Pb-C_8S thiolate shows the $4f_{7/2}$ peak at 138.9 eV and the spectrum also indicates that some trace amount of Pb-oxides (PbO or PbO_2) could be present. On the other hand, the same spectrum of PbS NCs shows the $4f_{7/2}$ peak at 137.8 eV which is in good agreement with previous report (for PbS).[37,38] In addition there is a small peak at 139.1 eV (which could be from the Pb-C_8DTCA). In case of the S $2p_{3/2}$ peak the Pb-C_8S sample displays a peak at 161.5 eV and the spectrum of PbS NCs is characterized with three peaks; one at 161 eV (for PbS), 162.4 eV (for - the sulfur attached to C or H) and a much smaller peak at higher BE (may be attributed to strongly oxidized species, such as sulfate and sulphite). All these, match very well with those previously reported PbS NCs data.[37,38] The isolated yield of purified PbS NCs turned out to be 44 %.

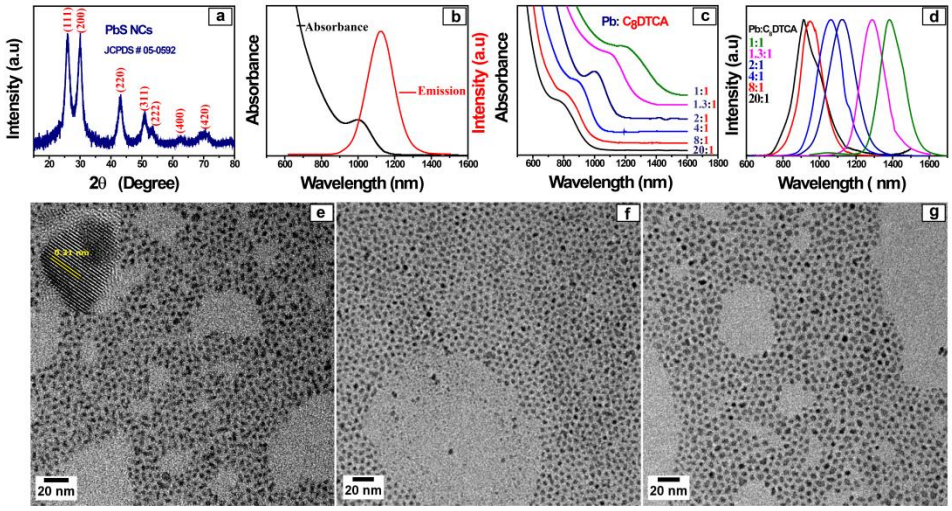

Figure 4.6 a) PXRD of PbS NCs. b) NIR UV-Vis spectra(black solid line) and PL spectra (red solid line) of PbS NCs synthesized by solid state (Pb:C_8DTCA 2:1). c) NIR UV-Vis spectra of PbS NCs synthesized at different Pb:C_8DTCA stoichiometry ratio. d) NIR PL spectra of PbS NCs synthesized at different Pb:C_8DTCA stoichiometry ratio. TEM images of different sized PbS NCs prepared at different Pb:C_8DTCA precursor ratio; e) 8:1, f) 2:1 and g) 1:1.

The absorption spectra of the PbS NCs obtained by the above method showed only one peak at 1005 nm (Figure 4.6b -black solid line). This sample also displayed a strong emission in the infra-red region. The emission spectra (red solid line, Figure 4.6b, excitation max = 1125 nm) has a FWHM of ~170 nm (137 meV) with a minimal Stokes shift (~120 nm or ~97 meV). The intense photoluminescence (quantum yield as determined relative to the standard dye Rhodamine-800 in methanol ~40 %) indicates that the emission is purely band gap emission, significantly devoid of trapped state emission. TEM image of this sample unveils the presence of monodispersed particles (~3.63 ± 0.64 nm; σ = 6.4 %; size distribution plot showed in Annexure Chapter 4 Figure A.C.4.4b) which is also exemplified by their self-assembly into two dimensional hexagonally close packed structures. High resolution TEM images shown in Figure 4.6d indicate that the particles are highly crystalline with well-resolved lattice planes corresponding to an inter-planar spacing of 0.29 ± 0.02 nm, consistent with the (200) d-spacing of the PbS bulk rock salt structure (lattice fringes shown in Figure 4.6d inset).

After ensuring the preparation of PbS NCs with good optical properties by this solid state route, we moved ahead to find reaction conditions that allow us to gain control over the particle sizes and their optical properties. To achieve this, we synthesized PbS at different Pb: C_8DTCA molar ratio at room temperature in open air atmosphere. The absorption spectra of PbS NCs obtained at different the Pb: C_8DTCA ratios are plotted in Figure 4.6c. It can be clearly seen that each of the sample displays well defined excitonic peak and the peak position varied gradually from 780 to 1200 nm (1.58 – 1.03 eV) as the Pb: C_8DTCA precursors molar stoichiometry ratio is varied in the range 20:1 to 1:1.

It can be noticed that as the C_8DTCA precursors concentration is increased the first excitonic peak position gets red shifted, indicating formation of bigger sized particles. In Figure 4.6d, the near infrared emission spectra of all the samples are plotted, which demonstrate that all the samples display bright and narrow emission peaks (FWHM of PL peaks ranges 130-170 nm). The Stokes shift changes observed with different samples obtained at various Pb: C_8DTCA ratios are found to be minimal (180 - 120 nm), which indicate pure band gap emission from the NCs formed. In Figure 4.6e-g the TEM images of PbS NCs synthesized at different Pb: C_8DTCA ratio, are presented which clearly point to the monodispersity in the particle sizes. The average particles sizes, size dispersion value (size distribution plot presented in Annexure Chapter 4 Figure AC4.4a-c) and results are shown in Table 4.1.

Table 4.1. Summary of optical spectral parameter and particles sizes of PbS NCs prepared at different Pb:C_8DTCA molar ratio.

PbS at different Pb:C_8DTCA	Absorption Wavelength (nm)	Emission wavelength (nm)	Stokes Shift (nm)	Particle Size from TEM (nm)
20:1	780	911	131	
8:1	827	949	122	2.90 ± 0.49
4:1	896	1059	163	
2:1	1002	1121	119	3.63 ± 0.64
1.3:1	1115	1287	172	
1:1	1206	1384	178	4.15 ± 0.65

Interestingly this simple grinding of metal thiolate with C_8DTCA alone did not result in the formation of good quality metal sulfide NCs in case of Cd, Zn, Mn and Cu systems. Therefore, we had changed the strategy and used C_8DTCA-OlAm (C_8DTCA dissolved in few µL of oleylamine) as sulfur source. We explain this procedure in detail by taking the CdS system as an example. Briefly, 500 mg (~1 mmol) of cadmium octanethiolate (Cd-C_8S) was ground with a mixture of C_8DTCA-OlAm (~ 0.5 mmol of C_8DTCA dissolved in 200 µL of oleyl amine). Once again as soon as we start grinding all the ingredients a colour changes from white to pale yellow was seen indicating the formation of CdS NCs. The PXRD pattern of the purified materials clearly matched with the CdS cubic phases (for PXRD pattern of this samples please see Figure 4.7a (solid black line)), which corresponds to JCPDS card No#65-2887. These CdS NCs (dispersed in toluene) display a sharp band gap absorption peak at 322 nm, (Figure 4.7b, solid black line) indicating the formation of nearly monodisperse CdS NCs and their PL spectra (Figure 4.7b, solid red line) reveal the presence of broad trap state emission centred at 480 nm (trap state emission dominated the pure band gap emission). TEM images of these CdS reveal a near-spherical ultra-small NCs with average size 2.1 nm with standard deviation value 3.9 % (standard deviation plot shown in Annexure Chapter 4 Figure A.C.4.4.) and HRTEM images reveal the lattice with d-spacing of 2.8Å, corresponding to (100) planes of cubic CdS (Figure 4.7e inset). Similar to PbS NCs, the size, absorption and emission of CdS NCs could be tuned by varying the Cd-C_8S: C_8DTCA precursor ratio. For example, when Cd: C_8DTCA ratio was increased to 1:~0.75 (1 mmol CdC_8S and 0.75 mmol of C_8DTCA) the absorption and emission position shifted towards red (Figure 4.7b, dotted lines) indicating the size of CdS NCs increased.

Similar to CdS NCs, monodisperse sub-3 nm ZnS and MnS could also be synthesized by solid state grinding of corresponding metal-octanethiolate with C_8DTCA-OlAm. The PXRD patterns of the purified materials are presented in Figure 4.7a, where ZnS NCs featured with zinc blend structure (Figure 4.7a JCPDF no-05-0566) and MnS NCs with hexagonal structure (Figure 4.7a JCPDS Card No. 40-1289) could be seen. The photoluminescence spectra of ZnS and MnS NCs are plotted in Figure 4.7c and both show sharp bandgap emission at 410 nm (for ZnS NCs, red lines) and 480 nm (for MnS NCs, blue lines). TEM images of these materials are presented in Figure

4.7f (ZnS NCs) and Figure 4.7g (MnS NCs) and their average sizes are deduced to be 2.19 ± 0.54 nm (for ZnS) and 5.65 ± 1.36 nm (for MnS) (size distribution plots of ZnS and MnS NCs are showed in Annexure Chapter 4 Figure A.C.4.4f and Figure A.C.4.4g respectively).

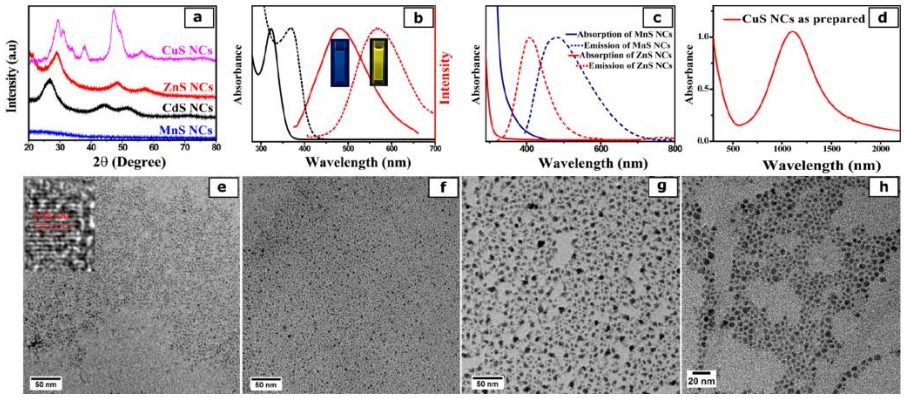

Figure 4.7 a) PXRD of different metal sulfide NCs, UV-Vis. and Photoluminescence (PL) spectra of b) CdS; two different sized CdS, c) ZnS (red solid line (absorbance) and red dotted line (PL)) and MnS ((blue solid line (absorbance) and blue dotted line for (PL)). TEM images of metal sulfide NCs of e) CdS; inset HRTEM of CdS NCs, f) ZnS and g) MnS and h) CuS NCs.

We next moved to the preparation of CuS plasmonic NCs. Copper sulfide is a p-type semiconductor with a direct band-gap (E_g) that depends on its stoichiometry and crystal phase (1.1−2.0 eV).[39-42] Its suitable band gap, low toxicity, and high absorbance coefficient make it a promising absorber material for optoelectronic[43] applications such as NIR optical switches and future photovoltaic devices.[44,45] CuS NCs possess highly tunable localized surface plasmon resonances (LSPR) in the near-infrared (NIR) spectral region, making it one of the most sought after materials. The LSPR in copper chalcogenide nanomaterials originates from excess holes in the top of the valence band, which are compensated by Cu^+ deficiencies in the lattice.[46,47] We found that the room temperature solid state grinding of copper (I) octanethiolate (Cu-C_8S) with C_8DTCA-OlAm (in air) produces nearly monodispersed covellite CuS NCs. PXRD pattern of as prepared purified CuS NCs shown in Figure 4.7a clearly matches with the CuS with covellite structure (JCPDS card no. 00-006-0464) and TEM images obtained from this sample (Figure 4.7h), display nearly monodispersed and spherical sized particles with the average particle size of 4.5±0.96 nm (size distribution plot

showed in Annexure Chapter 4 Figure A.C.4.4). The absorption spectra of as prepared samples (see Figure 4.7d) show that the CuS NCs exhibit sharp absorption in the NIR region at 1105 nm due to LSPR of free holes in the valence band of CuS NCs.

4.2.4 Characterization of metal selenide NCs

The PXRD pattern of the as synthesized and purified CdSe NCs clearly matched with the cubic CdSe structure (Figure 4.8a), which corresponds to JCPDSNo. # 91-0191. The absorption spectra of the as synthesized CdSe NCs obtained by the above method showed one sharp peak at 395 nm and one broad peak at 341 nm (Figure 4.8b−black solid line). This sample also displayed a strong emission in the visible region. The emission spectra (red solid line, Figure 4.8b) showed two peaks one at 415 nm (less intense) and one very broad peak at 560 nm (intense peak) with a FWHM of ∼185 nm and a Stokes shift of 165 nm with respect to the sharp absorption peak at 395 nm. As synthesized CdSe NCs shows intense greenish yellow color under UV lamp and photoluminescence spectra indicates that the emission is purely trap state emission as the high intense emission peak positioned at 565 nm has a high Stokes shift value (∼165 nm) and the first peak at 415 nm (band gap emission) has a stokes shift of 20 nm only and is of significantly less intensity.

This clearly indicates that the as prepared cubic CdSe NCs are featured with trap state emission. This may be due to surface defects or crystal defects as the materials were synthesised in open air atmosphere at room temperature. Quite gratifyingly, these defects could be reduced and crystal structure also can be transferred to hexagonal system by simply heating the as prepared materials in a high boiling solvent with oleicacid. When the cubic CdSe NCs, prepared by solid state (with Cd: Se= 4: 1 molar ratio) were heated at 140 °C under argon atmosphere, it got transformed to hexagonal system. This could be confirmed by the changes in PXRD patterns as shown in Figure 4.8c. Here the cubic CdSe structure (Figure 4.8a), corresponding JCPDS No. # 91-0191 is featured with peaks at 2θ values of 25.10°, 41.7° and 49.29° indexed to the (111), (220) and (311) planes respectively.On the other hand the hexagonal CdSe shows two extra peaks at 34.9° and 45.5° that can be indexed to the (102) and (103) planes (Figure 4.8c corresponding JCPDS No. # 08-0459). The absorption and emission spectra of the CdSe NCs after heating are presented in Figure 4.8d. It is very

clear that the excitonic peak got red shifted (from 395 nm to 490 nm) upon heating (Figure 4.8b).

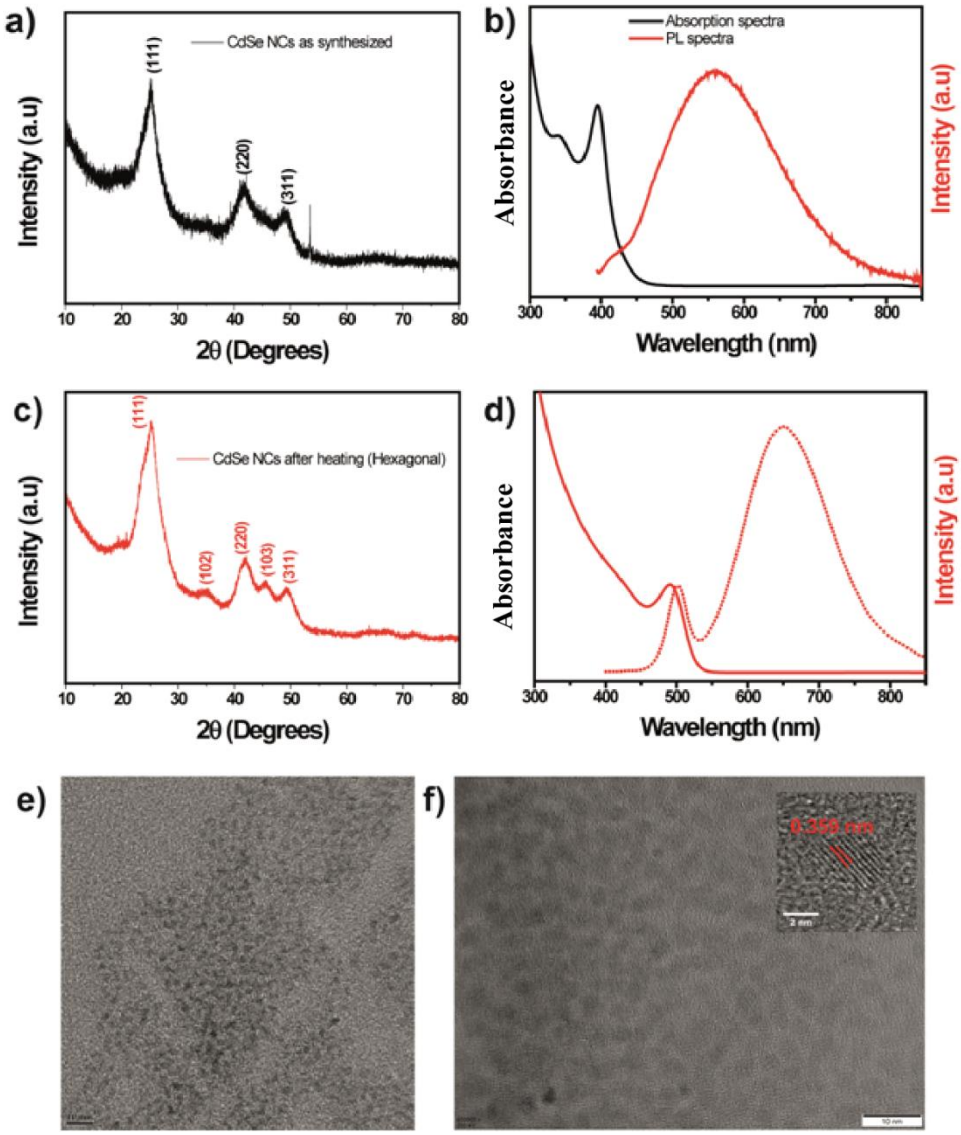

Figure 4.8 a) PXRD of as synthesised CdSe NCs; b) absorption (black) and emission spectra (red) of as synthesised CdSe NCs; c) PXRD of CdSe NCs after heating; d) optical properties of CdSe NCs after heating, absorption spectra (red solid line) and emission spectra (red dotted line); TEM images of CdSe NCs e) as synthesised and f) those after heating, Inset HRTEM image of CdSe after heating.

As mentioned previously, the emission spectra of as synthesised CdSe NCs showed two peaks one broad peak at 415 nm (less intense, where FWHM could not be calculated) and one very broad peak at 560 nm (intense peak) with a FWHM of ~185

nm and a Stokes shift of 165 nm (Figure 4.8.b). The emission spectra of the CdSe NCs after heating with oleic acid at 140°C showed in Figure 4.8d (red dotted line) display a sharp band edge emission peak at 505 nm with a FWHM of 36 nm and a Stokes shift of 15 nm only along with a comparatively low intense broad peak at 650 nm which clearly suggests the reduction of surface defects possibly due to the improved crystallinity as well as reducing the surface dangling bonds. TEM images of CdSe NCs shown in Figure 4.8e (as synthesised) and Figure 4.8f (after heating), clearly point to the monodispersity of the sample. The average particle size of CdSe NCs as synthesised is deduced to be 1.8 nm and after heating to the average size changed to 3.5 nm. The lattice fringes value 0.36 nm shown in inset of the Figure 4.8f, correspond to the (103) plane of the hexagonal CdSe NCs.

Interestingly, we could also tune the particle size and absorption spectra by varying the Cd-precursor to Se-precursor molar ratio at room temperature by grinding them under open atmospheric conditions. The absorption spectra of CdSe NCs obtained at different Cd: Se ratios are plotted in Figure 4.9a. It can be clearly seen that each of the sample displays well-defined excitonic peak and the peak position varied gradually from 418 to 434 nm as the Cd: Se precursor's molar stoichiometry ratio is varied in the range 2:1 to 1:1. It can be noticed that as the Se- precursors concentration is increased the first excitonic peak position gets red-shifted, indicating formation of larger sized NCs. Although, absorption spectral position of CdSe NCs prepared by different Cd: Se molar ratio gets red shifted and the emission spectra also shows intense broad peak with slight red shifted from 580 nm to 620 nm with the Cd: Se molar ratio change (Figure 4.9b). Figure 4.9c and 4.9d, the TEM images of as synthesized CdSe NCs synthesized at different Cd: Se ratio, are presented which clearly point to the monodispersity in their sizes and the average sizes of different CdSe NCs are 2.2 nm (when Cd: Se=2:1; Figure 4.9c) and 2.8 nm (when Cd: Se=1:1; figure 4.9d). It may be noted that if needed we can reduce the defects in these NCs also by heating them in a high boiling solvent under inert atmosphere.

Interestingly, this is a generic method for the synthesis of a series of metal selenide NCs. Similar to CdSe NCs, nearly monodisperse Ag_2Se, PbSe, CuSe and ZnSe NCs could also be synthesized by solid state grinding of corresponding metal thiolate with Se-precursor solution. The PXRD patterns of these materials are shown in Annexure

Chapter 4 Figure A.C.4.6. TEM images of these materials are presented in Figure 4.10a (Ag_2Se NCs), Figure 4.10b (PbSe NCs), Figure 4.10c (CuSe NCs) and Figure 4.10d (ZnSe NCs) and their average sizes are deduced to be 9 nm (for Ag_2Se), 5.5 nm (for PbSe), 4.5 nm (for CuSe) and 1.5 nm (for ZnSe) respectively. The as synthesised PbSe and Ag_2Se NCs did not show any characteristic absorption and emission peaks. This may be due to surface defects but CuSe NCs shows characteristic broad plasmonic peak at ~2000nm (please see the inset of the Figure 4.10c) and also ZnSe NCs shows sharp emission peak at ~422 nm (please see the inset of 4.10d)with a FWHM of ~87 nm.

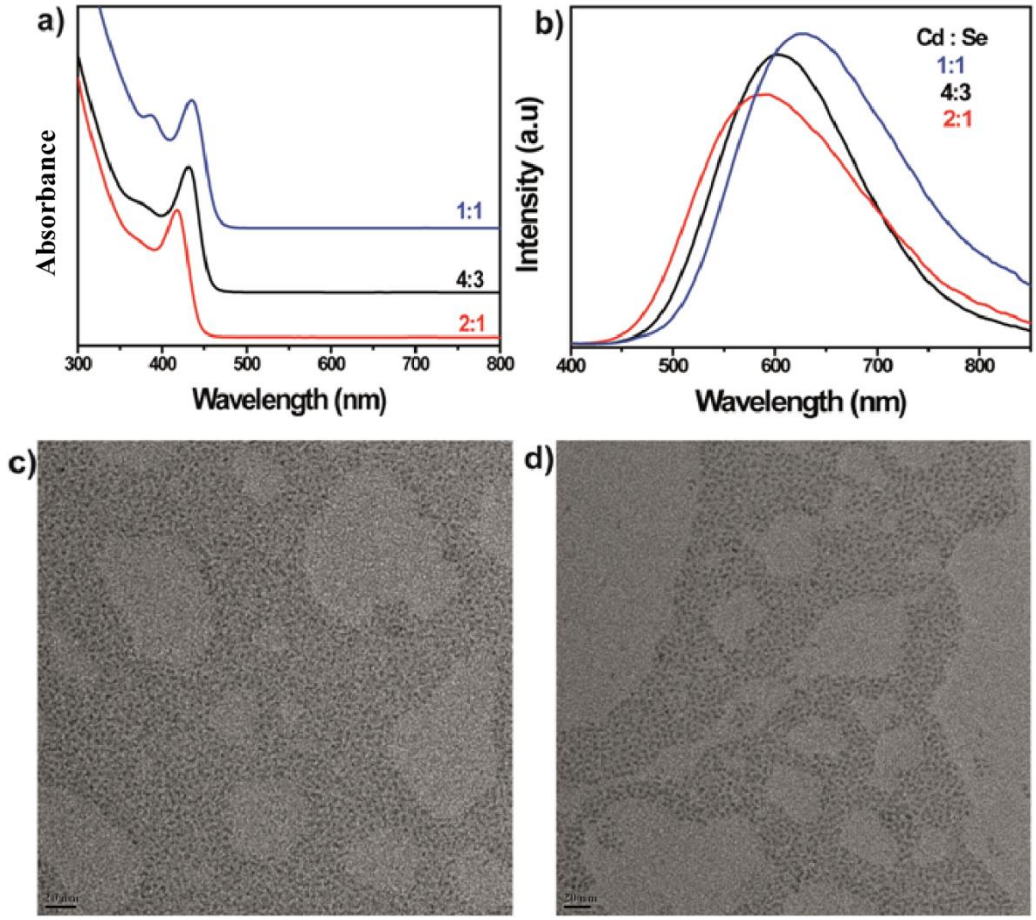

Figure 4.9 a) absorption spectra and b) emission spectra of as synthesised CdSe NCs with different Cd: Se precursor molar ratio, TEM images of CdSe NCs with different Cd: Se precursor molar ratio c) Cd: Se 2:1 and d) Cd: Se 1:1. Both cases scale bar is 20 nm.

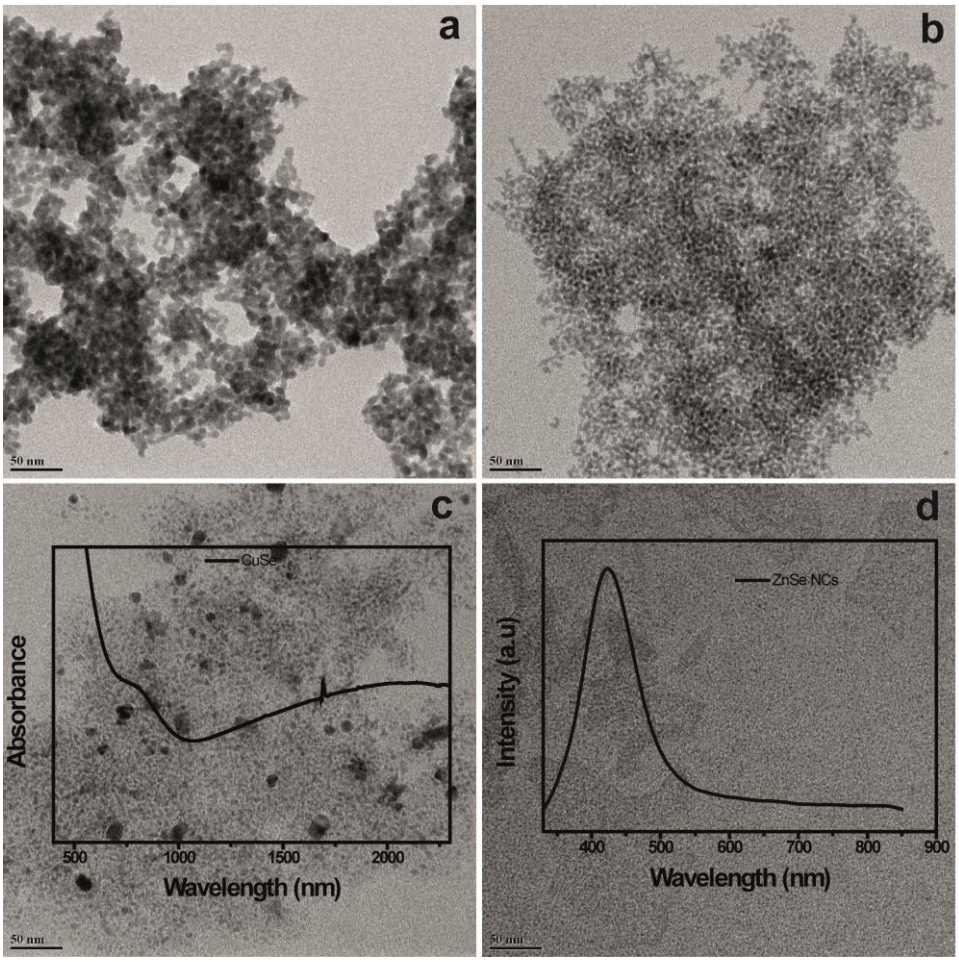

Figure 4.10 TEM images of other metal selenides NCs; a) Ag_2Se, b) PbSe, c) CuSe and inset shows absorption spectra of as synthesised CuSe NCs, d) ZnSe and inset shows emission spectra of ZnSe NCs. All TEM images scale bar is 50 nm.

4.2.5 How can NCs be synthesized by solid state grinding? Understanding the mechanism

4.2.5.1 Metal NCs

The solid state grinding of Ag-octanethiolate (Ag-C_8S) or Au-octanethiolate (Au-C_8S) with reducing agent sodium borohydride yields nearly monodispersed Ag and Au nanoparticle respectively. Sodium borohydride acts as a reducing agent and reduces the metal ions in the thiolates to their elemental form. This action would also involve a simultaneous generation of a stabilizing agent (alkane thiolate) *in situ*. We believe it is the presence of this thiolate that controls the growth of the metal crystals and stabilizes them in the nanosize regime.

4.2.5.2 Metal sulfide NCs

This chapter also discusses the utilization of metal thiolates as a precursor for the synthesis of metal sulfide NCs. The only difference here is that instead of adding a reducing agent a sulfur source is added so that metal sulfide NCs can be obtained. As mentioned above, the solid state grinding of Pb-C_8S or Ag-C_8S with C_8DTCA yields highly monodispersed PbS or Ag_2S which display excellent optical properties. In case of PbS, just varying the Pb: C_8DTCA ratio offered exceptional control over the particle size and size distributions that results in the tunability of absorption and emission band of these NCs (Figure 4.6c and 4.6d). This is very similar to that of hot injection based methods wherein with increase of metal: S ratio, excitonic peak was found to red shift with a concomitant peak broadening.[31,48,49]This raises the important question of what is actually happening during this procedure and how C_8DTCA reacts with metal thiolates during the grinding process. The C_8DTCA is a bidentate ligand and contains two sulfur atoms in a single molecule. It can easily bind with metal ions like Pb (II) and Ag (I) to form an M-C_8DTCA complex. So when we add C_8DTCA to a metal thiolate and grind them together two possible reactions can occur. One, formation of M-C_8DTCA complex, which decomposes to metal sulfide by grinding, two, the C_8DTCA molecules itself gets converted to thiourea while grinding and releases H_2S, which then reacts with metal thiolates (thiourea does not react with metal thiolates at room temperature) resulting in the formation of metal sulfides.

To gain more insights in to this aspect we recorded the ^{1}H NMR spectra of as prepared C_8DTCA and C_8DTCA after solid state grinding (at room temp. 25° C) which clearly revealed that this molecule remains intact and does not undergo any change by simple grinding (no extra peaks observed, please see in Annexure Chapter 4 Figure A.C.4.7 and Figure A.C.4.8). Therefore, we rule out the possibility that the H_2S species released by solid state grinding of pure C_8DTCA acting as sulfur source in the present case. The other possibility that we postulate as the reaction mechanism is as follows. While grinding of M-thiolate with C_8DTCA, the stronger bidentate ligand (C_8DTCA) first reacts with M-thiolate to form M-C_8DTCA complex. This contention is supported by the observation that pure yellow Pb-C_8S becomes deep orange colour when ground with C_8DTCA (the changes of PXRD pattern showed in Annexure Chapter 4 Figure A.C.4.9a-b). The unstable Pb-C_8DTCA complex

decomposes to PbS after further grinding as concluded from the observation that the orange Pb-C_8DTCA complex becomes brownish black upon further grinding. So, this clearly indicates that the path of metal sulfides NCs synthesis involves the formation of a metal-dithiocarbamic acid complex by solid state grinding with the concomitant release of an alkane thiolate and the decomposition of the metal-dithiocarbamate upon further grinding into a metal sulfide. These metal sulfide NCs are immediately protected by the alkane thiolate. It may be noted that while the solid state grinding of metal thiolate and C_8DTCA together is good enough to make many metal sulfide NCs, in some cases addition of small amount of oleylamine while grinding is necessary. For example, while the unstable M-C_8DTCA complexes like Pb-C_8DTCA yield PbS NCs, in case of metals like Cd, Mn, Zn and Cu they form highly stable M-C_8DTCA complexes which do not undergo complete decomposition by simple grinding itself at room temperature (25 ºC). This is supported by the PXRD pattern of the product obtained by the grinding of C_8DTCA with Cd-C_8S where a set of equidistant peaks ascribed to the formation of Cd-C_8DTCA complexes appear (along with the peaks corresponding to the Cd-C_8S Annexure Chapter 4 Figure A.C.4.10a). Interestingly even after prolonged grinding of the Cd-C_8S with C_8DTCA, though the entire Cd-C_8S converts to Cd-C_8DTCA complex the same does not readily decompose to CdS. This is supported by the fact that the PXRD patterns of the product obtained after prolonged grinding indicates the conversion of some Cd-C_8DTCA complex to CdS, but the maximum Cd-C_8DTCA remains intact, indicating its stability and resistance to decompose at room temperature (Annexure Chapter 4 Figure A.C.4.10b) by simple grinding. We suggest that the same must be happening with other M-C_8DTCA complexes like Mn, Zn and Cu. Quite satisfactorily, the resistance of such stable M-C_8DTCA complexes to decomposition could be overcome by simply adding a few µL of OlAm to C_8DTCA before grinding. It is well known that primary amines attack metal-dithiocarbamate complexes helping them to decompose faster and at lower temperature to metal sulfide when the reactions are carried out in solution state.[50,51] We believe that here also as the M-C_8S complexes are ground with C_8DTCA, the M-C_8DTCA complex forms first which is attacked by the OlAm present in the reaction milieu enhancing the decomposition rate of the M-C_8DTCA complex and ensues the formation good quality metal sulfide NCs (probable reaction mechanism showed in Annexure Chapter 4 Figure A.C.4.11).[51]

In case of metal selenide NCs, the Se-precursor solution readily reacts with the highly reactive metal ions present in the thiolates to form their metal selenides. This action would also involve a simultaneous generation of a stabilizing agent (alkyl thiolate anion) *in situ*. We believe it is the presence of this thiolate that controls the growth of the metal selenide crystals and stabilizes them in the nanosize regime.

4.2.6 Scalability of metal chalcogenide NC synthesis by solid state grinding

One of the most attractive features of the procedure we present here is the possibility to scale up by simply grinding larger amount of metal thiolates and C_8DTCA. For example, the optical properties of the product did not change much when the reaction was carried out between 0.5 mmol (250 mg) of PbC_8S and 0.25 mmol of C_8DTCA or if the reaction was carried out between 5 g (10 mmol) of PbC_8S and 5 mmol of C_8DTCA. In the former case the yield of PbS was 70 mg (yield 44%, based on Pb-C_8S used), while in latter case it was ~1.1 g (yield 35%, based on Pb-C_8S used). The optical spectral comparisons of these two samples are presented in Figure 4.11a. Similarly, almost 5 g of plasmonic CuS NCs (covellite phase) could be synthesized by this simple solid state grinding (optical spectra shown in Figure 4.11b).

4.2.7 Surface passivation of metal sulfide NCs

As mentioned previously, as most of the as prepared metal sulfides NCs are thiol capped/passivated, they could be easily dispersed in non-polar solvents. Such dispersions like the alkane thiol capped PbS NCs were stable for 5-7 days, after that the particles started to settle down. For better stability and better surface passivation, we had done dynamic ligand exchange with oleic acid at 50-60 °C (details ligand exchange procedure showed in experimental section 4.2.6). Quite satisfactorily, there was no difference in the absorbance spectra after ligand exchange with oleic acid, but emission intensity quite improved (may be due to proper surface passivation) without any change in the emission position. The characterization details like absorption, emission, FTIR, and TEM images of PbS NCs after and before ligand exchanged are shown in Annexure Chapter 4 Figure A.C.4.12. In a similar fashion, though the CdS NCs synthesized by the current method show trap state emission, the same could be minimized by simply heating the nanocrystal dispersion at 120-140°C in inert atmosphere with oleic acid and cadmium oleate.[52,53]

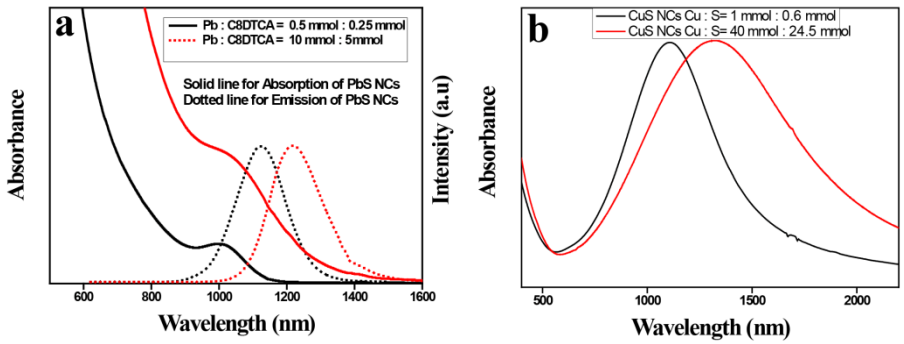

Figure 4.11: Scalability of metal sulfide NC synthesis by solid state grinding method. a) absorbance (solid line) and emission spectra (dotted line) of PbS NCs synthesized at different ~mmol scale. Black line represent 0.5 mmol of Pb-precursors and red line is the spectrum recorded from 10 mmolbatch. b) absorbance spectra of CuS NCs synthesized at different ~mmol scale. Black solid line represents 1 mmol of Cu-precursors and red solid line is for 40 mmol batch.

Another strategy that is routinely followed in literature to reduce the trap state density is known as hybrid passivation strategy.[33] Briefly, this hybrid passivation strategy involves introducing halide anions and metal cations during the synthesis and was shown to be effective in removing surface trap states within the bandgap. It is reported that metal cation will go and bind to the exposed sulfur atoms on the surface in submonolayer quantities and the halide anions passivate the surfaces where organic ligands are unable to reach due to steric hindrance or unfavourable surface topology. In order to check whether the metal sulfide NCs prepared by the solid state grinding could also be subjected to such hybrid passivation strategy, we added the $CdCl_2$ in a mixture of tetradecylphosphonic acid (TDPA) and oleyl amine to the metal sulfides obtained by the solid state grinding procedure described above (following the reported procedure).[33] The PXRD pattern in case of PbS after this surface passivation is shown in Annexure Chapter 4 Figure A.C.4.13 which is exactly similar to the as-prepared PbS NCs indicating that the $CdCl_2$ passivated the surface only and had not formed any core-shell type material.[33] As expected, the absorbance spectra of surface passivated material slightly shifted towards red and absorption coefficient also increased hugely. The emission spectra also shifted towards red and FWHM of emission peak also improved (to 128 nm from 161 nm). Similarly, the quantum yield also increased from

40% to 52% (for absorbance and PL spectra please see in Annexure Chapter 4 Figure A.C.4.14).

4.3 Summary and leads for the next chapter

In summary, we have developed a the generic solvent-less solid state synthesis for the preparation of metallic and metal sulfide nanocrystals by employing same single source precursor (metal thiolates) as metal source. We have developed a very useful air stable reactive sulphur source called octyl ammonium octyldithiocarbamate and utilised it here in the solid state synthesis of various metal sulfide nanocrystals. The materials synthesized by these solid state routes could be re-dispersed as desired in non-polar organic solvents and displayed very good structural characteristics and optical properties. The optical properties of the metal sulfide nanocrystals could further be improved by ligand exchange and hybrid passivation strategies if necessary.

The successful implementation of a solid state grinding method to prepare metal sulfide NCs of PbS, CdS and ZnS lead to a very interesting but yet highly challenging question –can this be extended to the synthesis of ternary system like $CuInS_2$, $AgInS_2$ and $AgBiS_2$ nanocrystals?

It may be noted that for such bimetallic sulfide NC synthesis, we need two metals and for this we may have to use bimetallic thiolates as precursors. Our literature search indicated that the synthesis of such bimetallic thiolates is not well explored (no reports as far as we could see). Therefore, it would be even more interesting to prepare such bimetallic thiolates and understand their structure and properties. Subsequently we could also try them as single source precursors of the prepared bimetallic sulfide and selenide NCs by the solid state grinding methods. The results of our experiments in this direction are included in the next chapter.

4.4 References

1. Wang, Y.; Xia, Y. Bottom-up and top-down approaches to the synthesis of monodispersed spherical colloids of low melting-point metals. *Nano Lett.* **2004,***4*, 2047-2050.

2. Li, W.; Zheng, G.; Yang, Y.; Seh, Z. W.; Liu, N.; Cui, Y. High-performance hollow sulfur nanostructured battery cathode through a scalable, room temperature, one-step, bottom-up approach. *PNAS* **2013,***110*, 7148-7153.
3. Hoeppener, S.; Maoz, R.; Cohen, S. R.; Chi, L.; Fuchs, H.; Sagiv, J. Metal Nanoparticles, Nanowires, and Contact Electrodes Self-Assembled on Patterned Monolayer Templates—A Bottom-up Chemical Approach. *Adv. Mater.* **2002,***14*, 1036-1041.
4. Acharya, S.; Das, B.; Thupakula, U.; Ariga, K.; Sarma, D.; Israelachvili, J.; Golan, Y. A bottom-up approach toward fabrication of ultrathin PbS sheets. *Nano Lett.* **2013,***13*, 409-415.
5. Debnath, D.; Kim, S. H.; Geckeler, K. E. The first solid-phase route to fabricate and size-tune gold nanoparticles at room temperature. *J. Mater. Chem.* **2009,***19*, 8810-8816.
6. Murugadoss, A.; Kai, N.; Sakurai, H. Synthesis of bimetallic gold–silver alloy nanoclusters by simple mortar grinding. *Nanoscale* **2012,***4*, 1280-1282.
7. Rao, T. U. B.; Nataraju, B.; Pradeep, T. Ag_9 quantum cluster through a solid-state route. *J. Am. Chem. Soc.* **2010,***132*, 16304-16307.
8. Malca, M. Y.; Bao, H.; Bastaille, T.; Saadé, N. K.; Kinsella, J. M.; Friščić, T.; Moores, A. Mechanically activated solvent-free assembly of ultrasmall Bi_2S_3 nanoparticles: A novel, simple, and sustainable means to access chalcogenide nanoparticles. *Chem. Mater.* **2017,***29*, 7766-7773.
9. Wang, W.; Liu, Z.; Zheng, C.; Xu, C.; Liu, Y.; Wang, G. Synthesis of CdS nanoparticles by a novel and simple one-step, solid-state reaction in the presence of a nonionic surfactant. *Mater. Lett.* **2003,***57*, 2755-2760.
10. Chawla, P.; Sharma, G.; Lochab, S.; Singh, N. Photoluminescence and optical characterization of CdS nanoparticles prepared by solid-state method at low temperature. *Radiation Effects & Defects in Solids* **2009,***164*, 755-762.
11. Liu, J.; Cao, J.; Li, Z.; Ji, G.; Deng, S.; Zheng, M. Low-temperature solid-state synthesis and phase-controlling studies of CdS nanoparticles. *J. Mater. sci.* **2007,***42*, 1054-1059.

12. Liu, J.; Zhao, C.; Li, Z.; Chen, J.; Zhou, H.; Gu, S.; Zeng, Y.; Li, Y.; Huang, Y. Low-temperature solid-state synthesis and optical properties of CdS–ZnS and ZnS–CdS alloy nanoparticles. *J. Alloys Compd.* **2011,***509*, 9428-9433.
13. Wang, W.; Liu, Y.; Zhan, Y.; Zheng, C.; Wang, G. A novel and simple one-step solid-state reaction for the synthesis of PbS nanoparticles in the presence of a suitable surfactant. *Mater. Res. Bull.* **2001,***36*, 1977-1984.
14. Liu, Q.; Ni, Y.; Yin, G.; Hong, J.; Xu, Z. High yield synthesis of PbS nanocubes using one-step solid-state reaction in the presence of an anionic surfactant. *Mater. Chem. Phys.* **2005,***89*, 379-382.
15. Busupalli, B.; Kummara, S.; Kumaraswamy, G.; Prasad, B. L. Ultrathin sheets of metal or metal sulfide from molecularly thin sheets of metal thiolates in solution. *Chem. Mater.* **2014,***26*, 3436-3442.
16. Dance, I. G.; Fisher, K. J.; Banda, R. H.; Scudder, M. L. Layered structure of crystalline compounds silver thiolates (AgSR). *Inorg. Chem.* **1991,***30*, 183-187.
17. Ye, Z.; Lito, P.; Efremov, M. Y.; Zuo, J.-M.; Allen, L. H. Approaching the size limit of organometallic layers: synthesis and characterization of highly ordered silver–thiolate lamellae with ultra-short chain lengths. *Dalton Trans.* **2016,***45*, 18954-18966.
18. Bensebaa, F.; Ellis, T. H.; Kruus, E.; Voicu, R.; Zhou, Y. Characterization of self-assembled bilayers: Silver− alkanethiolates. *Langmuir* **1998,***14*, 6579-6587.
19. Parikh, A.; Gillmor, S.; Beers, J.; Beardmore, K.; Cutts, R.; Swanson, B. Characterization of chain molecular assemblies in long-chain, layered silver thiolates: a joint infrared spectroscopy and X-ray diffraction study. *J. Phys. Chem. B* **1999,***103*, 2850-2861.
20. Cha, S.-H.; Kim, J.-U.; Kim, K.-H.; Lee, J.-C. Preparation and photoluminescent properties of gold (I)− alkanethiolate complexes having highly ordered supramolecular structures. *Chem. Mater.* **2007,***19*, 6297-6303.
21. Cha, S.-H.; Kim, K.-H.; Kim, J.-U.; Lee, W.-K.; Lee, J.-C. Thermal Behavior of Gold (I)− Thiolate Complexes and Their Transformation into Gold Nanoparticles under Heat Treatment Process. *J. Phys. Chem. C* **2008,***112*, 13862-13868.

22. Bhuvana, T.; Boley, W.; Radha, B.; Dolash, B.; Chiu, G.; Bergstrom, D.; Reifenberger, R.; Fisher, T.; Kulkarni, G. Inkjet printing of palladium alkanethiolates for facile fabrication of metal interconnects and surface-enhanced Raman scattering substrates. *Micro & Nano Lett.* **2010,***5*, 296-299.
23. Luo, Z.; Yuan, X.; Yu, Y.; Zhang, Q.; Leong, D. T.; Lee, J. Y.; Xie, J. From aggregation-induced emission of Au (I)–thiolate complexes to ultrabright Au (0)@ Au (I)–thiolate core–shell nanoclusters. *J. Am. Chem. Soc.* **2012,***134*, 16662-16670.
24. Nakamoto, M.; Yamamoto, M.; Fukusumi, M. Thermolysis of gold (I) thiolate complexes producing novel gold nanoparticles passivated by alkyl groups. *Chem. Comm.* **2002,** 0, 1622-1623.
25. Rosemary, M.; Pradeep, T. Solvothermal synthesis of silver nanoparticles from thiolates. *J. Colloid Interface Sci.* **2003,***268*, 81-84.
26. Sagade, A. A.; Radha, B.; Kulkarni, G. Intricate nature of Pd nanocrystal–hydrogen interaction investigated using thermolysed Pd hexadecylthiolate films. *Sens. Actuators B: Chem.* **2010,***149*, 345-351.
27. Rohner, C.; Pekkari, A.; Härelind, H.; Moth-Poulsen, K. Synthesis of Cu nanoparticles: Stability and conversion into Cu_2S nanoparticles by decomposition of alkanethiolate. *Langmuir* **2017,***33*, 13272-13276.
28. Zhuang, Z.; Lu, X.; Peng, Q.; Li, Y. A facile "dispersion–decomposition" route to metal sulfide nanocrystals. *Chem. A Eur. J.* **2011,***17*, 10445-10452.
29. van Embden, J.; Chesman, A. S.; Jasieniak, J. J. The heat-up synthesis of colloidal nanocrystals. *Chem. Mater.* **2015,***27*, 2246-2285.
30. Larsen, T. H.; Sigman, M.; Ghezelbash, A.; Doty, R. C.; Korgel, B. A. Solventless synthesis of copper sulfide nanorods by thermolysis of a single source thiolate-derived precursor. *J. Am. Chem. Soc.* **2003,***125*, 5638-5639.
31. Bera, A.; Mandal, D.; Goswami, P. N.; Rath, A. K.; Prasad, B. L. A generic and scalable method for the preparation of monodispersed metal sulfide nanocrystals with tunable optical properties. *Langmuir* **2018**, *34*, 5788-5797.
32. Liu, Y.; Yao, D.; Shen, L.; Zhang, H.; Zhang, X.; Yang, B. Alkylthiol-enabled Se powder dissolution in oleylamine at room temperature for the phosphine-free synthesis of copper-based quaternary selenide nanocrystals. *J. Am. Chem. Soc*. **2012**, *134*, 7207-7210.

33. Yuan, M.; Kemp, K. W.; Thon, S. M.; Kim, J. Y.; Chou, K. W.; Amassian, A.; Sargent, E. H. High-performance quantum-dot solids via elemental sulfur synthesis. *Adv. Mater.* **2014,***26*, 3513-3519.
34. Bera, A.; Busupalli, B.; Prasad, B. L. Solvent-less solid state synthesis of dispersible metal and semiconducting metal sulfide nanocrystals. *ACS Sustain. Chem. Eng*. **2018**, *6*, 12006-12016.
35. Chakraborty, I.; Erusappan, J.; Govindarajan, A.; Sugi, K.; Udayabhaskararao, T.; Ghosh, A.; Pradeep, T. Emergence of metallicity in silver clusters in the 150 atom regime: a study of differently sized silver clusters. *Nanoscale* **2014,***6*, 8024-8031.
36. Du, T.; Liang, J.; Dong, N.; Lu, J.; Fu, Y.; Fang, L.; Xiao, S.; Han, H. Glutathione-Capped Ag_2S Nanoclusters Inhibit Coronavirus Proliferation through Blockage of Viral RNA Synthesis and Budding. *ACS Appl. Mater. Interfaces* **2018,***10*, 4369-4378.
37. Cant, D. J.; Syres, K. L.; Lunt, P. J.; Radtke, H.; Treacy, J.; Thomas, P. J.; Lewis, E. A.; Haigh, S. J.; O'Brien, P.; Schulte, K. Surface properties of nanocrystalline PbS films deposited at the water–oil interface: a study of atmospheric aging. *Langmuir* **2015,***31*, 1445-1453.
38. Laajalehto, K.; Kartio, I.; Nowak, P. XPS study of clean metal sulfide surfaces. *Appl. Surface science* **1994,***81*, 11-15.
39. van der Stam, W.; Berends, A. C.; de Mello Donega, C. Prospects of colloidal copper chalcogenide nanocrystals. *Chem. Phys. Chem.* **2016,***17*, 559-581.
40. Wang, F.; Li, Q.; Lin, L.; Peng, H.; Liu, Z.; Xu, D. Monodisperse copper chalcogenide nanocrystals: controllable synthesis and the pinning of plasmonic resonance absorption. *J. Am. Chem. Soc.* **2015,***137*, 12006-12012.
41. Luther, J. M.; Jain, P. K.; Ewers, T.; Alivisatos, A. P. Localized surface plasmon resonances arising from free carriers in doped quantum dots. *Nat. Mater.* **2011,***10*, 361-366.
42. Zhao, Y.; Pan, H.; Lou, Y.; Qiu, X.; Zhu, J.; Burda, C. Plasmonic $Cu_{2-x}S$ nanocrystals: optical and structural properties of copper-deficient copper (I) sulfides. *J. Am. Chem. Soc.* **2009,***131*, 4253-4261.

43. Su, Y.; Lu, X.; Xie, M.; Geng, H.; Wei, H.; Yang, Z.; Zhang, Y. A one-pot synthesis of reduced graphene oxide–Cu_2S quantum dot hybrids for optoelectronic devices. *Nanoscale* **2013,***5,* 8889-8893.
44. Yu, X. L.; Cao, C. B.; Zhu, H. S.; Li, Q. S.; Liu, C. L.; Gong, Q. H. Nanometer-Sized Copper Sulfide Hollow Spheres with Strong Optical-Limiting Properties. *Adv. Func. Mater.* **2007,***17,* 1397-1401.
45. Wu, Y.; Wadia, C.; Ma, W.; Sadtler, B.; Alivisatos, A. P. Synthesis and photovoltaic application of copper (I) sulfide nanocrystals. *Nano Lett.* **2008,***8,* 2551-2555.
46. Dorfs, D.; Härtling, T.; Miszta, K.; Bigall, N. C.; Kim, M. R.; Genovese, A.; Falqui, A.; Povia, M.; Manna, L. Reversible Tunability of the Near-Infrared Valence Band Plasmon Resonance in Cu_{2-x} Se Nanocrystals. *J. Am. Chem. Soc.* **2011,***133,* 11175-11180.
47. Kriegel, I.; Scotognella, F.; Manna, L. Plasmonic doped semiconductor nanocrystals: Properties, fabrication, applications and perspectives. *Phys. Rep.* **2017,***674,* 1-52.
48. Hines, M. A.; Scholes, G. D. Colloidal PbS nanocrystals with size-tunable near-infrared emission: observation of post-synthesis self-narrowing of the particle size distribution. *Adv. Mater.* **2003,***15,* 1844-1849.
49. Weidman, M. C.; Beck, M. E.; Hoffman, R. S.; Prins, F.; Tisdale, W. A. Monodisperse, air-stable PbS nanocrystals via precursor stoichiometry control. *ACS Nano* **2014,***8,* 6363-6371.
50. Hollingsworth, N.; Roffey, A.; Islam, H.-U.; Mercy, M.; Roldan, A.; Bras, W.; Wolthers, M.; Catlow, C. R. A.; Sankar, G.; Hogarth, G. Active nature of primary amines during thermal decomposition of nickel dithiocarbamates to nickel sulfide nanoparticles. *Chem. Mater.* **2014,***26,* 6281-6292.
51. Jung, Y. K.; Kim, J. I.; Lee, J.-K. Thermal decomposition mechanism of single-molecule precursors forming metal sulfide nanoparticles. *J. Am. Chem. Soc.* **2009,***132,* 178-184.
52. Kim, J. I.; Kim, J.; Lee, J.; Jung, D.-R.; Kim, H.; Choi, H.; Lee, S.; Byun, S.; Kang, S.; Park, B. Photoluminescence enhancement in CdS quantum dots by thermal annealing. *Nanoscale Res. Lett.* **2012,***7,* 482.

53. Torimoto, T.; Ogawa, S.; Adachi, T.; Kameyama, T.; Okazaki, K.-i.; Shibayama, T.; Kudo, A.; Kuwabata, S. Remarkable photoluminescence enhancement of ZnS–AgInS 2 solid solution nanoparticles by post-synthesis treatment. *Chem. Comm.* **2010,***46*, 2082-2084.

Chapter 5

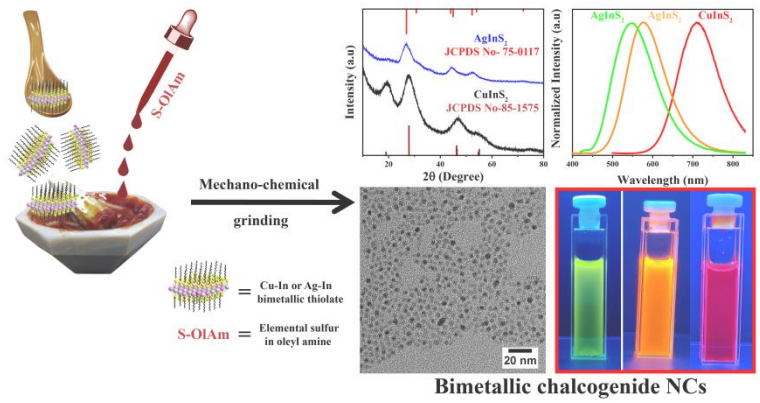

Bimetallic chalcogenide NCs

This chapter presents the preparation of two bimetallic thiolates, namely, copper-indium thiolate and silver-indium thiolate. The results of the synthesis and characterization of these bimetallic thiolates and their utilization for the preparation of bimetallic chalcogenide NCs by mechano-chemical grinding ($AgInS_2$, $CuInS_2$, as well as $AgInSe_2$ and $CuInSe_2$ NCs) are incorporated in this chapter.

5.1 Introduction

We have already discussed in the previous chapters that binary metal thiolates could be used as precursors for the preparation of monolayer protected metal chalcogenide nanocrystals (NCs) via thermolysis method or solid state grinding method using different chalcogen sources.[1,2] In this background, we thought it would be highly beneficial if we could extend these procedures and prepare bimetallic NCs or bimetallic chalcogenide NCs especially by solid state grinding method. We felt that this could be only realised if we can get access to bimetallic thiolates. However, we noticed that no reports exist as far as the preparation, isolation and characterization of bimetallic thiolates.

It may be noted that the structures of many single metal thiolates have been characterized in detail and it has been established that they consist of a network of metal ions covalently linked to sulfur atoms of the alkyl thiolate anion (Scheme A and B were shown in Figure 5.1).[3-11] Quite interestingly while few of these metal thiolates get de-laminated into individual sheets (eg. Pd-alkyl thiolate, Ni-alkyl thiolate, Pb-alkyl thiolate)[10] when a non-polar solvent is added, many others are quite insoluble (Ag-alkyl thiolate, Cu-alkyl thiolate, Au-alkyl thiolate) in these solvents under normal circumstances.[2]

In this premise it would be pertinent to ask (i) would it be possible to prepare metal thiolates consisting of two metal ions? (ii) what would be the bulk structure of such bimetallic thiolates? and (iii) whether they can be used as precursors for the preparation of bimetallic sulfide NCs? Here, the second question assumes greater significance because one can envisage three different structural scenarios. The first one is the formation of a segregated/mixed stack where both metal thiolates exist as separate non-interacting individual lamellar sheets and the final materials is nothing but a physical mixture of the individual thiolates (Scheme 1C, was shown in Figure 5.1). The second possibility is an alternating stacks where one individual metal thiolate sheet is above the second one forming an A-B-A-B type structure (Scheme 1D, was shown in Figure 5.1). The third and final possibility is a structure where both metal ions are intricately mixed and are present in each sheet of the lamellar structure (Scheme 1E, was shown in Figure 5.1).

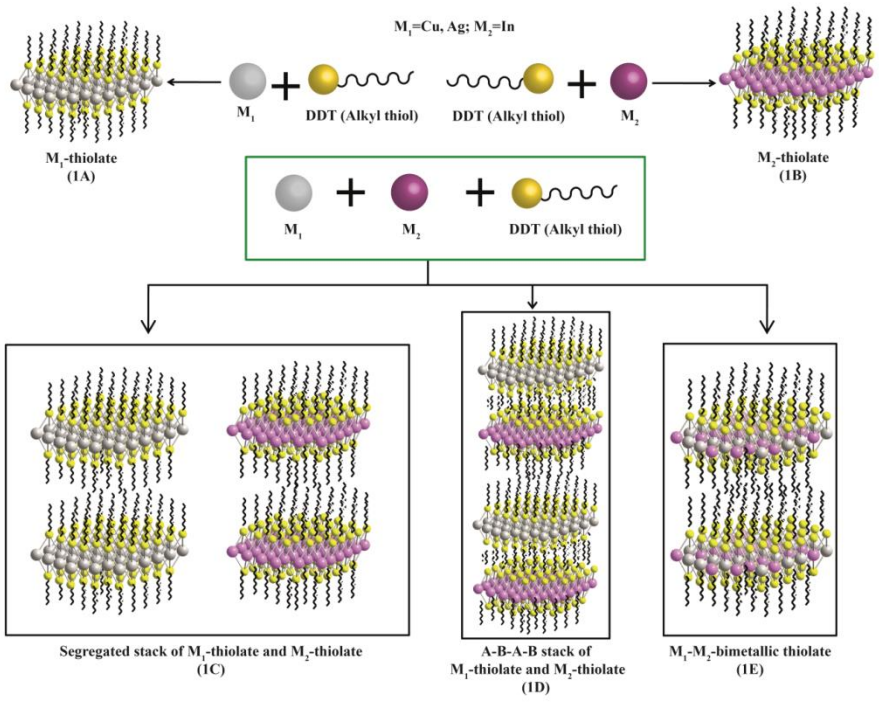

Figure 5.1 Plausible structures of the metal thiolates. 1A) M_1-thiolate, 1B) M_2-thiolate, 1C) mixture of M_1-thiolate and M_2-thiolate (mixed stack), 1D) Alternating stacks of M_1-thiolate and M_2-thiolate (2D Heterostructure) and 1E) M_1-M_2-bimetallic thiolate where each sheet contains both the metal ions.

To find answers to above listed questions and to see whether these bimetallic thiolates could be used as precursors for the solid state synthesis of bimetallic sulfides/selenides we started our work by preparing two of them, namely, copper-indium thiolate and silver-indium thiolate. The results of the synthesis and characterization of the above bimetallic thiolates and their utilization for the preparation of bimetallic sulfide NCs ($AgInS_2$, $CuInS_2$, as well as $AgInSe_2$ and $CuInSe_2$ NCs) are incorporated in this chapter. Our results clearly suggest these bimetallic thiolates are featured with structures of the third type (each sheet consisting of both the metal ions) described above (Scheme 1E, Figure 5.1). Quite satisfyingly, these bimetallic thiolates turned out to be excellent single source precursors for the preparation of $AgInS_2$, $CuInS_2$, as well as $AgInSe_2$ and $CuInSe_2$ NCs by simple mechano-chemical grinding. Even more satisfying was the fact that these bimetallic chalcogenide NCs displayed good optical properties which could further be enhanced by just simply heating them or by passivating them with ZnI_2. Such post synthetic

passivation is a commonly practiced technique to reduce the anionic surface defects and improve the optical properties of binary and ternary metal chalcogenide NCs even when they are prepared by the high-temperature solvent based methods.[12-14] Indeed after surface passivation, the $CuInS_2$ NCs displayed a relative quantum yield (QY) of 60% (compared to a mere ~1% QY in the as prepared materials) and in case of $AgInS_2$ NCs the QY enhanced up to 85% from 30%.

5.1.1 Experimental section

Chemicals required:

1-Dodecanethiol ($C_{12}H_{25}SH$), 1-octadecene, oleyl amine, and oleic acid were purchased from Sigma Aldrich and were used as received. Cuprous (I) bromide, Cuprous (I) iodide, Silver (I) iodide, Zinc iodide and Indium acetate were purchased from Sigma Aldrich. Solvents such as acetone, methanol, ethanol and toluene etc were also purchased from Merck Chemicals and were used as received.

5.1.1.1 Reaction 5.A: Preparation of bimetallic thiolates

About 0.5 mmol of metal salt A^+ and metal salt B^{3+} (where A=Cu and Ag, B=In^{3+}) were taken together in mortar and ground well with pestle to get uniform mixture of fine powder. To this uniformly mixed powder, about 200 µL of oleyl amine was added and they were ground well to get a homogeneous thick paste. To this homogeneous thick paste about 400 µL of 1-DDT was added stepwise (200 µL in each step) and ground thoroughly which resulted in the formation of bimetallic thiolates.

Note 1: Copper (I) iodide or copper (I) bromide, Ag (I) iodide or Ag(I) acetate could be used as metal A^+ precursor and Indium (III) acetate was used as B^{3+} metal source.

Note 2: The reactivity of two different Cu(I) salts, Cu(I)I and Cu(I)Br are found to be different when alkyl thiol is added to them. Here while Cu(I)Br directly reacts with alkyl thiol and converts to the corresponding metal thiolate, Cu(I)I does not react with alkyl thiol directly at room temperature. So, for the copper-indium bimetallic thiolate preparation, the Cu(I) salts, either Cu(I)I or Cu(I)Br are first treated with oleyl amine resulting in the formation of a Cu-amine complex which was found to readily react with alkyl thiol to form copper-indium bimetallic thiolate at room temperature.

5.1.1.2 Reaction 5.B1: Preparation of sulfur precursor solution

About 35 mg of elemental S powder were taken in 2 mL Eppendorf tube and 100-200 µL of DDT was added into that. Subsequently 100-200 µL of oleyl amine was added to this and the mixture was shaken vigorously. Immediately a deep orange clear solution was observed and this solution was used for the preparation of bimetallic sulfide NCs. This sulfur precursor solution is referred to as S-OlAm complex in the rest of the manuscript.

5.1.1.2 Reaction 5.B2: Preparation of selenium precursor solution

The Se^{2-} precursor solution was prepared following reported procedures with slight modifications.[15] About 82 mg of elemental Se powder was taken in an Eppendorf tube and 200 µL of 1-DDT was added to it. Then 200 µL of OlAm was added to this mixture and immediately the color changed to deep brownish red in color. This solution was used for the preparation of bimetallic selenide NCs.

5.1.1.3 Reaction 5.C1: Synthesis of $CuInS_2$ (ternary) NCs

The copper-indium bimetallic thiolate paste was prepared as mentioned in reaction A. To this 0.4 mL (~1.1mmol) of S-precursor solution (prepared as detailed in reaction 5.B1) was added and this mixture was ground thoroughly using a mortar and pestle. After 2-4 mins the color of the mixture changed to deep brownish red indicating the formation of $CuInS_2$. Then few mL of toluene was added to this product mixture which led to the dispersion of $CuInS_2$ NCs in it. No unreacted metal thiolate was noticed after the reaction. These $CuInS_2$ NCs were separated/purified from the excess thiol and oleyl amine by adding acetone or methanol into the dispersion, followed by centrifugation and the extracted NCs were again dispersed in toluene. The purified $CuInS_2$ NCs were characterized by PXRD, UV-Vis spectroscopy, PL-spectra and TEM.

5.1.1.3 Reaction 5.C2: Synthesis of $AgInS_2$ (ternary) NCs

The silver-indium bimetallic thiolate paste was prepared as mentioned in reaction A and 0.4 mL (~1.1 mmol) of S-precursor solution (preparation details in reaction 5.B1) was added and this mixture was ground thoroughly using a mortar and pestle. After 2-

4 mins the color of the mixture changed to deep brownish black indicating the formation of $AgInS_2$. Then few mL of toluene was added to this product mixture which led to the dispersion of $AgInS_2$ NCs in it. No unreacted metal thiolate was noticed after the reaction. These $AgInS_2$ NCs were separated/purified from the excess thiol and oleyl amine by adding acetone or methanol into the dispersion, followed by centrifugation and the extracted NCs were again dispersed in toluene. The purified $AgInS_2$ NCs were characterized by PXRD, UV-Vis spectroscopy, PL-spectra and TEM.

5.1.1.3 Reaction 5.C3: Synthesis of ternary metal selenides NCs

Ternary metal selenides like $CuInSe_2$and $AgInSe_2$NCs also were synthesized by the same procedure mentioned above. The only change was instead of the sulfur precursor solution 0.4 mL (~1.1mmol) selenium precursor solution (as mentioned in reaction B2) was used here as a chalcogenide source.

5.1.1.4 Reaction 5.D1: Heating of the ternary metal chalcogenide NCs

The ternary metal chalcogenide NCs prepared by the grinding method were first purified by washing with acetone or ethanol and dispersion of such purified particles were taken in 3 neck RB flask along with oleic acid and 1-DDT and 1-octadecene as a solvent. Then the mixture was heated and degassed under vacuum at 90°C for 1-2 h. Then temperature was increased gradually and was kept at 120 °C for 30 min.

5.1.1.4 Reaction 5.D2: ZnI_2 passivation of ternary metal chalcogenide NCs

Z-type passivation of binary metal chalcogenide NC surfaces by metal halides like $CdCl_2$, $ZnCl_2$ and ZnI_2 via solution based methods is routinely practiced to remove the chalcogen related trap states and for enhancing the PL QY. The distinguishing feature of our work is that though the particles were initially prepared by mechano-chemical grinding with no involvement of any solvent, they also are amenable to solvent based surface modification leading to the betterment in their optical properties. Here for Z-type passivation by metal halides the ternary metal chalcogenide NCs prepared by the grinding method were first purified with washing and the dispersion of such purified particles was taken in 3 neck RB flask along with oleic acid, oleyl amine (or DDT)

and 1-octadecene as a solvent. Then the mixture was heated and degassed under vacuum at 90°C for 2 h. Then temperature was set at 100°C. 2 mmol of ZnI_2(~640 mg) was taken in another separate 3 neck RB flask along with 18 mL of 1-ODE and 2 mL of oleyl amine and heated, degassed under vacuum at 100 °C for 1 h and stored it as a stock solution at argon atmosphere. Subsequently, 1-5 mL of this hot ZnI_2 solution was injected slowly (drop wise) into the ternary metal chalcogenide NCs dispersion at 90-120 °C and the heating was continued for 15-30 min. The flask was allowed to cool down gradually to room temperature under stirring and the passivated ternary metal chalcogenide NCs were purified in air by adding acetone, followed by centrifugation. These purified passivated ternary metal chalcogenide NCs were then characterized by PXRD, UV-Vis spectroscopy, NIR-PL spectra and TEM.

5.2 Results and discussion

5.2.1 Synthesis and characterization of bimetallic thiolates

We started our work by preparing bimetallic thiolates with the combination of metals like copper with indium and silver with indium. Both these bimetallic thiolates were prepared by adding DDT to a mixture of individual metal salts, as per the previously reported protocol with slight modifications (reaction 5.A in experimental section).[10] To avoid repetitiveness we present the characterization details of only one system, namely, copper-indium bimetallic thiolate here (Figure 5.2 and Annexure Chapter 5 Figure A.C.5.2-4). The representative PXRD pattern of copper indium bimetallic thiolate $CuIn(C_{12}H_{25}S)_n$ shown in Figure 5.2a (red solid line), reveals periodically spaced *(00l)* reflections, indicating their lamellar nature. The pure individual metal thiolates $Cu(C_{12}H_{25}S)$ and $In(C_{12}H_{25}S)_3$ were also prepared and their PXRD patterns are also included in Figure 5.2a (blue solid line for $Cu(C_{12}H_{25}S)$ and black solid line for $In(C_{12}H_{25}S)_3$), which as expected also display only *(00l)* reflections again signifying their lamellar nature.[2,10] The interlayer spacing calculated from the (*00l*) reflection for $CuIn(C_{12}H_{25}S)_n$ bimetallic thiolates turned out to be 3.48 nm whereas the interlayer spacing of pure $Cu(C_{12}H_{25}S)$ and $In(C_{12}H_{25}S)_3$ were determined to be 3.35 nm and 3.66 nm, respectively (for details please see Annexure Chapter 5 Table A.C.5.1). It also may be noted that silver-indium thiolate displays exactly similar

features and these details are provided in Annexure of chapter 5 (Annexure Chapter 5 Figure A.C.5.5-7).

It is clear from the figure that the (*00l*) peaks of $CuIn(C_{12}H_{25}S)_n$ are shifted towards higher 2θ value as compared to the pure $In(C_{12}H_{25}S)_3$ and to the lower 2θ value with respect to pure $Cu(C_{12}H_{25}S)$. The SEM image of the $CuIn(C_{12}H_{25}S)_n$ clearly display layered (sheet like) structure (Figure 5.2b and inset of 5.2b, and Annexure Chapter 5 Figure A.C.5.2a-d). These bimetallic thiolates were also analyzed by TEM which clearly show the presence of sheet like structures though at very few places some branched structures (Figure 5.2d, for more representative data please see Annexure Chapter 5 Figure A.C.5.4) are also seen. The TEM images obtained by tilting the grid to 8-14° unambiguously establish the layered nature of the sample. It can be clearly seen that the image consists of 10-20 layers that are stacked together (Figure 5.2e, 5.2f and 5.2g).

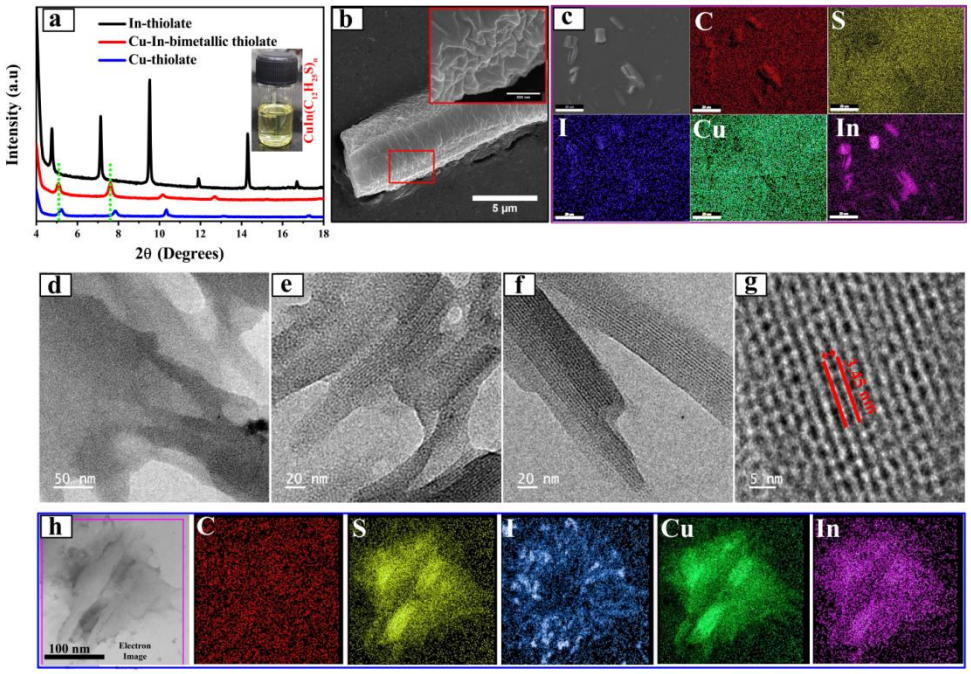

Figure 5.2 a) PXRD patterns of In-thiolate (black), Cu-In thiolate (red) and Cu-thiolate (blue)(the green line is a guide to the eye) and inset image shows the dispersion of Cu-In-thiolates (using Cu(I)) as a Cu-source, b) SEM image of Cu-In-thiolate (inset shows high resolution SEM image), c) EDS mapping from SEM, d) TEM image of Cu-In-thiolates e-g) after tilting (tilt angle 8 -14°), h) EDS mapping of Cu-In-thiolate from TEM.

As we stated in the introduction section, the bimetallic thiolates could form either segregated or mixed stack. In the bulk state this would mean that the bimetallic thiolate would consist of alternating sheets of individual metal thiolates overlapping with each other or stacks of non-interacting individual metal thiolates existing like a physical mixture. If the bimetallic thiolates were indeed made up of segregated stack (Scheme 1C, Figure 5.1) the PXRD pattern should display the peaks of both the individual thiolates. Similarly we could expect a partial solubility of such system where one of the thiolate is soluble while the other one is not. In the event that the bimetallic thiolate is constituted of an alternating stack where the one individual metal thiolates sheet lays above the second one forming an A-B-A-B type structure (Scheme 1D, Figure 5.1), the PXRD pattern should be completely different from the parent thiolates with an interlayer spacing that would be a combination/integer multiple of the individual metal thiolate's d-spacing.

As can be seen from Figure 5.2a and Annexure Chapter 5 Figure A.C.5.5a, Cu-In bimetallic thiolates and Ag-In bimetallic thiolates respectively, show a totally new set of lamellar peaks, which peak positions in between their individual metal thiolates are being observed. This strongly suggests that both the metal ions are intricately mixed and are present in each sheet of the lamellar structure. Also the fact that the these bimetallic thiolates are quite soluble in a non-polar solvent (as compared to the individual Cu-thiolate and Ag-thiolate which are otherwise insoluble)[2] adds credence to the contention that each sheet of this bimetallic thiolate probably contains both the metal atoms.

Similarly, the interlayer distance calculated from the tilted HRTEM images (Figure 5.2g and Annexure Chapter 5 Figure A.C.5.7b, Annexure), turned out to ~3.45 nm for ($CuIn(C_{12}H_{25}S)_n$) and 3.2 nm ($AgIn(C_{12}H_{25}S)_n$). These values were very close to the d spacing calculated from the PXRD patterns. Unfortunately we could not get the chemical information by EDS mapping from a single layer of bimetallic thiolate as the thin layer sheets of these materials were highly sensitive towards the high energy electron beam and were getting converted to spherical particles. Nevertheless, the EDS mapping (Figure 5.2h) captured from many sheets, clearly showed that Cu, In and S are overlapping with each other indicating their uniform presence all over the

area analyzed. Based on all these facts we conclude that these bimetallic thiolates consist of both metals in each sheet and the metal ions are probably randomly distributed in each sheet.

Encouraged by the fact that we have been able to prepare bimetallic thiolates with each sheet containing both the metals mixed in an intricate manner, we proceeded to evaluate their utility in preparing the ternary metal chalcogenide NCs via mechano-chemical routes. In fact, the resultant bimetallic sulfide/selenideNCs turned out to be phase pure materials adding another level of confirmation that both metals were in close proximity in each sheet of the bimetallic thiolates as a physical mixture of individual metal thiolates failed to provide such phase pure materials (*vide infra*).

5.2.2 Synthesis and characterization of bimetallic sulfide/selenide NCs

All reactions were performed in fume hood, under ambient atmosphere by mechano-chemical grinding. For this to the bimetallic thiolates prepared by the procedures described above, freshly (separately) prepared chalcogenide (S^{2-} or Se^{2-}) sources were added and were subjected to a thorough grinding using a mortar-pestle (see experimental section reaction 5.A, reaction 5.B1, reaction 5.B2, reaction 5.C1, reaction 5.C2 and reaction 5.C3 for details). For brevity the characterization details of only $CuInS_2$ are being provided here. Furthermore, though we considered several reagents such as C_8DTCA (octyl ammonium octyldithiocarbamate,[16] which we have used earlier and described in chapter 3 and chapter 4 in the synthesis of various binary metal sulfide NCs by hot injection method[16] as well as solid state grinding method),[2] also thiourea and oleyl amine sulfur complex (S-OlAm) as sulfur source, our results indicated that the S-OlAm complex works well and provides phase pure materials (please see detailed in Annexure Chapter 5 Figure A.C.5.8 with explanation for details about the characterization of materials obtained with other sulfur sources). This could be due to the high reactive nature of S-OlAm complex that is known to release S^{2-} very rapidly as necessary for the formation of phase pure $CuInS_2$ NCs via mechano-chemical methods.[17]

The PXRD pattern of the $CuInS_2$ NCs prepared as part of this study are presented in Figure 5.3a and the same are compared with standard diffraction peaks of cubic CP

$CuInS_2$, CuS and Cu_2S. Gratifyingly, the PXRD of the purified $CuInS_2$ NCs (Figure 5.3a) matches excellently with CP phase (JCPDS card No#85-1575) and the previously published $CuInS_2$ NC PXRD patterns.[18,19] Further, the TEM image obtained from a purified sample of $CuInS_2$ NCs prepared by the above mentioned mechano-chemical route using S-OlAm complex as a sulfur source unveils the presence of monodispersed particles (2.3 ± 0.68 nm; σ = 6.7 %; more TEM images and size distribution plot presented in Annexure Chapter 5 Figure A.C.5.9d). High resolution TEM images (Figure 5.3b), indicate that the particles are crystalline with well-resolved lattice planes corresponding to an inter-planar spacing of 0.32 nm, consistent with the (112) d-spacing of the CP structure (lattice fringes shown in Figure 5.3b inset).The d-spacing observed in HRTEM and the FFTs of the HRTEM images are also consistent with CP $CuInS_2$. The d-spacing were also calculated from the FFTs and IFFTs ofthe HRTEM images (Annexure Chapter 5 Figure A.C.5.9) and again matching was consistent with CP $CuInS_2$. ICP-MS analysis showed that the Cu/In molar ratio is 1:1 and the composition of Cu:In:S in all particles measured by EDS was 1:1:2. All the above analyses definitively establish the obtained material through the mechano-chemical grinding method to be phase pure CP $CuInS_2$ NCs.

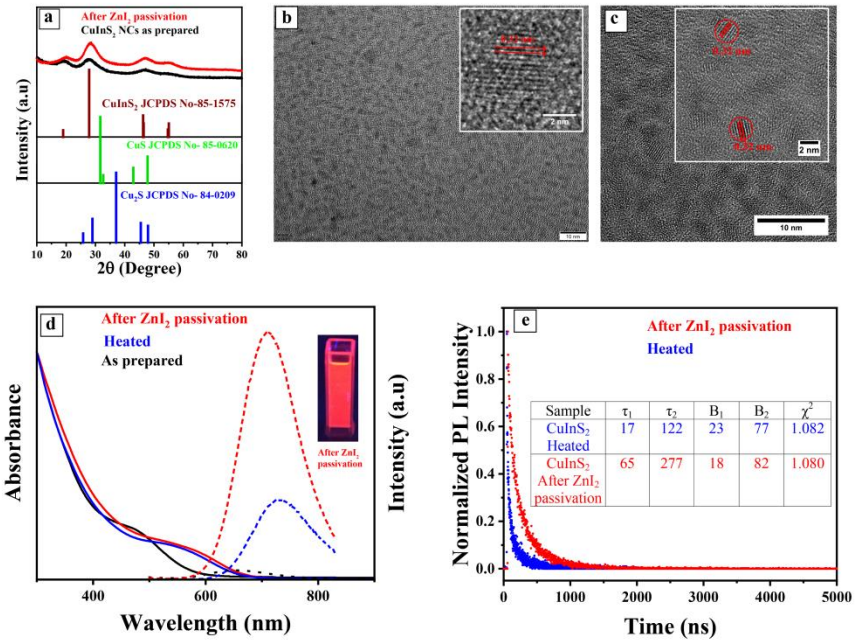

Figure 5.3 a) PXRD of the as synthesized $CuInS_2$ NCs (black solid line), after ZnI_2 passivation at 120°C (solid red line) and standard diffraction peaks for different metal sulfide; Cu_2S (blue), CP $CuInS_2$ (deep brown) and CuS (green) also were shown,

TEM image of b) as synthesized $CuInS_2$ NCs by mechano-chemical method (inset HRTEM image, lattice fringes), c) after ZnI_2 passivation at 120°C. d) absorbance (solid lines) and PL spectra (dotted lines) of as synthesized $CuInS_2$ NCs (black) and after heating at 120 °C (blue) and after ZnI_2 passivation (red), e) PL decay of $CuInS_2$ NCs after heating (blue) and after ZnI_2 passivation (red).

The absorbance spectrum of the as synthesized and purified $CuInS_2$ NCs is displayed in Figure 5.3d (solid black line) where it shows a broad peak with a small hump positioned at 475 nm. Emission spectra shown in Figure 5.3d (dotted black line) disclose a peak positioned at 650 nm, with a large full width half maxima (~130 nm) and a large Stokes shift about ~175 nm. The as synthesized $CuInS_2$ NCs are also characterized with very low quantum yield of <1%. The variation in bond lengths ($R_{Cu-S} \neq R_{In-S}$) in $CuInS_2$ resulting in anion displacement from a close-packed arrangement, is known to result in a tetragonal distortion of the crystal lattice. This distortion plus the structural complexity of I−III−VI_2 CP semiconductors having low band gap energy coupled with the abundant intrinsic defects, surface defects, also and the broad size distribution are all recognized to cause this characteristic broad emission. Also as we prepared the $CuInS_2$ under ambient atmosphere at room temperature through mechano-chemical methods, there is every chance of the material possessing intrinsic crystalline defects as well as surface defects and Cu oxidation related defects. In fact a recent report clearly ascertains that a direct correlation exists between the line width of the ensemble Cu^+/Cu^{2+} trap-state distribution and the broad PL feature of $CuInS_2$ NCs.[20] It further states that the Cu^{2+} states result in "dark" nanocrystals (PL off), whereas Cu^+ states result in "bright" (PL on) NCs.[20] It may be noted that these intrinsic defects and surface defects are routinely minimized by improving the crystallinity and surface passivation with appropriate ligands/high band gap materials.[21-23]The Cu oxidation related defects also have been shown to be minimized by heating with appropriate ligands such as oleyl amine and DDT that reduce the Cu^{2+} to Cu^+ in the overall ensemble of $CuInS_2$ NCs leading to better optical properties. We followed similar strategy and as expected after heating the $CuInS_2$ NCs in presence of oleyl amine and DDT at 120 ºC, their quantum yield increased from <1% to 20%, (see experimental section reaction 5.D1), indicating a considerable

reduction in the oxidation state related as well as intrinsic crystalline and surface defects. Obviously after heating the $CuInS_2$ NCs, there was a small red shift in the absorbance spectra (as after heating the size also increased to 2.5 nm, the size distribution plot was shown in Annexure Chapter 5 Figure A.C.5.10) with a small hump positioned at 550 nm (Figure 5.3d, solid blue line), and there was slight red shift in the position of the emission spectrum (Figure 5.3d, dotted blue line) though the peak positioned at 730 nm became comparatively narrower, with full width half maxima of 125 nm and a 180 nm Stokes shift. The PL decay of these $CuInS_2$ NCs could be well described by a bi-exponential fit, with a fast component τ_1 = 17 ns (23% component present) and slow component τ_2 = 122 ns (77% component present; Figure 5.3e). Based on the obtained lifetime values, we attribute the fast decay time component to be the radiative recombination process of the surface defect states (17 ns), whereas the slow decay time component could be due to the radiative recombination process of the donor-acceptor pairs (~122 ns). Surface-related trap states are usually shallow and therefore show faster decay lifetime compared to the intrinsic defect-related trap states.

To further improve the QY of the $CuInS_2$ NCs we simply injected freshly prepared ZnI_2 solution into $CuInS_2$ NC dispersion which has been preheated to 120 °C (please see details in experimental section Reaction5.D2). Subsequent to this treatment, though the absorption peak position remains almost same and emission peak slight blue shifted, the QY increased quite considerably to ~60% (PL spectra shown as red dotted line in the Figure 5.3d, also please see the details again in Annexure Chapter 5 Figure A.C.5.13). This can be attributed to the Z-type passivation by ZnI_2 on the under coordinated anionic sites eliminating the surface traps significantly [please see the Annexure Chapter 5 Figure A.C.5.11 to Figure A.C.5.13 for the details explanation and optimization the reaction condition (temperature and ZnI_2 concentration)]. Furthermore the PL decay of these ZnI_2 passivated $CuInS_2$ NCs could well be described again by a bi-exponential fit, with a fast component τ_1 = 65 ns (18%) and slow component τ_2 = 277 ns (82%; Figure 5.3e) indicating that surface passivation with ZnI_2 reduces the fast decay channel's contribution from ~23% to ~18%. This clearly establishes that on passivation with ZnI_2, the fast decay channels

associated with the recombination through surface defect-related trap states are reduced leading to the increase in QY to 60-65%.

Encouraged by the fact that we could synthesize $CuInS_2$ NCs (Cu:In=1:1) utilizing bimetallic thiolates through mechano-chemical methods we wanted to see whether we could control the stoichiometry of Cu_xInS_2 as this could provide PL tunability. For this we first prepared Cu-In bimetallic thiolates with varying compositions by taking different molar ratios of Cu without varying the In concentration (Cu : In= 1:1, 0.5:1 and 0.25:1). Quite satisfyingly, the Cu-In bimetallic thiolates with varying compositions of Cu and In turned out to be excellent precursors for Cu_xInS_2 NCs of different stoichiometries. The PXRD patterns of different stoichiometric Cu_xInS_2 NCs are shown in Figure 5.4, where with varying the Cu^+ content the crystal structure of Cu_xInS_2appears to remain the same. Absorbance spectra and PL spectra of as synthesized (under ambient atmosphere at RT) Cu_xInS_2 NCs with different Cu:In molar ratio (initial, starting material's molar ratio) are found to be slightly blue shifted for the In rich Cu_xInS_2 (Figure 5.5a).

Interestingly even these as-prepared materials display comparatively high PLQY of 15-20% in the as-prepared stated and with heating or ZnI_2passivation it could be further improved (up to 60-70%, Figure 5.5b and 5.5c). The PL peak position was also found to be slightly blue shifted with narrower peaks as compared to the stoichiometric $CuInS_2$ NCs. The PL decay spectra could be fitted to a bi-exponential curve with longer decay time (decay curve and life time value showed in Annexure Chapter 5 Figure A.C.5.14).

In a similar manner $CuInSe_2$ and the non-stiochiometric $Cu_{x1}InSe_2$ NCscould also be prepared by these mechano-chemical methods using an appropriate Se^{2-} precursor. The PXRD pattern of $CuInSe_2$ NCs and other characterizations including optical properties of these materials are shown in Figure 5.6 where quite surprisingly the absorption spectral peak position slightly red shifted after ZnI_2 passivation at 120 °C and the QY of the passivated $CuInSe_2$ NCs are 60-75% in range.

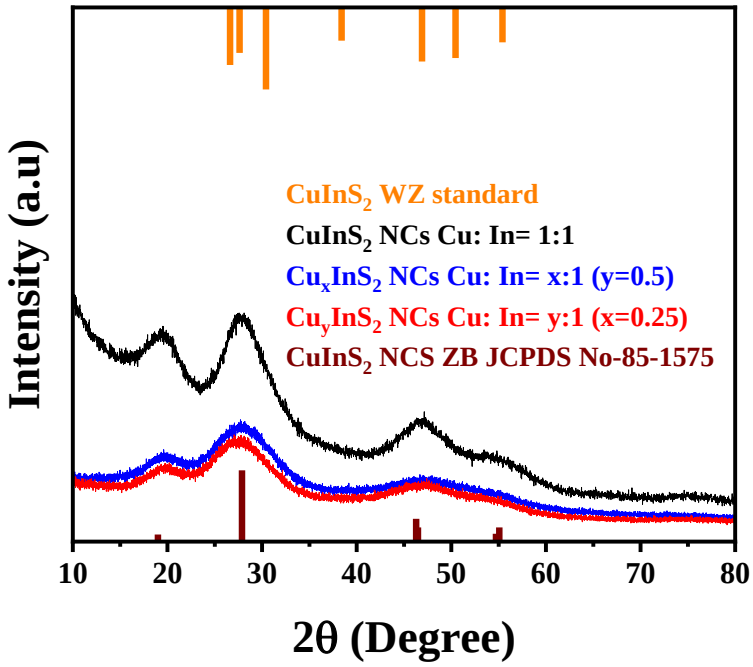

Figure 5.4 PXRD of stoichiometric Cu_xInS_2 NCs synthesized by mechano-chemical method using different amount of Cu without varying the In concentration, where with varying the Cu^+content the crystal structure of Cu_xInS_2 appears to remain the same. The as prepared Cu_xInS2 NCs matched with the ZB chalcopyrite structure (JCPDS NO- 85-1575).

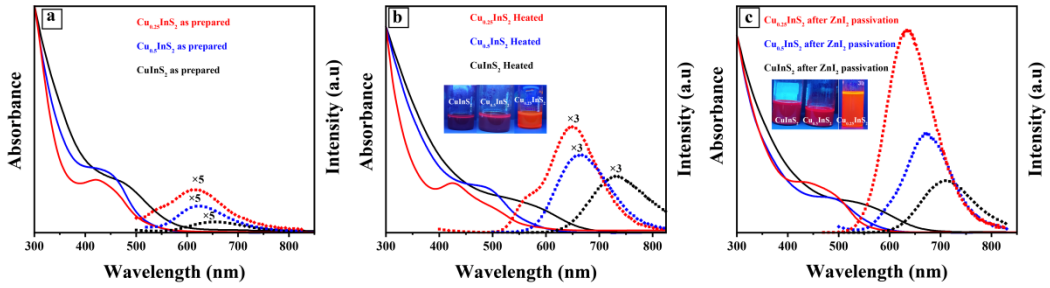

Figure 5.5 a) Absorption spectra and PL spectra of Cu_xInS_2 NCs with different Cu:In ratios, viz. 0.25:1 (red curves); 0.5:1 (blue curves); 1:1 (black curves). Solid lines represent the absorption spectra and dotted lines represent the PL spectra. The spectra in panel (a) correspond to the as-prepared samples, those in (b) to heated samples and those in (c) to samples after ZnI_2 passivation. Please note the PL intensities in (a) and (b) were scaled as indicated so that they become visible and the trends are discernible. Otherwise their intensities were very low.

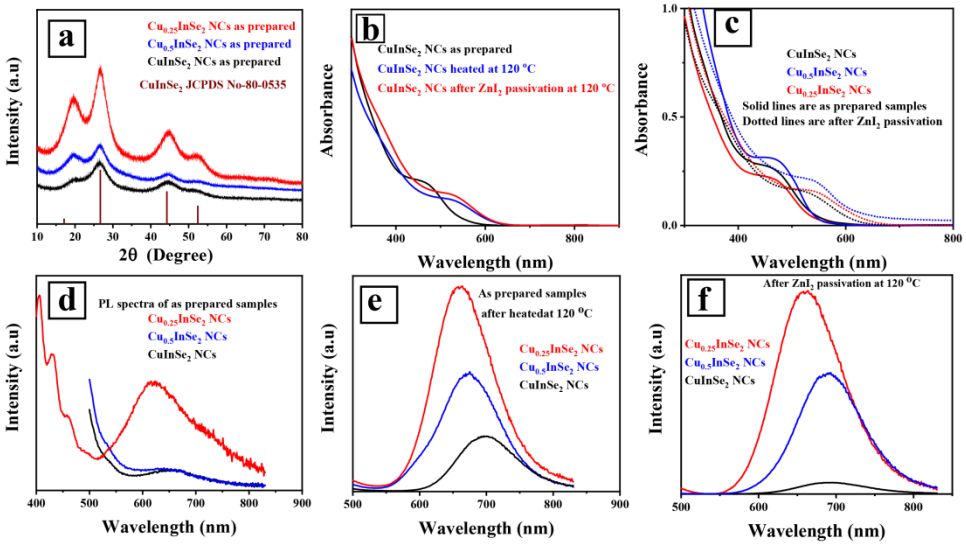

Figure 5.6 a) PXRD pattern of Cu_xInSe2 NCs b) Absorbance spectra of $CuInSe_2$ NCs (Cu:In=1:1) as synthesized (black) and after heated at 120 °C (blue) and after ZnI_2 passivation (red), c) absorption spectra of Cu_xInSe_2 NCs with different Cu: In ratios, as synthesized (solid line) and after heating at 120 °C (dotted line); PL spectra of d) as synthesized Cu_xInSe_2 NCs e) after heating at 120 °C and d) PL spectra after ZnI_2 passivation at 120 °C.

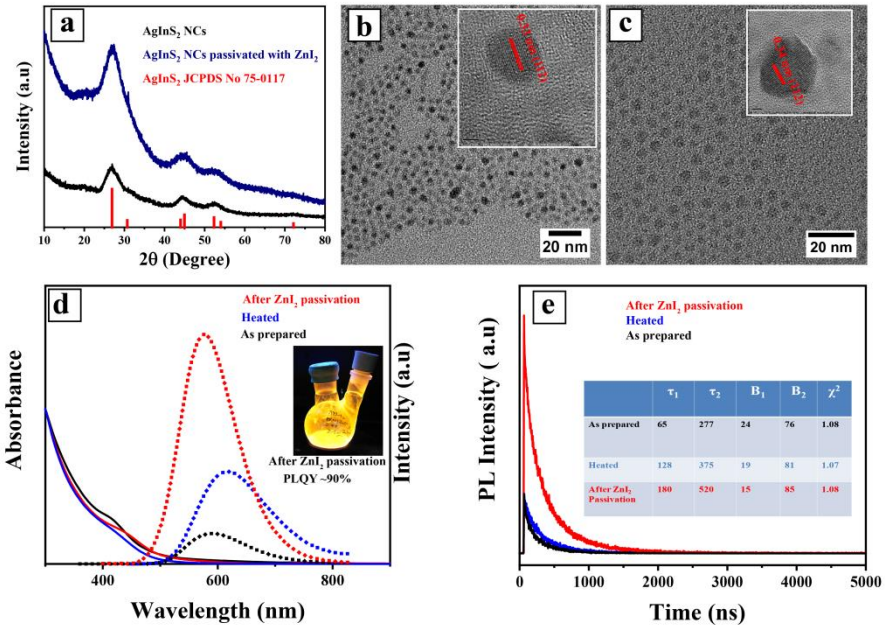

Figure 5.7 a) PXRD of the as synthesized $AgInS_2$ NCs (black line) and $AgInS_2$ NCs after passivation with ZnI_2 (blue line). The standard diffraction peaks of AgInS2 (JPPDS # 75-0117) are included. TEM image of, b) as synthesized $AgInS_2$ NCs by

mechano-chemical method (inset HRTEM image, lattice fringes), c) after ZnI_2 passivation at 120 °C. d) absorbance (solid lines) and PL spectra (dotted lines) of as synthesized $AgInS_2$ NCs (black) and after heating at 120 °C (blue) and after ZnI_2 passivation (red), e) PL decay of $AgInS_2$ NCs as-prepared (black) after heating (blue) and after ZnI_2 passivation (red).

Analogously $AgInS_2$ and $AgInSe_2$ NCs also could be synthesized by mechano-chemical methods using Ag-In bimetallic thiolates and an appropriate S^2- precursor and Se^2- precursor respectively. The PXRD of the purified $AgInS_2$ NCs (Figure 5.7a) matches excellently with tetragonal $AgInS_2$ phase (JCPDS card No#75-0117). The crystal structure was found to be retained after ZnI_2 passivation (Figure 5.7a) at 120 °C. From the TEM images (Figure 5.7b and 5.7c) the sizes of the as prepared $AgInS_2$ NCs were determined to be 4.1 ± 0.58 nm (σ = 5.8 %) whereas after ZnI_2 passivation the size was found to be increased slightly (4.4 ± 0.8 nm; σ = 8 %). More TEM images and size distribution plots are included in Annexure Chapter 5 Figure A.C.5.15. High resolution TEM images (inset of Figure 5.7b and 5.7c), indicate that the particles are crystalline with well-resolved lattice planes corresponding to an inter-planar spacing of 0.34 nm, consistent with the (112) d-spacing of the tetragonal $AgInS_2$ structure and the same was retained after passivation with ZnI_2. The most attractive feature of these silver systems is the absence of metal oxidation related trap states as silver only shows +1 (Ag^+) stable oxidation state. Due to this, the as synthesized (at room temperature by mechano-chemical methods) purified $AgInX_2$ (X=S or Se) show high QY of 30-65% even before any surface treatment by ZnI_2 (for the absorption and emission spectra please see Figure 5.7d). As expected the QY could be further improved to an impressive ~90% by just simply heating and surface passivation with ZnI_2 (Figure 5.7d). More characterization details of stoichiometric Ag_yInX_2 (y=1-0.25) NCs including optical properties are provided in the Figure 5.8 and 5.9.

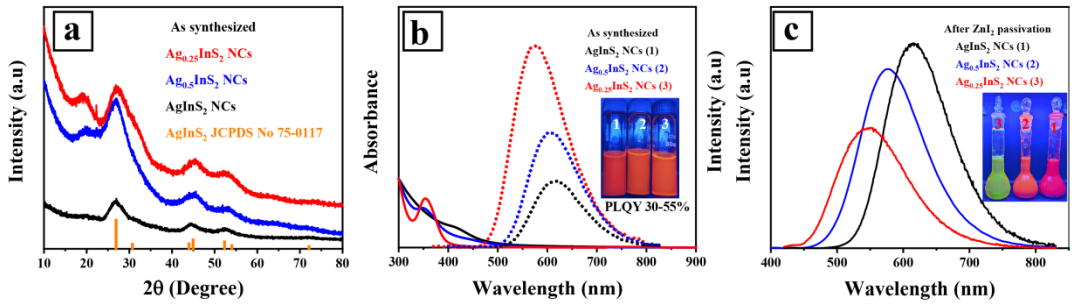

Figure 5.8 a) PXRD of as synthesized Ag_xInS_2 NCS, b) absorption and PL spectra of as synthesized Ag_xInS_2 NCS, where $AgInS_2$ (black Ag:In=1:1), $Ag_{0.5}InS_2$ (blue, Ag:In= 0.5: 1) and $Ag_{0.25}InS_2$ (red, Ag:In= 0.5: 1). The ratio indicating the starting Ag:In molar ratios. Solid lines represent the absorbance and dotted lines represent the PL spectra. c) PL spectra after ZnI_2 passivation.

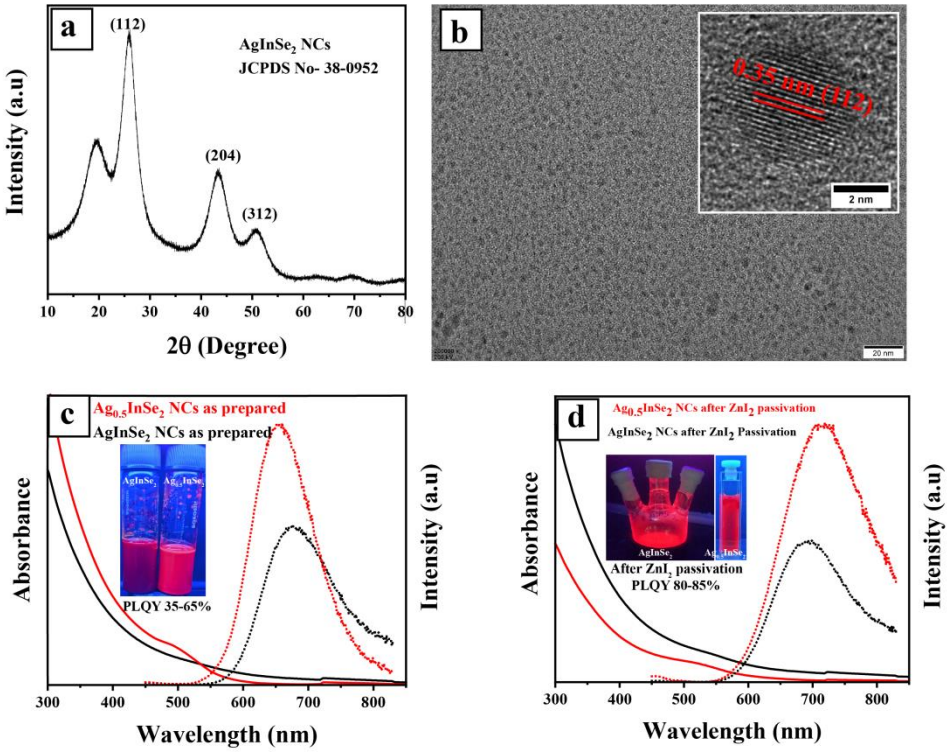

Figure 5.9 a) PXRD pattern of $AgInSe_2$ NCs b) TEM image of as prepared $AgInSe_2$ NCs synthesized by mechano-chemical grinding; inset images showed the lattice fringes of the same, c) absorbance (solid line) and emission spectra (dotted line) of as prepared $AgInSe_2$ NCs and $Ag_{0.5}InSe_2$ NCs with different Ag: In ratios, d) absorbance (solid line) and emission spectra (dotted) of $AgInSe_2$ NCs and $Ag_{0.5}InSe_2$ NCs after ZnI_2 passivation at 120 °C.

5.2.3 Mechanism of formation of ternary metal chalcogenide NCs

The efficacy of bimetallic thiolates to afford good quality, nearly monodisperse and more importantly phase pure bimetallic chalcogenide NCs invigorated us to probe deeper to understand the pathway this mechano-chemical reaction could be following. We actually could imagine three possible pathways for this reaction. The first of such pathway assumes that it is notactually necessary to have the bimetallic thiolate as a precursor to start with and that even when a physical mixture of two thiolates or a bimetallic thiolate with segregated stack like structure is ground with a chalcogenide source some type of an intermediate complex gets formed which then proceeds further to result in the bimetallic chalcogenide NCs (Figure 5.10, Pathway - I).

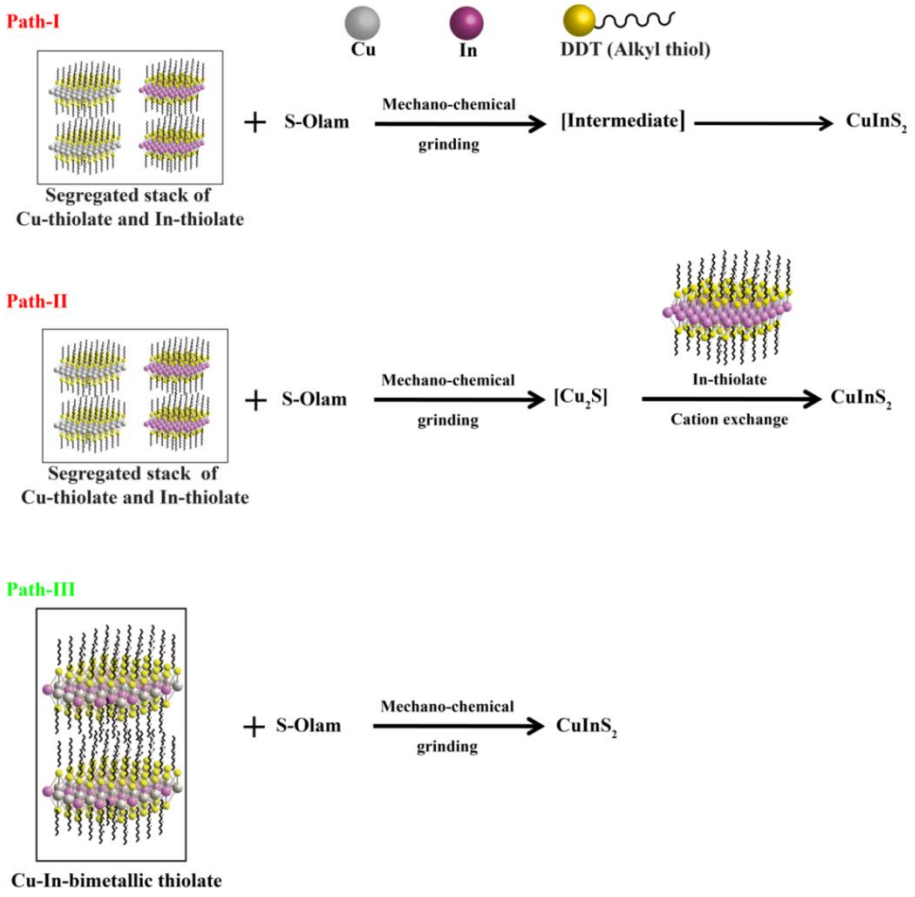

Figure 5.10.Probable pathway of bimetallic sulfide NCs formation by mechano-chemical grinding.

To check whether such scenario is possible, the individual thiolates of Cu and In (Figure 5.1B and 5.1C) were taken and after grinding them thoroughly, they were

treated with the freshly prepared S-OlAm complex (reaction 5.B1, experimental section). However, such a reaction resulted in the formation of Cu_2S NCs with $CuInS_2$ NCs as a minor phase (as concluded by the absorbance spectra which displays a major peak at 1550 nm corresponding to the Cu_2S NCs with an extremely small peak at 476 nm corresponding to the $CuInS_2$ NCs, Annexure Chapter 5 Figure A.C.5.16). This is not surprising considering the fact that copper ions react very fast with a sulfur source as compared to the In^{3+} ions and obviously the copper thiolate in this physical mixture probably reacted with the sulfur source faster leading to the formation of Cu_2S NCs. The small amount of $CuInS_2$ could have formed by the exchange of Cu ions with the In cations. Thus this formation of Cu_2S NCs as a major product negates Pathway - I to be the route for $CuInS_2$ NC formation in the present study. For the second route we again assumed that thiolates are only present as segregated stack like structure. When a sulfur source is added to this followed by grinding, the copper thiolate in the stack (as mentioned above) reacts first forming the Cu_2S NCs. However in this route it is assumed that these Cu_2S NCs further react with the indium thiolate leading to an extended cation exchange where half the copper is replaced by indium ultimately forming the $CuInS_2$ NCs (Figure 5.10, Pathway – II).

Such cation exchange reactions are abundantly reported in literature (albeit mostly in the solution phase).[24-26]To check whether this indeed is the route through which the bimetallic sulfide NCs are forming in the present study, we did the following reaction. First, we made the Cu_2S NCs separately (for characterization details of Cu_2S NCs please see Annexure Chapter 5 Figure A.C.5.17). We then added these Cu_2S NCs to indium thiolates and ground them well. Providentially even after grinding them together for long time (>30 min) no major changes were observed indicating that the majority of the Cu_2S NCs remained unreacted. This eliminates Pathway - II as the possible course for $CuInS_2$ NC formation as in the actual reaction (Reaction 5.C1) the $CuInS_2$ NCs get formed very rapidly (within minutes). The only remaining possibility then is that in the bimetallic thiolates both metals are present in each sheet as an intricate mixture (as indicated by the PXRD as well as the HRTEM analyses) and when they are ground with a reactive chalcogenide precursor like S-OlAm complex

formation of phase pure bimetallic chalcogenide NCs (Figure 5.10, Pathway – III) takes place.

In the literature it is well established that reaction of a reactive sulfur species with copper ions is much faster when compared to the same with In^{3+}ions.[27-31]Therefore, in the present case, the simultaneous reaction of Cu^{1+} and In^{3+}, with the S-OlAm complex is intriguing.[27] It may be noted that in most of the reported literature complexes/salts like copper (I) acetate, oleate, iodide, bromide are utilized as precursors which react rapidly with the sulfur reagents. In the present study the copper is present as a thiolate complex. We propose that the extra stability of copper in the thiolate form attenuates its reactivity with the S-OlAm and Se-OlAm complexes. This could result in similar reactivities of In^{3+} and Cu^{+} ensuing the formation of phase pure ternary $CuInS_2$/$CuInSe_2$ NCs. We believe a similar mechanism is operative in the Ag-In systems too.

5.3 Summary

The successful synthesis of many binary metal sulfide NCs in the previous chapters opened another interesting and of course challenging avenue, namely, the synthesis of bimetallic sulfide and selenideNCs. We could achieve great success in this endeavour by employing bimetallic thiolates as single source precursors. What was more satisfying was the fact that we could prepare the bimetallic sulfide and selenide NCs via a very simple and convenient solid state grinding method. The final $CuInS_2$, $AgInS_2$, $CuInSe_2$ and $AgInSe_2$not only turned out to be phase pure but also displayed reasonable photo luminescence quantum yields in the as-prepared state. We also demonstrated that the overgrowth of these bimetallic NCs with a few monolayers of metal halide like ZnI_2 significantly improve photo luminescence quantum yields close to 80-90%.

5.4 References

1. Bera, A.; Prasad, B. L., 2D molecular precursor for a one-pot synthesis of semiconducting metal sulfide nanocrystals. *Bull. Mater. Sci.* **2018,***41*, 125.

2. Bera, A.; Busupalli, B.; Prasad, B. L. Solvent-Less Solid State Synthesis of Dispersible Metal and Semiconducting Metal Sulfide Nanocrystals. *ACS Sustain. Chem. Eng.* **2018,***6*, 12006-12016.
3. Thomas, P. J.; Lavanya, A.; Sabareesh, V.; Kulkarni, G. Self-assembling bilayers of palladiumthiolates in organic media. *J. Chem. Sci.* **2001,***113*, 611-619.
4. John, N. S.; Kulkarni, G.; Datta, A.; Pati, S. K.; Komori, F.; Kavitha, G.; Narayana, C.; Sanyal, M. Magnetic interactions in layered nickel alkanethiolates. *J. Phys. Chem. C* **2007,***111*, 1868-1870.
5. Pokroy, B.; Aichmayer, B.; Schenk, A. S.; Haimov, B.; Kang, S. H.; Fratzl, P.; Aizenberg, J. Sonication-assisted synthesis of large, high-quality mercury thiolate single crystals directly from liquid mercury. *J. Am. Chem. Soc.* **2010,***132*, 14355-14357.
6. Wertheim, E. Derivatives for the identification of mercaptans. *J. Am. Chem. Soc.* **1929,***51*, 3661-3664.
7. Hu, L.; de la Rama, L. P.; Efremov, M. Y.; Anahory, Y.; Schiettekatte, F.; Allen, L. H. Synthesis and Characterization of Single-Layer Silver−Decanethiolate Lamellar Crystals. *J. Am. Chem. Soc.* **2011,***133*, 4367-4376.
8. Dance, I. G.; Fisher, K. J.; Banda, R. H.; Scudder, M. L. Layered structure of crystalline compounds silver thiolates (AgSR). *Inorg. Chem.* **1991,***30*, 183-187.
9. Sandhyarani, N.; Pradeep, T., An investigation of the structure and properties of layered copper thiolates. *J. Mater. Chem.* **2001,***11*, 1294-1299.
10. Busupalli, B.; Kummara, S.; Kumaraswamy, G.; Prasad, B. L., Ultrathin sheets of metal or metal sulfide from molecularly thin sheets of metal thiolates in solution. *Chem. Mater.* **2014,***26*, 3436-3442.
11. Busupalli, B.; Date, K.; Datar, S.; Prasad, B. L., Preparation of Ni_3S_2 and Ni_3S_2–Ni nanosheets via solution based processes. *Cryst. Growth Des.* **2015,***15*, 2584-2588.
12. Kirkwood, N.; Monchen, J. O.; Crisp, R. W.; Grimaldi, G.; Bergstein, H. A.; Du Fossé, I.; Van Der Stam, W.; Infante, I.; Houtepen, A. J. Finding and

fixing traps in II–VI and III–V colloidal quantum dots: The importance of Z-type ligand passivation. *J. Am. Chem. Soc.* **2018,***140*, 15712-15723.

13. Korala, L.; Braun, M. B.; Kephart, J. M.; Tregillus, Z.; Prieto, A. L. Ligand-exchanged CZTS nanocrystal thin films: does nanocrystal surface passivation effectively improve photovoltaic performance? *Chem. Mater.* **2017,***29*, 6621-6629.
14. Lee, W. S.; Kang, Y. G.; Woo, H. K.; Ahn, J.; Kim, H.; Kim, D.; Jeon, S.; Han, M. J.; Choi, J.-H.; Oh, S. J. Designing High-Performance CdSe Nanocrystal Thin-Film Transistors Based on Solution Process of Simultaneous Ligand Exchange, Trap Passivation, and Doping. *Chem. Mater.* **2019,***31*, 9389-9399.
15. Liu, Y.; Yao, D.; Shen, L.; Zhang, H.; Zhang, X.; Yang, B. Alkylthiol-enabled Se powder dissolution in oleylamine at room temperature for the phosphine-free synthesis of copper-based quaternary selenide nanocrystals. *J. Am. Chem. Soc.* **2012,***134*, 7207-7210.
16. Bera, A.; Mandal, D.; Goswami, P. N.; Rath, A. K.; Prasad, B. L. Generic and scalable method for the preparation of monodispersed metal sulfide nanocrystals with tunable optical properties. *Langmuir* **2018,***34*, 5788-5797.
17. Nose, K.; Soma, Y.; Omata, T.; Otsuka-Yao-Matsuo, S., Synthesis of ternary $CuInS_2$ nanocrystals; phase determination by complex ligand species. *Chem. Mater.* **2009**, 21, 2607-2613.
18. Castro, S. L.; Bailey, S. G.; Raffaelle, R. P.; Banger, K. K.; Hepp, A. F. Nanocrystalline chalcopyrite materials ($CuInS_2$ and $CuInSe_2$) via low-temperature pyrolysis of molecular single-source precursors. *Chem. Mater.* **2003,***15*, 3142-3147.
19. Ning, J.; Kershaw, S. V.; Rogach, A. L., Synthesis and Optical Properties of Cubic Chalcopyrite/Hexagonal Wurtzite Core/Shell Copper Indium Sulfide Nanocrystals. *J. Am. Chem. Soc.* **2019,***141*, 20516-20524.
20. van der Stam, W.; de Graaf, M.; Gudjonsdottir, S.; Geuchies, J. J.; Dijkema, J. J.; Kirkwood, N.; Evers, W. H.; Longo, A.; Houtepen, A. J., Tuning and probing the distribution of Cu^+ and Cu^{2+} trap states responsible for broad-band photoluminescence in $CuInS_2$ nanocrystals. *ACS Nano* **2018,***12*, 11244-11253.

21. Hirase, A.; Hamanaka, Y.; Kuzuya, T. Ligand-Induced Luminescence Transformation in $AgInS_2$ Nanoparticles: From Defect Emission to Band-Edge Emission. *J. Phys. Chem. Lett.* **2020,***11*, 3969-3974.
22. Ghosh, S.; Mandal, S.; Mukherjee, S.; De, C. K.; Samanta, T.; Mandal, M.; Roy, D.; Mandal, P. K. Near-Unity Photoluminescence Quantum Yield and Highly Suppressed Blinking in a Toxic-Metal-Free Quantum Dot. *J. Phys. Chem. Lett.* **2021,***12*, 1426-1431.
23. Berends, A. C.; Van Der Stam, W.; Hofmann, J. P.; Bladt, E.; Meeldijk, J. D.; Bals, S.; de Mello Donega, C. Interplay between surface chemistry, precursor reactivity, and temperature determines outcome of ZnS shelling reactions on $CuInS_2$ nanocrystals. *Chem. Mater.* **2018,***30*, 2400-2413.
24. De Trizio, L.; Prato, M.; Genovese, A.; Casu, A.; Povia, M.; Simonutti, R.; Alcocer, M. J.; D'Andrea, C.; Tassone, F.; Manna, L. Strongly Fluorescent Quaternary Cu–In–Zn–S Nanocrystals Prepared from Cu_{1-x} InS_2 Nanocrystals by Partial Cation Exchange. *Chem. Mater.* **2012,***24*, 2400-2406.
25. Van Der Stam, W.; Berends, A. C.; Rabouw, F. T.; Willhammar, T.; Ke, X.; Meeldijk, J. D.; Bals, S.; de Mello Donega, C. Luminescent $CuInS_2$ Quantum Dots by Partial Cation Exchange in Cu_{2-x} S Nanocrystals. *Chem. Mater.* **2015,***27*, 621-628.
26. Hinterding, S. O.; Berends, A. C.; Kurttepeli, M.; Moret, M.-E.; Meeldijk, J. D.; Bals, S.; Van Der Stam, W.; de Mello Donega, C. Tailoring Cu^+ for Ga^{3+} Cation Exchange in Cu_{2-x} S and $CuInS_2$ Nanocrystals by Controlling the Ga Precursor Chemistry. *ACS Nano* **2019,***13*, 12880-12893.
27. Leach, A. D.; Macdonald, J. E. Optoelectronic properties of $CuInS_2$ nanocrystals and their origin. *J. Phys. Chem. Lett.* **2016,***7* (3), 572-583.
28. Kolny-Olesiak, J.; Weller, H. Synthesis and application of colloidal CuInS2 semiconductor nanocrystals. *ACS Appl. Mater. Interfaces* **2013,***5*, 12221-12237.
29. Xie, R.; Rutherford, M.; Peng, X. Formation of high-quality I− III− VI semiconductor nanocrystals by tuning relative reactivity of cationic precursors. *J. Am. Chem. Soc.* **2009,***131*, 5691-5697.

30. Zhong, H.; Lo, S. S.; Mirkovic, T.; Li, Y.; Ding, Y.; Li, Y.; Scholes, G. D. Noninjection gram-scale synthesis of monodisperse pyramidal $CuInS_2$ nanocrystals and their size-dependent properties. *ACS Nano* **2010,***4*, 5253-5262.
31. Gromova, M.; Lefrançois, A. l.; Vaure, L.; Agnese, F.; Aldakov, D.; Maurice, A.; Djurado, D.; Lebrun, C.; de Geyer, A.; Schülli, T. U. Growth mechanism and surface state of $CuInS_2$ nanocrystals synthesized with dodecanethiol. *J. Am. Chem. Soc.* **2017,***139*, 15748-15759.

6.1 Conclusion and Future Perspective:

To summarize the work incorporated in this thesis, several simple and generic methods have been developed for the synthesis of various single source metal precursors like metal thiolates and metal dithiocarbamate complexes, comprising the main two constituents of metal chalcogenide nanocrystals (NCs), namely, the tiny inorganic metal chalcogenide complex as core and an organic molecule as shell. Specially, both binary metal thiolates and bimetallic (ternary) thiolates have been prepared and both of them turned out to be excellent precursors for the synthesis of metal sulfide/selenide NCs. The methods used to prepare these NCs included a direct-heating (solvo-thermal decomposition) method or solid state grinding method. We also observed that some of the metal thiolates like Pb-thiolate requires very high temperature to decompose into PbS resulting in particles bigger than their Bohr exciton radius and hence displayed poor optical properties. To reduce the decomposition temperature an active sulfur precursor called octyl ammonium octyldithiocarbamate (C_8DTCA) has been utilized for the synthesis of various metal sulfide NCs (including most challenging PbS NCs, with tunable optical properties) by solution based method (hot injection) or solid state grinding method. Importantly, the synthesis of starting materials (metal thiolate 2D sheets or metal dithiocarbamate complexes) was also very simple and scalable. We also show that the size of the nanocrystals could be controlled by changing the reaction temperature or metal: chalcogenide precursor ratio. We have also been successful in establishing that these methods are scalable without compromising their structural and optical properties. The binary or ternary materials synthesized by these solid state routes could be re-dispersed as desired in non-polar organic solvents allowing them to be solution processible. The optical properties of the metal chalcogenide nanocrystals could further be improved by post synthetic surface passivation.

These materials have many applications such as in LED, photovoltaic and biological cell imaging. For these emerging applications, there is a necessity to expand our synthetic repertoire and prepare good quality quaternary metal chalcogenide NCs and chalcogenide perovskites. Chalcopyrite semiconductors specifically $CuInX_2$, $CuGaX_2$ and their alloy $Cu(In,Ga)X_2$ (where X=S and Se) are well known direct band gap semiconductor used as absorbers in thin film solar cells. Copper zinc tin

sulfide/selenide (CZTS/Se) is similar to the chalcopyrite structure of $Cu(In,Ga)X_2$ but uses only earth-abundant elements and is regarded as potential candidate for photovoltaics because of the suitable bandgap (1.0−1.5 eV), high absorption coefficient (up to 105cm−1), good photo stability and low toxicity.

Another interesting chalcopyrite structure $CuFeS_2$ is also a good candidate as both the elements are earth abundant and non-toxic and this material exhibits a tunable band gap that spans the range 0.5−2 eV. The NCs of all of these above mentioned chalcopyrite structured materials are conventionally synthesized by wet chemical methods (hot injection or heat up). Interestingly, we have discussed the strategies in this thesis to synthesize some of the important bimetallic chalcogenide (S or Se) nanocrystals (NCs) like $AgInX_2$, and $CuInX_2$ etc using a solvent-less green approach, involving a simple and convenient solid state grinding route which could be easily scalable and we hope the above mentioned materials also could be synthesized using these strategies mentioned in this thesis. Another class of materials, bulk chalcogenide perovskite ($CaTiS_3$, $BaZrS_3$, $CaZrSe_3$) are also proposed for photovoltaic application as they possess direct bandgap within in the range 0.95−1.75 eV.

This makes them ideal candidate to harness the NIR region of the solar spectrum in multi-junction configuration. We believe the synthesis of bulk chalcogenide perovskite could be addressed using the novel 2D materials namely, metal thiolates or metal dithiocarbamate complexes, and we propose to use these precursors to make the desired QDs.

Even our single source precursor, metal thiolates are interesting class of materials which exist as 2D materials analogous to graphene or MoS_2. It has been postulated earlier that completely new and exotic materials could be prepared by making hetero-structures from 2D materials. As we already have established many of these metal thiolates could be easily delaminated into individual sheets by an easy and convenient route making them amenable for the preparation of composite 2D hetero-structures. Such composite 2D hetero-structures are expected to display unprecedented properties leading to novel applications in energy generation and catalysis. So, these mono metal thiolates and mixed bimetal thiolates, prepared by very convenient solid state method prescribed in this thesis, open another avenue for further realization of novel hetero-structures of two different metal thiolates. Such

hetero-structure could turn out to be extremely handy in the preparation of functional nanomaterials which could herald a new era in terms of improvement in the photovoltaic performance as well as in LED, biological cell imaging and catalysis.

Annexure

^{1}H NMR (200 MHz, Chloroform-d) δ 5.44 (s, 2H, N-H, S-H), 3.60 - 3.48 (m, 1H), 3.02 (t, *J* = 7.3 Hz, 1H), 1.70 - 1.59 (m, 2H), 1.27 (m, 10H), 0.88 (t, *J* = 6.1 Hz, 3H).

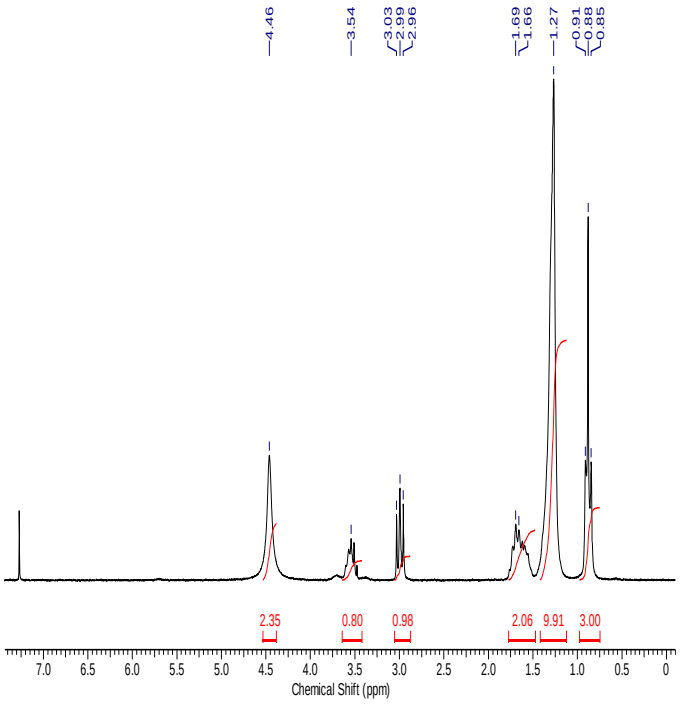

Figure A.C.2.1.^{1}H NMR spectra of the compound C_8DTCA

C_8DTCA= $[[C_8H_{17}NHCS_2]^-[C_8H_{17}NH_3]^+]$.

^{13}C NMR (50 MHz, CHLOROFORM-*d*) δ ppm 181.31, 77.63, 76.37, 44.37, 41.29, 31.73, 29.19, 29.12, 28.96, 26.88, 22.60, 14.04.

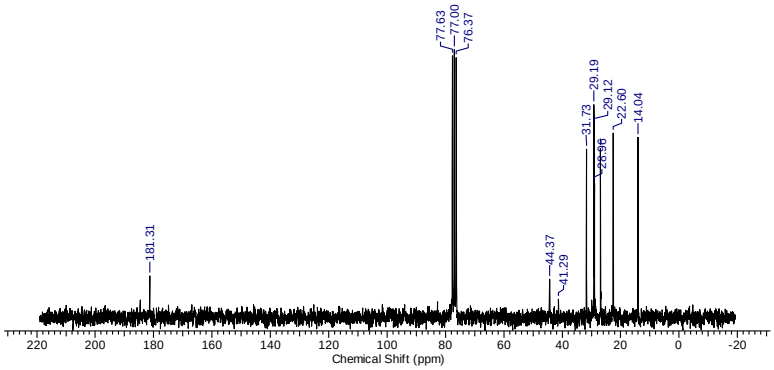

Figure A.C.2.2:^{13}C NMR spectra of the compound $[[C_8H_{17}NHCS_2]^-[C_8H_{17}NH_3]^+]$.

^{13}C NMR (DEPT-135, 50 MHz, CHLOROFORM-*d*) δ ppm 44.38, 41.31, 31.77, 29.24, 29.18, 29.00, 26.92, 22.64, 14.10.

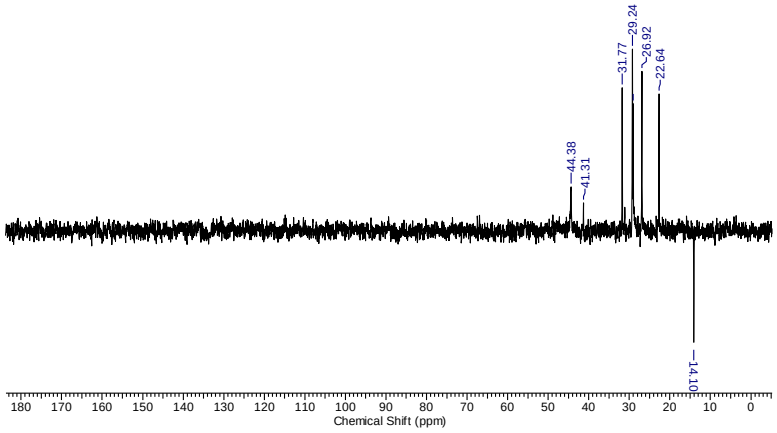

Figure A.C.2.3**:**^{13}C DEPT spectra of the compound $[C_8H_{17}NHCS_2][C_8H_{17}NH_3]$

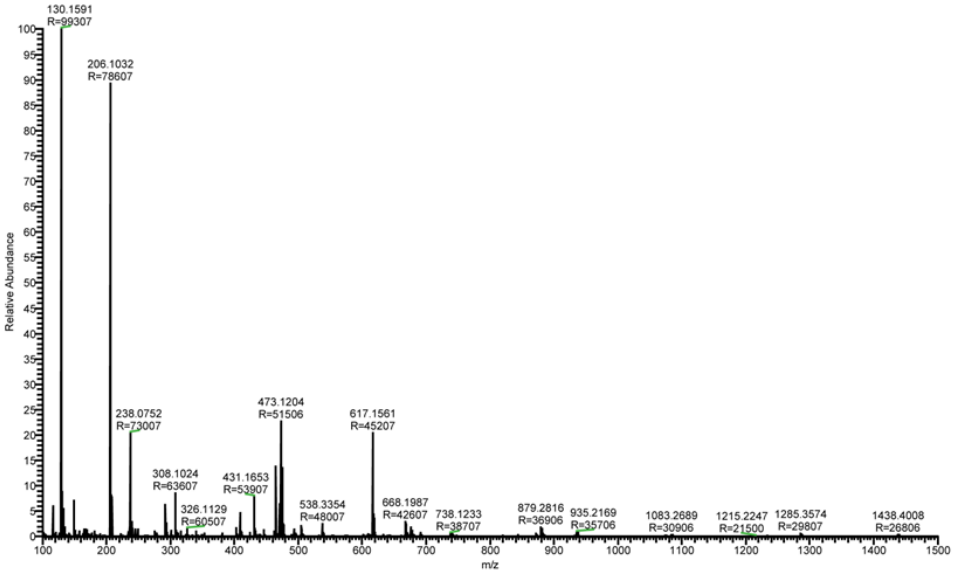

Figure A.C.2.4: HRMS spectrum of C_8DTCA. Two major peak observed at ~130 and 206 due to octyl amine and octyl dithiocarbamic acid respectively. In HRMS condition some of the compound (C_8DTCA) decomposed to octyl amine.

A.C.3.1 Synthesis of other different metal sulfide QDs

A.C.3.1.1 Synthesis of CdS QDs

Similar to in situ synthesis of PbS, cadmium acetate (2 mmol), oleic acid (1 mL), oleyl amine (1 mL) and 1-octadecene (6mL) was taken in a 3-neck Rb flask and heated and degassed under vacuum at 105 ºC for 2 – 4 h. Then the temperature was set to 160-200 ºC. About 75 mg C_8DTCA (0.45 mmol of "S") was dissolved in 0.5 mL oleyl amine and another 10 mL of 1-ODE added to it. Then the C_8DTCA-OlAm solution was injected very fast into the Cd-oleate solution at the set temperature (160-200 ºC). Immediately after the addition, colourless Cd-oleate became pale yellow indicating the formation of CdS. The heating was stopped immediately after the injection of C_8DTCA solution and the system was allowed to naturally cool to room temperature (which took ~1 h). The product of this reaction was collected by precipitating it with acetone addition and after washing it two times with acetone (centrifuged at 5000 rpm for 3 min) and one time with a mixture of acetone and methanol (1:3 by volume) the precipitate was dried under Argon flow. The precipitate was redispersed into toluene for various measurements. The purified CdS QDs were characterized by PXRD, UV-Vis spectroscopy, PL spectra and TEM.

A.C.3.1.2 Synthesis of ZnS QDs

Zinc acetate (2 mmol), oleic acid (1 mL), oleyl amine (1 mL) and 1-octadecene (6 mL) was taken in a 3 neck Rb flask, heated and degassed under vacuum at 105 ºC for 2-4 h.The temperature was set to 200 ºC. About 75mg C_8DTCA (0.45 mmol of "S") was dissolved in 0.5 mL oleyl amine and another 10 mL of 1-ODE added to it. Then the C_8DTCA-OlAm solution was injected very fast into the Zn-oleate solution at the set temperature (200 ºC). The heating was stopped immediately after the injection of C_8DTCA solution and the system was allowed to naturally cool to room temperature (which took ~1 h). The product of this reaction was collected by precipitating it with acetone addition and after washing it two times with acetone (centrifuged at 5000 rpm for 3 min) and one time with a mixture of acetone and methanol (1:3 by volume) the precipitate was dried under Argon flow. The precipitate was re-dispersed into toluene

for various measurements. The purified ZnS QDs were characterized by PXRD, UV-Vis spectroscopy, PL spectra and TEM.

A.C.3.1.3 Synthesis of MnS QDs

Manganese acetate (2 mmol), oleic acid (1 mL), oleyl amine (1 mL) and 1-octadecene (6 mL) was taken in a 3-neck Rb flask and heated and degassed under vacuum at 105 ºC for 2-4 h. Then the temperature was set to 160 ºC. About 75 mg C_8DTCA (0.45 mmol of "S") was dissolved in 0.5 mL oleyl amine and another 10 mL of 1-ODE added to it. Then the C_8DTCA-OlAm solution was injected very fast into the Mn-oleate solution at 160 °C. Immediately after the addition, pale yellow Mn-oleate became dark orange indicating the formation of MnS. The heating was stopped immediately after the injection of C_8DTCA solution and the system was allowed to naturally cool to room temperature (which took ~1 h). The product of this reaction was collected by precipitating it with acetone addition and after washing it two times with acetone (centrifuged at 5000 rpm for 3 min) and one time with a mixture of acetone and methanol (1:3 by volume) the precipitate was dried under Argon flow. The precipitate was redispersed into toluene for various measurements. The purified MnS QDs were characterized by PXRD, UV-Vis spectroscopy, PL spectra and TEM.

A.C.3.1.4 Synthesis of In_2S_3 QDs

Indium acetate (2 mmol), oleic acid (1 mL), oleyl amine (1 mL) and 1-octadecene (6 mL) was taken in a 3 neck Rb flask and heated and degassed under vacuum at 105 ºC for 2-4 h. Then the temperature was set to 160 ºC. About 75mg C_8DTCA (0.45 mmol of "S") was dissolved in 0.5 mL oleyl amine and another 10 mL of 1-ODE added to it. Then the C_8DTCA-OlAm solution was injected very fast into the In-oleate solution at 160 °C. Immediately after the addition, colourless In-oleate became dark orange indicating the formation of In_2S_3. The heating was stopped immediately after the injection of C_8DTCA solution and the system was allowed to naturally cool to room temperature (which took ~1 h). The product of this reaction was collected by precipitating it with acetone addition and after washing it two times with acetone (centrifuged at 5000 rpm for 3 min) and one time with a mixture of acetone and methanol (1:3 by volume) the precipitate was dried under Argon flow. The precipitate

was redispersed into toluene for various measurements. The purified In_2S_3 QDs were characterized by PXRD, UV-Vis spectroscopy, PL spectra and TEM.

A.C.3.1.5 Synthesis of SnS QDs

Tin (II) acetate (2 mmol), oleic acid (1 mL), oleyl amine (1 mL) and 1-octadecene (6 mL) was taken in a 3 neck Rb flask and heated and degassed under vacuum at 105 ºC for 2-4 h. Then the temperature was set to 160 °C. About 75mg C_8DTCA (0.45 mmol of "S") was dissolved in 0.5 mL oleyl amine and another 10 mL of 1-ODE added to it. Then the C_8DTCA-OlAm solution was injected very fast into the Sn-oleate solution at 160 °C. Immediately after the addition, colourless Sn-oleate became dark yellow indicating the formation of SnS. The heating was stopped immediately after the injection of C_8DTCA solution and the system was allowed to naturally cool to room temperature (which took ~1 h). The product of this reaction was collected by precipitating it with acetone addition and after washing it two times with acetone (centrifuged at 5000 rpm for 3 min) and one time with a mixture of acetone and methanol (1:3 by volume) the precipitate was dried under Argon flow. The precipitate was redispersed into toluene for various measurements. The purified SnS QDs were characterized by PXRD, UV-Vis spectroscopy, PL spectra and TEM.

A.C.3.1.6 Synthesis of Cu_2S QDs

Cupper (II) acetate, oleic acid (1 mL) and 1-octadecene (6 mL) was taken in a 3 neck Rb flask and heated, degassed under vacuum at 105 ºC for 2-4 h. Then the temperature was set to 140ºC. About 75 mg C_8DTCA (0.45 mmol of "S") was dissolved in 0.5 mL oleyl amine and another 10 mL of 1-ODE added to it. Then the C_8DTCA-OlAm solution was injected very fast into the Cu-oleate solution at 140 ºC. Immediately after the addition, Cu-oleate became greenish black indicating the formation of Cu_2S. The heating was stopped immediately after the injection of C_8DTCA solution and the system was allowed to naturally cool to room temperature (which took ~1 h). The product of this reaction was collected by precipitating it with acetone addition and after washing it two times with acetone (centrifuged at 5000 rpm for 3 min) and one time with a mixture of acetone and methanol (1:3 by volume) the precipitate was dried under Argon flow. The precipitate was redispersed into toluene

for various measurements. The purified Cu_2S QDs were characterized by PXRD, UV-UV-Vis spectroscopy and TEM.

A.C.3.2 Methods for solar cell device fabrication

A.C.3.2.1 Perovskite Ligand Exchange and film fabrication:

The oleic acid capped PbS CQDs were synthesized by using C_8DTCA as a sulfur source. The perovskite solution-phase ligand exchange was carried out in Argon atmosphere. The perovskite ligand exchange was carried out and purified by slightly modified to previously reported method.[1] The starting concentration of CQD solution was set at ~10 mg/mL in octane. For solution-phase ligand exchange, 5 mL of dimethyl formamide (DMF) solvent containing 0.1 M of PbI_2 and 0.02 M ocf $PbBr_2$ and 0.1 M of MAI were added to the vial and mixed vigorously at 45-50 °C for about 20-30 minutes. . A 5 mL of PbS CQD octane solution (10 $mgmL^{-1}$) was added to 5 mL of precursor solution in Argon atmosphere. These were mixed vigorously for 1–2 min until the CQDs completely transferred to the DMF phase. The DMF solution was washed three times with octane to remove the residual OA ligands. After ligand exchange, CQDs were precipitated via the addition of toluene, and were separated by centrifugation. After 20 min of drying, the CQDs were then redispersed in butylamine (200 $mgmL^{-1}$) to facilitate the film deposition. The exchanged ink was deposited by single-step spin-coating at 2,500 r.p.m. for 30s to achieve~200 nm thickness.

A.C.3.2.2 PbS CQDs Solar Cell Fabrication:

The solar cells were prepared on a pre-patterned ITO substrate (2.5 cm × 2.5 cm). Two layers of ZnO nanoparticles were deposited on the substrate by spin-coating at 3500 rpm. The perovskite-capped CQD film was further annealed at 70° C for 10 min under nitrogen atmosphere. Two layers of EDT ligand exchanged CQDs were deposited on top of perovskite-capped CQD film by spin-casting following reported method.[1] Top electrodes were deposited by thermal evaporator from Hind high vacuum, model BC-300 at a base pressure of 3 x 10^{-6} mBar. 10 nm MoO_3 was deposited at 0.1$Å s^{-1}$, followed by 50 nm of Au deposition at 0.5$Å s^{-1}$ and finally 100 nm Ag was deposited at 1$Å s^{-1}$ to complete the film formation.

A.C.3.2.3 Photovoltaic performance characterization:

Current-voltage measurement was carried out with a Keithley 2634B source-meter under ambient condition. The illumination intensity of AM1.5 was provided using class-AAA solar simulator from Peccell technologies (PEC-L01). A shadow mask was used before the device to match the illuminated area closely with the device area. The light intensity was set 100 mW/cm^2 at the position of the sample, using a Thor lab flat band thermal sensor S302C (aperture size 9.3 mm).

A.C.3.2.4 Capacitance-Voltage measurement:

The Cap–V and frequency response of the devices were performed by PSM1735 (N4L) LCR meter. Cap-V measurements were carried out at frequency of 1 kHz.

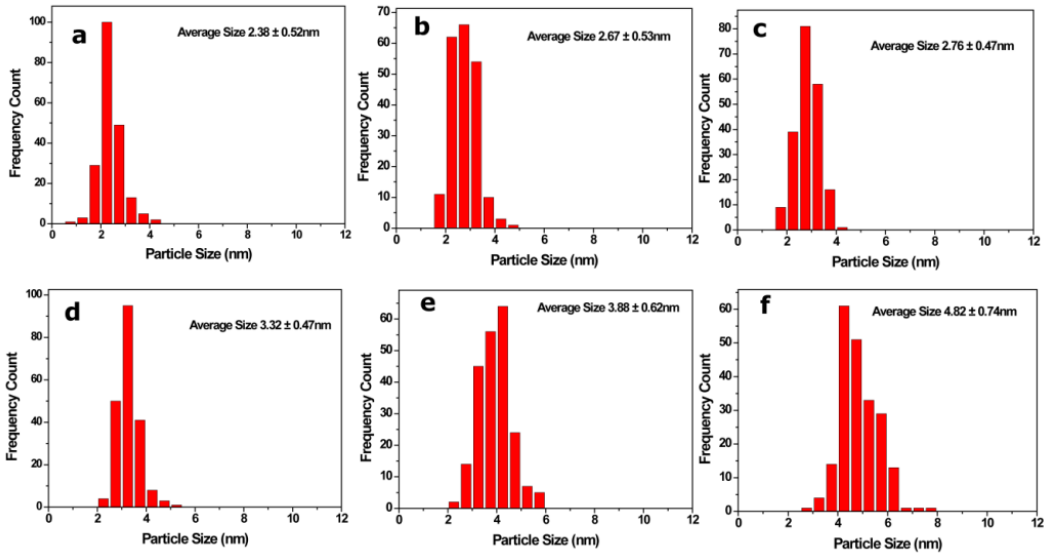

Figure A.C.3.1 Size distribution plots of PbS QDs synthesized at different temperatures (following path-IIB). (a) at 80 °C, (b) at 90 °C, (c) at 100 °C, (d) at 120 °C, (e) 130 °C and (f) at 160 °C.

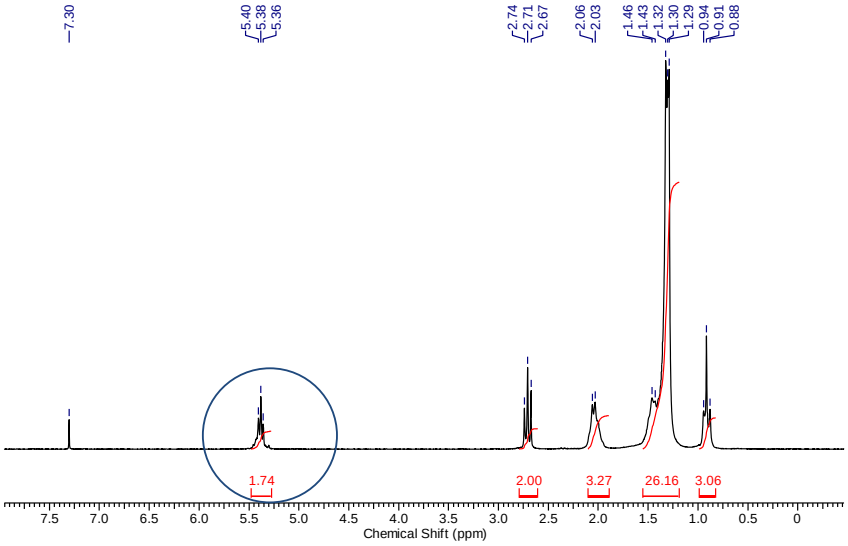

Figure A.C.3.2 ^{1}H NMR spectra of C_8DTCA and n-butyl amine mixture at room temperature. The spectrum shows a mixture of two compound C_8DTCA and n-butyl amine. There is no shift in CH_2 (near to –NH, marked in blue).

As n-butyl amine is more reactive than oleyl amine, so obviously it is expected that in presence of n-butyl amine the C_8DTCA can convert to corresponding thiourea (at ~25 ºC) but in Figure S15 showed it does not react at room temperature (it's a mixture of two compound only). Obviously it is expected oleyl amine will not react with C_8DTCA at room temperature, then we heated the C_8DTCA with oleyl amine at 50 ºC, again it didn't change (**Figure A.C.3.2**).

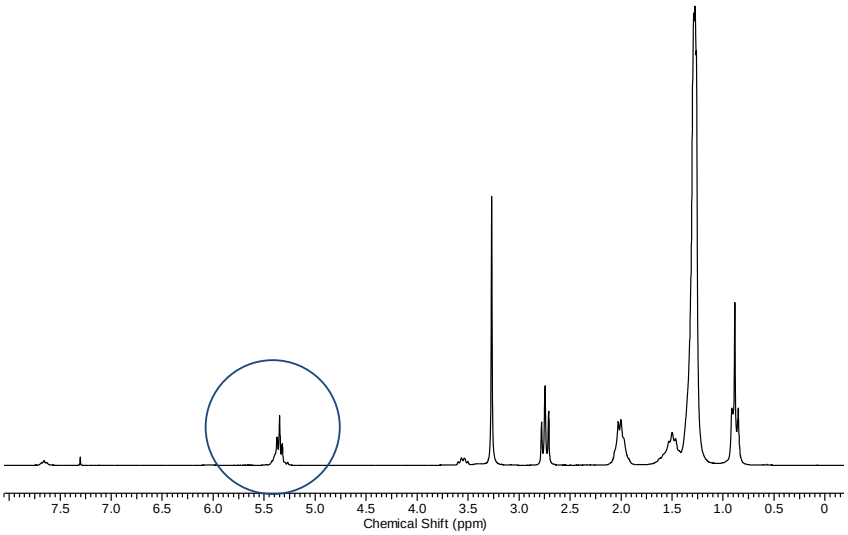

Figure A.C.3.3 ^{1}H NMR spectrum of C_8DTCA after heating at 50 ºC in oleyl amine. The spectrum shows that mixture of two compound C_8DTCA and oleyl amine. The blue marked peak corresponds to CH_2 (near to –NH of C_8DTCA) which has not changed.

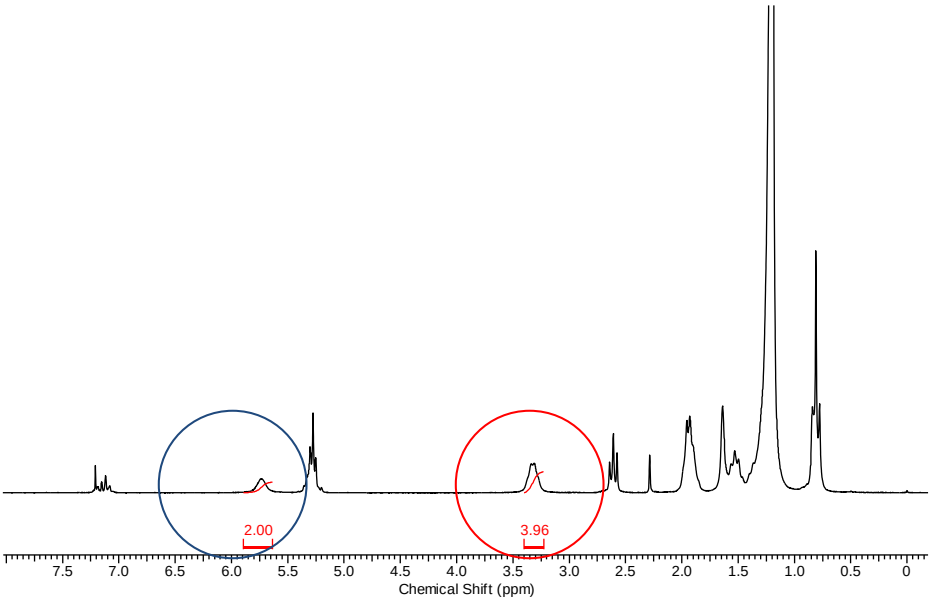

Figure A.C.3.4 ^{1}H NMR spectra of C_8DTCA after heating at 140 ºC in oleyl amine for 1h. The spectrum shows the transformation of C_8DTCA to thiourea. The two marked peaks arise due to the formation of thiourea. The blue marked peak due to –NH and red marked are for -CH_2 (near to –NH of thiourea).

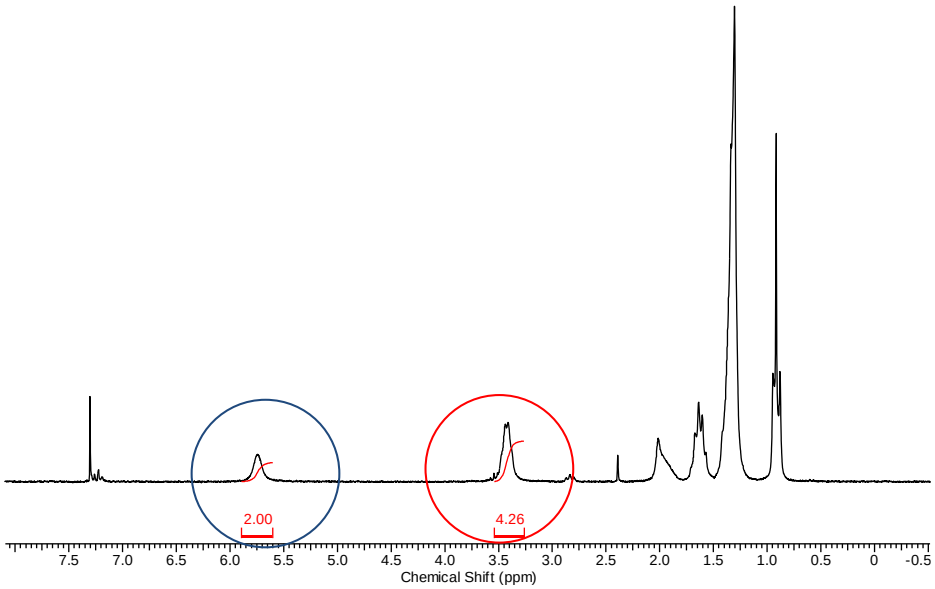

Figure A.C.3.5 ^{1}H NMR spectra of C_8DTCA after refluxing at in toluene for 1-2 h. Excess toluene were removed by using rotary evaporator. The spectra shows the C_8DTCA decomposed to thiourea. The two marked peaks arise due to the formation of thiourea. The blue marked peak due to –NH and red marked are for -CH_2 (near to –NH of thiourea).

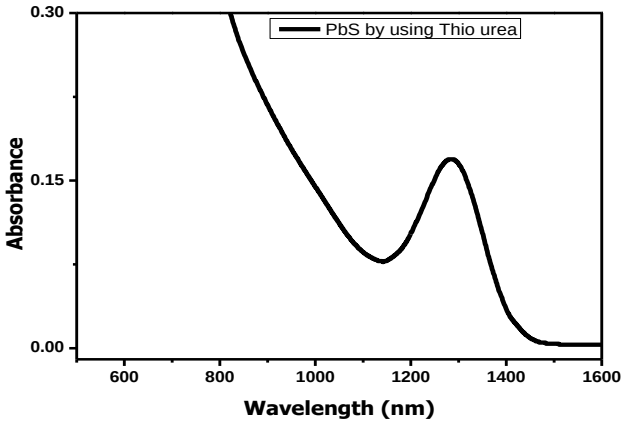

Figure A.C.3.6 NIR-Absorbance spectra of PbS QDs prepared by using N,N´-octyl thiourea as a sulfur source.

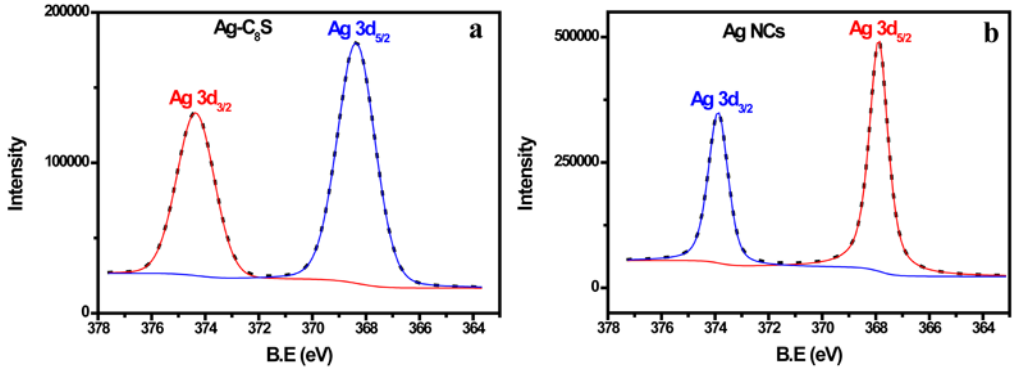

Figure A.C.4.1: XPS spectra of Ag3d region; a) for Ag-C_8S, and b) for Ag NCs.

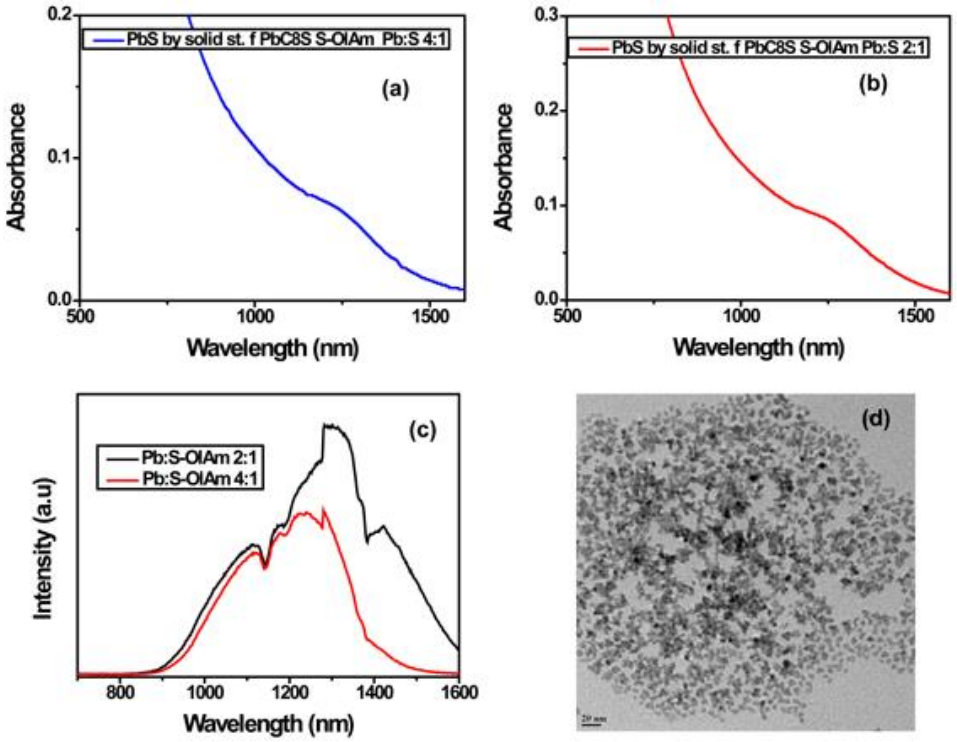

Figure A.C.4.2: PbS NCs synthesized by solid state using S-OlAm as a sulfur source; NIR absorption spectra of PbS; a) Pb:S-OlAm 4:1, b) Pb:S-OlAm 2:1. c) NIR-emission spectra of PbS NCs, black solid line is for Pb:S-OlAm 2:1and red solid line for Pb:S-OlAm 4:1. d) TEM image of PbS NCs synthesized by solid state using S-OlAm as a sulfur source.

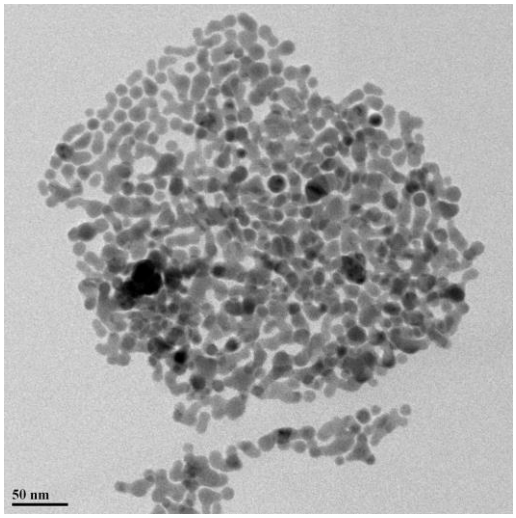

Figure A.C.4.3: TEM image of Ag_2S NCs synthesized by solid state grinding method using S-OlAm as a sulfur source.

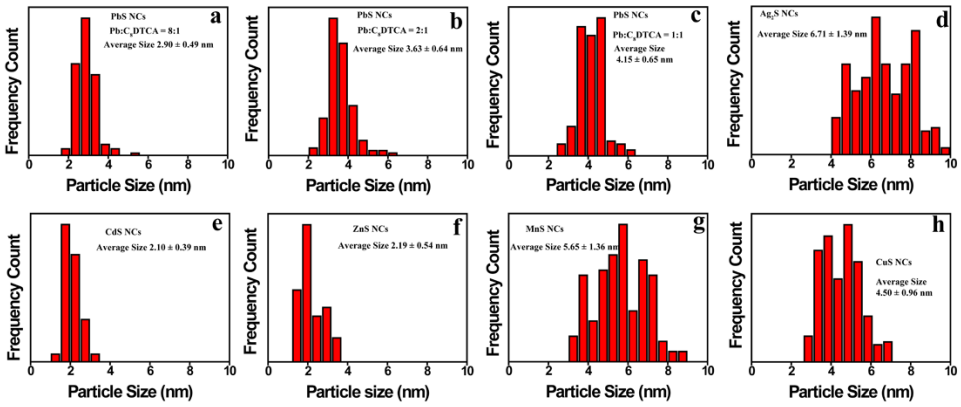

Figure A.C.4.4: Size distribution plot of different metal sulfide NCs synthesized by solid state method. PbS NCs synthesized at different Pb: C_8DTCA ratio; a) PbS NCs at 8:1, b) PbS NCs at 2:1, c) PbS NCs at 1:1. d) Ag_2S NCs, e) CdS NCs, f) ZnS NCs, g) MnS NCs, h) CuS NCs.

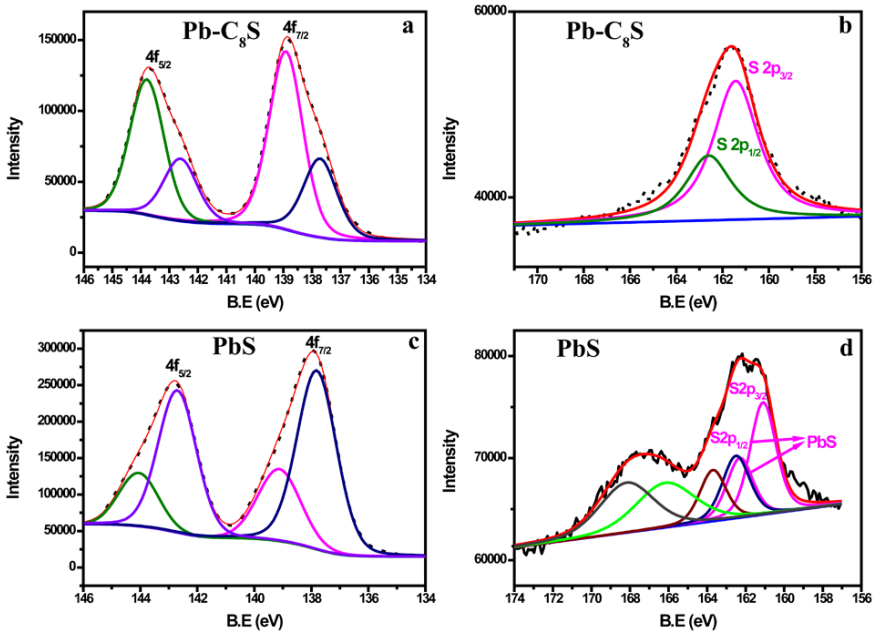

Figure A.C.4.5: XPS spectra of a) Pb 4f of Pb-C8S; b) S 2p of Pb-C8S; c) Pb 4f of PbS NCs and d) S 2p of PbS NCs.

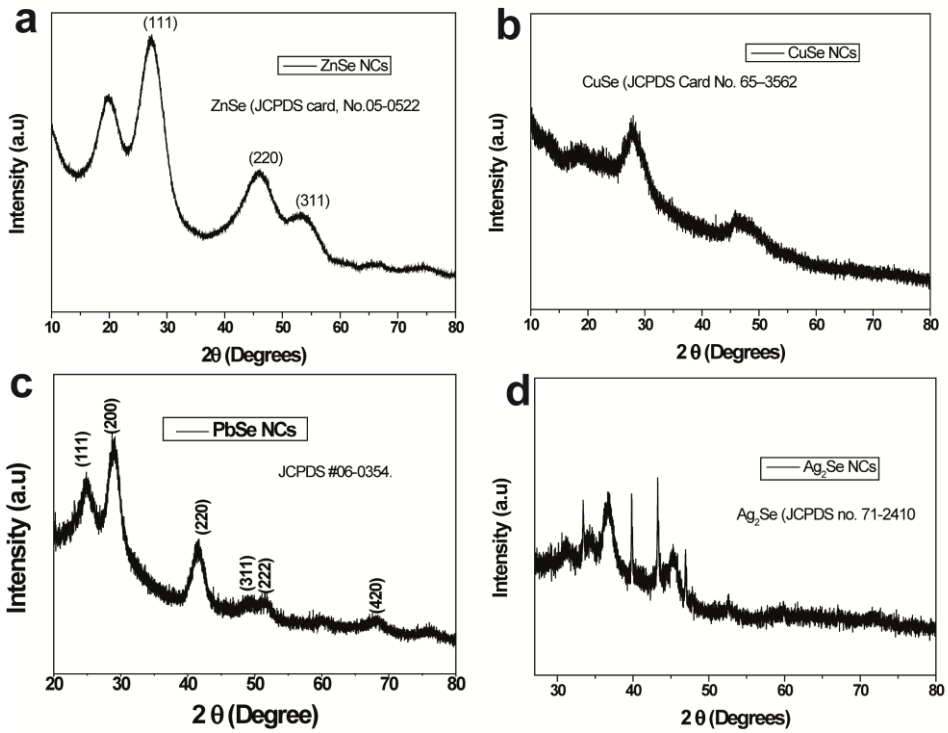

Figure A.C.4.6: PXRD of other metal selenide NCs, a) ZnSe, b) CuSe, c) PbSe and d) Ag_2Se NCs.

^{1}H NMR spectrum of C_8DTCA.**^{1}H NMR** (200 MHz, Chloroform-d) δ 5.44 (s, 2H, N-H, S-H), 3.60 - 3.48 (m, 1H), 3.02 (t, *J* = 7.3 Hz, 1H), 1.70 - 1.59 (m, 2H), 1.27 (m, 10H), 0.88 (t, *J* = 6.1 Hz, 3H).

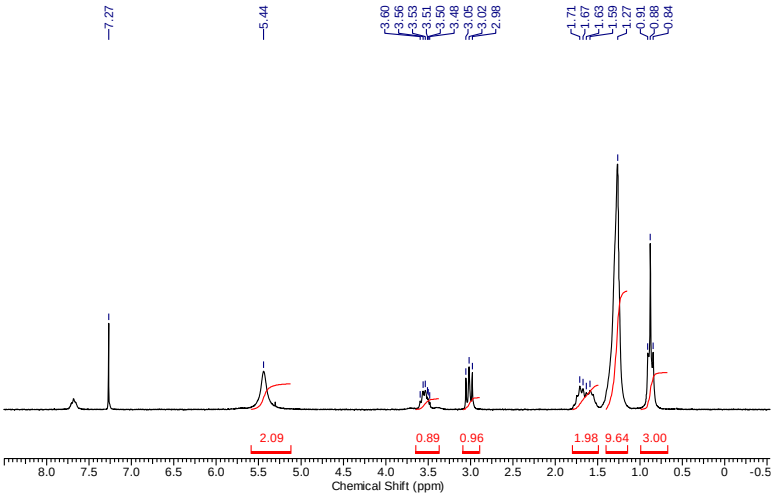

Figure A.C.4.7: ^{1}H NMR spectrum of C_8DTCA.

C_8DTCA was taken in mortar-pestle and ground it for 15-20 min in open air atmosphere at 25 °C. The NMR spectra show below indicates that it does not undergo any change under these grinding conditions.

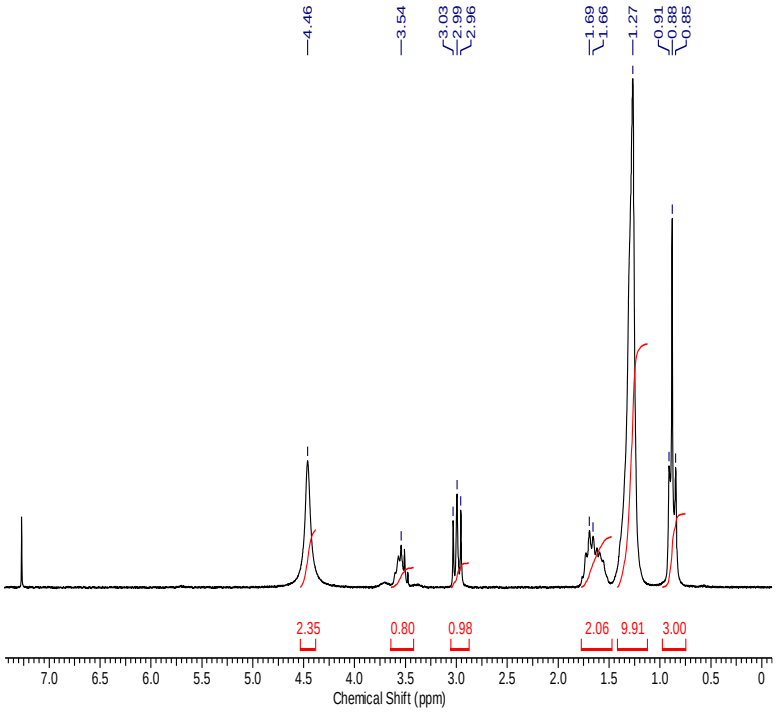

Figure A.C.4.8: ^{1}H NMR spectrum of octyl dithiocarbamic acid, after it was ground for 15 min at room temperature (25 °C).

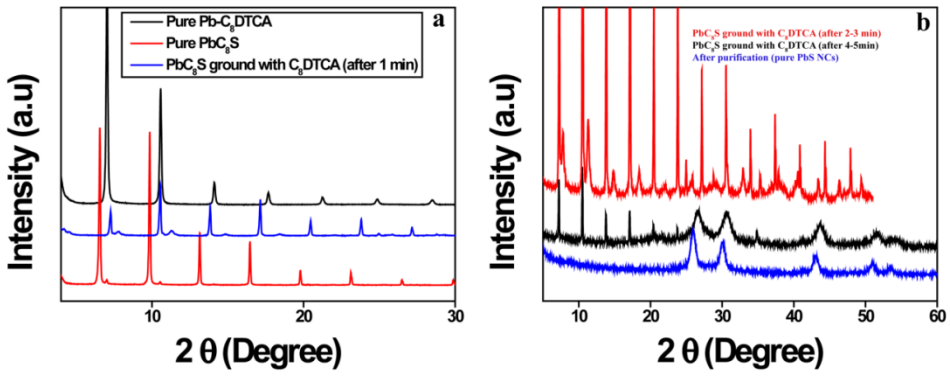

Figure A.C.4.9: PXRD data of (a) Pure Pb-C_8DTCA complex prepared at room temp. (black), pure Pb-octanethiolate (red) and solid state mixing of Pb-octanethiolate and C_8DTCA (after 1 min, solid blue line). (b) Pb-octanethiolate mixed with C_8DTCA by solid state, two different set of lamellar peaks appeared after 1-3 min (red), black solid line represent after 4-5 min of solid state grinding (before separation) and blue solid line represent after separation (pure PbS).

Both, the pure Pb-complex (Pb-C_8S or Pb-C_8DTCA), showed lamellar peaks in PXRD pattern and when Pb-C_8S was ground with highly reactive bidentate ligand (C_8DTCA), first Pb-C_8DTCA complex formed. This is confirmed by the appearance of two set of lamellar peaks in the PXRD pattern as showed in Figure A.C.4.9a (blue) and Figure A.C.4.9b. As we continued grinding, the new set of lamellar peaks shifted towards the pure Pb-C_8DTCA peaks indicating more of Pb-C_8DTCA complex forming with concomitant release of alkane thiolate ($^{-}SC_8H_{17}$) and slowly decomposes to PbS.

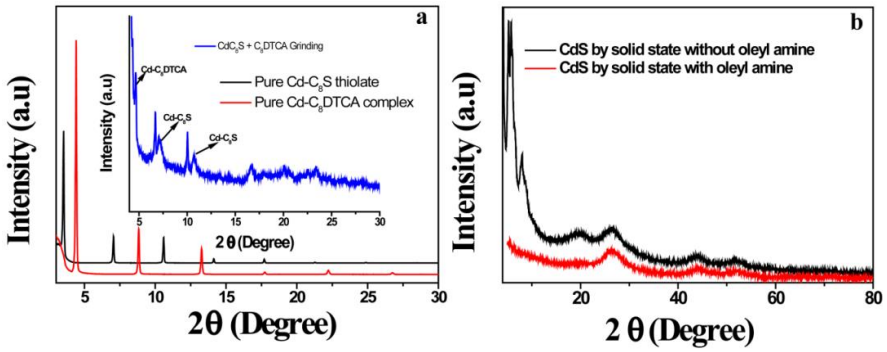

Figure A.C.4.10: PXRD of a) pure Cd-C_8S thiolate (black solid line); pure Cd-C_8DTCA complex (red solid line) and Cd-C_8S thiolate ground with C_8DTCA (blue solid line). It can be noticed that in the blue curve both of the Cd-C_8S and Cd-

C_8DTCA peaks are present indicating after grinding with C_8DTCA, Cd-C8S converts to Cd-C_8DTCA complex. b) CdS prepared by solid state using only C_8DTCA as sulfur source. Black solid line; Cd-octanethiolate ground with C_8DTCA where CdS formed as well as highly stable Cd-C_8DTCA complex also formed which is very difficult to separate from CdS. Here catalytic amount of Oleyal amine helps to decompose the Cd-C_8DTCA complex fully. Red line represents PXRD of CdS synthesized by using C_8DTCA-OlAm as a sulfur source (Figure A.C.4.10b).

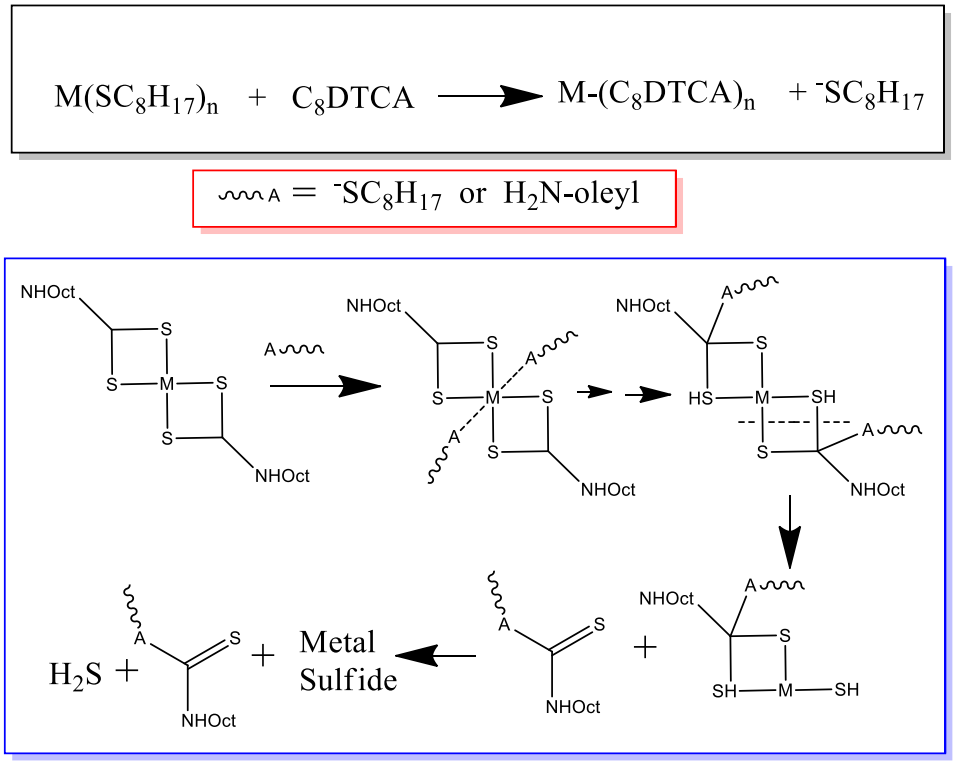

Figure A.C.4.11: Probable reaction mechanism of metal sulfide formation by solid state grinding method using only C_8DTCA or C_8DTCA-OlAm as a sulfur source. Adapted from ref. 1.

The grinding of metal thiolate with C_8DTCA or C_8DTCA-OlAm, the stronger bidentate ligand (C_8DTCA) first react with M-thiolate to form M-C_8DTCA complex (clear change in PXRD pattern showed in Figure A.C.4.9 and Figure A.C.4.10) with concomitant release of alkane thiolate ($^-SC_8H_{17}$). Here released alkane thiolate ($^-SC_8H_{17}$) or oleyl amine present in the medium (when C_8DTCA-OlAm used as sulfur source) helps to decompose the M-C_8DTCA complex to metal sulfide (probable reaction mechanism showed above in Figure A.C.4.11). Ref.1.

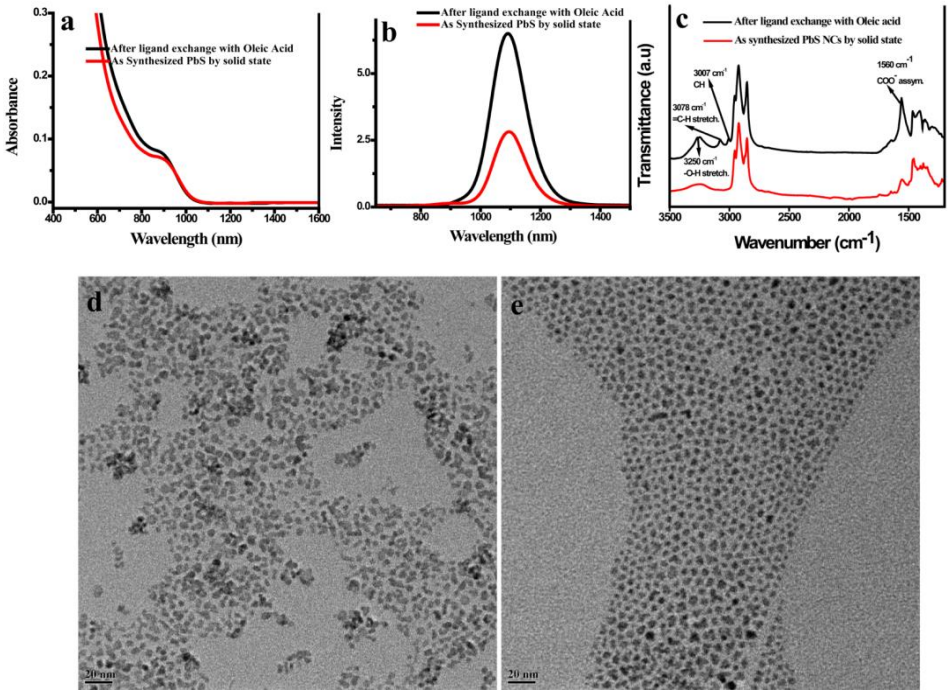

Figure A.C.4.12: PbS synthesized by solid state. a) Absorption spectra of PbS, b) NIR-Emission spectra of PbS; before ligand exchange (as prepared red solid line) and after ligand exchange with Oleic Acid (black solid line). c) ATR FTIR spectra of PbS NCs; as synthesized (thiol capped) showed in red solid line and after ligand exchange with oleic acid showed in black solid line. TEM images of PbS synthesized by solid state, d) as prepared (before ligand exchange) and e) after ligand exchange with oleic acid.

As synthesized PbS NCs are basically octane thiol capped. The peaks at wave numbers 2955 cm^{-1}, 2920 and 2652 cm^{-1} are assigned as CH_3 stretch, asymmetric and symmetric CH_2 stretching frequencies respectively (solid red line). After ligand exchange with oleic acid all peaks related to CH_3 stretching and CH_2 stretching (symmetric and asymmetric) are present and new set of peaks appear at 1560, 3007 and 3078 cm^{-1} which can be undoubtedly ascribed to the asymmetric stretching vibration of COO- (from bounded oleic acid) and stretching vibration (for cis and trans) of CH (-C=C-H) respectively. FTIR analysis thus confirms that the as synthesized PbS NCs are thiol capped and ligand exchange with oleic acid is successful.

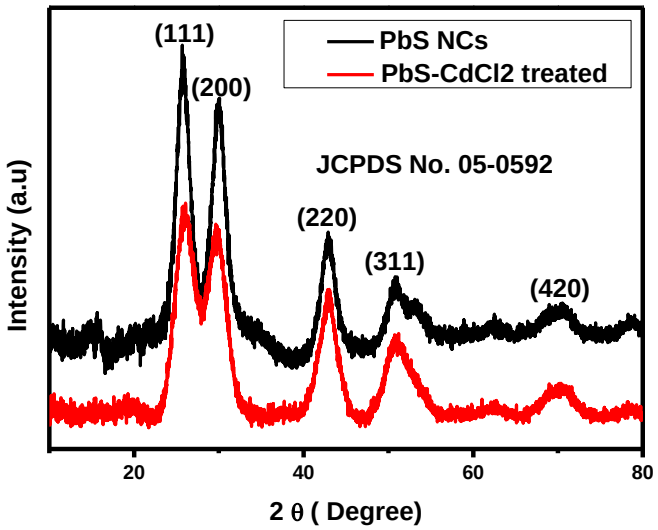

Figure A.C.4.13: PXRD of PbS NCs synthesized by solid state using C_8DTCA as a sulfur source (black) and after $CdCl_2$ surface passivation (red).

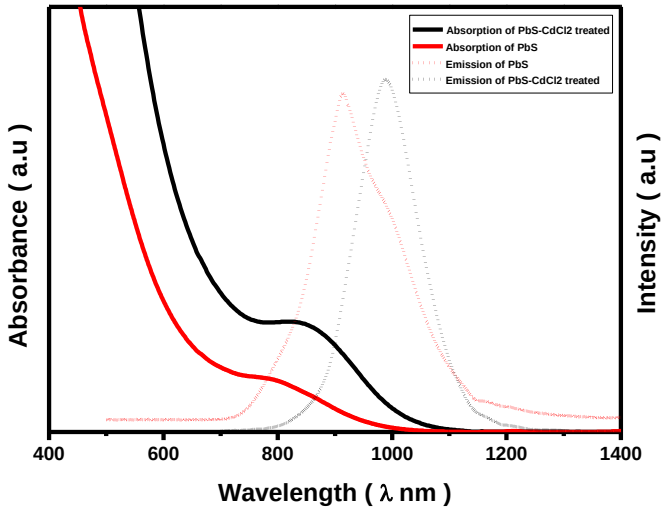

Figure A.C.4.14: NIR UV-Vis spectra and PL spectra of PbS NCs synthesized by solid state (Pb:C_8DTCA 2:1). Solid line for NIR- absorption spectra of PbS; as prepared (red solid line) and after $CdCl_2$ passivation (black solid line). Dotted line for NIR-Emission spectra of PbS; as prepared (red dotted line) and after $CdCl_2$ passivation (black dotted line).

Reference 1. Jung, Y. K.; Kim, J. I.; Lee, J.-K. Thermal decomposition mechanism of single-molecule precursors forming metal sulfide nanoparticles. *J. Am. Chem. Soc.* **2009,***132*, 178-184.

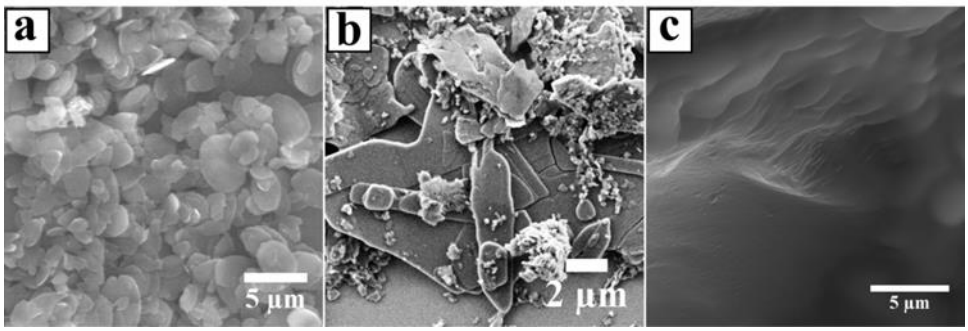

Figure A.C.5.1: SEM image of individual metal thiolates; a) Cu-thiolate, b) Ag-thiolate and c) In-thiolate.

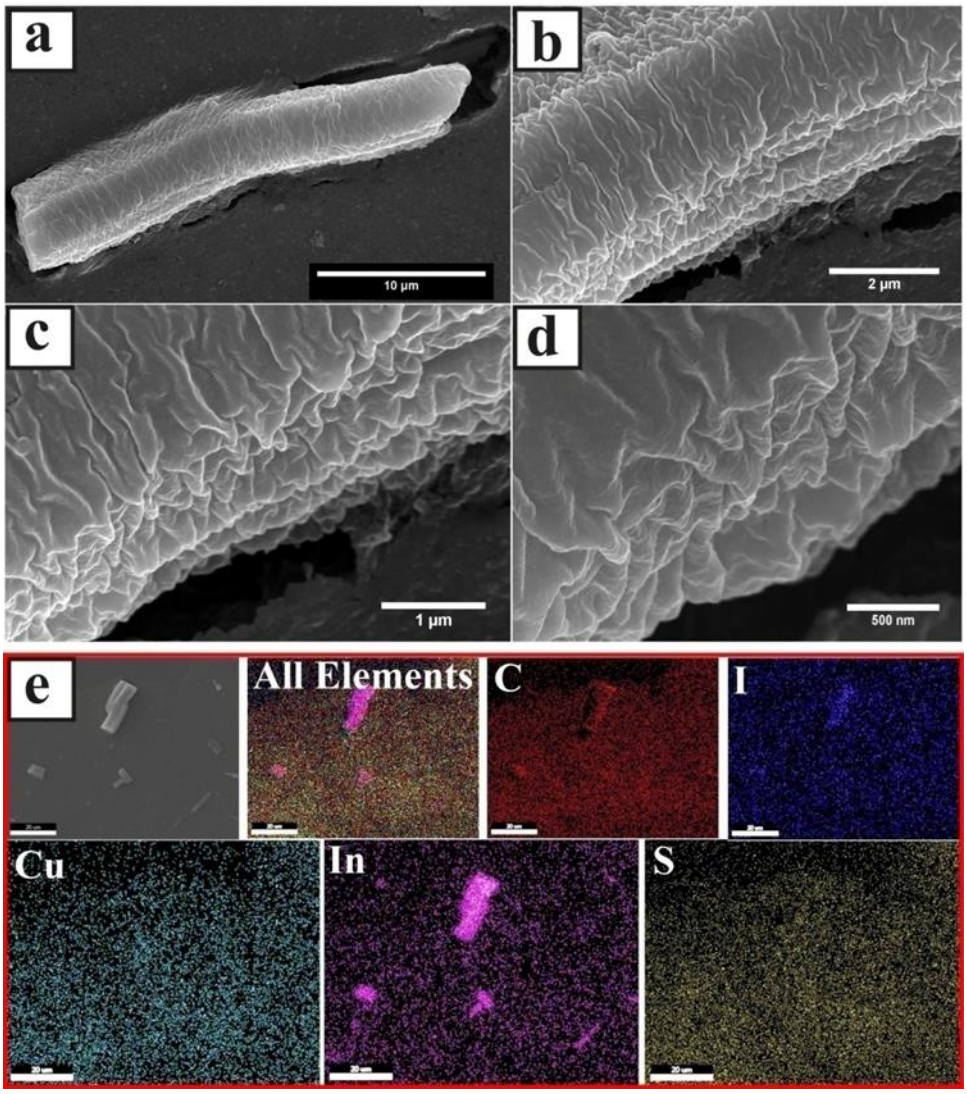

Figure A.C.5.2: a-d) SEM image of Cu-In bimetallic thiolate $CuIn(C_{12}H_{25}S)_n$ prepared using Cu(I)I as a Cu source, e) EDS mapping from SEM. SEM images

clearly show the presence of sheet like structures and EDS mapping clearly showed that Cu, In and S are overlapping with each other indicating their uniform presence all over the area analysed.

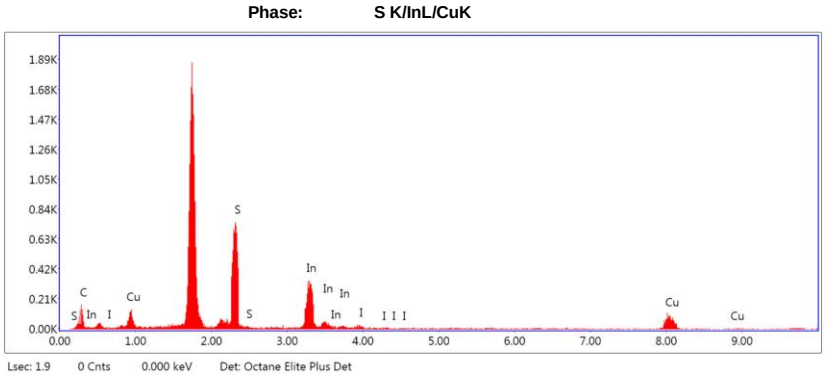

eZAF Smart Quant Results

Element	Weight %	Atomic %	Net Int.	Error %	Kratio	Z	R	A	F
C K	30.89	66.78	408.80	14.08	0.0612	1.2078	0.8693	0.1641	1.0000
S K	21.15	17.44	3213.50	5.24	0.1753	1.0483	0.9660	0.7783	1.0159
InL	27.76	8.19	1612.00	6.94	0.2230	0.7841	1.1727	1.0045	1.0201
I L	1.16	0.24	45.80	61.77	0.0087	0.7586	1.1851	0.9562	1.0303
CuK	19.03	7.92	645.70	8.49	0.1759	0.8779	1.0347	0.9791	1.0754

Figure A.C.5.3: Energy dispersive X-ray analysis of Cu-In bimetallic thiolate $CuIn(C_{12}H_{25}S)_n$ prepared using Cu(I)I as a Cu source. Atomic percentage shows Cu:In ratio ~1:1.

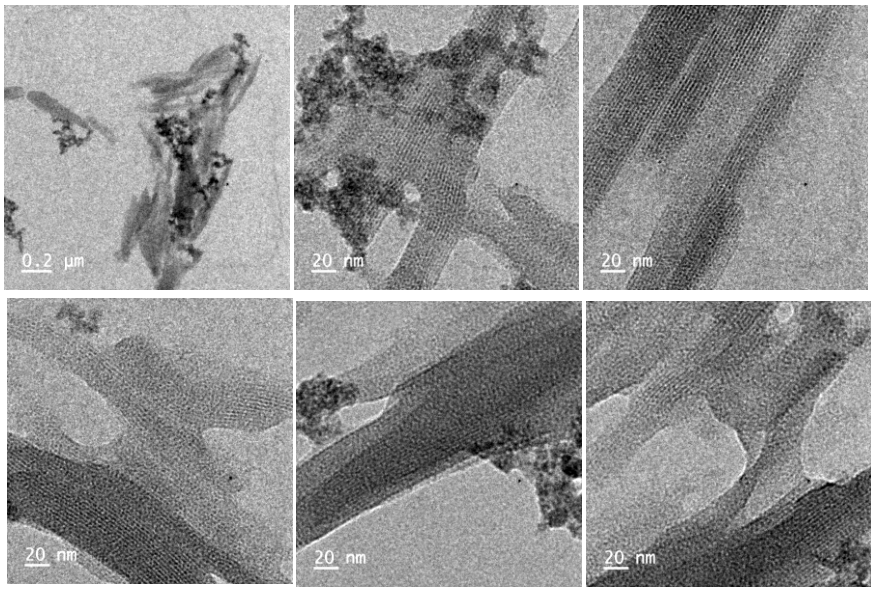

Figure A.C.5.4: TEM images of Cu-In bimetallic thiolates.

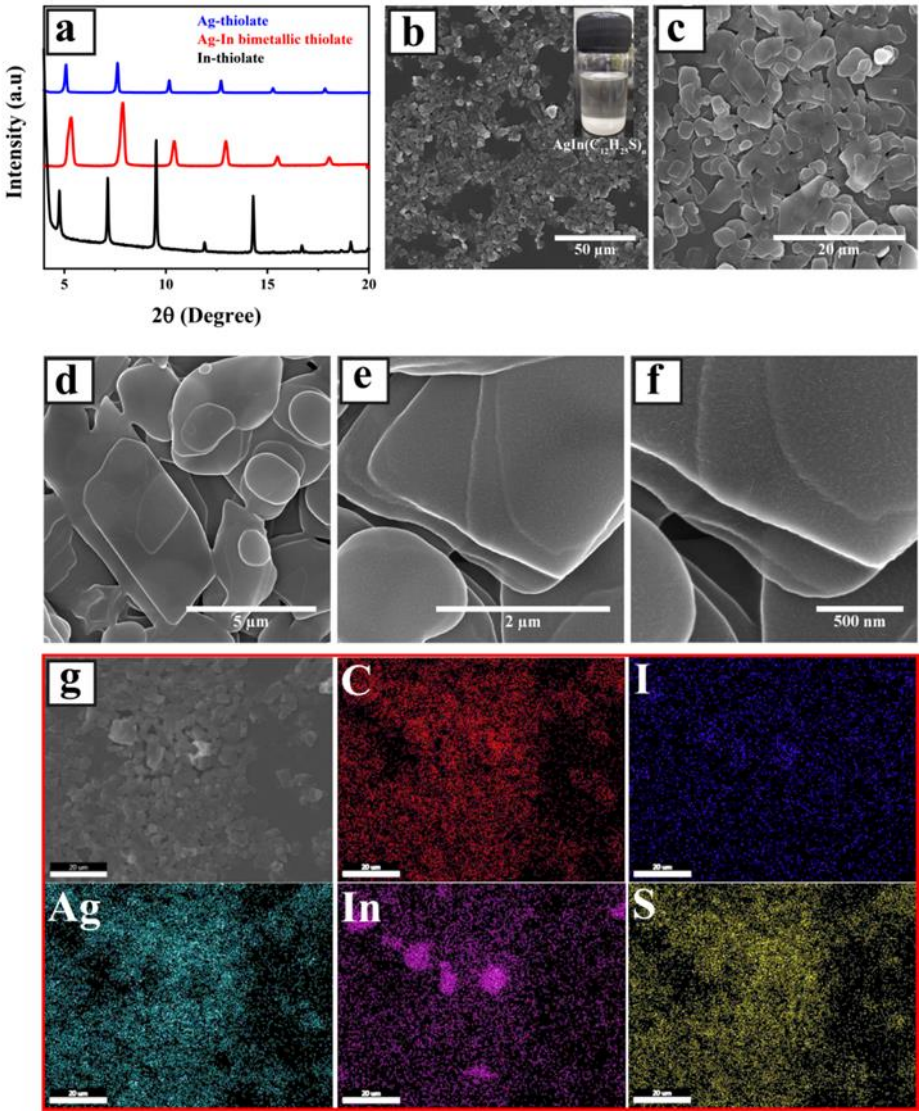

Figure A.C.5.5: a) PXRD patterns of In-thiolate (black), Ag-In bimetallic thiolate $AgIn(C_{12}H_{25}S)_n$ (red) and Ag-thiolate (blue), b-f) SEM image of Ag-In- bimetallic thiolate (inset of b is the photo of the Ag-In bimetallic thiolate dispersion), g) EDS mapping from SEM. The PXRD pattern shows (*00l*) reflection and it is clear from the PXRD pattern that the (*00l*) peaks of $AgIn(C_{12}H_{25}S)_n$ are shifted towards higher 2θ value as compared to the pure $In(C_{12}H_{25}S)_3$ and $Ag(C_{12}H_{25}S)$. The SEM image of the $AgIn(C_{12}H_{25}S)_n$ clearly display layered (sheet) like structure and EDS mapping clearly showed that Ag, In and S are overlapping with each other indicating their uniform presence all over the area analyzed.

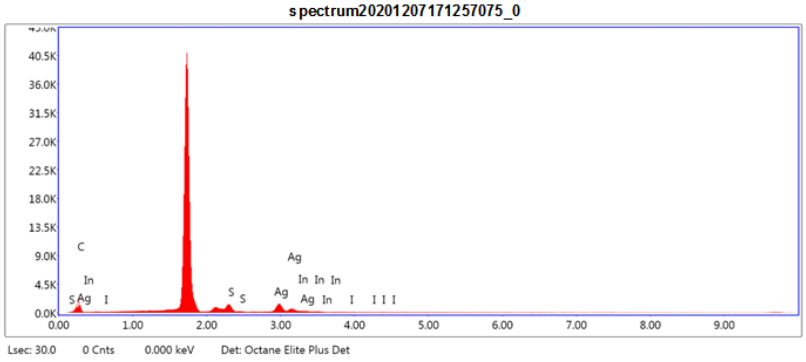

eZAF Smart Quant Results

Element	Weight %	Atomic %	Net Int.	Error %	Kratio	Z	R	A	F
C K	39.51	84.19	357.64	14.01	0.2047	1.1045	0.9217	0.3015	1.0000
S K	12.13	6.59	517.49	13.47	0.1078	0.9521	1.0102	0.9117	1.0240
Ag L	23.83	3.85	412.17	4.71	0.1940	0.7301	1.2142	1.0988	1.0154
In L	22.00	3.30	29.15	7.88	0.0154	0.7110	1.2208	1.0606	1.0194
I L	2.53	2.07	5.15	57.90	0.0037	0.6872	1.2305	0.9965	1.0266

Figure A.C.5.6: Energy dispersive X-ray analysis of Ag-In bimetallic thiolate ($AgIn(C_{12}H_{25}S)_n$). Atomic percentage shows Ag:In ratio ~1:1.

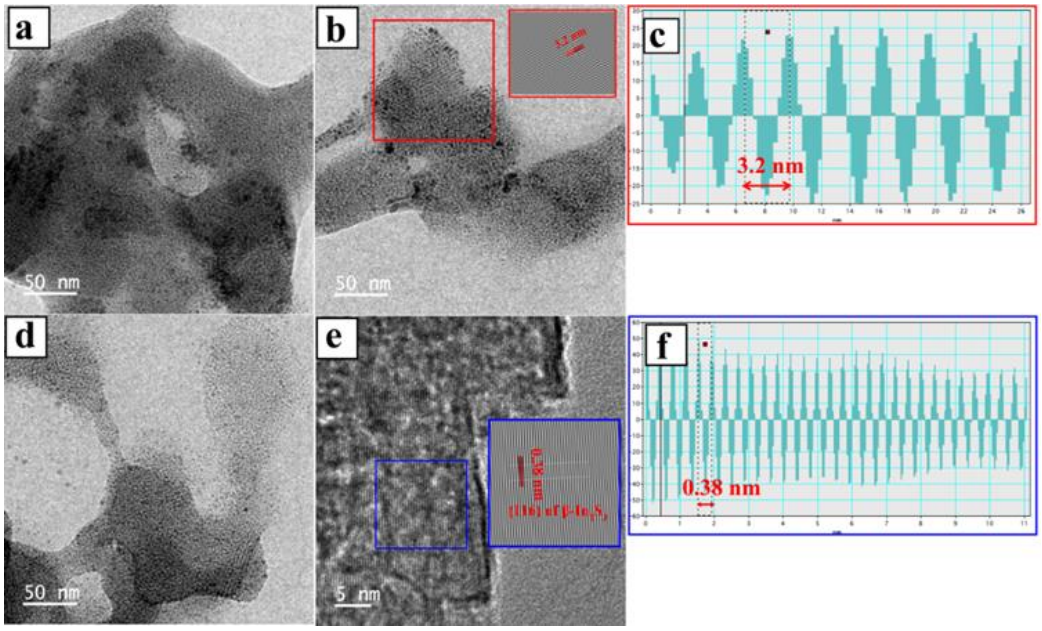

Figure A.C.5.7: TEM images of Ag-In bimetallic thiolates; a), b), d) and e). b) Inset shows the IFFT of the marked area (red) for the interlayer spacing calculation of Ag-In bimetallic thiolate, and c) shows the interlayer spacing of Ag-In bimetallic thiolate. Although Ag-In bimetallic thiolates shows sheet like structure but it is highly sensitive towards high power electron beam and reduced to Ag metallic particles can

be seen very small sized particles all over the area in a,b and d and also if we expose the sample to electron beam for longer time (4-10 mins), the thiolate decomposed to a new material with sheet like morphology. And the calculated d-spacing value 0.38 nm is matching with the (116) lattice planes of β-In_2S_3 ((JCPDS 25-0390).[1]

Table A.C.5.1: Interlayer spacing of metal thiolates

Metal thiolates	$\theta_{(001)}$	d (nm)
Cu-thiolate	2.64	3.35
Ag-thiolate	2.54	3.48
In-thiolate	2.41	3.66
Cu-In mixed metal thiolate	2.54	**3.48**
Ag-In mixed metal thiolate	2.782	**3.17**

We have tried the bimetallic sulfide NCs synthesis by mechano-chemical grinding method using different sulfur source such as C_8DTCA (octyl ammonium octyl dithiocarbamate, which we have used earlier in the synthesis of various binary metal sulfide NCs by hot injection method[2] as well as solid state grinding method),[3] thiourea and oleyl amine sulfur complex (OlAm-S) as sulfur source and we observed that C_8DTCA and thiourea both react very slowly due to their low reactivity. After grinding with C_8DTCA and thiourea for few mins (15 mins), the final products are purified and the PXRD patterns do not show any characteristic peak of $CuInS_2$ but the PXRD pattern is well matched with the Cu_2S. Whereas, the OlAm-S or OlAm-Se complex works well and provides phase pure bimetallic chalcogenide materials. This could be due to the comparatively high reactive nature of OlAm-S or OlAm-Se complex that is known to release S^{2-} or Se^{2-} very rapidly as necessary for the formation of phase pure bimetallicNCs via mechano-chemical methods.

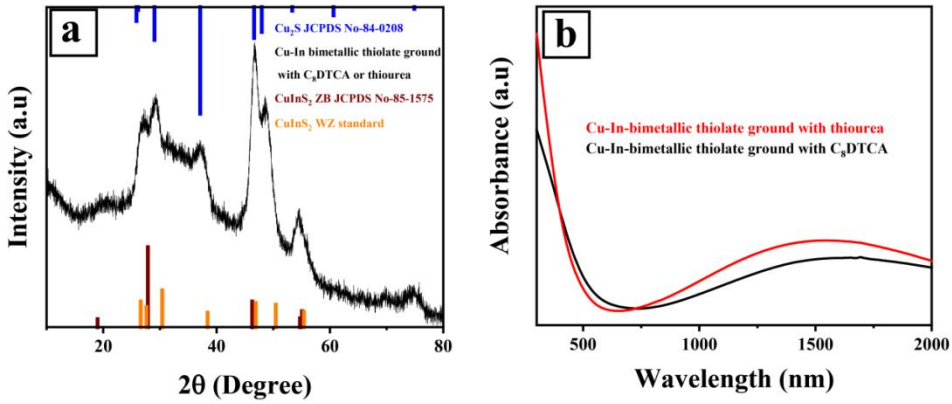

Figure A.C.5.8:PXRD patterns aftergrinding the bimetallic thiolates paste with different sulfur sourceC_8DTCA and thiourea where both react very slowly and due to distinct reactivity of two different metals (Cu and In in case of $CuInS_2$), the formation of copper sulfide binary system overtakes the formation of bimetallic sulfide NCs. a) PXRD data after grinding with Cu-In bimetallic thiolates which was matched with the hexagonal high chalcosite Cu_2S phase, b) absorption spectra aftergrinding the bimetallic thiolates paste with C_8DTCA and thiourea. In both cases absorption spectra shows characteristic surface Plasmon resonance of Cu_2S whereas no absorption peak for $CuInS_2$ observed.

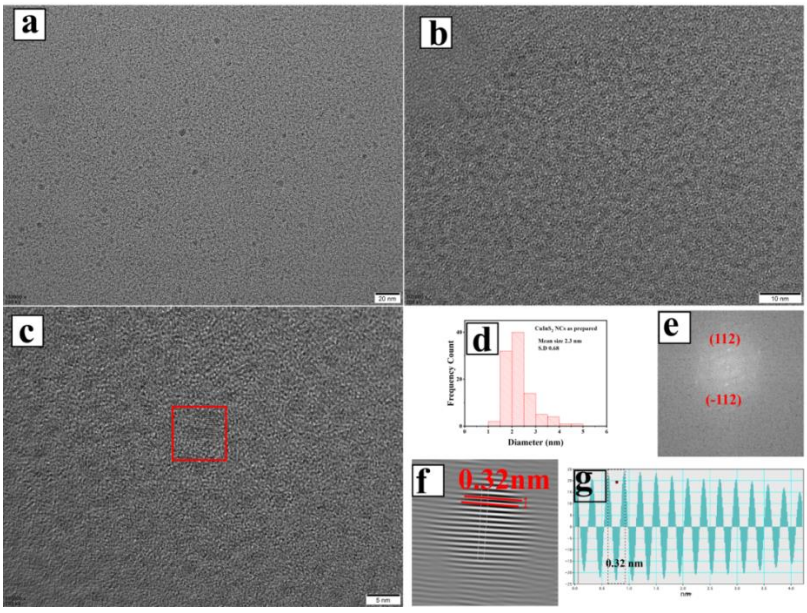

Figure A.C.5.9: a-c) TEM images of as synthesized $CuInS_2$ NCs by mechano-chemical method, d) size distribution plot of the $CuInS_2$ NCs, e) Fast Fourier transform (FFT) of a $CuInS_2$ NCs marked by a red cube in HRTEM image (c) where

diffraction from the CP lattice (112) of $CuInS_2$ NCs is observed, f) the corresponding IFFT image of the same and g) shows inter-planar spacing about 0.32 nm, consistent with the (112) d-spacing of the $CuInS_2$ bulk chalcopyrite (CP) structure.

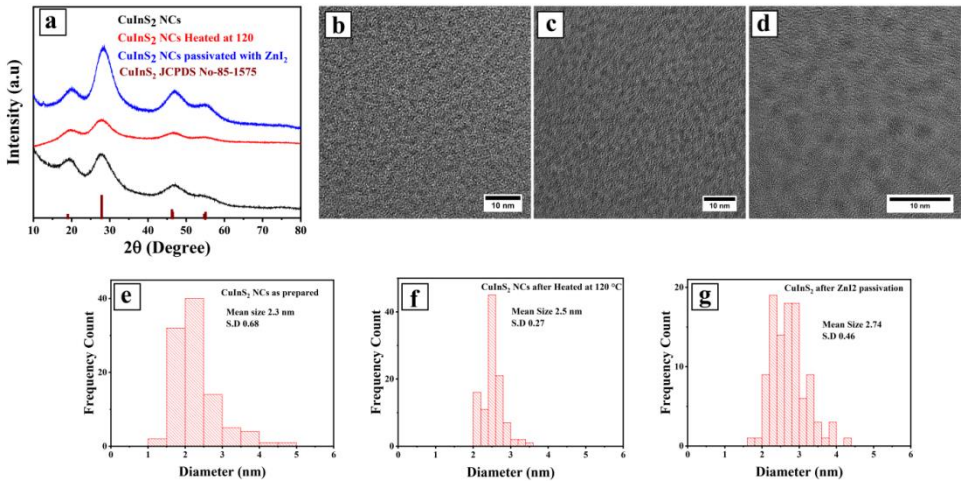

Figure A.C.5.10: a) PXRD of $CuInS_2$ NCs as synthesized by mechano-chemical method (black), after heating at 120 °C (red) and after ZnI_2 passivation (blue), TEM images of $CuInS_2$ NCs by b) mechano-chemical method, c) after heating at 120 °C and d) after ZnI_2 passivation, size distribution plot e) mechano-chemical method, f) after heating at 120 °C and g) after ZnI_2 passivation.

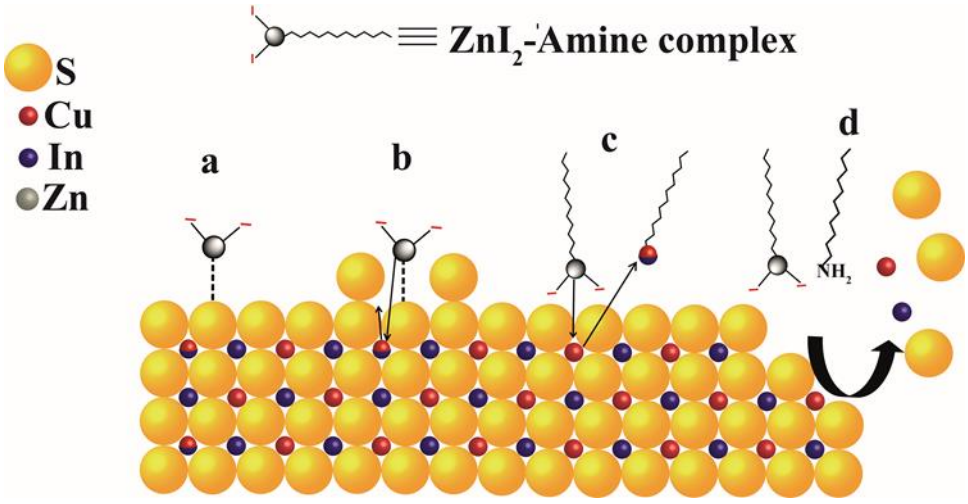

Figure A.C.5.11: Schematic representation of a $CuInS_2$ NC surface illustrating the chemical processes that can take place after ZnI_2 addition. (a) The ZnI_2 can adsorb on the CuIns2 NCs surface, which can be called as ZnI_2 passivation. (b) Alloying: the adsorbed ZnI_2 could diffuses inward as Zn^{2+}, while Cu^{+} and/or In^{3+} ions diffuse

outward. (c) Cation exchange: the adsorbed ZnI_2 complex as Zn-amine complex can take place exchange reaction at the $CuInS_2$ surface, through which Zn^{2+} is incorporated in the NC, while Cu^+ or In^{3+} cations are extracted as Cu-amine or In-amine complex. (d) Etching: chemical species in the reaction medium can promote the partial dissolution of the $CuInS_2$ NC by extracting cations and/or S^{2-} from the lattice. The schematic is true for the $AgInX_2$ cases too. Adapted from ref. 4.

The reaction temperature is a crucial parameter during the addition of ZnI_2 into the bimetallic chalcogenides NC and all the probable processes could be analyzed easily through the spectral shift in the absorbance spectra. If the ZnI_2 adsorbed on the NC surface then the spectral position could be intact or could be slightly red shifted where as other three possibilities obviously will show spectral blue shift. We observed at lower temperature 90-120 °C the ZnI_2 adsorb on the surface (passivated, as there is no shift in the absorption spectra, Annexure Figure A.C.5.12a) and at higher temperature (>140 °C), the ZnI_2 could help in alloying or cation exchange as it is clearly showing spectral blue shift in the absorption spectra (Annexure Figure A.C.5.12b). Although, alloying or through cation exchange help to improve the optical properties of bimetallic chalcogenides but we observe the improvement of optical properties by ZnI_2 surface passivation at comparatively lower temperature (90-120 °C). At very high temperature (200 °C), chemical species are etching from the NC surface so size reduced (Annexure Figure A.C.5.12f) and large blue shift in the absorption and emission spectra (Annexure Figure A.C.5.12c and Annexure Figure A.C.5.12d (deep brown spectra) and there is a possibility also that some of the species re-deposited such a high temperature. Although, some of the material shows high QY when ZnI_2 added at high temperature but due to very low yield we have chosen the surface passivation at lower temperature.

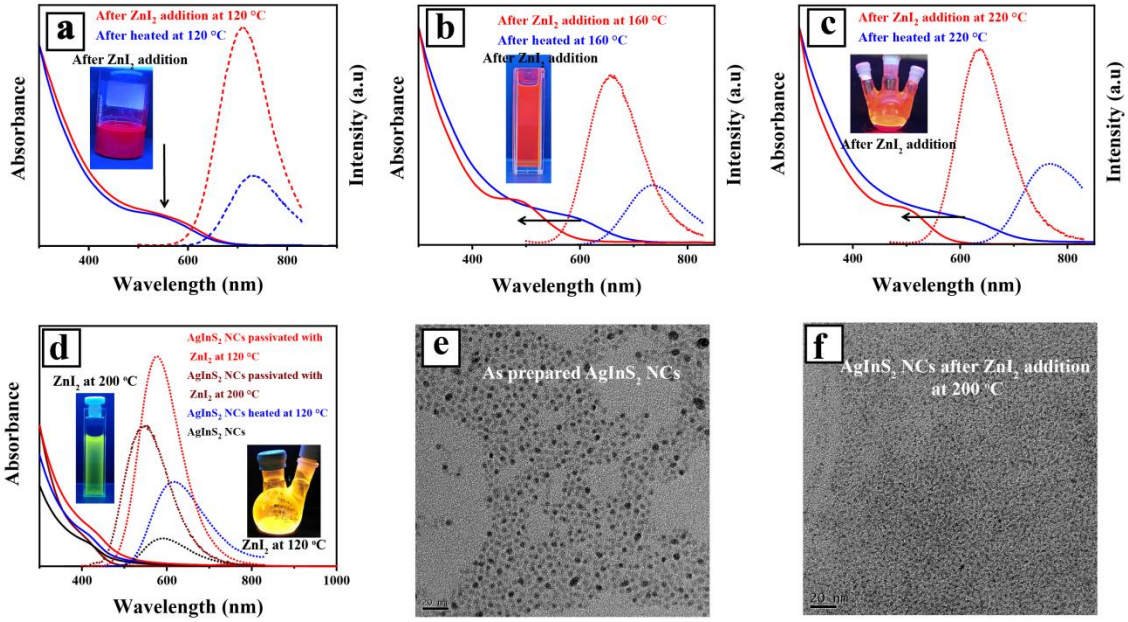

Figure A.C.5.12: As synthesized metal chalcogenides were heated at different temperature and ZnI_2 added at different temperature. Absorption and PL spectra of $CuInS_2$ heated at different temperature and ZnI_2 added at different temperature; a) heated at 120 °C and ZnI_2 added at 120 °C. b) heated at 160 °C and ZnI_2 added at 160 °C. c) heated at 220 °C and ZnI_2 added at 220 °C. d) absorption and PL spectra of $AgInS_2$ NCs, black solid line and dotted line are representing the as synthesized $AgInS_2$ NCs absorption and PL respectively, and after heated at 120 °C (blue solid line represent the absorption spectra and blue dotted line represent the PL spectra and after ZnI_2 addition at different temperature 120 °C (red solid line represent the absorption and red dotted line represent the PL spectra), 200 °C (brown dotted line reprent the absorption and brown dotted line represent the PL spectra). TEM images of $AgInS_2$ NCs e) as synthesized and f) after ZnI_2 addition at 200 °C and the size reduced due to etching.

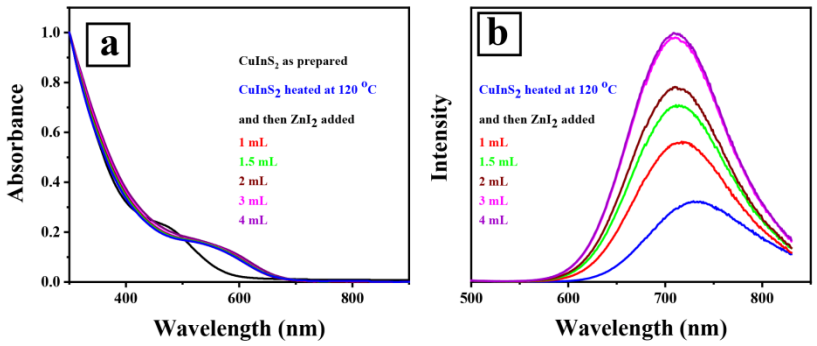

Figure A.C.5.13: a) absorption spectra of $CuInS_2$ as prepared (black), after heated at 120 °C (blue) and after addition of different amount of ZnI_2 1 mL (red), 1.5 mL (green), 2 mL(chocolate brown), 3 mL (pink), 4 mL (pale violet); b) PL spectra of $CuInS_2$ after heated at 120 °C (blue) and after addition of different amount of ZnI_2 1 mL (red), 1.5 mL (green), 2 mL(chocolate brown), 3 mL (pink), 4 mL (pale violet).

From 2 mmol of ZnI_2 (in 20 mL) stock solution was used to passivate the surface of bimetallic chalcogenide NCs. After addition of ZnI_2 at 120 °C absorption spectral position does not change much only red shifted or intact the spectral position indicating that Z-type of metal halide passivation. Here only PL Intensity (PLQY) increases and 3-4 mL of the ZnI_2 solution is the optimum concentration used for other metal chalcogenides too.

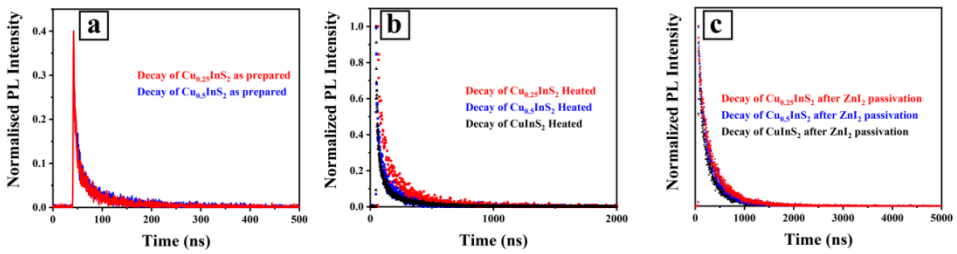

As prepared

Sample	τ_1	τ_2	B_1	B_2	χ^2
$CuInS_2$	.....	.....	.....	.....	.....
$Cu_{0.5}InS_2$	5	34	25	75	1.026
$Cu_{0.25}InS_2$	7	42	29	71	1.028

After heated at 120 °C

Sample	τ_1	τ_2	B_1	B_2	χ^2
$CuInS_2$	17	122	23	77	1.08
$Cu_{0.5}InS_2$	25	166	18	82	1.09
$Cu_{0.25}InS_2$	23	180	33	67	0.954

After ZnI_2 passivation at 120 °C

Sample	τ_1	τ_2	B_1	B_2	χ^2
$CuInS_2$	65	277	18	82	1.080
$Cu_{0.5}InS_2$	87	311	19	81	1.069
$Cu_{0.25}InS_2$	93	340	15	85	1.045

Figure A.C.5.14: Lifetime deecay curve of a) Cu_xInS_2 NCs as prepared samples, b) after heating at 120 °C and c) after ZnI_2 passivation at 120 °C. Here only Cu concentration varied without changing the In concentration where Cu:In ratios, viz.0.25:1 (red curves); 0.5:1 (blue curves); 1:1 (black curves). In the bottom panel, the lifetime values were shown in the tables.

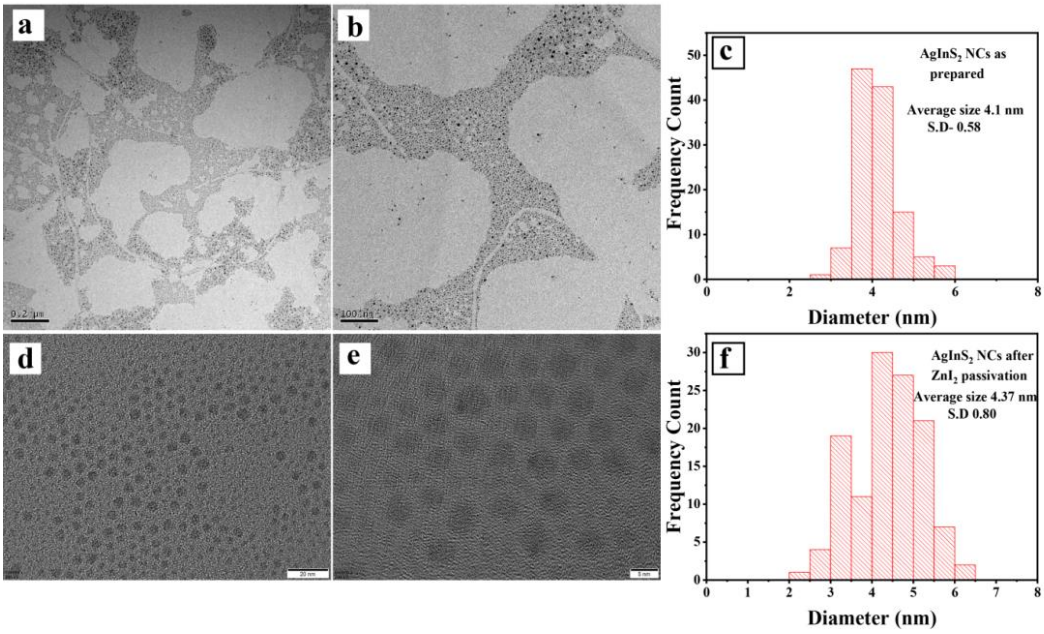

Figure A.C.5.15. TEM images of $AgInS_2$ NCs, a) and b) as synthesized; c) size distribution plot of as prepared $AgInS_2$ NCs. TEM images of $AgInS_2$ NCs, d) and e) after ZnI_2 passivation, f) size distribution plot of $AgInS_2$ NCs after ZnI_2 passivation.

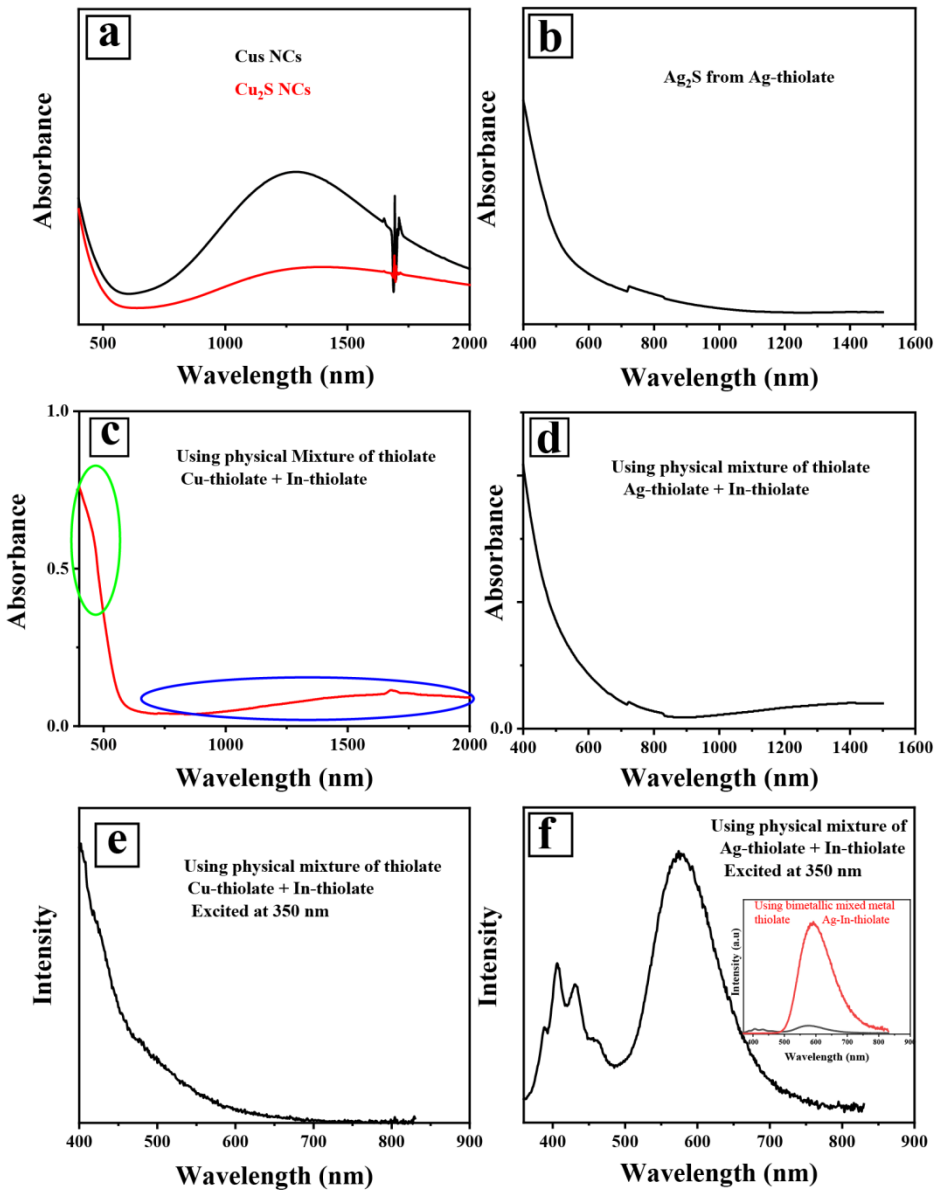

Figure A.C.5.16. Absorbance spectra of a) as prepared CuS (black) and Cu_2S NCs (red) by solid state grinding, b) as prepared Ag_2S NCs by solid state grinding; absorbance spectra of the material after mechano-chemical grinding with the individual thiolates of c) Cu and In with S-OlAm and d) Ag and In with S-OlAm; Steady state PL spectra of the as prepared materials prepared by mechano-chemical grinding with the individual thiolates (physical mixture of individual metal thiolate) of e) Cu and In with S-OlAm and f) Ag and In with S-OlAm.

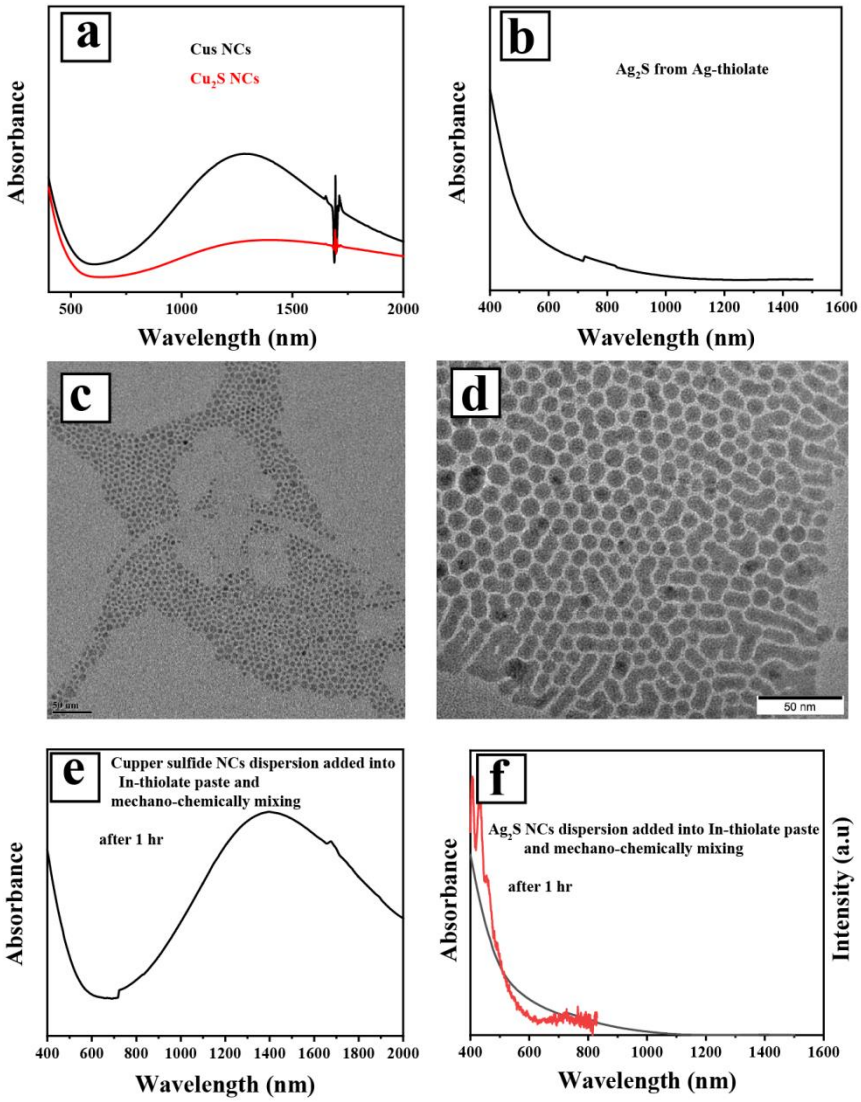

Figure A.C.5.17. Bimetallic sulfide NCs prepared by mechano-chemical mixing using as prepared Cu_2S and Ag_2S NCs through cation exchange. Absorbance spectra of a) as prepared CuS (black) and Cu_2S NCs (red) by solid state grinding, b) as prepared Ag_2S NCs by solid state grinding; TEM images of the c) Cu_2S and d) Ag_2S; absorbance spectra of the material after mechano-chemical grinding with bimetallic thiolate and binary metal sulfide dispersion, e) Cu-In bimetallic thiolate with Cu_2S, f) Ag-In bimetallic thiolate with Ag_2S. After grinding with binary metal sulfide dispersion, we did not see any change in the absorbance spectra after 30 min also.

We observed a major broad peak in the absorbance spectra (Figure A.C.5.16c) around 1500-1600 nm (marked in blue) along with a small hump at 475 nm (marked in green), which are corresponding to Cu_2S and $CuInS_2$ respectively. We also didn't see any emission (Figure A.C.5.16e) of the material after mechano-chemical grinding with the individual thiolates (physical mixture of Cu and In individual metal thiolates) with S-OlAm but in case of Ag and In with S-OlAm, shows very low intense emission peak at 590 nm along with multiple peak in between 400-450 nm. Whereas using bimetallic Cu-In or Ag-In thiolates gives phase pure material where we saw only characteristic $CuInS_2$ or $AgInS_2$ absorption peak with high intense single PL peak (for comparison $AgInS_2$ PL spectra showed in the inset of Figure A.C.5.16f, where red solid line represent the PL spectra of phase pure $AgInS_2$ NCs, prepared using bimetallic Ag-In thiolate) devoid of binary metal sulfide peak.

References:

1. Horani, F.; Lifshitz, E. Unraveling the growth mechanism forming stable γ-In_2S_3 and β-In_2S_3 colloidal nanoplatelets. *Chem. Mater.***2019**, 15, 1784-93.
2. Bera, A.; Mandal, D.; Goswami, P. N.; Rath, A. K.; Prasad, B. L. Generic and scalable method for the preparation of monodispersed metal sulfide nanocrystals with tunable optical properties. *Langmuir* **2018,***34*, 5788-5797.
3. Bera, A.; Busupalli, B.; Prasad, B. L. Solvent-Less Solid State Synthesis of Dispersible Metal and Semiconducting Metal Sulfide Nanocrystals. *ACS Sustainable Chem. Eng.* **2018,***6*, 12006-12016.
4. Berends, A. C.; Stam, W. V. D.; Hofmann, J.P.; Bladt, E.; Meeldijk, J.D.; Bals, S.; de Mello Donega C. Interplay between surface chemistry, precursor reactivity, and temperature determines outcome of ZnS shelling reactions on $CuInS_2$ nanocrystals. *Chem. Mater.* **2018**, 30, 2400-2413.

ABSTRACT

Name of the Student: Abhijit Bera **Registration No.:**10CC14A26022
Faculty of Study: Chemical Sciences **Year of Submission:** 2021
AcSIR academic centre/CSIR Lab: NCL, Pune **Name of the Supervisor(s):** Dr. B. L. V. Prasad

Title of the thesis: Scalable Synthesis of Dispersible Semiconducting Metal Chalcogenides Nanocrystals and their Application

The work incorporated in this thesis is mainly focused on various single source metal precursors like metal thiolates and metal dithiocarbamate complexes. Herein, several simple and general methods have been developed for the synthesis of various such single source metal precursors, which comprising the main two constituents of metal chalcogenide nanocrystals (NCs), namely, the tiny inorganic metal chalcogenide complex as core and an organic molecule as shell. Specially, both binary metal thiolates and bimetallic (ternary) thiolates have been prepared and both of them turned out to be excellent precursors for the synthesis of metal sulfide/selenide NCs.

The methods used to prepare metal chalcogenide NCs included a direct-heating (solvo-thermal decomposition) method or solid state grinding method. First, the large scale synthesis of various 2D molecular precursors like metal thiolates and metal dithiocarbamate complexes (M-C_8DTCA) have been developed and studied their thermal decomposition to metal sulfide NCs via solution based methods. We observed that some of the metal thiolates like Pb-thiolate requires very high temperature to decompose into PbS resulting in particles bigger than their Bohr exciton radius and hence displayed poor optical properties.

In the next, to reduce the decomposition temperature an active sulfur precursor called octyl ammonium octyldithiocarbamate (C_8DTCA) has been utilized for the synthesis of various metal sulfide NCs (including most challenging PbS NCs, with tunable optical properties) by solution based method (hot injection) or solid state grinding method. We also show that the size of the nanocrystals could be controlled by changing the reaction temperature or metal: chalcogenide precursor ratio. Interestingly, we have also been successful in establishing that these newly developed solid state grinding methods are scalable without compromising their structural and optical properties. The binary or ternary materials synthesized by these solid state routes could be re-dispersed as desired in non-polar organic solvents allowing them to be solution processible. The optical properties of the metal chalcogenide nanocrystals could further be improved by post synthetic surface passivation.

List of Publication(s) in SCI Journal(s) Emanating from the Thesis Work

List of publication (emanating from the thesis work)

1) **Bera, A.**; Prasad, B. L. V. 2D Molecular precursor for a one-pot synthesis of semiconducting metal sulphide nanocrystals. *Bull. Mater. Sci*. **2018**, *41*, 125.
2) **Bera, A.**; Mandal, D.; Goswami, P. N.; Rath, A. K.; Prasad, B. L. Generic and scalable method for the preparation of monodispersed metal sulfide nanocrystals with tunable optical properties. *Langmuir* **2018**, *34*, 5788-5797.
3) **Bera, A.**; Busupalli, B.; Prasad, B. L. Solvent-less solid state synthesis of dispersible metal and semiconducting metal sulfide nanocrystals. *ACS Sustain. Chem. Eng*. **2018**, *6*, 12006-12016.

List of papers with abstract presented (oral or poster) at national or international conferences/seminars.

1) Science Day Conference, 2016, 2017, 2018 CSIR-National Chemical Laboratory. (*poster presented*).
2) International Conference on Nano Science and Technology (*ICONSAT*), IISC Bangalore, 2018 (*poster presented*)
3) NCL-RF Annual Students' Conference, CSIR-National Chemical Laboratory, 2019 (*delivered oral presentation*).
4) Gordon Research Conference, (Nanomaterials for Applications in Energy Technology), Ventura, CA United States, 2019, (*poster presented*)

ACS Sustainable Chemistry & Engineering

pubs.acs.org/journal/ascecg

Correction

Correction to "Solvent-Less Solid State Synthesis of Dispersible Metal and Semiconducting Metal Sulfide Nanocrystals"

Abhijit Bera, Balanagulu Busupalli, and Bhagavatula L. V. Prasad*

ACS Sustainable Chem. Eng. **2018**, *6* (9), 12006−12016. DOI: 10.1021/acssuschemeng.8b02292

Cite This: *ACS Sustainable Chem. Eng.* 2020, 8, 17000−17000

Read Online

ACCESS | Metrics & More | Article Recommendations

In our published paper, the affiliations of the authors were incomplete. The complete affiliations are as follows:

Abhijit Bera, Balanagulu Busupalli, and Bhagavatula L. V. Prasad: Physical/Materials Chemistry Division, National Chemical Laboratory (CSIR-NCL), Dr. Homi Bhabha Road, Pune 411008, India

Abhijit Bera and Bhagavatula L. V. Prasad: Academy of Scientific and Innovation Research (AcSIR), Ghaziabad 201002, India.

Balanagulu Busupalli's present address: Department of Chemistry, Pandit Deendayal Petroleum University, Gandhinagar 382007, India.

Received: October 28, 2020
Published: November 5, 2020

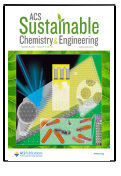

ACS Sustainable Chemistry & Engineering

Research Article

Cite This: ACS Sustainable Chem. Eng. 2018, 6, 12006−12016

pubs.acs.org/journal/ascecg

Solvent-Less Solid State Synthesis of Dispersible Metal and Semiconducting Metal Sulfide Nanocrystals

Abhijit Bera, Balanagulu Busupalli,† and Bhagavatula L. V. Prasad*

Physical/Materials Chemistry Division, National Chemical laboratory (CSIR-NCL), Dr. Homi Bhabha Road, Pune 411008, India

Supporting Information

ABSTRACT: Monolayer protected metal and metal sulfide nanocrystals (NCs) have mainly two constituents; the inorganic metal or metal chalcogenide complex as core and organic molecule as shell. Noticing that metal thiolates have these ingredients inbuilt in their structure, we investigated them as possible precursors for the preparation of monolayer protected metal and metal sulfide NCs via solid state grinding method. Accordingly silver and gold NCs have been prepared using a solvent less green approach, by the simple and convenient solid state grinding of the corresponding metal thiolate with sodium borohydride. Similarly, a large variety of uniform-sized semiconducting NCs of metal sulfides including PbS, CdS, ZnS, MnS, Ag_2S, and CuS could also be synthesized by the same solid state route by grinding the metal thiolates with octyl dithiocarbamic acid (C_8DTCA) and in some cases C_8DTCA plus small amount of oleylamine as sulfur source. Interestingly, this simple technique could be used to prepare sub-3 nm NCs like Ag_2S, PbS, and CuS which are otherwise difficult to prepare by the conventional high temperature solution routes also. Most gratifyingly, all these NCs, though were prepared by a solvent less grinding method, could be easily dispersed in nonpolar solvents as the preparation method ensued the formation of organic molecule capped NCs.

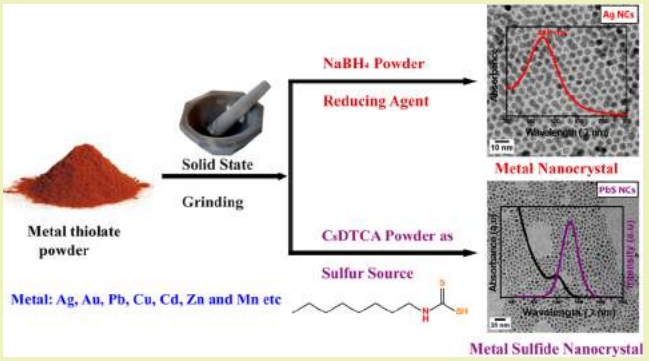

KEYWORDS: *Metal thiolates, Solid-state reaction, Nanocrystals, Optical properties, Surface modification*

INTRODUCTION

Monolayer protected metal nanocrystals (NCs), that can be dispersed in polar or nonpolar organic solvents, have tremendous application in biomedicine,[1,2] energy conversion,[3] magnetic data storage,[4] catalysis,[5,6] and other fields.[7,8] Similarly, highly dispersible transition metal chalcogenide NCs have been established as extremely useful materials for the development of numerous classes of solution processed optoelectronic devices,[9] including biological imaging,[10,11] photovoltaic devices,[12,13] photodetectors,[14] and light-emission devices.[15] All these applications require large quantities of these materials to be prepared. In fact, it is argued that obtaining large enough quantities of these materials is the main hurdle in translating their potential applications into practicing technologies. Thus, a large number of researchers have dedicated efforts to develop methods for large scale preparation of monolayer protected metal and metal sulfide NCs. In general, the synthesis of such metal or metal sulfide NCs is achieved via solvent based chemical methods (bottom-up approach) wherein metal ions are reduced/reacted with the appropriate precursor in the presence of a stabilizer to yield metal/metal sulfide NCs.[16−20] Although these chemical methods afford monolayer protected NCs with excellent control over their size and shape, unfortunately, they often result in the production of material at subgram quantities. Furthermore, many times these synthetic procedures are time-consuming and complicated and also require multiple reagents and lot of solvents during the reaction and for the purification of material. These become the main hurdles in scaling up these reactions and thus accessing large amounts of these materials turns out to be difficult. Thus, a method for synthesis of metal/metal sulfide NCs which can be scaled up and yet can be carried out under solvent-less environment, is highly desirable. In this context, engagement of reagents or some inorganic metal complexes consisting of distinct moieties that can play the role of different ingredients (such as the core of the desired NC, the capping agents etc.) would lead to the simplification of the synthetic procedure and thus is an attractive prospect. In addition, if the reaction is carried out under ambient atmosphere, at room temperature (~25 °C) and in a solvent-less environment, it adds greenness to the process and could lead to mass production of these materials that are highly sought after for many applications.

In fact, a few solid state routes were indeed reported for the synthesis of NCs. For example, high-speed vibration milling has been used for the synthesis of gold NCs, where sodium borohydride was used for the reduction of the gold salt and poly(vinylpyrrolidone) was used as a protecting agent.[21] In

Received: May 19, 2018
Revised: July 12, 2018
Published: July 22, 2018

DOI: 10.1021/acssuschemeng.8b02292
ACS Sustainable Chem. Eng. 2018, 6, 12006−12016

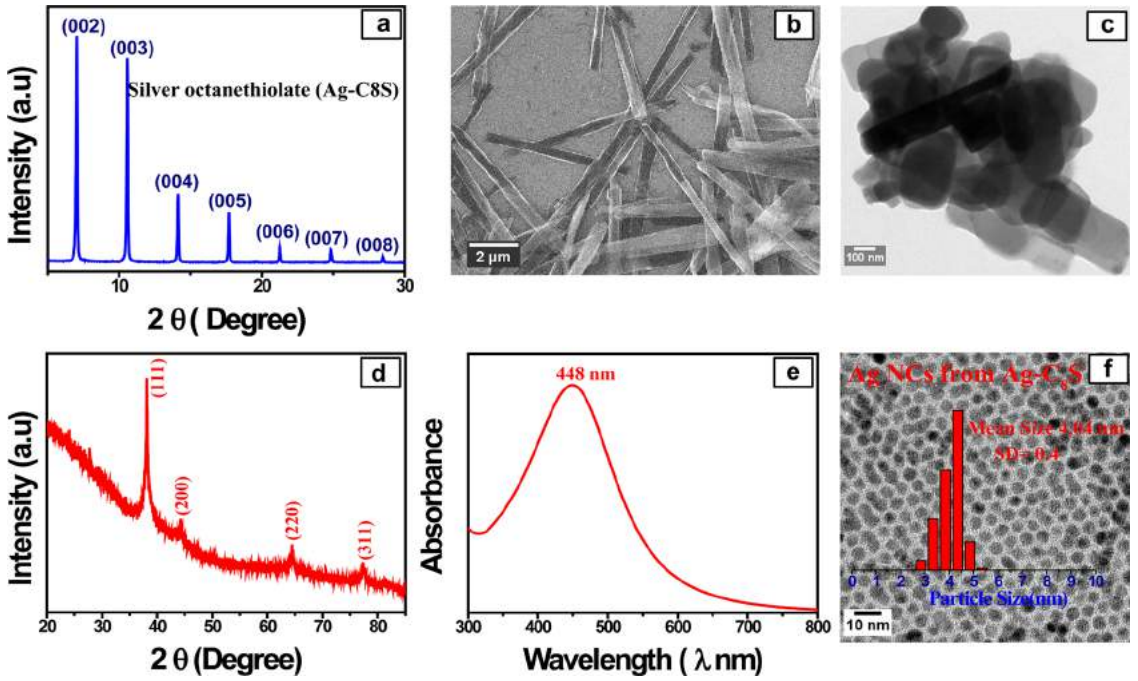

Figure 1. (a) PXRD of Ag-octanethiolate. (b) SEM image of Ag-octanethiolate. (c) TEM images of Ag-octanethiolate. (d) PXRD of Ag NCs obtained from Ag-octanethiolate. (e) UV−vis spectra of Ag NCs obtained from Ag−C_8S (Ag-octanethiolate). (f) TEM images of Ag NCs obtained from Ag−C_8S. The size distribution plot of the Ag NCs obtained is shown in the inset.

another report macroscopic quantities of bimetallic Au−Ag alloy NCs were prepared through sequential reduction by simple mortar grinding using a chitosan biopolymer as both a stabilizing and reducing agent.[22] Furthermore, there were few papers that reported the preparation of monometallic Au, Ag, Cu, Pd, and Ir and bimetallic CuAg and CuAu alloy NCs via solid state synthetic routes.[23,24] Here, the amine-borane and amine borane derivatives were employed to play dual roles—as a reducing agent and also as an in situ stabilizing agent.[24] Although, some other solid state processes also were reported, those were restricted to metallic NC systems.[25,26] While the above examples deal with NCs of slightly larger dimensions (>3 nm), the recent years have seen a surge in the synthesis of nanoclusters consisting of a fixed number of atoms and a few solid state based syntheses of these cluster systems have also been illustrated.[27−29] For instance, a silver cluster having the composition $Ag_9(H_2MSA)_7$ (H_2MSA = mercaptosuccinic acid) was synthesized in macroscopic quantities using a solid-state route.[27] More precisely, when a reaction between $AgNO_3$ and H_2MSA is carried out it was shown that silver thiolate gets formed by solid state reaction. In the next step this silver thiolate was ground with sodium borohydride resulting in the formation of a brownish black silver cluster powder consisting of a nine-atom core protected with mercaptosuccinic acid (H_2MSA). Like in the case of metallic NCs and nanoclusters described above, a few solid state routes for the preparation of semi conducting systems have also been published. Among these the noteworthy one is the synthesis of ultrasmall monodispersed 2 nm sized Bi_2S_3 NCs which are applicable for CT imaging in physiological media.[30] In addition, reports on the preparation of cadmium sulfide NCs have also appeared. In some of these nonanionic surfactants were employed as one ingredient and the resultant NCs were polydispersed and displayed broad absorption spectra.[31−34] It may be worth noting here that there have been few studies focused on the synthesis of PbS NCs based on solid state routes also. In one of them PbS NCs in the size regime 10−15 nm were prepared in the presence of a surfactant[35] while in the other paper the preparation of PbS nanocubes using lead dodecylsulfate and Na_2S as precursors was described.[36] In both cases the resulting PbS NCs did not display any characteristic excitonic peak, which are extremely important in terms of their application potential.

In this context, previously, we reported that thiolates of 2+ metal ions like Pd, Ni, Hg and Pb exist as lamellar sheets in the bulk form and these could be easily separated into individual one layer thick sheets by simply adding nonpolar solvents to the bulk material.[37] In the same way thiolates of metal ions like Ag (I),[38−41] Au (I),[42−44] and Cu (I)[45,46] have also been reported to exist as lamellar sheets in the bulk state. Realizing that these have the two main ingredients—the metal ion that can become part of the metal or metal sulfide NCs and an organic molecule, capable of becoming a capping/passivating agent—in built in their structures we reckoned that they could be utilized as precursors for the synthesis of metal or metal sulfide NCs. Indeed these metal alkyl thiolates were previously used for the synthesis of functional nanomaterials[47] like metal NCs[43,48−53] and metal sulfide[52,54−57] NCs by solution based solvo-thermal routes. Similarly metal-diethyldethiocarbamate complexes were also used previously for the synthesis of metal sulfide NCs,[58−62] but again via solvothermal conditions using high boiling solvents.

Different from the above descriptions, herein, we report the synthesis of NCs of metals like Ag, Au, and also NCs of metal chalcogenides like CdS, ZnS, MnS including the highly sought after PbS, Ag_2S, and CuS NCs through a simple and convenient solid state route wherein grinding the corresponding metal thiolate and a reducing agent (sodium borohydride) or a sulfur source (C_8DTCA or C_8DTCA dissolved in few μL of oleyl amine) yielded monolayer protected metal and metal

DOI: 10.1021/acssuschemeng.8b02292
ACS Sustainable Chem. Eng. 2018, 6, 12006−12016

Scheme 1. Preparation of Metal and Metal Sulfide NCs by Solid State Method

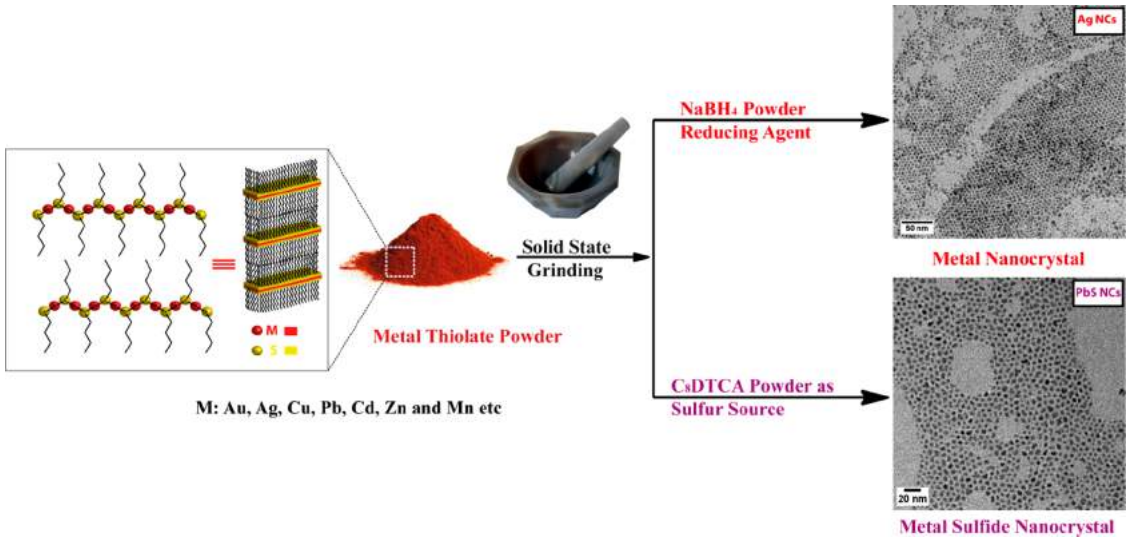

sulfide NCs, respectively. The most gratifying aspect of this procedure is that the resultant NCs were monodispersed and could be easily dispersed in nonpolar solvents though no solvent has been used during their preparation. In the case of metal NCs sodium borohydride reduces the metal thiolates to their elemental form and simultaneously generates a stabilizing agent (thiol) in situ which controls the growth of the crystals and stabilizes them in the nanosize regime. Here the extra advantage is that both of the starting materials (metal thiolates and sodium borohydride) are insoluble in nonpolar solvent, so the as formed NCs could be separated in a pure form by adding a nonpolar solvent to the product in which only the NCs get dispersed. In the case of metal chalcogenides NCs we employed layered metal thiolates as metal precursor and C_8DTCA or C_8DTCA-OlAm (C_8DTCA plus few μL oleyl amine) mixture as a sulfur source. These NCs were also dispersible in nonpolar organic solvents and displayed very good optical characteristics exemplifying their compositional purity and crystalline nature.

RESULTS

Metal Thiolates. All metal thiolates (Ag, Au, Cu, Pb, Cd, Mn, and Zn thiolates) were synthesized following our previously reported protocol[37] (for details see the Experimental Section in the Supporting Information (SI)). The representative PXRD pattern of silver octanethiolate is shown in Figure1a, revealing periodically spaced (00*l*) reflections. The SEM and TEM image (Figure 1b, c) of the silver octanethiolate also clearly indicate that they are featured with layered structures. Similarly all of the other metal thiolates also display PXRD pattern with periodically spaced (00*l*) reflections (please see in SI Figure S1a–c) and their SEM images (SI Figure S1d–i) show flaky features, revealing their lamellar nature. Energy dispersive X-ray analysis (see SI Figures S2 and S3) confirm the stoichiometry of metal thiolates as M(SR) [for M = Ag, Au, and Cu] and $M(SR)_2$ [for M = Pb, Cd, Mn, and Zn].

Metal Nanocrystals. The metal NCs were prepared from the above-mentioned metal thiolates by grinding them with sodium borohydride powder under ambient conditions. The overall synthetic procedure for metal NCs preparation is shown in Scheme 1 (for synthesis procedure details please see SI). We noticed that as soon as we start grinding the metal thiolates of noble metals like Au and Ag (which are white in color) with $NaBH_4$ in an agate mortar at room temperature, the color starts changing to brown indicating a change in the metal oxidation state (the color changes showed in SI Scheme S1) and the formation of metallic NCs. We continued the grinding for about 3–5 min until the color of the ground material was found to be uniform. It may be noted that no other capping agent has been added here. The product obtained by this method could be separated from the side products and unreacted reagents remaining after the grinding by simply adding a nonpolar organic solvent like toluene, hexane, etc. to the reaction mixture where only the NCs became dispersed because the other reagents were not soluble in these solvents. Moreover, we could reprecipitate the product by simply adding solvents like ethanol, acetone, etc. and this precipitate could be further redispersed in nonpolar solvents as desired.

The XRD pattern of the obtained Ag NCs, shown in Figure 1d, clearly display reflections for pure fcc phase Ag(0) that are in agreement with the JCPDS data (JCPDS No. 03-0931). It may be noticed that, no reflections corresponding to the silver thiolates can be seen. The conversion of Ag–C_8S to Ag NCs has also been supported by X-ray photoelectron spectroscopy (XPS). The high-resolution XPS spectra for Ag–C_8S and Ag NCs are presented in SI Figure S4(a,b). The Ag–C_8S thiolate shows the $3d_{5/2}$ peak at 368.37 eV and the corresponding spectra of Ag NCs shows the $3d_{5/2}$ peak at 367.88 eV, confirming the conversion of Ag(I) to Ag(0) as suggested by the previous studies.[63,64] The yield of Ag NCs obtained by the solid state grinding of Ag–C_8S with $NaBH_4$, determined from the TGA analysis, was 78% (for TGA data please see Figure S5. The yield calculation details are also presented in SI). The well-defined surface plasmon resonance (SPR) band in the UV–vis spectrum at 448 nm (as shown in the Figure 1e) further confirmed the formation of small size Ag NCs. The TEM images of Ag NCs obtained from Ag-octanethiolate (Ag–C_8S) are shown in Figure 1f (more images can be found in SI Figure S6). The TEM images clearly indicate that the NCs are nearly monodispersed with average size 4.04 ± 0.45 nm (size distribution plot shown in inset of Figure 1f). The UV–vis spectra of Ag NC dispersions obtained from other Ag-

DOI: 10.1021/acssuschemeng.8b02292
ACS Sustainable Chem. Eng. 2018, 6, 12006–12016

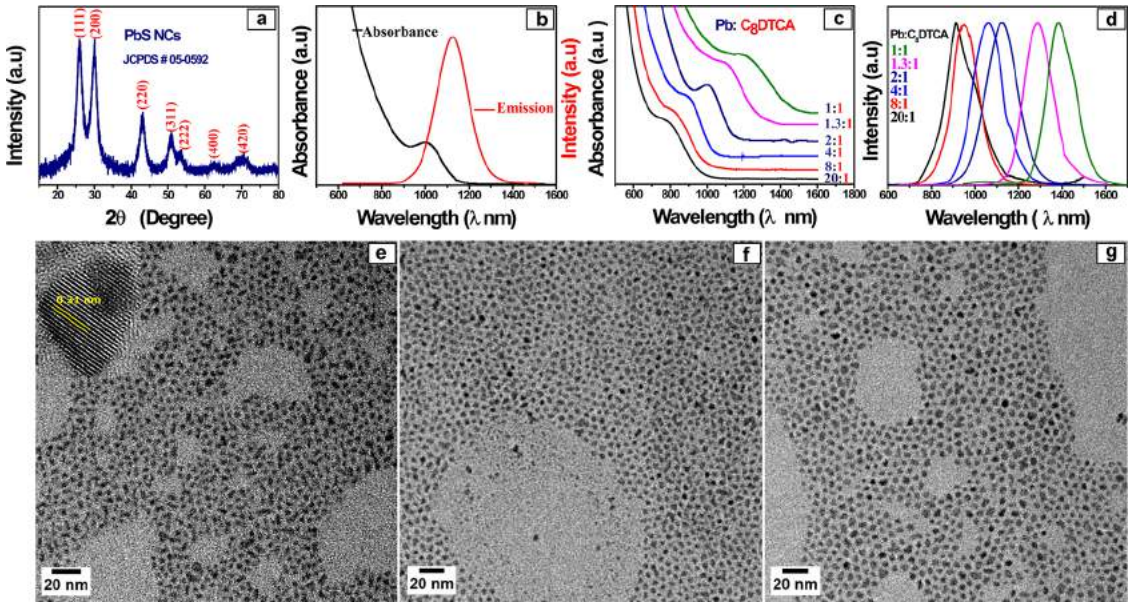

Figure 2. (a) PXRD of PbS NCs. (b) NIR UV−vis spectra (black solid line) and PL spectra (red solid line) of PbS NCs synthesized by solid state (Pb:C_8DTCA 2:1). (c) NIR UV−vis spectra of PbS NCs synthesized at different Pb:C_8DTCA stoichiometry ratio. (d) NIR PL spectra of PbS NCs synthesized at different Pb:C_8DTCA stoichiometry ratio. TEM images of different sized PbS NCs prepared at different Pb:C_8DTCA precursor ratio; (e) 8:1, (f) 2:1, and (g) 1:1.

thiolates are presented in SI Figure S7. From the full width at half maximum (fwhm) values of these SPR peaks we can see that as the chain length of thiol increases the fwhm also increases (fwhm values are tabulated in SI Table S1). The average sizes of Ag NCs prepared from other thiolates are 4.7 ± 1.2 nm (from Ag-decanethiolate, Ag−C_{10}S), 4.9 ± 1.4 nm (from Ag-dodecanethiolate, Ag−C_{12}S) and 5.2 ± 1.7 nm (from Ag-hexadecanethiolate, Ag−C_{16}S), respectively (see SI Figure S8).

In a similar manner Au NCs could also be prepared by the solvent-less solid state grinding of Au−C_8S with sodium borohydride. The XRD pattern (SI Figure S9a) of obtained Au NC samples clearly shows reflections for pure fcc phase Au(0) that are in agreement with the JCPDS data (JCPDS No. 04-0784). Here again no reflections corresponding to the gold thiolates could be seen. The UV−vis spectra (SI Figure S9b) displays a well-defined but broad surface plasmon resonance (SPR) peak positioned at 536 nm where the peak broadening could be to the presence of larger sized NCs. Very interestingly, the TEM images of the product revealed the presence NCs of two different sizes (SI Figure S9c−e) where the average size of the small Au NCs was 2.0 ± 0.4 nm and the larger sized Au NCs were of the size 17.4 ± 5.7 nm. When we separated these two NCs from one another by centrifugation and looked at the TEM images of them again, the small Au NCs (which formed flocculent precipitate upon standing) were seen to assemble in a 1D nanowire (NW) fashion. These NWs mostly consist of single strands with lengths of up to several hundred nanometers, as shown in SI Figure S9f,g.

It may be noted that metal thiolate: sodium borohydride ratio and the reaction time play an important role in the solid state synthesis of metal NCs. Increasing the molar ratio of metal thiolate:$NaBH_4$ leads to an increase in the average NC size and the size distribution also becomes broad. With very high amount of $NaBH_4$, NCs start aggregating. Similarly, reaction time (grinding time) also has a great influence. The reaction of metal thiolates with $NaBH_4$ leads to the formation of metal NCs within 1−2 min as indicated by the color change. In general we stopped grinding after noticing a uniform color change as further grinding led to an increase in the NC size as well as polydispersity. These data are not shown for brevity.

Semiconducting Metal Sulfide Nanocrystals. Semiconducting metal sulfide NCs could also be synthesized by similar solid-state methods where metal thiolates were ground along with a sulfur source. We had tried solid-state reaction with different sulfur sources like elemental sulfur (sulfur powder dissolved in oleyl amine), sodium sulfide, and thiourea. When all these sulfur sources were ground with different metal thiolates a precipitate which was more like bulk metal sulfide formed and the small amount of dispersible materials that formed on examination by electron microscopy and X-ray diffraction were found to be featured with broad size distributions. As expected the optical properties of these products were not good as concluded by the presence of very broad absorption peaks and multiple emission peaks (results are shown in SI Figures S10 and S11 where metal sulfides were prepared using S-OlAm as sulfur source). When we changed the sulfur source to thiourea no reaction took place when it was ground with different metal thiolates (especially with those of Pb, Cd, and Cu).

Our search for a suitable sulfur source lead us to octyl dithiocarbamic acid (C_8DTCA) which we have previously used to make a library of metal sulfide NCs in a solution based method.[65] The air stable large scale synthesis of C_8DTCA is a very simple one step process involving the reaction of octylamine with carbon disulfide (Caution: This reaction is exothermic). Here in this report, we employed the metal thiolates as metal source and this C_8DTCA or C_8DTCA-OlAm (C_8DTCA dissolved in few μL of oleylamine) as a sulfur source. To elaborate briefly, we took metal thiolate powder along with solid C_8DTCA in a mortar pestle and ground it for few minutes and gratifyingly this simple procedure lead to the formation of metal sulfide NCs, which are highly dispersible in nonpolar solvents. To confirm that this novel simple solid state

DOI: 10.1021/acssuschemeng.8b02292
ACS Sustainable Chem. Eng. 2018, 6, 12006−12016

Table 1. Summary of Optical Spectral Parameter and Sizes of PbS NCs Prepared at Different Pb:C_8DTCA Molar Ratio

PbS at different Pb:C_8DTCA	absorption wavelength (nm)	emission wavelength (nm)	stoke shift (nm)	NC size from TEM (nm)
20:1	780	911	131	
8:1	827	949	122	2.90 ± 0.49
4:1	896	1059	163	
2:1	1002	1121	119	3.63 ± 0.64
1.3:1	1115	1287	172	
1:1	1206	1384	178	4.15 ± 0.65

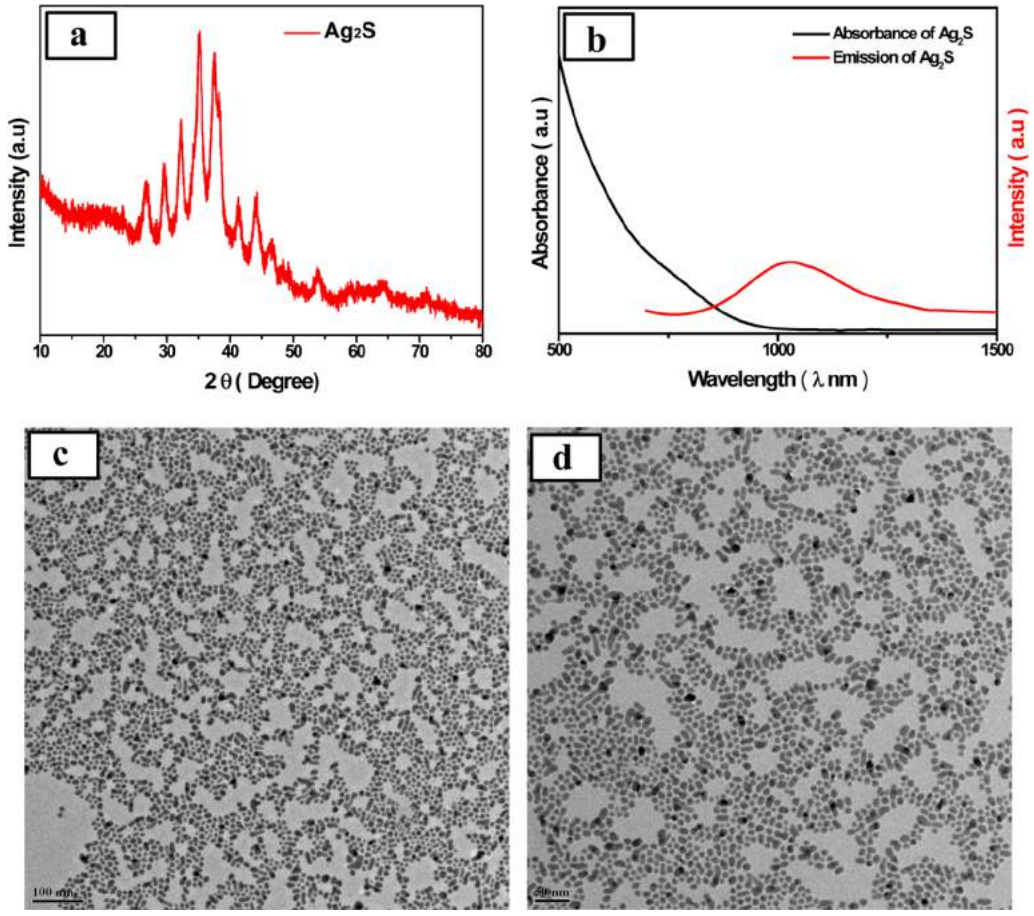

Figure 3. (a) PXRD of Ag_2S NCs synthesized by solid state, using C_8DTCA as a sulfur source. (b) NIR UV−vis spectra (black solid line) and NIR PL spectra (red solid line) of Ag2S NCs. (c,d) TEM images of Ag_2S NCs.

method can be used as a generic strategy to produce a broad variety of monodisperse metal sulfide colloidal NCs, we made several NCs including those in high demand like PbS, Ag_2S, and CuS as well as CdS, MnS, and ZnS. On the basis of the sulfur source used the type of NCs being prepared could be separated into two classes. For instance, for the synthesis of PbS and Ag_2S, the ingredients were the respective metal thiolates and only C_8DTCA as sulfur source. However, in the case of CdS, MnS, ZnS, and Cu_2S while the metal thiolates could still be used as the metal precursor, we had to use C_8DTCA-OlAm (C_8DTCA+few μL of oleylamine) as the sulfur source. In the following the full details of the study are described with the PbS and CdS systems from these two different classes. It may be noted that these semiconducting quantum dot systems are very sensitive and do not show good optical properties if their composition, crystallinity, and surface passivation are not good.[66−69]

To make PbS NCs, about 250 mg of lead-octanethiolate (Pb−C_8S, 0.5 mmol) powder was taken in a mortar pestle to which 50 mg of C_8DTCA (0.25 mmol) was added. These two were ground for 5−10 min in air atmosphere. During the grinding, the yellow color of Pb−C_8S changed to brownish black indicating PbS formation (for detailed synthesis procedures and isolation of dispersible PbS NCs please see SI). The PXRD pattern of the purified materials clearly matched with the PbS with rocksalt structure (please see Figure 2a solid black line), which corresponds to JCPDS Card No. 05-0592. The conversion of Pb−C_8S to PbS NCs has also been supported by X-ray photoelectron spectroscopy (XPS). The high-resolution XPS spectra of Pb and S for both Pb−C_8S and PbS NCs are presented in SI Figure S12a−d. The Pb−C_8S thiolate shows the $4f_{7/2}$ peak at 138.9 eV. The tiny peak at 137.7 eV could be ascribed to the remnant Pb-acetate present in the sample. However, the same spectrum of PbS NCs shows the $4f_{7/2}$ peak at 137.8 eV (which matched with the previous

DOI: 10.1021/acssuschemeng.8b02292
ACS Sustainable Chem. Eng. 2018, 6, 12006−12016

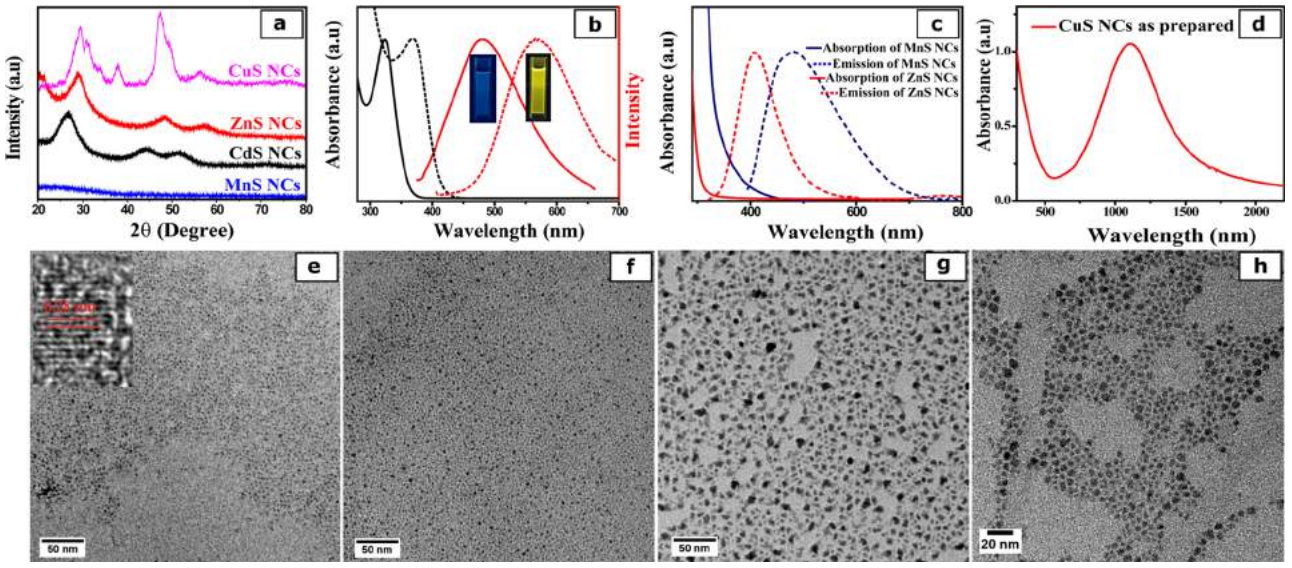

Figure 4. (a) PXRD of different metal sulfide NCs, UV−vis and Photoluminescence (PL) spectra of (b) CdS; two different sized CdS, (c) ZnS (red solid line (absorbance) and red dotted line(PL)) and MnS ((blue solid line (absorbance) and blue dotted line for (PL)). TEM images of metal sulfide NCs of (e) CdS; inset HRTEM of CdS NCs, (f) ZnS, (g) MnS, and (h) CuS NCs.

reports[70,71] for PbS) and a small intensity peak at 139.1 eV (which could be from the Pb−C_8DTCA). In case of the S $2p_{3/2}$ peak the Pb−C_8S sample displays a peak at 161.5 eV. In contrast the spetrum of PbS NCs is characterized with three peaks; one at 161 eV (for PbS), the second at 162.4 eV (for -the sulfur attached to C or H) and a much smaller peak at higher BE (may be attributed to strongly oxidized species, such as sulfate and sulphite). All these match very well with those previously reported.[70,71] The isolated yield of purified PbS NCs from Pb−C_8S was calculated from TGA analysis and was determined to be 44% (for TGA data please see Figure S13. The yield calculation details are also presented in the SI).

The absorption spectra of the PbS NCs obtained by the above method showed only one peak at 1005 nm (Figure 2b−black solid line). This sample also displayed a strong emission in the infrared region. The emission spectra (red solid line, Figure 2b, excitation max = 1125 nm) has a fwhm of ∼170 nm (137 meV) with a minimal Stokes shift (∼120 nm or ∼97 meV).

The intense photoluminescence (quantum yield as determined relative to the standard dye Rhodamine-800 in methanol ∼40%) indicates that the emission is purely band gap emission, significantly devoid of trapped state emission (please see the SI for the details of quantum yield calculations). TEM image of this sample unveils (Figure 2e) the presence of monodispersed NCs (∼3.63 ± 0.64 nm; σ = 6.4%; size distribution plot showed in SI Figure S14.b) which is also exemplified by their self-assembly into two-dimensional hexagonally close packed structures. High resolution TEM images showed in Figure 2e indicate that the NCs are highly crystalline with well-resolved lattice planes corresponding to an interplanar spacing of 0.29 ± 0.02 nm, consistent with the (200) *d*-spacing of the PbS bulk rock salt structure (lattice fringes shown in Figure 2e inset).

After ensuring that we could prepare PbS NCs with good optical properties by this solid state route, we moved ahead to find reaction conditions that allow us to gain control over the NC sizes and their optical properties. To achieve this, we synthesized PbS at different Pb:C_8DTCA molar ratio at room temperature in open air atmosphere. The absorption spectra of PbS NCs obtained at different the Pb:C_8DTCA ratios are plotted in Figure 2c. It can be clearly seen that each of the sample displays well-defined excitonic peak and the peak position varied gradually from 780 to 1200 nm (1.58−1.03 eV) as the Pb: C_8DTCA precursors molar stoichiometry ratio is varied in the range 20:1 to 1:1. It can be noticed that as the C_8DTCA precursors concentration is increased the first excitonic peak position gets red-shifted, indicating formation of larger sized NCs. In Figure 2d, the near-infrared emission spectra of all the samples are plotted, which demonstrate that all the samples display bright and narrow emission peaks (fwhm of PL peaks ranges 130−170 nm). The stoke shift changes observed with different samples obtained at various Pb: C_8DTCA ratio are found to be minimal (180−120 nm), which indicate pure band gap emission from the NCs formed.

Figure 2(e−g) the TEM images of PbS NCs synthesized at different Pb:C_8DTCA ratio, are presented which clearly point to the monodispersity in their sizes. The average NC sizes, size dispersion value (size distribution plot shown in SI Figure S14.a−c), and results are shown in Table 1.

We next describe the preparation of Ag_2S NCs by the solid state grinding method which was accomplished in a similar manner to that of PbS NCs synthesis. Here again the Ag−C_8S was taken along with C_8DTCA in mortor pestle and ground to make a consistent mixture. As soon as we start grinding the white color of Ag−C_8S changed to deep brownish black indicating Ag_2S formation. PXRD pattern of as prepared purified Ag_2S NCs shown in Figure 3a is consistent with the pattern of monoclinic α-Ag_2S (JCPDS 14-0072) and TEM images obtained from this sample (Figure 3c,d), display nearly monodispersed NCs with the average NC size of 6.71 nm and a standard deviation of 13.9% (size distribution plot shown in SI Figure S14.d). It is observed that the absorption spectra of as-prepared purified Ag_2S NCs are featureless with no discrete absorption feature (Figure 3b, black solid line), which is different from the II−VI NCs that usually exhibit an evident absorption feature. This could be due to overlap of other transitions with the excitonic transition. Figure 3b (solid red

DOI: 10.1021/acssuschemeng.8b02292
ACS Sustainable Chem. Eng. 2018, 6, 12006−12016

line) presents the PL of Ag_2S NCs, in which the fluorescence of Ag_2S NCs is slightly broad with fwhm of 316 nm and peak position at 1027 nm.

Interestingly this simple grinding of metal thiolate with C_8DTCA alone did not result in the formation of good quality and quantity metal sulfide NCs in case of Cd, Zn, Mn, and Cu systems. Therefore, we had changed the strategy and used C_8DTCA-OlAm (C_8DTCA dissolved in few μL of oleylamine) as sulfur source. We explain this procedure in detail by taking the CdS system as an example. Briefly, 500 mg (~1 mmol) of cadmium octanethiolate (Cd−C_8S) was ground with a mixture of C_8DTCA-OlAm (~0.5 mmol of C_8DTCA dissolved in 200 μL of oleyl amine). Once again as soon as we start grinding all the ingredients a color changes from white to pale yellow was seen indicating the formation of CdS NCs. The PXRD pattern of the purified materials clearly matched with the CdS cubic phases (for PXRD pattern of this samples please see Figure 4a (solid black line)), which corresponds to JCPDS Card No. 65-2887. These CdS NCs (dispersed in toluene) display a sharp band gap absorption peak at 322 nm, (Figure 4b, solid black line) indicating the formation of nearly monodisperse CdS NCs and their PL spectra (Figure 4b, solid red line) reveal the presence of broad trap state emission centered at 480 nm (trap state emission dominated the pure band gap emission). TEM images of these CdS reveal a near-spherical ultrasmall NCs with average size 2.10 nm with standard deviation value 3.9% (please see SI Figure S14e) and HRTEM images reveal the lattice with *d*-spacing of 2.8 Å, corresponding to (100) planes of cubic CdS (Figure 4e inset). Similar to PbS NCs, the size, absorption and emission of CdS NCs could be tuned by varying the Cd−C_8S: C_8DTCA ratio. For example, when Cd: C_8DTCA ratio was increased to 1: ~0.75 (1 mmol CdC_8S and 0.75 mmol of C_8DTCA) the absorption and emission position shifted toward red (Figure 4b, dotted lines) indicating the size of CdS NCs increased.

Similar to CdS NCs, monodisperse sub-3 nm ZnS and MnS could also be synthesized by solid state grinding of corresponding metal octanethiolate with C_8DTCA-OlAm. For the details of their synthesis please see SI. The PXRD patterns of the purified materials are presented in Figure 4a, where ZnS NCs featured with zinc blend structure (Figure 4a JCPDF No. 05-0566) and MnS NCs with hexagonal structure (Figure 4a JCPDS Card No. 40-1289) could be seen. The photoluminescence spectra of ZnS NCs and MnS NCs are plotted in Figure 4c and both show sharp bandgap emission at 410 nm (for ZnS NCs, red lines) and 480 nm (for MnS NCs, blue lines). TEM images of these materials are presented in Figure 4f (ZnS NCs) and Figure 4g (MnS NCs), and their average sizes are deduced to be 2.19 ± 0.54 nm (for ZnS) and 5.65 ± 1.36 nm (for MnS) (size distribution plots of ZnS and MnS NCs are shown in SI Figure S14f,g, respectively).

We next moved to the prepartion of CuS plasmonic NCs. Copper sulfide is a p-type semiconductor with a direct band gap (E_g) that depends on its stoichiometry and crystal phase (1.1−2.0 eV).[72−75] Its suitable band gap, low toxicity, and high absorbance coefficient make it a promising absorber material for optoelectronic applications[76] such as NIR optical switches and future photovoltaic devices.[77,78] CuS NCs possess highly tunable localized surface plasmon resonances (LSPR) in the near-infrared (NIR) spectral region, making it one of the most sought after materials. The LSPR in copper chalcogenide nanomaterials originates from excess holes in the top of the valence band, which are compensated by Cu^+ deficiencies in the lattice.[79,80] We found that the room temperature solid state grinding of copper(I) octanethiolate (Cu−C_8S) with C_8DTCA-OlAm produces nearly monodispersed covellite CuS NCs in air. PXRD pattern of as prepared purified CuS NCs shown in Figure 4a clearly matches with the CuS with covellite structure (JCPDS Card No. 00-006-0464) and TEM images obtained from this sample (Figure 4h), display nearly monodispersed and spherical sized NCs with the average size of 4.5 ± 0.96 nm (size distribution plot shown in SI Figure S14h). The absorption spectra of as prepared samples (see Figure 4d) show that the CuS NCs exhibit sharp absorption in the NIR region at 1105 nm due to LSPR of free holes in the valence band of CuS NCs.

Similar to the case of metal NCs, the reaction time (solid state grinding time) also has a great influence on the semiconducting NC size and size distribution. In general we see a color change after 1−2 min of grinding the metal thiolate with C_8DTCA. We usually stopped the grinding at this point as further continuation of the grinding led to an increase in NCs size and eventually to their aggregation. These results are not shown for brevity.

DISCUSSION

Metal alkyl thiolates are coordination compounds and exist as lamellae or stacked sheets in the solid state. Metal thioates are characterized with zigzag strands of − S(R)−M−S(R)−M− segments and these zigzag seagments associate into lamellar or multibilayer type structures (please see in SI Figure S15).[37]

For example, in Ag(I) thiolates, the silver ions sit in a plane and the sulfur atoms are attached to them from both above and below their plane and the carbon chain conformation are almost exclusively in trans orientation.[38−41] This structure can be very well correlated with the two-dimensional self-assembled monolayers (2D-SAMs).[40,41] The pioneering study of Dance et al. showed that the interlayer spacing (*d* spacing) of Ag-octanethiolate is 24.8 Å (for (001) reflection) and it increases with the chain length of the alkane thiol.[38] We found similar trends where from the PXRD patterns of these metal thiolates it can be noticed that as the chain length of these thiolates increases the lamellar peak positions shift to lower 2θ angle indicating increase in the "*d*" value (please see SI Figure S1a). A schematic of the layered silver(I) thiolate structure is shown in SI Figures S15 and S16.

The solid state grinding of Ag-octanethiolate (Ag−C_8S) or Au-octanethiolate (Au−C_8S) with reducing agent sodium borohydride yields nearly monodispersed Ag and Au NCs, respectively. Sodium borohydride acts as a reducing agent and reduces the metal ions in the thiolates to their elemental form. This action would also involve a simultaneous generation of a stabilizing agent (alkane thiolate) in situ. We believe it is the presence of this thiolate that controls the growth of the metal crystals and stabilizes them in the nanosize regime. It is noticed that the metal NCs size increases as the chain length of thiol increases. This may be ascribed to the fact that as the chain length of the alkane moiety increases so does the interlayer interdigitation between the alkyl chains of adjancent layers. So, these highly interdigitated silver thiolates sheets would resist the reduction resulting in a nonuniform growth and the formation of polydispersed and larger sized NCs.

This report also discusses the utilization of metal thiolates as a precursor for the synthesis of metal sulfide NCs. The only difference here is that instead of adding a reducing agent a sulfur source (C_8DTCA or C_8DTCA-OlAm) is added so that

DOI: 10.1021/acssuschemeng.8b02292
ACS Sustainable Chem. Eng. 2018, 6, 12006−12016

metal sulfide NCs can be obtained. As mentioned above, the solid state grinding of Pb−C_8S or Ag−C_8S with C_8DTCA yields highly monodispersed PbS or Ag_2S which display excellent optical properties. In case of PbS, just varying the Pb:C_8DTCA ratio offered exceptional control over the NC size and size distributions that results in the tunability of absorption and emission band of these NCs (Figure 2c,d). This is very similar to that of hot injection based methods wherein with increase of metal:S ratio, the excitonic peak was found to red shift with a concomitant peak broadening.[65,81,82] This raises the important question of what is actually happening during this procedure and how C_8DTCA reacts with metal thiolates during the grinding process. The C_8DTCA is a bidentate ligand and contains two sulfur atoms in a single molecule. It can easily bind with metal ions like Pb (II) and Ag (I) to form an M−C_8DTCA complex. So when we add C_8DTCA to a metal thiolate and grind them together two possible reactions can occur. One, formation of M−C_8DTCA complex, which decomposes to metal sulfide by grinding, two, the C_8DTCA molecules itself gets converted to thiourea while grinding and releases H_2S, which then reacts with metal thiolates (thiourea does not react with metal thiolates at room temperature) resulting in the formation of metal sulfides.

To gain more insights in to this aspect we recorded the ^{1}H NMR spectra of as prepared C_8DTCA and C_8DTCA after solid state grinding (at room temp. 25 °C) which clearly revealed that this molecule remains intact and does not undergo any change by simple grinding (no extra peaks observed, please see in SI Figures S17 and S18). Therefore, we rule out the possibility that the H_2S species released by solid state grinding of pure C_8DTCA acting as sulfur source in the present case. The other possibility that we postulate as the reaction mechanism is as follows. While grinding of metal−thiolate with C_8DTCA, the stronger bidentate ligand (C_8DTCA) first reacts with metal−thiolate to form M−C_8DTCA complex. This contention is supported by the observation that pure yellow Pb−C_8S becomes deep orange color when ground with C_8DTCA (the changes of PXRD pattern shown in SI Figure S19a,b). The unstable Pb−C_8DTCA complex decomposes to PbS after further grinding as concluded from the observation that the orange Pb−C_8DTCA complex becomes brownish black upon further grinding. So, this clearly indicates that the path of metal sulfides NCs synthesis involves the formation of a metal-dithiocarbamic acid complex by solid state grinding with the concomitant release of an alkane thiolate and the decomposition of the metal-dithiocarbamate upon further grinding into a metal sulfide. These metal sulfide NCs are immediately protected by the alkane thiolate. It may be noted that while the solid state grinding of metal thiolate and C_8DTCA is good enough to make many metal sulfide NCs, in some cases addition of small amount of oleylamine while grinding is necessary to obtain better NCs systems in terms of their sizes and optical properties. For example, the unstable M−C_8DTCA complexes like Pb−C_8DTCA yield small size NCs due to the fast decomposition this complex by simple grinding. However, metal ions like Cd, Mn, Zn, and Cu form highly stable M−C_8DTCA complexes which do not undergo complete decomposition by simple grinding itself at room temperature (25 °C). This is supported by the PXRD pattern of the product obtained by the grinding of Cd−C_8S where a set of equidistant peaks ascribed to the formation of Cd−C_8DTCA complexes appear (along with the peaks corresponding to the Cd−C_8S, SI Figure 20a) as we start grinding Cd−C_8S with C_8DTCA. Interestingly even after prolonged grinding of the Cd−C_8S with C_8DTCA, while entire Cd−C_8S converts to Cd−C_8DTCA complex the same does not readily decompose to CdS. This is supported by the fact that the PXRD patterns of the product obtained after prolonged grinding indicates the conversion of some Cd−C_8DTCA complex to CdS, but the maximum Cd−C_8DTCA remains intact, indicating its stability and resistance to decompose at room temperature (SI Figure 20b). We reckon that the same must be happening with other M−C_8DTCA complexes like Mn, Zn, and Cu. Quite satisfactorily, the resistance of such stable M-C_8DTCA complexes to decomposition could be overcome by simply adding a few μL of OlAm to C_8DTCA before grinding. It is well-known that primary amines attack metal−dithiocarbamate complexes helping them to decompose faster and at lower temperature to metal sulfide when the reactions are carried out in solution state.[83,84] We believe that here also as the metal thiolates are ground with C_8DTCA, the M−C_8DTCA complex forms first which is attacked by the OlAm present in the reaction milieu enhancing the decomposition rate of the M−C_8DTCA complex and ensues the formation good quality metal sulfide NCs (probable reaction mechanism shown in SI Figure S21).

One of the most attractive features of the procedure we present here is the possibility to scale up by simply grinding larger amount of metal thiolates and C_8DTCA. For example, the optical properties of the product did not change much when the reaction was carried out between 0.5 mmol (250 mg) of PbC_8S and 0.25 mmol of C_8DTCA or if the reaction was carried out between 5 g (10 mmol) of PbC_8S and 5 mmol of C_8DTCA. In the former case the yield of PbS was 70 mg (yield 44%, based on Pb−C_8S used, details shown in SI), while in latter case it was ∼1.1 g (yield 35%, based on Pb−C_8S used, details shown in SI), (the optical spectral comparisons of these two samples are presented in SI Figure S22a). Similarly, almost 5 g of plasmonic CuS NCs (covellite phase) could be synthesized by this simple solid state grinding (optical spectra shown in SI Figure S22b).

As mentioned previously, as most of the as prepared metal sulfides NCs are thiol capped/passivated, they could be easily dispersed in nonpolar solvents. Such dispersions like the alkane thiol capped PbS NCs were stable for 5−7 days, after that they started to settle down. For better stability and better surface passivation, we had done dynamic ligand exchange with oleic acid at 50−60 °C (details ligand exchange procedure showed in SI). Quite satisfactorily, there was no difference in the absorbance spectra after ligand exchange with oleic acid, but emission intensity quite improved (may be due to proper surface passivation) without any change in the emission position. The characterization details like absorption, emission, FTIR, and TEM images of PbS NCs after and before ligand exchanged are shown in SI Figure S23. In a similar fashion, though the CdS NCs synthesized by the current method show trap state emission, the same could be minimized by simply heating the nanocrystal dispersion at 120−140 °C in inert atmosphere with oleic acid and cadmium oleate.[85,86]

Another strategy that is routinely followed in literature to reduce the trap state density is known as hybrid passivation strategy.[87] Briefly, this hybrid passivation strategy involves introducing halide anions and metal cations during the synthesis and was shown to be effective in removing surface trap states within the bandgap. It is reported that metal cation

DOI: 10.1021/acssuschemeng.8b02292
ACS Sustainable Chem. Eng. 2018, 6, 12006−12016

will go and bind to the exposed sulfur atoms on the surface in submonolayer quantities and the halide anions passivate the surfaces where organic ligands are unable to reach due to steric hindrance or unfavorable surface topology.[87] In order to check whether the metal sulfide NCs prepared by the solid state grinding could also be subjected to such hybrid passivation strategy, we added the $CdCl_2$ in a mixture of tetradecylphosphonic acid (TDPA) and oleylamine to the metal sulfides obtained by the solid state grinding procedure described above (following the reported procedure).[87] The PXRD pattern showed in case of PbS after this surface passivation is shown in SI Figure S24 which is exactly similar to the as-prepared PbS NCs indicating that the $CdCl_2$ passivated the surface only and had not formed any core−shell type material. As expected, the absorbance spectra of surface passivated material slightly shifted toward red and absorption coefficient also increased hugely. The emission spectra also shifted toward red and fwhm of emission peak also improved (to 128 nm from 161 nm). Similarly, the quantum yield also increased from 40% to 52% (for absorbance and PL spectra please see SI Figure S25).

CONCLUSIONS

We have developed a generic solvent-less solid state approach for the preparation of metallic and metal sulfide nanocrystals by employing same single source precursor (metal thiolates) as metal source. The materials synthesized by these solid state routes could be redispersed as desired in nonpolar organic solvents and displayed very good structural characteristics and optical properties. The optical properties of the metal sulfide nanocrystals could further be improved by ligand exhange and hybrid passivation strategies if necessary.

ASSOCIATED CONTENT

Supporting Information

The Supporting Information is available free of charge on the ACS Publications website at DOI: 10.1021/acssuschemeng.8b02292.

Experimental section, additional materials characterization, and supporting PXRD data and NMR spectrometry results (PDF)

AUTHOR INFORMATION

Corresponding Author

*Tel: 91-20-25902013. Fax: 91-20-25902036. E-mail: pl.bhagavatula@ncl.res.in (B.L.V.P.).

ORCID

Abhijit Bera: 0000-0002-7480-5245

Bhagavatula L. V. Prasad: 0000-0002-3115-0736

Present Address

†College of Science and Mathematics, University of Massachusetts, Boston MA 02125−3393

Notes

The authors declare no competing financial interest.

ACKNOWLEDGMENTS

We acknowledge Ms. Sneha Sreekumar, Ms. Ruchira Chattopadhyay, and Ms. Aparna Shindhe for their help with some of the experiments. A.B. thanks UGC, New Delhi for research fellowship. The authors thank Council of Scientific and Industrial Research (CSIR), New Delhi for financial assistance through the 12th Five Year Plan Project (CSC 0134).

REFERENCES

(1) Jain, P. K.; Lee, K. S.; El-Sayed, I. H.; El-Sayed, M. A. Calculated absorption and scattering properties of gold nanoparticles of different size, shape, and composition: applications in biological imaging and biomedicine. *J. Phys. Chem. B* **2006**, *110*, 7238−7248.

(2) Dykman, L.; Khlebtsov, N. Gold nanoparticles in biomedical applications: recent advances and perspectives. *Chem. Soc. Rev.* **2012**, *41*, 2256−2282.

(3) Linic, S.; Christopher, P.; Ingram, D. B. Plasmonic-metal nanostructures for efficient conversion of solar to chemical energy. *Nat. Mater.* **2011**, *10*, 911−921.

(4) Ethirajan, A.; Wiedwald, U.; Boyen, H. G.; Kern, B.; Han, L.; Klimmer, A.; Weigl, F.; Kaestle, G.; Ziemann, P.; Fauth, K. A Micellar Approach to Magnetic Ultrahigh-Density Data-Storage Media: Extending the Limits of Current Colloidal Methods. *Adv. Mater.* **2007**, *19*, 406−410.

(5) Daniel, M.-C.; Astruc, D. Gold nanoparticles: assembly, supramolecular chemistry, quantum-size-related properties, and applications toward biology, catalysis, and nanotechnology. *Chem. Rev.* **2004**, *104*, 293−346.

(6) Crooks, R. M.; Zhao, M.; Sun, L.; Chechik, V.; Yeung, L. K. Dendrimer-encapsulated metal nanoparticles: synthesis, characterization, and applications to catalysis. *Acc. Chem. Res.* **2001**, *34*, 181−190.

(7) Nie, S.; Emory, S. R. Probing single molecules and single nanoparticles by surface-enhanced Raman scattering. *Science* **1997**, *275*, 1102−1106.

(8) Li, K.; Stockman, M. I.; Bergman, D. J. Self-similar chain of metal nanospheres as an efficient nanolens. *Phys. Rev. Lett.* **2003**, *91*, 227402.

(9) Oh, S. J.; Berry, N. E.; Choi, J.-H.; Gaulding, E. A.; Paik, T.; Hong, S.-H.; Murray, C. B.; Kagan, C. R. Stoichiometric control of lead chalcogenide nanocrystal solids to enhance their electronic and optoelectronic device performance. *ACS Nano* **2013**, *7*, 2413−2421.

(10) Fu, A.; Gu, W.; Larabell, C.; Alivisatos, A. P. Semiconductor nanocrystals for biological imaging. *Curr. Opin. Neurobiol.* **2005**, *15* (5), 568−575.

(11) Allen, P. M.; Liu, W.; Chauhan, V. P.; Lee, J.; Ting, A. Y.; Fukumura, D.; Jain, R. K.; Bawendi, M. G. InAs (ZnCdS) quantum dots optimized for biological imaging in the near-infrared. *J. Am. Chem. Soc.* **2010**, *132*, 470−471.

(12) Chuang, C.-H. M.; Brown, P. R.; Bulović, V.; Bawendi, M. G. Improved performance and stability in quantum dot solar cells through band alignment engineering. *Nat. Mater.* **2014**, *13*, 796−801.

(13) Nozik, A. Quantum dot solar cells. *Phys. E* **2002**, *14*, 115−120.

(14) Liu, H.; Gao, M.; McCaffrey, J.; Wasilewski, Z.; Fafard, S. Quantum dot infrared photodetectors. *Appl. Phys. Lett.* **2001**, *78*, 79−81.

(15) Sun, Q.; Wang, Y. A.; Li, L. S.; Wang, D.; Zhu, T.; Xu, J.; Yang, C.; Li, Y. Bright, multicoloured light-emitting diodes based on quantum dots. *Nat. Photonics* **2007**, *1*, 717−722.

(16) Wang, Y.; Xia, Y. Bottom-up and top-down approaches to the synthesis of monodispersed spherical colloids of low melting-point metals. *Nano Lett.* **2004**, *4*, 2047−2050.

(17) Li, W.; Zheng, G.; Yang, Y.; Seh, Z. W.; Liu, N.; Cui, Y. High-performance hollow sulfur nanostructured battery cathode through a scalable, room temperature, one-step, bottom-up approach. *Proc. Natl. Acad. Sci. U. S. A.* **2013**, *110*, 7148−7153.

(18) Hoeppener, S.; Maoz, R.; Cohen, S. R.; Chi, L.; Fuchs, H.; Sagiv, J. Metal Nanoparticles, Nanowires, and Contact Electrodes Self-Assembled on Patterned Monolayer Templates—A Bottom-up Chemical Approach. *Adv. Mater.* **2002**, *14*, 1036−1041.

(19) Acharya, S.; Das, B.; Thupakula, U.; Ariga, K.; Sarma, D.; Israelachvili, J.; Golan, Y. A bottom-up approach toward fabrication of ultrathin PbS sheets. *Nano Lett.* **2013**, *13*, 409−415.

(20) Moores, A. Bottom up, solid-phase syntheses of inorganic nanomaterials by mechanochemistry and aging. *Curr. Op. Green Sustainable Chem.* **2018**, *12*, 33−37.

(21) Debnath, D.; Kim, S. H.; Geckeler, K. E. The first solid-phase route to fabricate and size-tune gold nanoparticles at room temperature. *J. Mater. Chem.* **2009**, *19*, 8810−8816.
(22) Murugadoss, A.; Kai, N.; Sakurai, H. Synthesis of bimetallic gold−silver alloy nanoclusters by simple mortar grinding. *Nanoscale* **2012**, *4*, 1280−1282.
(23) Kalidindi, S. B.; Sanyal, U.; Jagirdar, B. R. Metal nanoparticles via the atom-economy green approach. *Inorg. Chem.* **2010**, *49*, 3965−3967.
(24) Sanyal, U.; Jagirdar, B. R. Metal and alloy nanoparticles by amine-borane reduction of metal salts by solid-phase synthesis: atom economy and green process. *Inorg. Chem.* **2012**, *51*, 13023−13033.
(25) Li, Y.; Cao, Y.; Jia, D. A general strategy for synthesis of metal nanoparticles by a solid-state redox route under ambient conditions. *J. Mater. Chem. A* **2014**, *2*, 3761−3765.
(26) Rak, M. J.; Saadé, N. K.; Friščić, T.; Moores, A. Mechanosynthesis of ultra-small monodisperse amine-stabilized gold nanoparticles with controllable size. *Green Chem.* **2014**, *16*, 86−89.
(27) Rao, T. U. B.; Nataraju, B.; Pradeep, T. Ag9 quantum cluster through a solid-state route. *J. Am. Chem. Soc.* **2010**, *132*, 16304−16307.
(28) Udayabhaskararao, T.; Bootharaju, M.; Pradeep, T. Thiolate-protected Ag 32 clusters: mass spectral studies of composition and insights into the Ag−thiolate structure from NMR. *Nanoscale* **2013**, *5*, 9404−9411.
(29) Chakraborty, I.; Govindarajan, A.; Erusappan, J.; Ghosh, A.; Pradeep, T.; Yoon, B.; Whetten, R. L.; Landman, U. The superstable 25 kDa monolayer protected silver nanoparticle: measurements and interpretation as an icosahedral Ag152 (SCH2CH2Ph) 60 cluster. *Nano Lett.* **2012**, *12*, 5861−5866.
(30) Malca, M. Y.; Bao, H.; Bastaille, T.; Saadé, N. K.; Kinsella, J. M.; Friščić, T.; Moores, A. Mechanically activated solvent-free assembly of ultrasmall Bi2S3 nanoparticles: A novel, simple, and sustainable means to access chalcogenide nanoparticles. *Chem. Mater.* **2017**, *29*, 7766−7773.
(31) Wang, W.; Liu, Z.; Zheng, C.; Xu, C.; Liu, Y.; Wang, G. Synthesis of CdS nanoparticles by a novel and simple one-step, solid-state reaction in the presence of a nonionic surfactant. *Mater. Lett.* **2003**, *57*, 2755−2760.
(32) Chawla, P.; Sharma, G.; Lochab, S.; Singh, N. Photoluminescence and optical characterization of CdS nanoparticles prepared by solid-state method at low temperature. *Radiat. Eff. Defects Solids* **2009**, *164*, 755−762.
(33) Liu, J.; Cao, J.; Li, Z.; Ji, G.; Deng, S.; Zheng, M. Low-temperature solid-state synthesis and phase-controlling studies of CdS nanoparticles. *J. Mater. Sci.* **2007**, *42*, 1054−1059.
(34) Liu, J.; Zhao, C.; Li, Z.; Chen, J.; Zhou, H.; Gu, S.; Zeng, Y.; Li, Y.; Huang, Y. Low-temperature solid-state synthesis and optical properties of CdS−ZnS and ZnS−CdS alloy nanoparticles. *J. Alloys Compd.* **2011**, *509*, 9428−9433.
(35) Wang, W.; Liu, Y.; Zhan, Y.; Zheng, C.; Wang, G. A novel and simple one-step solid-state reaction for the synthesis of PbS nanoparticles in the presence of a suitable surfactant. *Mater. Res. Bull.* **2001**, *36*, 1977−1984.
(36) Liu, Q.; Ni, Y.; Yin, G.; Hong, J.; Xu, Z. High yield synthesis of PbS nanocubes using one-step solid-state reaction in the presence of an anionic surfactant. *Mater. Chem. Phys.* **2005**, *89*, 379−382.
(37) Busupalli, B.; Kummara, S.; Kumaraswamy, G.; Prasad, B. L. Ultrathin sheets of metal or metal sulfide from molecularly thin sheets of metal thiolates in solution. *Chem. Mater.* **2014**, *26*, 3436−3442.
(38) Dance, I. G.; Fisher, K. J.; Banda, R. H.; Scudder, M. L. Layered structure of crystalline compounds silver thiolates (AgSR). *Inorg. Chem.* **1991**, *30*, 183−187.
(39) Ye, Z.; de la Rama, L. P.; Efremov, M. Y.; Zuo, J.-M.; Allen, L. H. Approaching the size limit of organometallic layers: synthesis and characterization of highly ordered silver−thiolate lamellae with ultra-short chain lengths. *Dalton Trans.* **2016**, *45*, 18954−18966.
(40) Bensebaa, F.; Ellis, T. H.; Kruus, E.; Voicu, R.; Zhou, Y. Characterization of self-assembled bilayers: Silver− alkanethiolates. *Langmuir* **1998**, *14*, 6579−6587.
(41) Parikh, A.; Gillmor, S.; Beers, J.; Beardmore, K.; Cutts, R.; Swanson, B. Characterization of chain molecular assemblies in long-chain, layered silver thiolates: a joint infrared spectroscopy and X-ray diffraction study. *J. Phys. Chem. B* **1999**, *103*, 2850−2861.
(42) Cha, S.-H.; Kim, J.-U.; Kim, K.-H.; Lee, J.-C. Preparation and photoluminescent properties of gold (I)− alkanethiolate complexes having highly ordered supramolecular structures. *Chem. Mater.* **2007**, *19*, 6297−6303.
(43) Cha, S.-H.; Kim, K.-H.; Kim, J.-U.; Lee, W.-K.; Lee, J.-C. Thermal Behavior of Gold (I)− Thiolate Complexes and Their Transformation into Gold Nanoparticles under Heat Treatment Process. *J. Phys. Chem. C* **2008**, *112*, 13862−13868.
(44) Zhang, Y. X.; Zeng, H. C. Gold (I)−alkanethiolate nanotubes. *Adv. Mater.* **2009**, *21*, 4962−4965.
(45) Espinet, P.; Lequerica, M. C.; Martín-Alvarez, J. M. Synthesis, structural characterization and mesogenic behavior of copper (I) n-alkylthiolates. *Chem. - Eur. J.* **1999**, *5*, 1982−1986.
(46) Sandhyarani, N.; Pradeep, T. An investigation of the structure and properties of layered copper thiolates. *J. Mater. Chem.* **2001**, *11*, 1294−1299.
(47) Bhuvana, T.; Boley, W.; Radha, B.; Dolash, B.; Chiu, G.; Bergstrom, D.; Reifenberger, R.; Fisher, T.; Kulkarni, G. Inkjet printing of palladium alkanethiolates for facile fabrication of metal interconnects and surface-enhanced Raman scattering substrates. *Micro Nano Lett.* **2010**, *5*, 296−299.
(48) Luo, Z.; Yuan, X.; Yu, Y.; Zhang, Q.; Leong, D. T.; Lee, J. Y.; Xie, J. From aggregation-induced emission of Au (I)−thiolate complexes to ultrabright Au (0)@ Au (I)−thiolate core−shell nanoclusters. *J. Am. Chem. Soc.* **2012**, *134*, 16662−16670.
(49) Nakamoto, M.; Yamamoto, M.; Fukusumi, M. Thermolysis of gold (I) thiolate complexes producing novel gold nanoparticles passivated by alkyl groups. *Chem. Commun.* **2002**, *0*, 1622−1623.
(50) Rosemary, M.; Pradeep, T. Solvothermal synthesis of silver nanoparticles from thiolates. *J. Colloid Interface Sci.* **2003**, *268*, 81−84.
(51) Sagade, A. A.; Radha, B.; Kulkarni, G. Intricate nature of Pd nanocrystal−hydrogen interaction investigated using thermolysed Pd hexadecylthiolate films. *Sens. Actuators, B* **2010**, *149*, 345−351.
(52) Rohner, C.; Pekkari, A.; Härelind, H.; Moth-Poulsen, K. Synthesis of Cu nanoparticles: Stability and conversion into Cu2S nanoparticles by decomposition of alkanethiolate. *Langmuir* **2017**, *33*, 13272−13276.
(53) Bhuvana, T.; Gregoratti, L.; Heun, S.; Dalmiglio, M.; Kulkarni, G. Electron Resist Behavior of Pd Hexadecanethiolate Examined Using X-ray Photoelectron Spectroscopy with Nanometric Lateral Resolution. *Langmuir* **2009**, *25*, 1259−1264.
(54) Yang, Z.; Smetana, A. B.; Sorensen, C. M.; Klabunde, K. J. Synthesis and characterization of a new tiara Pd (II) thiolate complex, [Pd (SC12H25) 2] 6, and its solution-phase thermolysis to prepare nearly monodisperse palladium sulfide nanoparticles. *Inorg. Chem.* **2007**, *46*, 2427−2431.
(55) Zhuang, Z.; Lu, X.; Peng, Q.; Li, Y. A facile "dispersion−decomposition" route to metal sulfide nanocrystals. *Chem. - Eur. J.* **2011**, *17*, 10445−10452.
(56) van Embden, J.; Chesman, A. S.; Jasieniak, J. J. The heat-up synthesis of colloidal nanocrystals. *Chem. Mater.* **2015**, *27*, 2246−2285.
(57) Larsen, T. H.; Sigman, M.; Ghezelbash, A.; Doty, R. C.; Korgel, B. A. Solventless synthesis of copper sulfide nanorods by thermolysis of a single source thiolate-derived precursor. *J. Am. Chem. Soc.* **2003**, *125*, 5638−5639.
(58) Du, Y.; Xu, B.; Fu, T.; Cai, M.; Li, F.; Zhang, Y.; Wang, Q. Near-infrared photoluminescent Ag2S quantum dots from a single source precursor. *J. Am. Chem. Soc.* **2010**, *132*, 1470−1471.
(59) Zhang, Y.; Xu, H.; Wang, Q. Ultrathin single crystal ZnS nanowires. *Chem. Commun.* **2010**, *46*, 8941−8943.

DOI: 10.1021/acssuschemeng.8b02292
ACS Sustainable Chem. Eng. 2018, 6, 12006−12016

(60) Shen, S.; Zhang, Y.; Peng, L.; Xu, B.; Du, Y.; Deng, M.; Xu, H.; Wang, Q. Generalized synthesis of metal sulfide nanocrystals from single-source precursors: size, shape and chemical composition control and their properties. *CrystEngComm* **2011**, *13*, 4572−4579.
(61) Shen, S.; Zhang, Y.; Peng, L.; Du, Y.; Wang, Q. Matchstick-Shaped Ag2S−ZnS Heteronanostructures Preserving both UV/Blue and Near-Infrared Photoluminescence. *Angew. Chem.* **2011**, *123*, 7253−7256.
(62) Zhang, Y.; Liu, Y.; Li, C.; Chen, X.; Wang, Q. Controlled synthesis of Ag2S quantum dots and experimental determination of the exciton Bohr radius. *J. Phys. Chem. C* **2014**, *118*, 4918−4923.
(63) Chakraborty, I.; Erusappan, J.; Govindarajan, A.; Sugi, K.; Udayabhaskararao, T.; Ghosh, A.; Pradeep, T. Emergence of metallicity in silver clusters in the 150 atom regime: a study of differently sized silver clusters. *Nanoscale* **2014**, *6*, 8024−8031.
(64) Du, T.; Liang, J.; Dong, N.; Lu, J.; Fu, Y.; Fang, L.; Xiao, S.; Han, H. Glutathione-Capped Ag2S Nanoclusters Inhibit Coronavirus Proliferation through Blockage of Viral RNA Synthesis and Budding. *ACS Appl. Mater. Interfaces* **2018**, *10*, 4369−4378.
(65) Bera, A.; Mandal, D.; Goswami, P. N.; Rath, A. K.; Prasad, B. L. A generic and scalable method for the preparation of monodispersed metal sulfide nanocrystals with tunable optical properties. *Langmuir* **2018**, *34*, 5788−5797.
(66) Thomson, J. W.; Nagashima, K.; Macdonald, P. M.; Ozin, G. A. From sulfur− amine solutions to metal sulfide nanocrystals: peering into the oleylamine− sulfur black box. *J. Am. Chem. Soc.* **2011**, *133*, 5036−5041.
(67) Cademartiri, L.; Montanari, E.; Calestani, G.; Migliori, A.; Guagliardi, A.; Ozin, G. A. Size-dependent extinction coefficients of PbS quantum dots. *J. Am. Chem. Soc.* **2006**, *128*, 10337−10346.
(68) Moreels, I.; Lambert, K.; De Muynck, D.; Vanhaecke, F.; Poelman, D.; Martins, J. C.; Allan, G.; Hens, Z. Composition and size-dependent extinction coefficient of colloidal PbSe quantum dots. *Chem. Mater.* **2007**, *19*, 6101−6106.
(69) Kim, D.; Kim, D.-H.; Lee, J.-H.; Grossman, J. C. Impact of stoichiometry on the electronic structure of PbS quantum dots. *Phys. Rev. Lett.* **2013**, *110*, 196802.
(70) Cant, D. J.; Syres, K. L.; Lunt, P. J.; Radtke, H.; Treacy, J.; Thomas, P. J.; Lewis, E. A.; Haigh, S. J.; O'Brien, P.; Schulte, K. Surface properties of nanocrystalline PbS films deposited at the water−oil interface: a study of atmospheric aging. *Langmuir* **2015**, *31*, 1445−1453.
(71) Laajalehto, K.; Kartio, I.; Nowak, P. XPS study of clean metal sulfide surfaces. *Appl. Surf. Sci.* **1994**, *81*, 11−15.
(72) van der Stam, W.; Berends, A. C.; de Mello Donega, C. Prospects of colloidal copper chalcogenide nanocrystals. *ChemPhysChem* **2016**, *17*, 559−581.
(73) Wang, F.; Li, Q.; Lin, L.; Peng, H.; Liu, Z.; Xu, D. Monodisperse copper chalcogenide nanocrystals: controllable synthesis and the pinning of plasmonic resonance absorption. *J. Am. Chem. Soc.* **2015**, *137*, 12006−12012.
(74) Luther, J. M.; Jain, P. K.; Ewers, T.; Alivisatos, A. P. Localized surface plasmon resonances arising from free carriers in doped quantum dots. *Nat. Mater.* **2011**, *10*, 361−366.
(75) Zhao, Y.; Pan, H.; Lou, Y.; Qiu, X.; Zhu, J.; Burda, C. Plasmonic Cu2− x S nanocrystals: optical and structural properties of copper-deficient copper (I) sulfides. *J. Am. Chem. Soc.* **2009**, *131*, 4253−4261.
(76) Su, Y.; Lu, X.; Xie, M.; Geng, H.; Wei, H.; Yang, Z.; Zhang, Y. A one-pot synthesis of reduced graphene oxide−Cu 2 S quantum dot hybrids for optoelectronic devices. *Nanoscale* **2013**, *5*, 8889−8893.
(77) Yu, X. L.; Cao, C. B.; Zhu, H. S.; Li, Q. S.; Liu, C. L.; Gong, Q. H. Nanometer-Sized Copper Sulfide Hollow Spheres with Strong Optical-Limiting Properties. *Adv. Funct. Mater.* **2007**, *17*, 1397−1401.
(78) Wu, Y.; Wadia, C.; Ma, W.; Sadtler, B.; Alivisatos, A. P. Synthesis and photovoltaic application of copper (I) sulfide nanocrystals. *Nano Lett.* **2008**, *8*, 2551−2555.
(79) Dorfs, D.; Härtling, T.; Miszta, K.; Bigall, N. C.; Kim, M. R.; Genovese, A.; Falqui, A.; Povia, M.; Manna, L. Reversible Tunability of the Near-Infrared Valence Band Plasmon Resonance in Cu2−x Se Nanocrystals. *J. Am. Chem. Soc.* **2011**, *133*, 11175−11180.
(80) Kriegel, I.; Scotognella, F.; Manna, L. Plasmonic doped semiconductor nanocrystals: Properties, fabrication, applications and perspectives. *Phys. Rep.* **2017**, *674*, 1−52.
(81) Hines, M. A.; Scholes, G. D. Colloidal PbS nanocrystals with size-tunable near-infrared emission: observation of post-synthesis self-narrowing of the particle size distribution. *Adv. Mater.* **2003**, *15*, 1844−1849.
(82) Weidman, M. C.; Beck, M. E.; Hoffman, R. S.; Prins, F.; Tisdale, W. A. Monodisperse, air-stable PbS nanocrystals via precursor stoichiometry control. *ACS Nano* **2014**, *8*, 6363−6371.
(83) Hollingsworth, N.; Roffey, A.; Islam, H.-U.; Mercy, M.; Roldan, A.; Bras, W.; Wolthers, M.; Catlow, C. R. A.; Sankar, G.; Hogarth, G. Active nature of primary amines during thermal decomposition of nickel dithiocarbamates to nickel sulfide nanoparticles. *Chem. Mater.* **2014**, *26*, 6281−6292.
(84) Jung, Y. K.; Kim, J. I.; Lee, J.-K. Thermal decomposition mechanism of single-molecule precursors forming metal sulfide nanoparticles. *J. Am. Chem. Soc.* **2010**, *132*, 178−184.
(85) Kim, J. I.; Kim, J.; Lee, J.; Jung, D.-R.; Kim, H.; Choi, H.; Lee, S.; Byun, S.; Kang, S.; Park, B. Photoluminescence enhancement in CdS quantum dots by thermal annealing. *Nanoscale Res. Lett.* **2012**, *7*, 482.
(86) Torimoto, T.; Ogawa, S.; Adachi, T.; Kameyama, T.; Okazaki, K.-i.; Shibayama, T.; Kudo, A.; Kuwabata, S. Remarkable photoluminescence enhancement of ZnS−AgInS 2 solid solution nanoparticles by post-synthesis treatment. *Chem. Commun.* **2010**, *46*, 2082−2084.
(87) Yuan, M.; Kemp, K. W.; Thon, S. M.; Kim, J. Y.; Chou, K. W.; Amassian, A.; Sargent, E. H. High-performance quantum-dot solids via elemental sulfur synthesis. *Adv. Mater.* **2014**, *26*, 3513−3519.

DOI: 10.1021/acssuschemeng.8b02292
ACS Sustainable Chem. Eng. 2018, 6, 12006−12016

Bull. Mater. Sci. (2018) 41:125
https://doi.org/10.1007/s12034-018-1639-6

2D molecular precursor for a one-pot synthesis of semiconducting metal sulphide nanocrystals

ABHIJIT BERA and BHAGAVATULA L V PRASAD*
Physical/Materials Chemistry Division, National Chemical Laboratory (CSIR-NCL), Pune 411008, India
*Author for correspondence (pl.bhagavatula@ncl.res.in)

MS received 19 March 2018; accepted 1 May 2018; published online 6 September 2018

Abstract. 2D molecular materials, namely, metal alkyl thiolates, have been used as a single-source precursor for the synthesis of semiconducting metal sulphide nanocrystals (NCs) by thermal decomposition. These 2D molecular precursors have all the ingredients required for metal sulphide synthesis (metal source, sulphur source and protecting ligand). In this study, we demonstrate a simple and general 'solvothermal decomposition' approach for the synthesis of high-quality Cu_2S, PbS, CdS, MnS and ZnS NCs. The size of the NC can also be controlled by changing the decomposition temperature. Furthermore, the optical properties of the NCs have also been studied.

Keywords. Single-source precursor; nanocrystal; thermal decomposition; optical properties.

1. Introduction

Over the past few decades, there has been great interest in the utilization of semiconducting nanocrystals (NCs) for biomedical [1–3], electronic [4–6] and alternative-energy applications [7–9]. This interest stems from their optical properties, which can be tuned by particle size via quantum confinement or changing the composition. Even a slight change of size, morphology or composition of NCs has a considerable effect on the optical properties, including the energies of the absorption onset, fluorescence emission and surface plasmons [10]. Thus, the synthesis of monodisperse, single-crystalline metal sulphide NCs is highly desired. While there are many ways to synthesize NCs, solution-based colloidal synthesis often yields the high-quality materials, with desired monodispersity displaying uniform properties [10]. Over the past several years, several groups have reported the synthesis of metal sulphide NCs using various synthesis routes, including the thermolysis of single-source precursors [11–13], solvent-less synthesis [14], thermolysis of metal–oleylamine complexes [15] and a simple organic-amine-assisted hydrothermal process [16].

In this communication, a general 'solvothermal decomposition' approach has been carried out for synthesizing metal sulphide NCs. It is a direct-heating approach without any subsequent reagent injection. Both the 'direct-heating' and 'hot-injection' processes are very convenient and are suitable for large-scale synthesis. However, to obtain high-quality NCs, the hot-injection method poses some drawbacks as the reagents used are characterized with high reactivity [17]. Therefore, modulating size via this 'hot-injection' process becomes tricky for many systems. On the other hand, the 2D molecular precursors (metal alkyl thiolates) that we propose here have ideal reactivity and have all the ingredients required for metal sulphide synthesis (metal source, sulphur source and protecting ligand). Because of their low reactivity below a certain temperature (i.e., the reaction temperature) a short nucleation process can be achieved simply by direct heating of these metal thiolates at or above the decomposition temperature. Thus, at these high temperatures, the decomposition of thiols leads to the formation of metal sulphides and at the termination of the reaction, the particles get *in-situ* capped with a layer of intact thiols. Furthermore, metal thiolates of different metals are easy to prepare in large scale by a simple solvent-less process, which are highly stable in air below the decomposition temperature. Accordingly, we show in this work that by the decomposition of a suitable metal thiolate in a high boiling solvent like 1-octadecene a series of metal sulphide NCs, such as Cu_2S, PbS, ZnS, MnS and CdS, can be successfully synthesized. Interestingly their size also can be controlled by varying the decomposition temperature. This method avoids injecting a second reagent during the reaction and uses air-free manipulation, which is very suitable for large-scale synthesis.

Electronic supplementary material: The online version of this article (https://doi.org/10.1007/s12034-018-1639-6) contains supplementary material, which is available to authorized users.

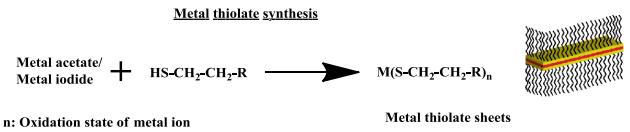

Scheme 1. Schematic representation of the metal thiolate synthesis.

2. Experimental

2.1 *General procedure for metal sulphide NCs*

A quantity of 200 mg of metal thiolates powder was taken along with 15 ml of 1-ODE in a 100 ml RB flask. First, the reaction mixture was heated at mild temperature (130–140°C); the homogeneous clear solution formed was then further heated at high temperature (200–240°C) for 30 min. This reaction mixture was precipitated and washed with methanol to obtain pure metal sulphide NCs. These products were re-dispersed into toluene or tetrachloroethylene and characterized by PXRD and UV–vis absorption, fluorescence spectra and transmission electron microscopy (TEM).

3. Results and discussion

A series of 2D molecular precursors (metal thiolates of different metals like Cu, Pb, Cd, Mn and Zn) were synthesized following our previously reported protocol [18].

Briefly, metal precursors (such as metal acetate or metal iodide) were taken in a glass vial and alkyl thiol (octane thiol) was added into this (the generic procedure for metal thiolate synthesis is shown in scheme 1). This immediately led to a colour change due to M–S co-ordination (synthesis and cleaning of materials are explained in detail in the Experimental section in supplementary information). These metal alkyl thiolates are coordination compounds and exist as lamellae or stacked sheets in the solid state [18]. The PXRD patterns of different metal thiolates are shown in figure 1a, which shows periodically spaced (00*l*) reflections. SEM images (shown in figure 1b–f) of these metal thiolates also clearly indicate that all of the metal thiolates are featured with layer-like structures and justify the sheet-like (2D) morphology. It is confirmed by energy-dispersive X-ray analysis (see supplementary figure S1) that the stoichiometry of metal thiolates is $M_n(SR)_n$ (where M = Cu, Pb, Cd, Mn and Zn and n = oxidation state of metal). This simple and generic solvent-less synthesis of 2D single-source precursors is scalable and the resulting materials are also highly stable in air [18].

Subsequently, the semiconducting metal sulphide NCs were synthesized using these 2D molecular precursors as a starting material (the generic procedure for metal sulphide synthesis is shown in scheme 2). The main advantage is that the 2D metal thiolates used here are single-source precursors,

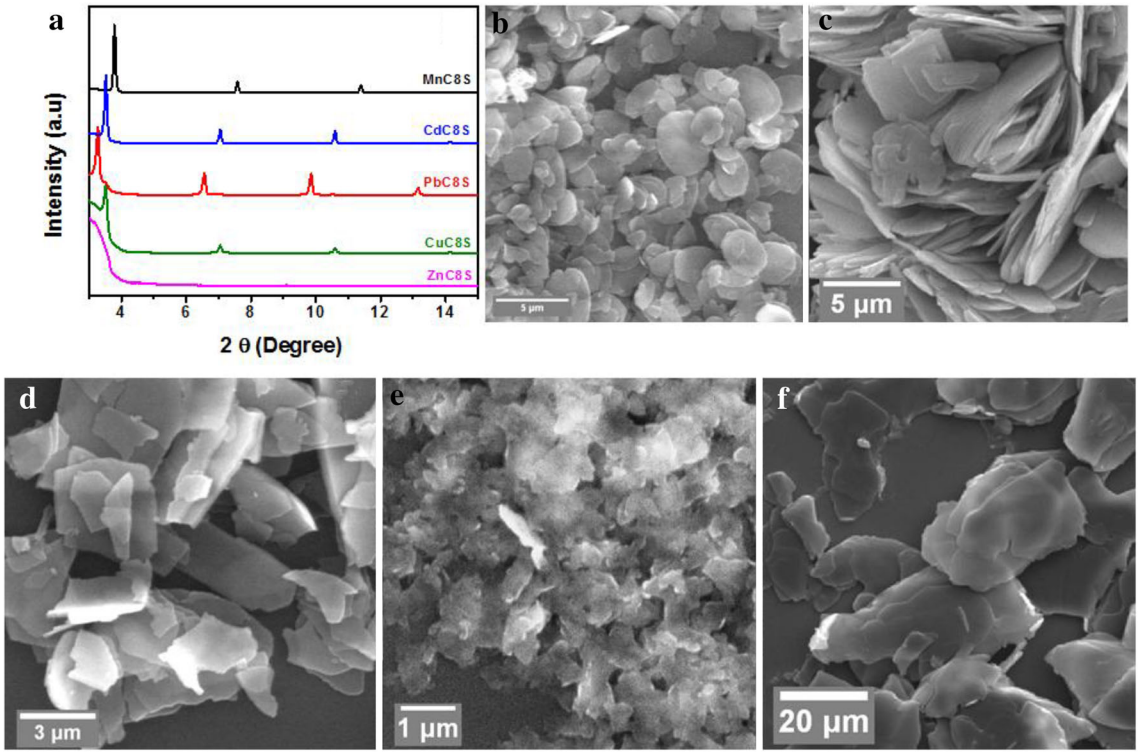

Figure 1. (**a**) PXRD of metal thiolates; PXRD of manganese octanethiolate (MnC_8S) is in black, cadmium octanethiolate (CdC_8S) in blue, lead octanethiolate (PbC_8S) in red, copper octanethiolate (CuC_8S) in green and zinc octanethiolate (ZnC_8S) in pink. SEM images of metal thiolates: (**b**) CuC_8S, (**c**) CdC_8S, (**d**) PbC_8S, (**e**) ZnC_8S and (**f**) MnC_8S.

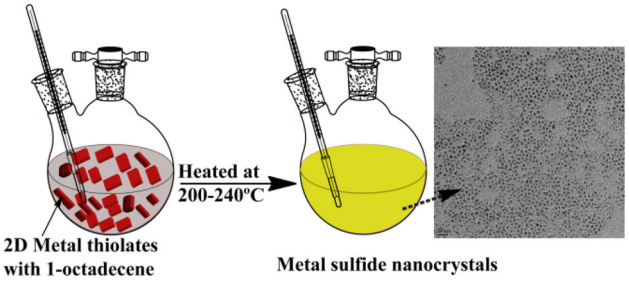

Scheme 2. Method for generic metal sulphide NCs synthesis.

Thermal decomposition of metal thiolates

$$Cd(S\text{-}CH_2\text{-}CH_2\text{-}R)_2 \xrightarrow[240\ ^oC]{\triangle} CdS + R\text{-}CH{=}CH_2 + R\text{-}_2HC\text{-}_2HC\text{-}S\text{-}CH_2\text{-}CH_2\text{-}R$$

Scheme 3. Proposed reaction mechanism for thermal decomposition of metal thiolates to metal sulphide NCs (following Ref. [19]). The equation has not been balanced.

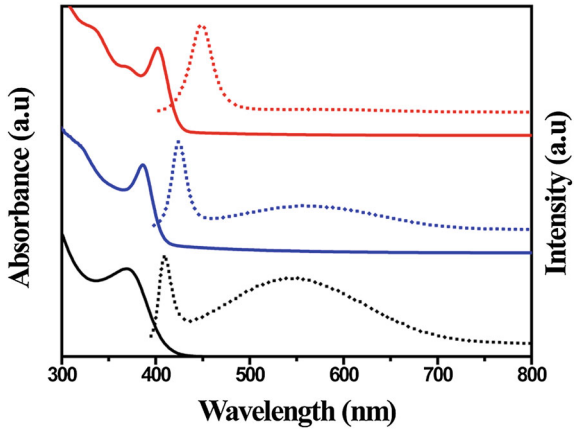

Figure 2. Absorption (solid line) and emission (dotted line) spectra of CdS NCs synthesized at different temperatures (200–240°C).

where all the ingredients required for metal sulphide NCs are inbuilt in their structure (metal source, sulphur source and capping agent). These metal thiolates are highly stable and are dispersible at mild temperatures (120–140°C) in a high boiling solvent like 1-octadecene. After or at a certain temperature (decomposition temperature) the uniform dispersion of metal thiolates (which have been shown to exist as individual sheet-like structures in solution) [18] can decompose into metal sulphide and an alkene [19] and some of the undecomposed alkyl thiol passivate the surface of the NCs to control the growth (proposed reaction mechanism is shown in scheme 3, according to Choi *et al* [19]). In the following, the synthesis procedure is explained in detail through the synthesis of cadmium sulphide NCs as an example. First, 200 mg of the Cd-octanethiolate 2D molecular complex was taken along with a solvent (1-octadecene) and the temperature was raised to 130°C to get a homogeneous clear solution. The temperature was then raised to 200–240°C in argon flow and the reaction was kept at this temperature for 30 min. The colourless solution became pale yellow, indicating formation of CdS. The heating was stopped immediately after the colour change and the system was allowed to naturally cool to room temperature (which took ∼45 min). The product of this reaction was collected by precipitating it with acetone/ethanol addition, and after washing it two times with acetone/ethanol (centrifuged at 5000 rpm for 3 min) the precipitate was dried in argon flow. The precipitate was re-dispersed into tetrachloroethylene or toluene for various measurements. The PXRD pattern of the purified materials clearly matched those of the CdS cubic phases (for PXRD pattern of these samples, see supplementary figure S2), which corresponds to JCPDS card No#43-1469. Figure 2 shows the UV–vis absorption spectra of CdS NCs synthesized between 200 and 240°C. As can be noticed, all spectra exhibit sharp bandgap absorption features, indicating the formation of nearly monodisperse CdS NCs. It may be noticed that the samples display a well-defined excitonic peak and the peak position varied gradually from 370 to 385 to 405 nm as the reaction temperature was varied to 200 to 220 to 240°C (figure 2). The absorption peak also becomes narrow and the peak shifts towards red (figure 2). The photoluminescence (PL) of CdS NCs (figure 2) shows both a sharp bandgap emission as well as trap state emission centred around 450–700 nm. The trap state emission is significantly depressed on increasing reaction temperature and bandgap emission dominates the fluorescence of CdS NCs for synthesis temperatures over 200°C (figure 2).

TEM images show near-spherical NCs with average size of ∼3 nm and the size of CdS NCs can be tuned between ∼3 and 5 nm, with longer reaction times and higher reaction temperatures favouring the formation of larger NCs (figure 3a–c).

Similar to the synthesis of CdS NCs, nearly monodisperse sub-13 nm PbS NCs can be synthesized by heating Pb-octanethiolate precursor in ODE solution at 200°C. The PXRD pattern of the purified materials clearly matched that of the PbS with rock salt structure (see supplementary figure S2), which corresponds to JCPDS card No#05-0592. TEM images showed NCs with nearly spherical shape and average size of 13 nm (figure 3d). As in the case of CdS and PbS NCs, monodisperse ∼sub-3 nm ZnS and MnS can also be synthesized by thermal decomposition of zinc octanethiolate and Mn-octanethiolate, respectively, in ODE at 240°C. The PXRD pattern of the purified materials shows zinc blende ZnS phase (supplementary figure S2; JCPDF no-75-1546), and the average size of NCs in both these cases was found to be ∼3.5 nm (see figure 3e for TEM image of ZnS NCs and figure 3f for TEM image of MnS NCs).

The PL of ZnS NCs (figure 4a) shows a sharp bandgap emission at ∼410 nm. The PXRD pattern of MnS NCs (supplementary figure S2) is broad in nature, which we ascribe

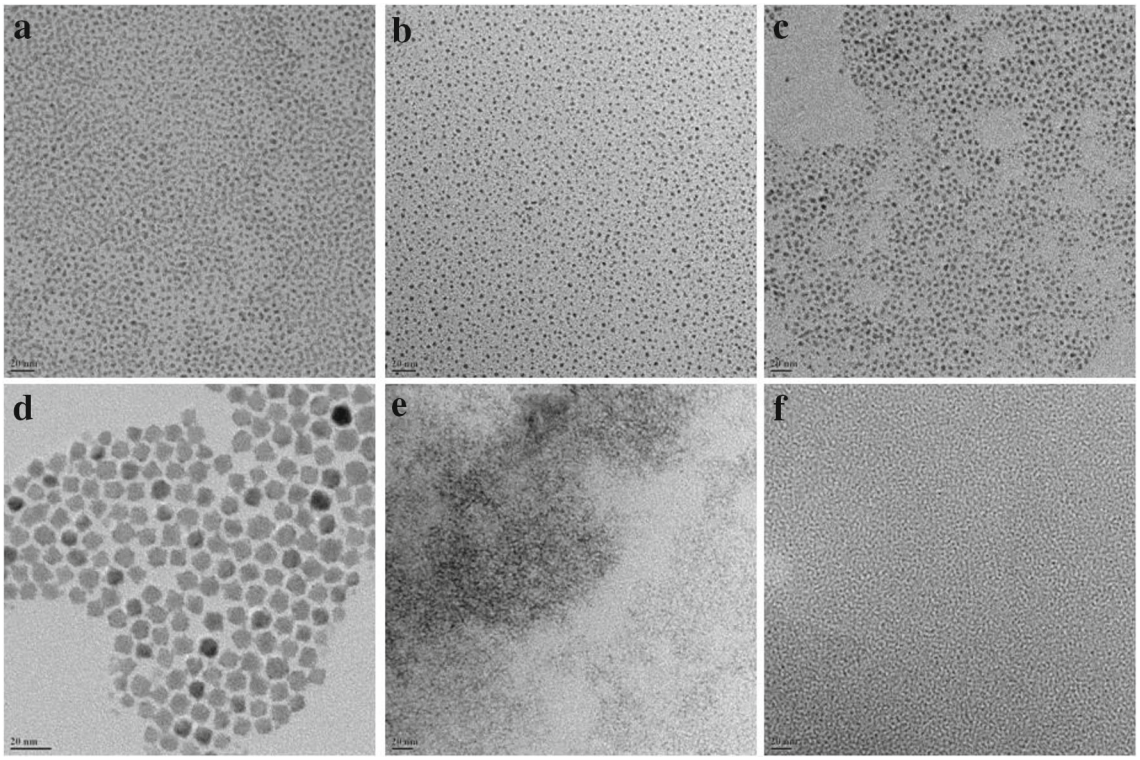

Figure 3. TEM images of different metal sulphide quantum dots synthesized using their corresponding thiolates as precursors. CdS at different temperatures: (**a**) 200, (**b**) 220 and (**c**) 240°C. (**d**) PbS at 200°C, (**e**) ZnS at 200°C and (**f**) MnS at 200°C. In all images, the scale bar corresponds to 20 nm.

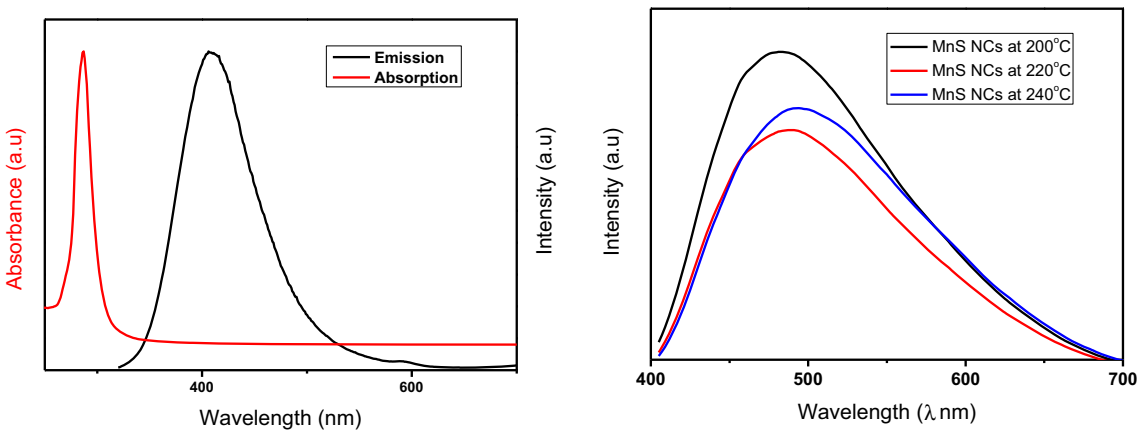

Figure 4. Optical spectra of ZnS and MnS NCs. (**a**) Absorption (red line) and emission (black line) spectra of ZnS NCs. (**b**) Emission spectra of MnS NCs synthesized at different temperatures.

to the small-sized particles (2.5–3 nm). The PL of MnS NCs, synthesized at different reaction temperatures, shows a sharp bandgap emission range of 470–490 nm (figure 4b). The TEM image of the MnS NCs synthesized at 200°C (figure 3f) reveals the presence of small spherical-shaped NCs.

Similar to the synthesis of different NCs described earlier, monodisperse NCs of ~6−10 nm Cu_2S were also synthesized by the thermal decomposition of copper octanethiolate in ODE at 200–240°C. For this, first, 200 mg of the Cu-octanethiolate (prepared using cupper acetate as Cu source) 2D molecular complex was taken in a solvent (1-octadecene) and the temperature was raised to 130°C to get a homogeneous clear solution. The temperature was then raised to 200°C in argon flow and the reaction was kept at this

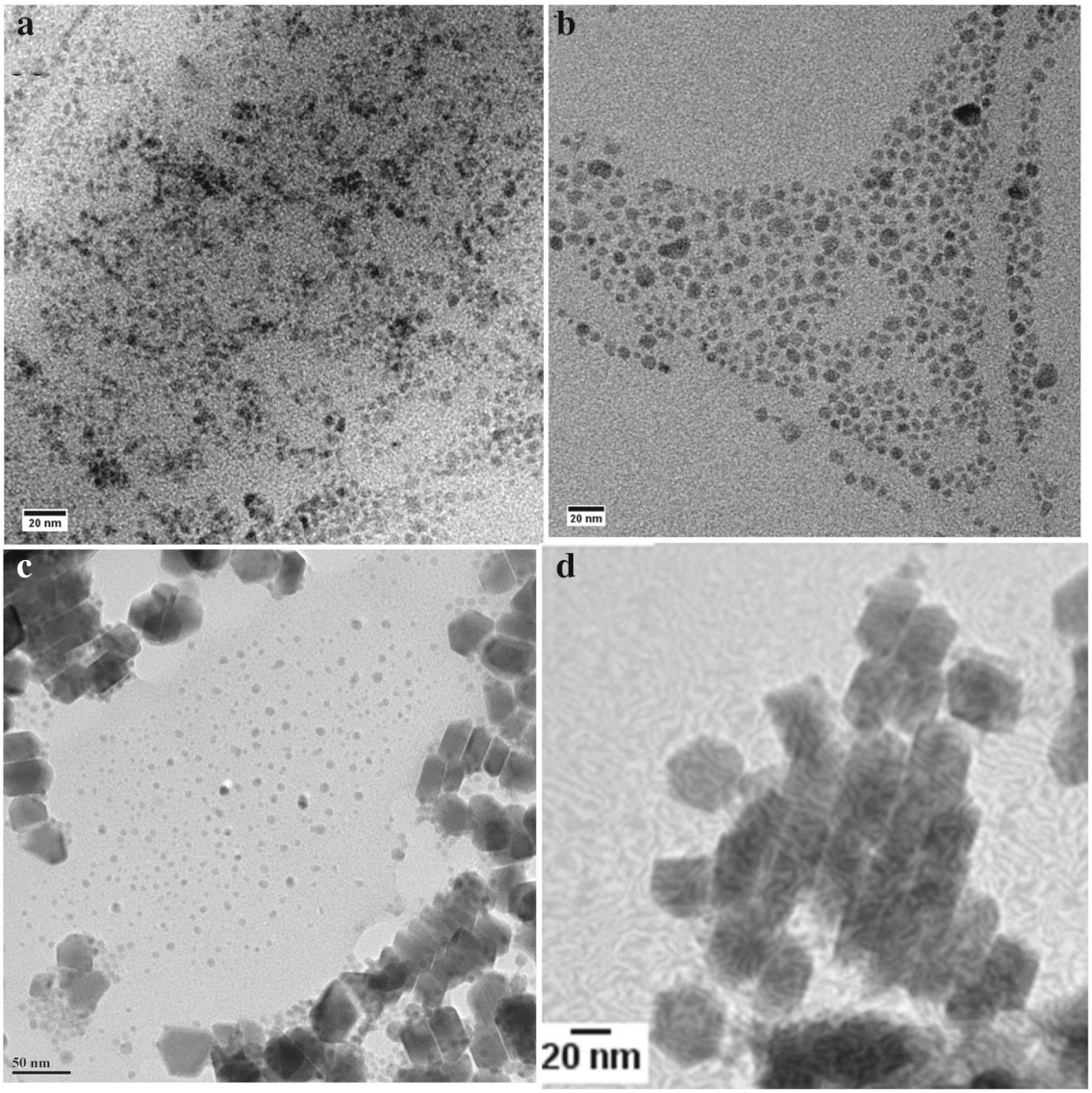

Figure 5. TEM images of Cu_2S prepared by thermolysis from Cu-octanethiolate ($Cu(ac)_2$ as metal precursor) at (**a**) 200 and (**b**) 240°C. (**c**, **d**) Effect of iodide in thermolysis of Cu-octanethiolate (CuI as metal precursor); mixed shape of particles formed (like plates, sheets as well as spherical particles are present).

temperature for 30 min. The pale yellow coloured solution became brownish black, indicating formation of Cu_2S. The heating was stopped immediately after the colour change; the system was allowed to naturally cool to room temperature (which took ∼45 min) and later the material was purified, similar to the CdS NCs synthesis. The PXRD pattern of the purified materials clearly matched with the chalcocite Cu_2S structure (for PXRD pattern of these samples, see supplementary figure S2), which corresponds to JCPDS 84-0206. TEM images (figure 5a) reveal that the NCs are almost uniform in size and spherical in shape with a particle diameter of ∼6 nm. One of the notable features of this synthesis procedure is the tunability of NCs size by changing the reaction temperature. For instance, when the Cu-thiolate clear solution (obtained by heating the Cu-thiolate in 1-octadecene to 130°C) was heated to 240°C for 30 min, ∼10-nm-sized spherical Cu_2S NCs were obtained (TEM images shown in figure 5b).

Interestingly, not only the size of Cu_2S NCs but also the shape (morphology) can be controlled by changing the metal source during synthesis of metal thiolate preparation. For instance, we found that the high-temperature decomposition of Cu-octanethiolate prepared from CuI at 240°C in 1-ODE resulted in the formation of plate-like Cu_2S NCs (with very few spherical NCs, see figure 5c and d). This is in agreement with the results of Wu *et al* [20], where they reported that introduction of halide ions slows down the growth kinetics and therefore the Cu_2S NCs with plate-like morphology

are more favoured. In our case as the Cu-octanethiolate was prepared from CuI, some iodide ions were found to be left behind as confirmed from the EDS results (see supplementary figures S3 and S4) of the Cu-octanethiolate sample. We strongly believe that these iodide ions act as shape-directing agents, resulting in the formation of Cu_2S plates, similar to the previous studies [20].

We believe that the simple process described here can be easily extended to prepare heterostructure of different metal sulphides like CdS–ZnS, CdS–MnS and ZnS–MnS; $Cd_xZn_{1-x}S$, $Zn_xCd_{1-x}S$, etc. by simply heating the corresponding metal thiolates (in a proper ratio) in a high boiling solvent. It is well known that the afore-mentioned heterostructure NCs show high quantum yield; hence these type of heterostructures are expected to be highly useful in LED (optoelectronic devices) applications. Similarly, synthesis of doped NCs like Mn:CdS and Mn:ZnS could also be attempted by heating manganese thiolates (taken in a proper ratio) with cadmium or zinc thiolates in a high boiling solvent.

4. Conclusion

In conclusion, a simple and general direct-heating solvothermal decomposition synthesis method using 2D molecular precursor (metal thiolates as single-source precursor) has been developed for the synthesis of different metal sulphide NCs like Cu_2S, PbS, CdS, MnS and ZnS. The synthesis of starting material (metal thiolate 2D sheets) is also very simple and scalable. We also showed that the size and shape of the NCs could be controlled by changing the reaction temperature and changing the metal precursor (used for metal thiolate preparation).

Acknowledgements

AB thanks UGC, New Delhi, for research fellowship. We thank the Council of Scientific and Industrial Research (CSIR), New Delhi, for financial assistance through the 12th Five-Year Plan Project (CSC 0134).

References

[1] Medintz I L, Uyeda H T, Goldman E R and Mattoussi H 2005 *Nat. Mater.* **4** 435
[2] Brunchez M P, Moronne M, Gin P, Weiss S and Alivisatos A P 1998 *Science* **281** 2013
[3] Chan W C and Nie W S 1998 *Science* **281** 2016
[4] Talapin D V, Lee J S, Kovalenko M V and Shevchenko E V 2010 *Chem. Rev.* **110** 389
[5] Filankembo A, Giorgio S, Lisiecki I and Pileni M P 2003 *J. Phys. Chem. B* **107** 7492
[6] Pileni M P 1997 *Langmuir* **13** 3266
[7] Chen X B, Li C, Gratzel M, Kostecki R and Mao S S 2012 *Chem. Soc. Rev.* **41** 7909
[8] Sakamoto T, Sunamura H, Kawaura H, Hasegawa T, Nakayama T and Aonob M 2003 *Appl. Phys. Lett.* **82** 3032
[9] Hu J, Li L S, Yang W, Manna L, Wang L W and Alivisatos A P 2001 *Science* **292** 2060
[10] Park J, Joo J, Kwon S G, Jang Y and Hyeon T 2007 *Angew. Chem. Int. Ed.* **46** 4630
[11] Lee S M, Jun Y W, Cho S N and Cheon J 2002 *J. Am. Chem. Soc.* **124** 11244
[12] Lee S M, Cho S N and Cheon J 2003 *Adv. Mater.* **15** 441
[13] Aldana J, Lavelle N, Wang Y and Peng X 2005 *J. Am. Chem. Soc.* **127** 2496
[14] Chen L, Chen Y B and Wu L M 2004 *J. Am. Chem. Soc.* **126** 16334
[15] Yu J H, Joo J, Park H M, Baik S I, Kim Y W, Kim S C *et al* 2005 *J. Am. Chem. Soc.* **127** 5662
[16] Lu Q, Gao F and Zhao D 2002 *Nano Lett.* **2** 725
[17] Murray C, Norris D J and Bawendi M G 1993 *J. Am. Chem. Soc.* **115** 8706
[18] Busupalli B, Kummara S, Kumaraswamy G and Prasad B L V 2015 *Chem. Mater.* **26** 3436
[19] Choi S H, An K, Kim E G, Yu J H, Kim J H and Hyeon T 2009 *Adv. Funct. Mater.* **19** 1645
[20] Wu W Y, Chakrabortty S, Chang C K L, Guchhait A, Lin M and Chan Y 2014 *Chem. Mater.* **26** 6120

LANGMUIR Article
Cite This: Langmuir 2018, 34, 5788−5797
pubs.acs.org/Langmuir

Generic and Scalable Method for the Preparation of Monodispersed Metal Sulfide Nanocrystals with Tunable Optical Properties

Abhijit Bera, Debranjan Mandal, Prasenjit N. Goswami, Arup K. Rath,* and Bhagavatula L. V. Prasad*

Physical/Materials Chemistry Division, National Chemical laboratory (CSIR-NCL), Dr. Homi Bhabha Road, Pune 411008, India

Supporting Information

ABSTRACT: A rational synthetic method that produces monodisperse and air-stable metal sulfide colloidal quantum dots (CQDs) in organic nonpolar solvents using octyl dithiocarbamic acid (C_8DTCA) as a sulfur source, is reported. The fast decomposition of metal-C_8DTCA complexes in presence of primary amines is exploited to achieve this purpose. This novel technique is generic and can be applied to prepare diverse CQDs, like CdS, MnS, ZnS, SnS, and In_2S_3, including more useful and in-demand PbS CQDs and plasmonic nanocrystals of Cu_2S. Based on several control reactions, it is postulated that the reaction involves the in situ formation of a metal−C_8DTCA complex, which then reacts in situ with oleylamine at slightly elevated temperature to decompose into metal sulfide CQDs at a controlled rate, leading to the formation of the materials with good optical characteristics. Controlled sulfur precursor's reactivity and stoichiometric reaction between C_8DTCA and metal salts affords high conversion yield and large-scale production of monodisperse CQDs. Tunable and desired crystal size could be achieved by controlling the precursor reactivity by changing the reaction temperature and reagent ratios. Finally, the photovoltaic devices fabricated from PbS CQDs displayed a power conversion efficiency of 4.64% that is comparable with the reported values of devices prepared with PbS CQDs synthesized by the standard methods.

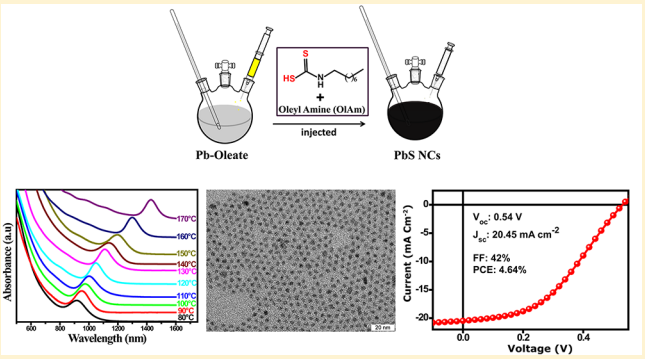

INTRODUCTION

Over the past few decades, highly dispersible colloidal quantum dots (CQDs) capped with surfactant molecules have emerged as extremely useful materials for the development of numerous classes of solution-processed optoelectronic devices, including photovoltaic cells,[1−8] photodetectors,[9−12] and light-emission devices.[13−17] In addition to solution processing, a key advantage of their synthesis in solvents is the ability to tune their sizes, allowing their optical and electrical properties to be readily modulated.[18−20] Among the different classes of CQDs, lead sulfide (PbS) based ones have particularly captured the attention due to their tunable absorption edge from the near-infrared through the visible region, which makes them suitable for solar energy conversion. Accordingly, solar cells based on the p−n junction[21,22] between a wide band gap n-type semiconductor (e.g., TiO_2, ZnO) and a p-type lead-rich PbS colloidal quantum dot (CQD) film have seen rapid advances in recent years, progressing from the first report of an infrared solar cell[11,23] to recent reports of a ∼11.28% solar AM1.5 power conversion efficiency (PCE).[24]

Therefore, it is not surprising to see that a large number of researchers have dedicated their efforts to find methods for the preparation of large-scale high-quality metal sulfide QDs, including PbS. Among the different physical and chemical processes that are currently being used to synthesize metal sulfide CQDs with the desired characteristics, hot-injection method is considered the best.[25] Several metal sulfide quantum dots like CdS, MnS, ZnS, SnS, In_2S_3, and Cu_2S have been synthesized using hot-injection method using elemental sulfur or sulfur-containing ligands (like thiourea),[26] ammonium sulfide,[27] and thioacetamide[28] as sulfur source. In the methods involving elemental sulfur, a solution is prepared by dissolving the sulfur powder in oleylamine that leads to the generation of alkylamonium-S^{2-} disulfide or alkylamonium-S_n^{2-} polysulfide species.[26,29] These species then react with cations like Pb^{2+}, Cd^{2+}, etc., resulting in the formation of the respective nanocrystals. Unfortunately, due to the high reactivity and relatively low nucleation threshold with the Pb^{2+} ion,[30] the above procedure leads to the formation of many sulfur-containing byproducts, damaging the reaction yield when it is employed for PbS CQD synthesis. This also causes batch-to-batch variability and gives wide size distribution associated with imperfect surface passivation, including poor air stability.[31] Therefore, these PbS CQDs are subjected to size selective precipitation and cadmium chloride passivation to improve the power conversion efficiency of the photovoltaic devices made with them.[32] Among the other methods, the one using thioacetamide provides access to a large amount of PbS

Received: March 7, 2018
Revised: April 23, 2018
Published: May 1, 2018

DOI: 10.1021/acs.langmuir.8b00741
Langmuir 2018, 34, 5788−5797

QDs,[33] but this method suffers from lack of sharp excitonic peak of the PbS CQDs due to their broad size distributions (>8%), again preventing their utility in many applications like solar cells.[34] Substituted thiourea derivatives are another option that has been suggested to prepare good quality metal sulfide, especially PbS CQDs.[35] Although this procedure does provide PbS CQDs with tunable band gap, including narrower size distribution and good optical properties, the size control in this procedure is achieved by the differences in the decomposition rate and the associated release of active sulfur species from different thiourea derivatives. Thus, if one desires to prepare different sized PbS, different thiourea derivatives will be needed.

Compared to the procedures listed above, the method that involves the usage of a highly reactive sulfur source—bis (trimethylsilyl) sulfide $[(TMS)_2S]$[36]—is considered to be the best as far as PbS CQDs preparation is concerned. The use of $[(TMS)_2S]$ provides a fast reaction, yielding CQDs with a relatively narrow size distribution. Till date, all the reported performance records for photovoltaic devices based on PbS CQDs have relied on the $[(TMS)_2S]$-based synthesis.[24,34] Unfortunately $[(TMS)_2S]$ is pyrophoric, toxic, and expensive. Though $[(TMS)_2S]$ can be used to prepare PbS near room temperature, as it is highly reactive, this rapid reactivity causes problems due to limitations in mixing during the injection step that may also hinder the reaction scalability.

Consequently, there is an obvious need for an alternative and safe method for large-scale, high-quality CQD production. Addressing this, we present here a method involving a safe and air-stable octyl dithiocarbamic acid (C_8DTCA) as a sulfur source. We demonstrate that highly reactive bidentate ligand C_8DTCA first reacts with metal-oleate and a metal−C_8DTCA complex gets formed, which reacts with oleylamine at slightly elevated temperature and decomposes to metal sulfide CQDs at a controlled rate, resulting in the formation of a material with good optical characteristics. We also show that great control over the particle sizes and size distribution can be achieved by just adjusting the reaction parameter like temperature, time, and oleylamine concentration. Although the full details of the study are described with the more difficult PbS system, we also show that this method could be easily extended to obtain others metal sulfide like CdS, MnS, ZnS etc., without compromising their optical properties. Finally, to prove that the prepared PbS CQDs thus prepared could indeed be used for device fabrication, we prepared photovoltaic devices using the PbS CQDs that displayed a power conversion efficiency of 4.64%, which is comparable with the reported values,[37] where PbS CQDs synthesized using $[(TMS)_2S]$ have been utilized.

EXPERIMENTAL SECTION

Synthesis. *Reaction A—Synthesis of Octyl Dithiocarbamic Acid (C_8DTCA).* About 10 mL dry dichloromethane was taken in 100 mL Rb flask and cooled. To this, 50 mmol of CS_2 (large excess) was added and stirred for some time in argon atmosphere. After 15 min, 10 mmol of octyl amine was added dropwise into the CS_2 solution and stirred for 30 min. A white precipitate was formed immediately. This was dried under vacuum. The powder was recrystallized from toluene. The dried shiny crystals were analyzed by NMR and high-resolution mass spectrometry (see in Supporting Information (SI) Figures S1−S3). The other dithiocarbamic acids with different chain length alkyl amines were prepared in similar ice cold conditions (the detailed procedures are described in the Supporting Information).

Caution: Reaction is exothermic; solution became warm upon addition of amine, so reaction should be performed in ice cold condition and addition of amine should be dropwise. Otherwise, some part of desired compound can convert to thiourea.

Reaction B—Preparation of Lead Oleate. PbO (450 mg, 2 mmol) was mixed with 1.5 mL of oleic acid and 10 mL of 1-octadecene (1-ODE) in the 100 mL three-neck round-bottom flask. The system was connected to the vacuum gas manifold and heated to 100 °C under vacuum. The turbid yellow solution turns colorless, indicating the formation of a lead(II) oleate solution.[36]

Reaction C—Preparation of Lead Octyl Dithiocarbamate (Pb-C_8DTCA) Complex. Initially, the lead oleate was made as mentioned in Reaction B. First, C_8DTCA dissolved in dry $CHCl_3$ (used very less amount of $CHCl_3$ mixed with toluene) was injected into this lead oleate solution at room temperature (25 °C). Immediately, the colorless lead oleate solution became pale yellow. Addition of dry acetone to this solution led to the formation of a yellowish brown precipitate. This precipitate is highly soluble in nonpolar solvents like toluene and chloroform. Based on different characterizations, this compound was determined to be $Pb(C_8DTCA)_2$.

Note: The Pb-C_8DTCA complex is highly moisture sensitive; it can decompose to PbS NPs in the presence of air and moisture. The yellowish brown Pb-$(C_8DTCA)_2$ turns black when exposed to moisture.

Reaction D—Preparation of PbS by Heating Pb-C_8DTCA Complex without OlAm. Initially, the lead oleate was prepared as mentioned in Reaction B. After 2 h, the setup was backfilled with nitrogen and left for an additional 20 min for temperature stabilization (100 °C). Into this lead oleate solution, C_8DTCA dissolved in dry $CHCl_3$ (at room temperature) was injected. Immediately, the colorless lead oleate solution became pale yellow. Then, the temperature was increased slowly to 140−150 °C, leading to the formation of a dark brownish black product. When dry acetone was added, a brownish black precipitate got separated from the solution. This precipitate was washed two times with acetone (centrifuged at 5000 rpm for 3 min) to remove excess surfactants. This precipitate was then dried under Argon flow and redispersed into tetrachloroethylene or toluene for various measurements. Analysis of this product indicated the formation of PbS nanoparticles.

Reaction E—Preparation of PbS by Heating Pb-C_8DTCA Complex with OlAm. The Pb-C_8DTCA complex was prepared as mentioned in Reaction C. The system was connected to the vacuum gas manifold and heated to 50−100 °C under vacuum. Into this, 0.5 mL of OlAm was injected very fast (<1 sec). Immediately, the pale yellow Pb-C_8DTCA solution turned into brownish black, indicating the formation of PbS. Immediately after OlAm injection, heating was stopped and the system was removed from the heating bath and allowed to naturally cool to room temperature (which took ∼45 min). The product of this reaction was collected by precipitating it with acetone addition, and after washing it two times with acetone (centrifuged at 5000 rpm for 3 min) and one time with a mixture of acetone and methanol (1:3 by volume), the precipitate was dried under Argon flow. The precipitate was redispersed into tetrachloroethylene or toluene for various measurements. Analysis of this product indicated the formation of PbS nanoparticles.

Reaction F—In Situ Preparation of PbS Using Pb-Oleate, C_8DTCA, and OlAm. Initially, the lead oleate was made as mentioned in Reaction B. Into this, the mixture of C_8DTCA and OlAm (0.3−0.75 mL) solution in 1-octadecene (1-ODE) was injected very fast (<1 s). During the injection, the temperature of the Pb-oleate was maintained between 80 to 160 °C at different levels. Immediately after the C_8DTCA-OlAm addition, colorless Pb-oleate became brownish black. The heating was stopped immediately after the injection of C_8DTCA plus OlAm and the system was allowed to naturally cool to room temperature (which took ∼45 min). The product of this reaction was collected by precipitating it with acetone addition, and after washing it two times with acetone (centrifuged at 5000 rpm for 3 min) and one time with a mixture of acetone and methanol (1:3 by volume), the precipitate was dried under Argon flow. The precipitate was redispersed into tetrachloroethylene or toluene for various measurements. Analysis of this product indicated the formation of PbS nanoparticles.

DOI: 10.1021/acs.langmuir.8b00741
Langmuir 2018, 34, 5788−5797

Materials Characterization. Optical absorption measurements were carried out by Shimadazu UV−vis−IR-3600 Plus spectrophotometer. The NIR-fluorescence spectra were recorded using Qunata Master 400, PTI spectrofluorometer. The X-ray diffraction (XRD) profiles were recorded on an X'pert Pro model PANalytical diffractometer from Philips PANalytical instruments operated at a voltage of 40 kV and a current of 30 mA with Cu Kα (1.5418 Å) radiation. The samples were scanned in a 2θ range from 5 to 80° with a scan rate of 0.4° per minute. Transmission electron microscopy (TEM) was carried out on a TECHNAI G2-20 S-TWIN (T-20) instrument operating at 200 keV and with LaB_6 filament as the source of electrons. The metal sulfide QDs were dispersed in toluene through vigorous sonication and placed on carbon-coated Cu grid for TEM measurement. The particle size distributions were determined by measuring the size of a minimum of 200 particles manually from multiple images. The device fabrication and characterization details have been provided in the SI.

RESULTS

We present here a generic method for metal sulfide CQDs preparation, involving a safe and air-stable octyl dithiocarbamic acid (C_8DTCA) as a sulfur source. We conclude that the C_8DTCA possesses the optimum alkyl chain length for controlled CQDs formation (please see SI Figure S4 for more details). In fact, we found that C_8DTCA can be used to produce a broad variety of nearly monodisperse metal sulfide CQDs, including PbS, CdS, ZnS, MnS, In_2S_3, SnS, and Cu_2S (the generic procedure followed is shown in Scheme 1). In all these cases, the sulfur precursor solution—prepared by dissolving C_8DTCA into OlAm (at room temperature 25 °C)—was injected into the previously prepared metal-oleate solution at an appropriate temperature (140−200 °C) depending on the type of CQDs to be prepared. The TEM images of all the metal sulfide CQDs prepared by this simple method are presented in SI Figure S5 and other characterizations (powder X-ray diffraction (PXRD), UV−vis, and photoluminescence (PL) spectra) of all these metal sulfides are summarized in the SI (Table A and Figures S6−S10). Thus it is clearly established that this simple one-step synthesis process can be easily applied for the synthesis of different metal sulfide CQDs.

Scheme 1. Method for Generic Metal Sulfide CQDs Synthesis

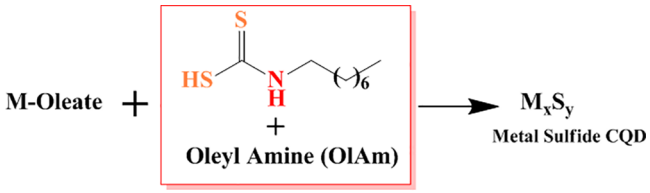

After demonstrating that this generic method could be used to prepare a variety of metal sulfide CQDs, we wanted to find the best conditions that will provide nearly monodispersed CQDs with good optical properties, and for this we chose the more difficult and in-demand PbS system as the test case.

Quite gratifyingly, we could effectuate great control over the size and size distribution of the PbS CQDs and tune their optical properties in a controlled fashion by varying the reaction parameters such as the OlAm concentration and Pb:C_8DTCA ratio in a systematic way (for full experimental details, see the Supporting Information, and for the optical spectra of the samples obtained under these different conditions, see Figures S11−S13). As can be noticed from these results, 0.5 mL of OlAm and a Pb:C_8DTCA ratio of 6:1 (which corresponds to an actual Pb:S ratio of 3:1, as C_8DTCA contains two sulfur atoms in a single molecule) were determined to be the optimum. In the following, we first present the characterization details of the sample obtained using the above reagent concentrations and a temperature of 120 °C. When C_8DTCA dissolved in OlAm was injected into the hot Pb-oleate solution (120 °C), an immediate color change, from colorless to deep brownish black, took place. The reaction was immediately stopped by removing the round-bottom flask from the heating bath. The system was allowed to cool naturally to room temperature, which took ∼45 min. From the reaction mixture, the product was isolated by precipitation by adding dry acetone and washing with acetone and methanol mixtures. The isolated product was found to be easily redispersibe in toluene or tetrachloroethylene, and the dispersions were stable for a long time (∼3 months, vide infra).

The absorption spectra of the PbS CQDs obtained under the above-mentioned condition showed only one sharp peak at 1050 nm (Figure 1a—black solid line) with an full width at half-maximum (FWHM) of ∼95 nm (∼76 meV). In addition to the narrow absorption linewidth, this sample also displayed a strong emission in the infrared region. The emission spectra (red solid line, Figure 1a, excitation max = 1125 nm) has a FWHM of ∼100 nm with a minimal Stokes shift (∼75 nm or ∼40 meV). The intense photoluminescence (quantum yield ∼42%) indicates that the emission is purely band gap emission, devoid of any significant emission from trapped states. The PXRD pattern of the PbS nanocrystals prepared by this method is shown in Figure 1b, which shows a high degree of crystallinity, with all the peaks matching with the Bragg reflections of the standard cubic rock-salt structure of PbS (JCPDS #05-0592). The TEM image of this sample (Figure 1c,d) unveils the presence of monodispersed particles (size 3.32 ± 0.47 nm; σ = 4.7%; size distribution plot shown in SI Figure S14d), which is also exemplified by their self-assembly into two-dimensional hexagonally close-packed structures. The high-resolution TEM images shown in Figure 1d (inset) indicate that the particles are highly crystalline with well-resolved lattice planes corresponding to an interplanar spacing of 0.29 ± 0.02 nm, consistent with the (200) d-spacing of the PbS bulk rock-salt structure (lattice fringes shown in Figure 1d inset).

Our next aim was to find the reaction conditions that allow us to gain control over the particle sizes and their optical properties. To achieve this, we synthesized PbS at different injection temperatures (T_{inj}) by keeping the reaction parameters like OlAm concentration and Pb:C_8DTCA ratio same as above. The absorption spectra of PbS CQDs obtained by varying the T_{inj} temperatures (80−160 °C) are plotted in Figure 2a. It can be clearly seen that each of the sample displays a well-defined excitonic peak and the peak position varied gradually from 915 to 1300 nm (1.35−0.95 eV) as the T_{inj} temperature is varied in the range 80−160 °C. At 80 °C, the excitonic peak is positioned at 915 nm (1.35 eV), and the peak is comparatively broader (the FWHM for this peak could not be determined exactly). The TEM images (Figure 2c) of this sample indicate that the average particle size is ∼2.4 nm, with a slightly broader particle size dispersion (5.1%, see Figure S14a for size distribution plots). As T_{inj} is raised to 90 °C, the excitonic peak becomes noticeably narrower (FWHM = 157 nm). As T_{inj} is increased further (100−120 °C), the FWHM of

DOI: 10.1021/acs.langmuir.8b00741
Langmuir 2018, 34, 5788−5797

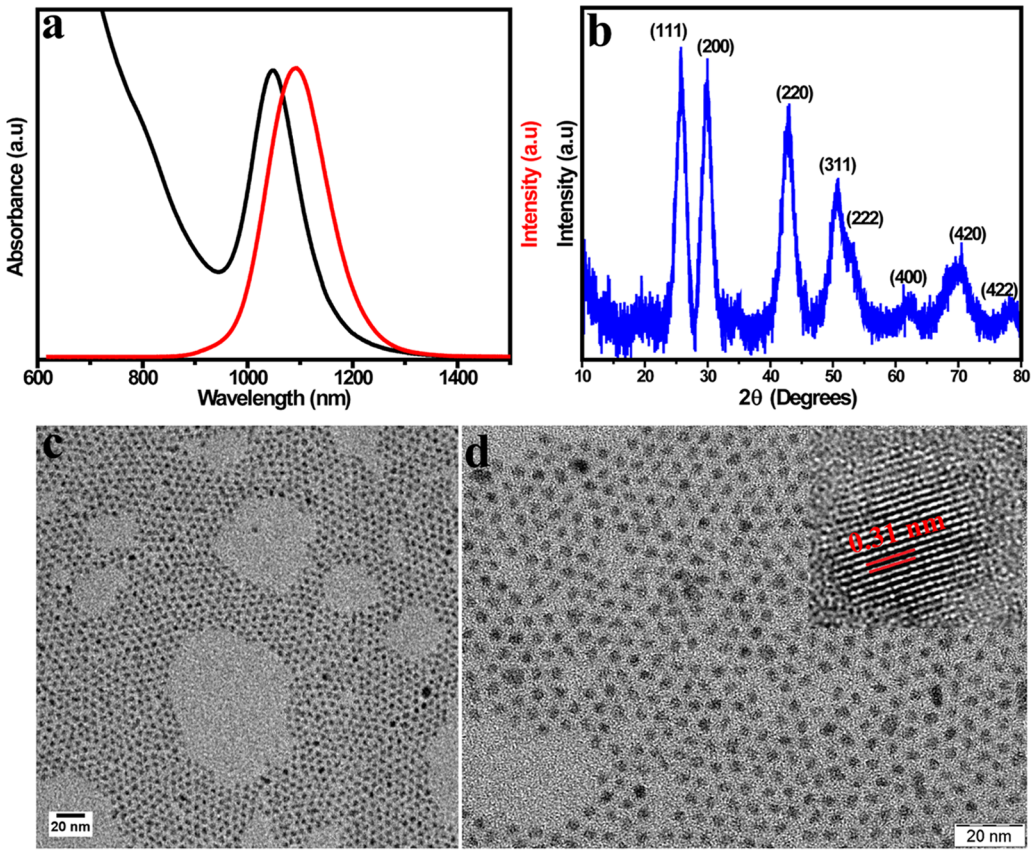

Figure 1. (a) Optical characterization of PbS QDs prepared at 120 °C. Absorption spectra (black solid line) and photoluminescence spectra (red solid line), normalized for same peak amplitude. (b) PXRD of PbS QDs and (c, d) TEM images of PbS QDs. The high-resolution TEM image of one PbS QD is shown in the inset of (d).

the first excitonic peak gets further narrowed down to 95 nm, with a concomitant red shift in the peak. After a certain T_{inj} temperature (120 °C), no further change in the FWHM is observed, whereas the peak position keeps shifting to the right. In Figure 2b, the near-infrared emission spectra of all the samples are plotted, which demonstrate that all the samples display bright and narrow emission peaks. The Stokes shift changes observed with different samples obtained at various T_{inj} are found to be minimal (110−50 nm), which indicate a pure band gap emission from these CQDs. In Figure 2c−h, the TEM images of PbS CQDs synthesized at different T_{inj} temperatures are presented, which clearly point to the monodispersity in the the particle sizes. The average particles sizes for these particles are shown in Table 1, and for the size distribution plots of the same, see SI Figure S14.

One of the most attractive features of the procedure we present here is the possibility to scale up without compromising the product quality. This is demonstrated by carrying out the above reaction at 10 mmol scale. As may be noticed, the optical properties of the product remain almost the same even when the precursor plus sulfur source concentration was increased five times (Figure 3a).

In addition, the PbS CQDs synthesized using the recipe developed here showed excellent air stability, as evidenced by the intact optical characteristics from the sample recorded after storing it in a normal laboratory atmosphere (not in inert atmosphere) for several months. In Figure 3b, we compare the absorbance spectra for three different sized PbS QDs immediately after synthesis and after 3 months of storage. It can be easily noticed that the absorption peak positions remain almost the same even when the sample is stored for 3 months under ambient conditions.

DISCUSSION

It may be recalled that the successful synthetic strategy to obtain metal sulfide CQDs with controlled sizes comprised the addition of C_8DTCA and OlAm together into preheated metal-oleate. We reckoned that there could be several possible ways through which these metal sulfide CQDs are formed. In the first of such scenarios, the OlAm could react with C_8DTCA releasing H_2S gas (path I, Scheme 2). This H_2S gas could then react with metal-oleate and form metal sulfide CQDs. To gain more insights into this aspect, we recorded the ^{1}H NMR spectra of C_8DTCA and *n*-butyl amine (as it is more reactive) mixture (at room temperature 25 °C) and C_8DTCA and OlAm mixture (at 50 °C), which clearly revealed the presence of the individual species that are intact (no extra peaks observed that can be related to the reaction products (thiourea) between C_8DTCA and amine—see in SI Figures S15 and S16). However, when the same mixture was heated to 140 °C for several hours (1−2 h), we could see signatures of thiourea with a concomitant release of H_2S (as evidenced by the blackening of lead acetate paper). For NMR spectra of the reaction products, see SI Figures S17 and S18. We also noticed that the liberation rate of H_2S species by this route is much slower (30 min−1 h) than the overall reaction time take to form different metal CQDs (few minutes) in this study. Thus, we ruled out path I (possibility of H_2S gas getting released by the reaction

DOI: 10.1021/acs.langmuir.8b00741
Langmuir 2018, 34, 5788−5797

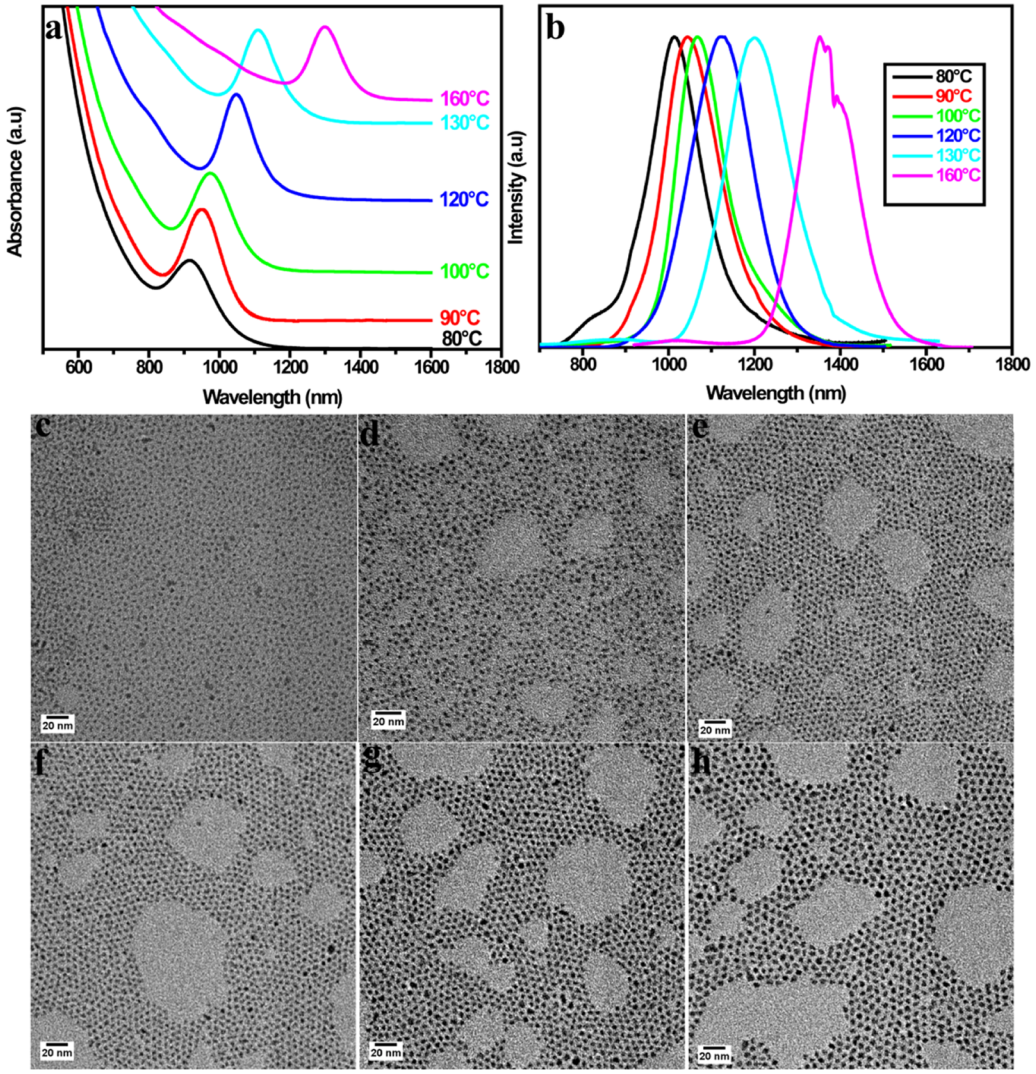

Figure 2. (a) Absorbance spectra of PbS QDs prepared by adding C_8DTCA and OlAm to Pb-oleate at a Pb/S ratio of 3:1 at different temperatures. (b) Near-infrared photoluminescence spectra of the PbS QDs synthesized at different temperatures. All the emission spectra were normalized to have the same peak amplitude. The absorbance spectra were offset vertically for clarity. (c–h) TEM images of PbS QDs synthesized at different temperatures (c) 80 °C, (d) 90 °C, (e) 100 °C, (f) 120 °C, (g) 130 °C, and (h) 160 °C. All the QDs were dispersed in tetrachloroethylene for the absorption and PL spectra.

Table 1. Summary of Particle Sizes and Optical Spectral Parameters of PbS QDs Prepared at Different Temperatures

PbS at different temp (°C)	particle size from TEM (nm)	absorption wavelength (nm)	FWHM	emission wavelength (nm)	Stoke shift (nm)
80	2.4 ± 0.5	915		1015	100
90	2.7 ± 0.5	946	157	1045	99
100	2.8 ± 0.5	972	147	1068	96
120	3.3 ± 0.5	1050	95	1125	75
130	3.9 ± 0.6	1110	95	1200	90
160	4.8 ± 0.7	1300	92	1371	71

between OlAm and C_8DTCA) as the possible route by which metal sulfide CQDs are getting formed in the current study.

The other possibility is the formation of a stable M–C_8DTCA complex, which undergoes self-decomposition when subjected to high-temperature heating, giving rise to the respective CQDs, which get subsequently capped/passivated by the oleic acid/OlAm present in the system (path IIA). To test whether this true or not, we prepared the Pb-C_8DTCA complex first (see Experimental Section Reaction A, Reaction B, and Reaction C for the preparation of C_8DTCA, lead oleate, and Pb-C_8DTCA, respectively). The PXRD pattern (see SI Figure S19a,b) of Pb-C_8DTCA complex is characterized with equidistant peaks, suggesting its lamellar structure similar to several other metal thiolates.[38] We wish to mention that the Pb-C_8DTCA complex is very unstable (in air) and decomposes to form PbS even at room temperature as evidenced by the peaks corresponding to PbS (Supporting Information Figure S19c,d) even in this PXRD pattern. Further, when this partially decomposed Pb-C_8DTCA complex was heated to 150 °C in 1-ODE (Figure 4, path IIC), a black precipitate was seen to form within 1–2 min. The PXRD pattern of this powder could be assigned to the PbS rock-salt structure (SI Figure S19e). The formation of PbS by this route is similar to those accomplished using the thermal decomposition of single-source precursors.[39–42] However, when the precipitate obtained by this high temperature decomposition of Pb-C_8DTCA complex was redispersed in tetrachloroethylene, the absorption specrum (shown in Figure 4a, black curve) displayed two absorption

DOI: 10.1021/acs.langmuir.8b00741
Langmuir 2018, 34, 5788–5797

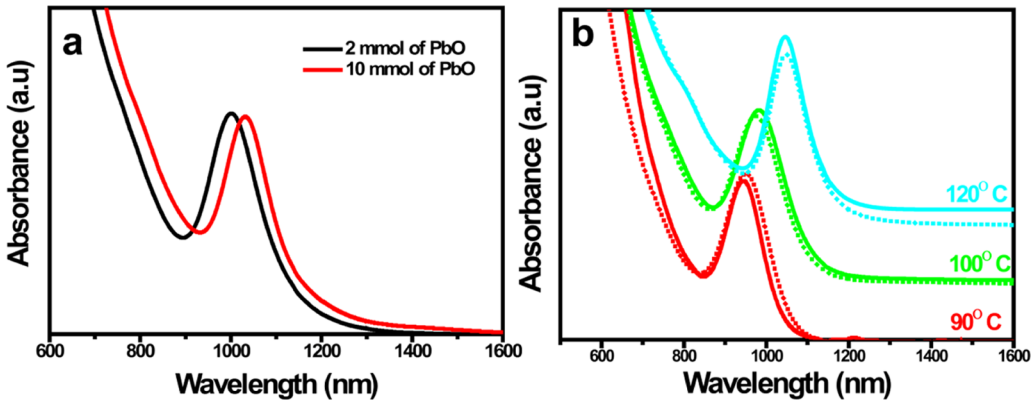

Figure 3. (a) Absorption spectra of PbS QDs synthesized at different ~mmol scales. Black solid line represent 2 mmol batch synthesis and red solid line is the spectrum recorded from 10 mmol batch. (b) Absorption spectra of different-sized PbS QDs immediately after the synthesis (solid line) and after 3 months of storage (dotted line).

Scheme 2. Probable Pathways of PbS Formation[a]

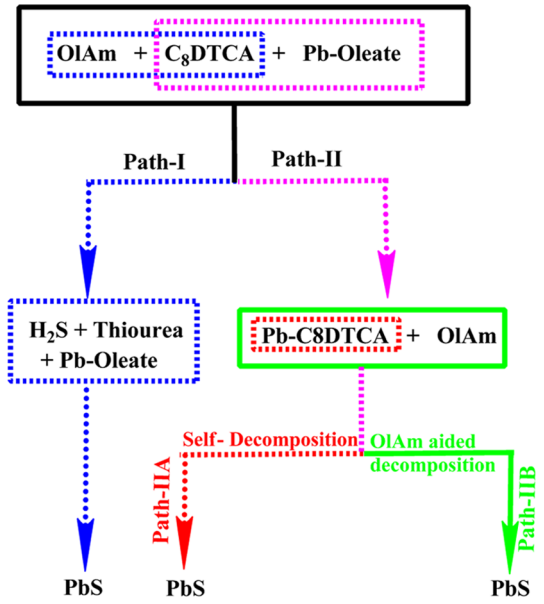

[a]Please see text for details.

features, one at ~1500 nm and the other one at 2000 nm (major peak). This could be due to the formation particles of varied sizes and morphologies. The TEM images obtained from this sample attests the same with the average particle size and size distribution (Figure 4b, more images and size distribution plot are shown in SI Figure S20), turning out to be 9.86 nm and 12.6%, respectively. Thus, it is clear that the high-temperature self-decomposition of Pb-C_8DTCA complex alone would not provide the nearly monodispersed PbS CQDs.

In the literature, it has been shown that the addition of oleylamine to the thermally stable $[Ni(S_2CNBui_2)_2]$ complex reduces its solvothermal decomposition temperature from 310 to 145 °C, resulting in the formation of NiS NPs.[43] Similarly, several groups reported the synthesis of monometallic sulfide[39,40] (like CdS and ZnS) and bimetallic self-coupled sulfide heterostructures[41,42,44] (like $Cu_{2-x}S$–ZnS, $Cu_{2-x}S$–CuS Ag–$AgInS_2$) by simply heating the single-source precursors in the presence of amine. We thus wanted to see whether the addition of any primary amine would lead to a drop in the Pb-C_8DTCA decomposition (see Experimental Section Reaction E for details) temperature too. Indeed, when oleylamine was injected to the preformed Pb-C_8DTCA complex in 1-ODE at different temperatures, its color immediately changed to deep brownish black, indicating that the Pb-C_8DTCA complex is decomposed to PbS NPs (schematic shown in Figure 4, path IID). The PXRD patterns of the product obtained from this reaction clearly matched with that of PbS with rock-salt structure (for PXRD pattern of this samples, see SI Figure S19f, which corresponds to JCPDS card no. #05-0592). The absorption spectra of the samples obtained when oleylamine was injected at lower temperatures (25–70 °C) are featured with broad peaks (SI Figure S21), whereas those recorded with the sample that resulted by adding OlAm at a slightly higher temperature (~100 °C) displayed a sharp peak at 1427 nm, as may be noticed from Figure 4c. The FWHM of this sharp peak is deduced to be 92 nm. However, this sharp peak is overlaid on a broad absorbance, which is characterized by four more shoulder/humplike features, indicating the formation of particles of different size and morphologies. The TEM image (Figure 4d) of this sample also exhibits the presence of different sized particles (more TEM images and size distribution plot are shown in SI Figure S22). Thus, all our initial attempts in trying to make PbS from preformed Pb-C_8DTCA led to the formation of large particles or polydispersed particles, which are not suitable for the intended photovoltaic applications.[34] Hence, the results of the above two experiments suggested that either the reaction of H_2S gas with Pb-oleate or the self-decomposition of preformed Pb-C_8DTCA complex does not provide the metal sulfide CQDs with the desired optical characteristics.

We attribute the failure to obtain good quality PbS CQDs when preformed Pb-C_8DTCA was subjected to heating to the uncontrollable decomposition of the very unstable Pb-C_8DTCA complex. As could be seen, using OlAm as a reagent to control the decomposition of preformed Pb-C_8DTCA complex also did not offer much improvement. This could be due to two reasons: (i) the autodecomposition of Pb-C_8DTCA (Figure 4, path IIC) and (ii) the decomposition of Pb-C_8DTCA aided by oleylamine (Figure 4, path IID) in an uncontrollable (as oleylamine reacts with Pb-C_8DTCA at room temperature also) fashion, both occurring simultaneously. Thus, the addition of OlAm to preformed Pb-C_8DTCA and heating them do not offer any improvement as far as the quality of PbS CQDs is concerned. Then, how does the current procedure afford highly monodispersed PbS CQDs with

DOI: 10.1021/acs.langmuir.8b00741
Langmuir 2018, 34, 5788–5797

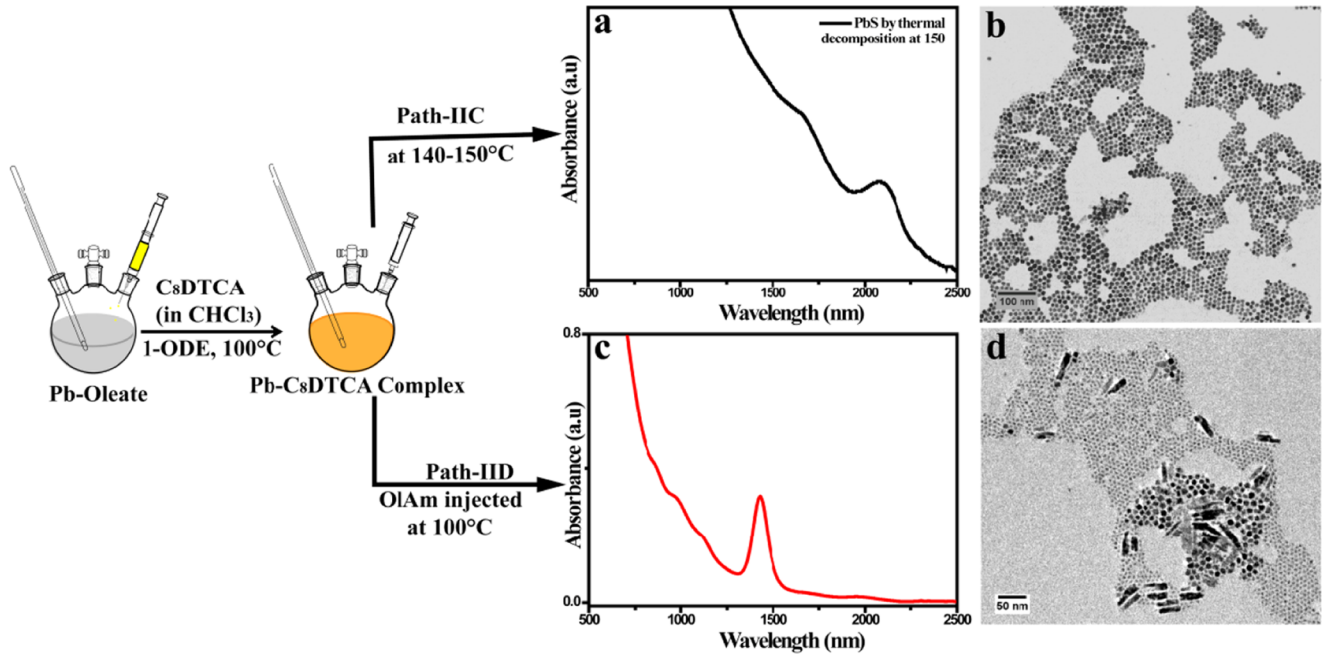

Figure 4. Schematic presentation of the preparation of PbS QDs from Pb-C_8DTCA complex. (a) Absorption spectra of the PbS QDs prepared by thermal decomposition of Pb-C_8DTCA complex. (b) TEM images of the same. (c) Absorption spectra of PbS QDs prepared by solvothermal decomposition by adding OlAm to Pb-C_8DTCA complex and their TEM images (d).

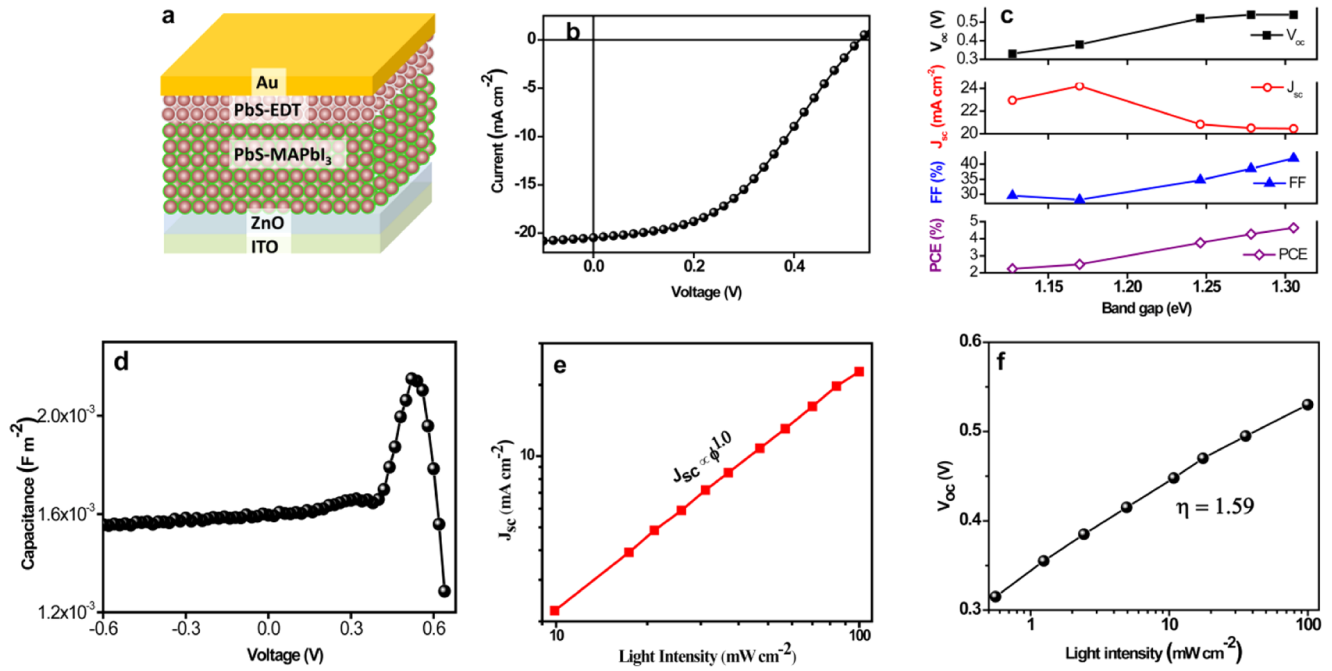

Figure 5. (a) Schematic device structure of the photovoltaic device. (b) J–V characteristics of the best-performing solar cell under 1.5 AM illumination. (c) Comparison of photovoltaic figure of merits for different band gap PbS QDs. (d) Capacitance–voltage plot for best-performing PbS QD (1.3 eV band gap) based solar. (e, f) The evolution of short-circuit current (J_{sc}) and open-circuit voltage (V_{oc}), respectively, for best-performing PbS QD-based solar cell.

tunable optical characteristics? The third and final possibility we envisaged is that Pb-oleate and C_8DTCA react first, forming Pb-C_8DTCA complex, which then reacts in situ with OlAm to form the PbS nanocrystals (Scheme 2, path IIB). This could happen as follows. After the injection of C_8DTCA-OlAm solution into Pb-oleate, the bidentate ligand (C_8DTCA) first reacts with Pb-oleate to form the highly reactive and unstable Pb-C_8DTCA complex. The OlAm present in the solution immediately attacks this complex (as proposed by Jung et al)[45] in situ, resulting in the formation of PbS nanoparticles (the reaction mechanism drawn on the basis of the one suggested by Jung et al. is shown in SI Figure S23). We further postulate that the reaction of Pb-C_8DTCA with oleylamine results in the formation of *N*,*N*′-octylthiourea as the side product and no further decomposition of this thiourea takes place. To support this, we have independently prepared the *N*,*N*′-octylthiourea

DOI: 10.1021/acs.langmuir.8b00741
Langmuir 2018, 34, 5788–5797

derivative. It was seen that this compound required a temperature of ∼150−170 °C to decompose, which is higher than that we have generally used in our reaction. Also, when we used *N*,*N*′-octylthiourea as a sulfur source for PbS synthesis, particles with poor optical properties (with excitonic peak near around ∼1300 nm, SI Figure S24) were found to be formed. This supports our contention that the attack of oleylamine on Pb-C_8DTCA with the release of H_2S and the formation of thiourea as a byproduct is the main reaction. The H_2S thus released reacts with the liberated Pb^{2+} species to form PbS nanoparticles. We hasten to add here that we cannot rule out the possibility of some amount of thiourea decomposing and releasing active sulfur species, which also participate in the formation of PbS.

We surmise that the formation of the other metal sulfide CQDs would be following the same pathway because we followed the same sequence of reagent addition for their preparation also. This generic approach is optimized for PbS CQD synthesis, and as has been demonstrated, we could exercise great control over the particle sizes and size distribution of these CQDs by just adjusting the reaction parameter like temperature, time, and oleylamine concentration. However, it may be noted that some of the other metal sulfide CQDs as prepared here are characterized with broad size distribution as well as irregular size. This could be due to the fact that the decomposition temperature and other reaction conditions (e.g., amount of OlAm needed) for different M−C_8DTCA complexes will be different, and each may need further optimization of the conditions, which are currently being pursued by us.

For any CQDs, to perform as an active layer in photovoltaic application, both good optical and electronic properties are a perquisite. Therefore, to test the usefulness of the PbS QDs synthesized from the presented strategy, we have tested their performance as an active layer in photovoltaic devices. Solar cell devices are made according to the earlier report and the device structure is shown in Figure 5a.[37] Here, ZnO layer acts as n-type window layer through which light can pass without any absorption to shine upon the active layer. $MAPbI_3$-capped PbS QD layer acts as the main light-absorbing layer and 1,2-ethane dithiol (EDT)-caped PbS QD layer acts as p-type electron-blocking and hole-transport layer for the solar cell. Au was deposited as a counter electrode to establish ohmic contact with the EDT-capped PbS layer for seamless collection of holes from the solar cell. The *J*−*V* characteristic under solar illumination for the best-performing solar cell is shown in Figure 5b. As can be seen, power conversion efficiency (PCE) as high as 4.64% is achieved in the PbS QD-based solar cells synthesized using the present approach. We further studied the photovoltaic figure of merits of the different sized PbS QDs. Shockley−Queisser equation[46] predicts that the semiconductor band gap between 1.1 and 1.3 eV is best suited for single-junction solar cell application.

This is the main driving factor for the researchers to tune the size of the PbS QDs so that their band gap can be varied from 1.1 to 1.3 eV as desired for solar cell development. Figure 5c shows the evolution of V_{oc}, J_{sc}, fill factor (FF), and power conversion efficiency (PCE) with the band gap of PbS QDs. It can be seen that the lower band gap of PbS QDs produces higher J_{sc} values, but both V_{oc} and FF decrease significantly with decrease in band gap. Best PCE is achieved in the case of 1.3 eV band gap PbS QDs. Doping density and depletion width of the best-performing PbS QD layer (1.3 eV band gap) are determined to further assess their quality from capacitance−voltage study, as shown in Figure 5d.[47] Capacitance−voltage study suggests a near-complete depletion of the PbS-$MAPbI_3$ layer at short-circuit condition. Doping density of the PbS QD layer as determined from Mott−Schottky analysis is found to be 5×10^{16} cm^{-3}, matching closely with the high-performing PbS QD-based photovoltaic devices.[37] We further characterized the electronic properties of the PbS QD layer through light-intensity-dependent current and voltage generation measurements. Photocurrent generation in solar cells with illumination intensity is governed by the equation $J \infty \phi^{\alpha}$, where J is the current density, ϕ is the illumination intensity, and α is the power exponent.[48] As shown in Figure 5e, the slope of the logarithmic plot of J_{sc} and the light intensity is determined to be 1. This implies that current extraction is generation limited and transport of both electron and hole carriers is balanced through the PbS layer in our photovoltaic devices. Diode ideality factor η is determined from the intensity vs V_{oc} evolution measurement (Figure 5f).[49] η = 1.59 suggests the involvement of intermediate trap states of PbS QD layer in the recombination process of the photocarriers. Further, literature reports suggest that PbS QD synthesized from the established optimized method shows similar η values in their solar cell applications.[49]

CONCLUSIONS

An easy and convenient procedure to make metal sulfide quantum dots is unveiled. It is disclosed that the metal-octyl dithiocarbamic acid complex's decomposition can be delicately controlled by adjusting the reaction parameter like temperatures and oleylamine concentration. The QDs synthesized have tunable infrared emission with small Stokes shifts and quantum yields of 15−40%. The synthesis was easily scaled up to produce 1.2−3.5 gm of PbS QDs from one batch of reaction. We observed that the as-synthesized QDs are air-stable for several months (more than 3 months), and they readily self-assemble into ordered lattices. Our simple low-cost method resulted in a record solar power conversion efficiency of 4.64%. These working PbS QD solar cells, prepared by this prescribed method, open another avenue for further investigation to improve the photovoltaic performance.

ASSOCIATED CONTENT

Supporting Information

The Supporting Information is available free of charge on the ACS Publications website at DOI: 10.1021/acs.langmuir.8b00741.

Synthesis and characterization (Section S1); Details of solar cell device fabrication and characterization (Section S2) (PDF)

AUTHOR INFORMATION

Corresponding Authors

*E-mail: ak.rath@ncl.res.in (A.K.R.).

*E-mail: pl.bhagavatula@ncl.res.in. Tel: 91-20-25902013. Fax: 91-20-25902036 (B.L.V.P.).

ORCID

Arup K. Rath: 0000-0003-2261-7215

Bhagavatula L. V. Prasad: 0000-0002-3115-0736

Notes

The authors declare no competing financial interest.

DOI: 10.1021/acs.langmuir.8b00741
Langmuir 2018, 34, 5788−5797

■ ACKNOWLEDGMENTS

A.B. thanks UGC, New Delhi, for research fellowship. The authors thank Council of Scientific and Industrial Research (CSIR), New Delhi, for financial assistance through 12th Five Year Plan Project (CSC 0134). A.K. thanks the Nanomission and Science and Engineering Research Board of Department of Science and Technology, New Delhi, for funding through the grants SR/NM/NT-1011/2105 (G) EMR/2015/002415, respectively.

■ REFERENCES

(1) Ma, W.; Luther, J. M.; Zheng, H.; Wu, Y.; Alivisatos, A. P. Photovoltaic devices employing ternary PbS_x Se_{1-x} nanocrystals. *Nano Lett.* **2009**, *9*, 1699−1703.
(2) Kim, J. Y.; Kim, S. H.; Lee, H. H.; Lee, K.; Ma, W.; Gong, X.; Heeger, A. J. New Architecture for high efficiency polymer photovoltaic cells using solution based titanium oxide as an optical spacer. *Adv. Mater.* **2006**, *18*, 572−576.
(3) Kojima, A.; Teshima, K.; Shirai, Y.; Miyasaka, T. Organometal halide perovskites as visible-light sensitizers for photovoltaic cells. *J. Am. Chem. Soc.* **2009**, *131*, 6050−6051.
(4) Li, G.; Shrotriya, V.; Huang, J.; Yao, Y.; Moriarty, T.; Emery, K.; Yang, Y. High-efficiency solution processable polymer photovoltaic cells by self-organization of polymer blends. *Nat. Mater.* **2005**, *4*, 864−868.
(5) Lunt, R. R.; Osedach, T. P.; Brown, P. R.; Rowehl, J. A.; BuloviÄ, V. Practical roadmap and limits to nanostructured photovoltaics. *Adv. Mater.* **2011**, *23*, 5712−5727.
(6) Zhitomirsky, D.; Kramer, I. J.; Labelle, A. J.; Fischer, A.; Debnath, R.; Pan, J.; Bakr, O. M.; Sargent, E. H. Colloidal quantum dot photovoltaics: the effect of polydispersity. *Nano Lett.* **2012**, *12*, 1007−1012.
(7) Kamat, P. V. Quantum dot solar cells. Semiconductor nanocrystals as light harvesters. *J. Phys. Chem. C* **2008**, *112*, 18737−18753.
(8) Robel, I.; Subramanian, V.; Kuno, M.; Kamat, P. V. Quantum dot solar cells. Harvesting light energy with CdSe nanocrystals molecularly linked to mesoscopic TiO2 films. *J. Am. Chem. Soc.* **2006**, *128*, 2385−2393.
(9) Konstantatos, G.; Howard, I.; Fischer, A.; Hoogland, S.; Clifford, J.; Klem, E.; Levina, L.; Sargent, E. H. Ultrasensitive solution-cast quantum dot photodetectors. *Nature* **2006**, *442*, 180−183.
(10) Levine, B. F. Quantum well infrared photodetectors. *J. Appl. Phys.* **1993**, *74*, R1−R81.
(11) McDonald, S. A.; Konstantatos, G.; Zhang, S.; Cyr, P. W.; Klem, E. J. D.; Levina, L.; Sargent, E. H. Solution-processed PbS quantum dot infrared photodetectors and photovoltaics. *Nat. Mater.* **2005**, *4*, 138−142.
(12) Peumans, P.; Yakimov, A.; Forrest, S. R. Small molecular weight organic thin-film photodetectors and solar cells. *J. Appl. Phys.* **2003**, *93*, 3693−3723.
(13) Colvin, V. L.; Schlamp, M. C.; Alivisatos, A. P. Light-emitting diodes made from cadmium selenide nanocrystals and a semiconducting polymer. *Nature* **1994**, *370*, 354−357.
(14) Ali, M.; Chattopadhyay, S.; Nag, A.; Kumar, A.; Sapra, S.; Chakraborty, S.; Sarma, D. D. White-light emission from a blend of CdSeS nanocrystals of different Se: S ratio. *Nanotechnology* **2007**, *18*, No. 075401.
(15) Talapin, D. V.; Lee, J.-S.; Kovalenko, M. V.; Shevchenko, E. V. Prospects of colloidal nanocrystals for electronic and optoelectronic applications. *Chem. Rev.* **2009**, *110*, 389−458.
(16) Sun, L.; Choi, J. J.; Stachnik, D.; Bartnik, A. C.; Hyun, B.-R.; Malliaras, G. G.; Hanrath, T.; Wise, F. W. Bright infrared quantum-dot light-emitting diodes through inter-dot spacing control. *Nat. Nanotechnol.* **2012**, *7*, 369−373.
(17) Li, L.; Pandey, A.; Werder, D. J.; Khanal, B. P.; Pietryga, J. M.; Klimov, V. I. Efficient synthesis of highly luminescent copper indium sulfide-based core/shell nanocrystals with surprisingly long-lived emission. *J. Am. Chem. Soc.* **2011**, *133*, 1176−1179.
(18) de Mello Donegá, C. Synthesis and properties of colloidal heteronanocrystals. *Chem. Soc. Rev.* **2011**, *40*, 1512−1546.
(19) Peng, X.; Wickham, J.; Alivisatos, A. P. Kinetics of II-VI and III-V colloidal semiconductor nanocrystal growth: focusing of size distributions. *J. Am. Chem. Soc.* **1998**, *120*, 5343−5344.
(20) Ellingson, R. J.; Beard, M. C.; Johnson, J. C.; Yu, P.; Micic, O. I.; Nozik, A. J.; Shabaev, A.; Efros, A. L. Highly efficient multiple exciton generation in colloidal PbSe and PbS quantum dots. *Nano Lett.* **2005**, *5*, 865−871.
(21) Carey, G. H.; Abdelhady, A. L.; Ning, Z.; Thon, S. M.; Bakr, O. M.; Sargent, E. H. Colloidal quantum dot solar cells. *Chem. Rev.* **2015**, *115*, 12732−12763.
(22) Pal, B. N.; Robel, I.; Mohite, A.; Laocharoensuk, R.; Werder, D. J.; Klimov, V. I. High Sensitivity p-n Junction Photodiodes Based on PbS Nanocrystal Quantum Dots. *Adv. Funct. Mater.* **2012**, *22*, 1741−1748.
(23) Wang, X.; Perzon, E.; Delgado, J. L.; de la Cruz, P.; Zhang, F.; Langa, F.; Andersson, M.; InganÃ¤s, O. Infrared photocurrent spectral response from plastic solar cell with low-band-gap polyfluorene and fullerene derivative. *Appl. Phys. Lett.* **2004**, *85*, 5081−5083.
(24) Liu, M.; Voznyy, O.; Sabatini, R.; de Arquer, F. P. G.; Munir, R.; Balawi, A. H.; Lan, X.; Fan, F.; Walters, G.; Kirmani, A. R.; Hoogland, S.; Laquai, F.; Amassian, A.; Sargent, E. H. Hybrid organic-inorganic inks flatten the energy landscape in colloidal quantum dot solids. *Nat. Mater.* **2017**, *16*, 258−263.
(25) Murray, C.; Norris, D. J.; Bawendi, M. G. Synthesis and characterization of nearly monodisperse CdE (E = sulfur, selenium, tellurium) semiconductor nanocrystallites. *J. Am. Chem. Soc.* **1993**, *115*, 8706−8715.
(26) Joo, J.; Na, H. B.; Yu, T.; Yu, J. H.; Kim, Y. W.; Wu, F.; Zhang, J. Z.; Hyeon, T. Generalized and facile synthesis of semiconducting metal sulfide nanocrystals. *J. Am. Chem. Soc.* **2003**, *125*, 11100−11105.
(27) Zhang, H.; Hyun, B.-R.; Wise, F. W.; Robinson, R. D. A generic method for rational scalable synthesis of monodisperse metal sulfide nanocrystals. *Nano Lett.* **2012**, *12*, 5856−5860.
(28) Zhang, L.-j.; Shen, X. C.; Liang, H.; Guo, S.; Liang, Z. H. Hot-injection synthesis of highly luminescent and monodisperse CdS nanocrystals using thioacetamide and cadmium source with proper reactivity. *J. Colloid Interface Sci.* **2010**, *342*, 236−242.
(29) Li, Z.; Ji, Y.; Xie, R.; Grisham, S. Y.; Peng, X. Correlation of CdS nanocrystal formation with elemental sulfur activation and its implication in synthetic development. *J. Am. Chem. Soc.* **2011**, *133*, 17248−17256.
(30) Thomson, J. W.; Nagashima, K.; Macdonald, P. M.; Ozin, G. A. From sulfur amine solutions to metal sulfide nanocrystals: peering into the oleylamine-sulfur black box. *J. Am. Chem. Soc.* **2011**, *133*, 5036−5041.
(31) Cademartiri, L.; Montanari, E.; Calestani, G.; Migliori, A.; Guagliardi, A.; Ozin, G. A. Size-dependent extinction coefficients of PbS quantum dots. *J. Am. Chem. Soc.* **2006**, *128*, 10337−10346.
(32) Yuan, M.; Kemp, K. W.; Thon, S. M.; Kim, J. Y.; Chou, K. W.; Amassian, A.; Sargent, E. H. High Performance Quantum Dot Solids via Elemental Sulfur Synthesis. *Adv. Mater.* **2014**, *26*, 3513−3519.
(33) Huang, Z.; Zhai, G.; Zhang, Z.; Zhang, C.; Xia, Y.; Lian, L.; Fu, X.; Zhang, D.; Zhang, J. Low cost and large scale synthesis of PbS quantum dots with hybrid surface passivation. *CrystEngComm* **2017**, *19*, 946−951.
(34) Chuang, C.-H. M.; Brown, P. R.; BuloviÄ, V.; Bawendi, M. G. Improved performance and stability in quantum dot solar cells through band alignment engineering. *Nat. Mater.* **2014**, *13*, 796−801.
(35) Hendricks, M. P.; Campos, M. P.; Cleveland, G. T.; Jen-La Plante, I.; Owen, J. S. A tunable library of substituted thiourea precursors to metal sulfide nanocrystals. *Science* **2015**, *348*, 1226−1230.
(36) Hines, M. A.; Scholes, G. D. Colloidal PbS nanocrystals with size tunable near infrared emission: observation of post synthesis self

DOI: 10.1021/acs.langmuir.8b00741
Langmuir 2018, 34, 5788−5797

narrowing of the particle size distribution. *Adv. Mater.* **2003**, *15*, 1844−1849.
(37) Yang, Z.; Janmohamed, A.; Lan, X.; García de Arquer, F. P.; Voznyy, O.; Yassitepe, E.; Kim, G.-H.; Ning, Z.; Gong, X.; Comin, R.; Sargent, E. H. Colloidal Quantum Dot Photovoltaics Enhanced by Perovskite Shelling. *Nano Lett.* **2015**, *15*, 7539−7543.
(38) Busupalli, B.; Kummara, S.; Kumaraswamy, G.; Prasad, B. L. V. Ultrathin sheets of metal or metal sulfide from molecularly thin sheets of metal thiolates in solution. *Chem. Mater.* **2014**, *26*, 3436−3442.
(39) Pradhan, N.; Katz, B.; Efrima, S. Synthesis of High-Quality Metal Sulfide Nanoparticles from Alkyl Xanthate Single Precursors in Alkylamine Solvents. *J. Phys. Chem. B* **2003**, *107*, 13843−13854.
(40) Pradhan, N.; Efrima, S. Single-Precursor, One-Pot Versatile Synthesis under near Ambient Conditions of Tunable, Single and Dual Band Fluorescing Metal Sulfide Nanoparticles. *J. Am. Chem. Soc.* **2003**, *125*, 2050−2051.
(41) Han, S. K.; Gong, M.; Yao, H. B.; Wang, Z. M.; Yu, S. H. One-Pot Controlled Synthesis of Hexagonal-Prismatic $Cu_{1.94}S$-ZnS, $Cu_{1.94}S$-ZnS-$Cu_{1.94}S$, and $Cu_{1.94}S$-ZnS-$Cu_{1.94}S$-ZnS-$Cu_{1.94}S$ Heteronanostructures. *Angew. Chem., Int. Ed.* **2012**, *51*, 6365−6368.
(42) Han, S. K.; Gu, C.; Zhao, S.; Xu, S.; Gong, M.; Li, Z.; Yu, S. H. Precursor Triggering Synthesis of Self-Coupled Sulfide Polymorphs with Enhanced Photoelectrochemical Properties. *J. Am. Chem. Soc.* **2016**, *138*, 12913−12919.
(43) Hollingsworth, N.; Roffey, A.; Islam, H.-U.; Mercy, M.; Roldan, A.; Bras, W.; Wolthers, M.; Catlow, C. R. A.; Sankar, G.; Hogarth, G.; et al. Active nature of primary amines during thermal decomposition of nickel dithiocarbamates to nickel sulfide nanoparticles. *Chem. Mater.* **2014**, *26*, 6281−6292.
(44) Han, S. K.; Gu, C.; Gong, M.; Yu, S. H. A Trialkylphosphine-Driven Chemical Transformation Route to Ag and Bi-Based Chalcogenides. *J. Am. Chem. Soc.* **2015**, *137*, 5390−5396.
(45) Jung, Y. K.; Kim, J. I.; Lee, J.-K. Thermal decomposition mechanism of single-molecule precursors forming metal sulfide nanoparticles. *J. Am. Chem. Soc.* **2009**, *132*, 178−184.
(46) Shockley, W.; Queisser, H. J. Detailed Balance Limit of Efficiency of p-n Junction Solar Cells. *J. Appl. Phys.* **1961**, *32*, 510−519.
(47) Johnston, K. W.; Pattantyus-Abraham, A. G.; Clifford, J. P.; Myrskog, S. H.; Hoogland, S.; Shukla, H.; Klem, E. J. D.; Levina, L.; Sargent, E. H. Efficient Schottky-quantum-dot photovoltaics: The roles of depletion, drift, and diffusion. *Appl. Phys. Lett.* **2008**, *92*, No. 122111.
(48) Zhao, N.; Osedach, T. P.; Chang, L.-Y.; Geyer, S. M.; Wanger, D.; Binda, M. T.; Arango, A. C.; Bawendi, M. G.; Bulovic, V. Colloidal PbS quantum dot solar cells with high fill factor. *ACS Nano* **2010**, *4*, 3743−3752.
(49) Chuang, C.-H. M.; Maurano, A.; Brandt, R. E.; Hwang, G. W.; Jean, J.; Buonassisi, T.; BulovicÌ, V.; Bawendi, M. G. Open-circuit voltage deficit, radiative sub-bandgap states, and prospects in quantum dot solar cells. *Nano Lett.* **2015**, *15*, 3286−3294.

DOI: 10.1021/acs.langmuir.8b00741
Langmuir 2018, 34, 5788−5797